

**Design of an efficient venturi-scrubber for retention of  
radionuclides during severe accident of a nuclear reactor**

*By*

**PARIDHI GOEL**

**ENGG01201304009**

**BHABHA ATOMIC RESEARCH CENTRE,**

**MUMBAI 400085, INDIA**

*A thesis submitted to the Board of Studies in Engineering Sciences*

*In partial fulfilment of requirements for the Degree of*

**DOCTOR OF PHILOSOPHY**

*of*

**HOMI BHABHA NATIONAL INSTITUTE**

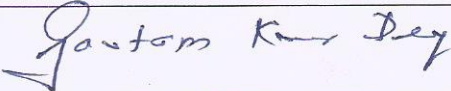
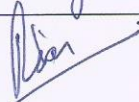
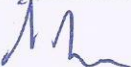
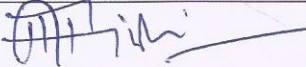
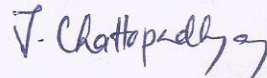
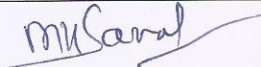
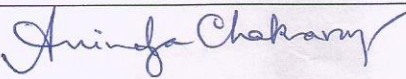


**March 2020**

# Homi Bhabha National Institute

## Recommendations of the Viva Voce Committee

As members of the Viva Voce Committee, we certify that we have read the dissertation prepared by *Paridhi Goel* entitled *Design of an efficient venturi-scrubber for retention of radionuclides during severe accident of a nuclear reactor* and recommend that it may be accepted as fulfilling the thesis requirement for the award of Degree of Doctor of Philosophy.

Chairman – Dr. G. K. Dey		Date 4/1/2020
Guide / Convener – Dr. A. K. Nayak		Date 4-1-2020
Co-guide – Dr. P. M. Ravi		Date 4/1/2020
Examiner – Prof. Sreenivas Jayanti		Date 4/1/2020
Member 1 – Dr. A. P. Tiwari		Date 04/1/2020
Member 2 – Dr. J. Chattopadhyay		Date 4/1/2020
Member 3 – Dr. M. K. Samal		Date 4/1/2020
Member 4 – Dr. A. Chakravarty		Date 4/1/2020

Final approval and acceptance of this thesis is contingent upon the candidate's submission of the final copies of the thesis to HBNI.

I/We hereby certify that I/we have read this thesis prepared under my/our direction and recommend that it may be accepted as fulfilling the thesis requirement.

Date: 4-1-2020

Place: Mumbai

Signature

Co-guide: Dr. P. M. Ravi

Signature

Guide: Dr. A. K. Nayak

## STATEMENT BY AUTHOR

This dissertation has been submitted in partial fulfilment of requirements for an advanced degree at Homi Bhabha National Institute (HBNI) and is deposited in the Library to be made available to borrowers under rules of the HBNI.

Brief quotations from this dissertation are allowable without special permission, provided that accurate acknowledgement of source is made. Requests for permission for extended quotation from or reproduction of this manuscript in whole or in part may be granted by the Competent Authority of HBNI when in his or her judgement the proposed use of the material is in the interests of scholarship. In all other instances, however, permission must be obtained from the author.

*Paridhi*  
PARIDHI GOEL

## DECLARATION

I, hereby declare that the investigation presented in the thesis has been carried out by me. The work is original and has not been submitted earlier as a whole or in part for a degree / diploma at this or any other Institution / University.

*Paridhi*  
PARIDHI GOEL

## List of Publications arising from the thesis

### Publications in Refereed Journal:

1. "Numerical Simulation of Injection Characteristics, Hydrodynamics and Absorption of Iodine Vapour in a Venturi Scrubber operating in Self-priming mode." Nuclear Engineering and Design, Volume 341, January 2019, Pages 360-367. P. Goel, A. Moharana and A. K. Nayak. <https://doi.org/10.1016/j.nucengdes.2018.11.020>
2. "Measurement of scrubbing behaviour of simulated radionuclide in a submerged venturi scrubber." Nuclear Engineering and Design, Volume 327, February 2018, Pages 92-99. P. Goel, A. Moharana and A. K. Nayak. <https://doi.org/10.1016/j.nucengdes.2017.12.003>
3. "Performance estimation of a venturi scrubber and its application to self-priming operation in decontaminating aerosol particulates." Nuclear Engineering and Design, Volume 320, March 2017, Pages 165-182. A. Moharana, P. Goel and A. K. Nayak. <https://doi.org/10.1016/j.nucengdes.2017.05.023>
4. "Experimental investigation of hydrodynamic behaviour of a submerged venturi scrubber." P. Goel, A. Moharana and A. K. Nayak. Multiphase Science and Technology, Volume 31, 2019, Pages 45-59. <https://doi.org/10.1615/MultScienTechn.2019029434>
5. "Simulation of the performance of the venturi scrubber for an advanced reactor containment venting conditions." P. Goel and A. K. Nayak. ASME Nuclear Engineering and Radiation Science, Volume 6, January 2020, Pages 011211. <https://doi.org/10.1115/1.4044845>

### Publications in the conferences:

6. "Development of a Computational Model to determine Performance of a Self-Priming Venturi Scrubber for Thorium Reactor." P. Goel, A. Moharana and A. K. Nayak. NCPTTh: Present Status and Future Directions, December 22-24, 2014, Mumbai, India. Paper no. NCPTTh1-2014/64 pp. 63-65.
7. "Development of a computational model to determine performance of a self-priming venturi scrubber for thorium reactor." P. Goel, A. Moharana and A. K. Nayak. International Topical Meeting on Nuclear Reactor Thermal Hydraulics 2015, NURETH 2015, 8, pp. 6208-6216.
8. "Experimental study of pressure drop in self-priming and submerged venturi Scrubber." P. Goel, A. Moharana and A. K. Nayak. The 8<sup>th</sup> ERMSAR-2017 Warsaw, Poland, 16-18 May 2017 Paper no. 309.
9. "Numerical investigation of aerosol collection efficiency in a venturi scrubber." P. Goel and A. K. Nayak. Proceedings of ICONE-26 July 22-26, 2018, London, England. doi:10.1115/ICONE26-82489.
10. "CFD Simulation of Hydrodynamics and Scrubbing Behaviour in a venturi scrubber in a Self-Priming mode." P. Goel and A. K. Nayak. IUSSTF Symposium on Advanced Sensors and Modeling Techniques for Nuclear Reactor Safety, December 15-19 2018, IIT Bombay.

*Paridhi*

PARIDHI GOEL

## **Dedications**

*To my family*

[For their unconditional support and motivation]

## **ACKNOWLEDGEMENTS**

I would like to acknowledge my deepest gratitude to my guide Dr A.K Nayak, O.S., Thermal Hydraulics Section, Reactor Engineering Division BARC for his invaluable guidance and continuous encouragement in carrying out my PhD work. His guidance helped me in understanding the critical aspects of the work, writing the research papers and the thesis.

I am highly obliged to my co-guide Dr P.M Ravi for helping me understand the chemistry aspects of the topic. He has also been very kind to give me his reviews on the report and improve it.

I would like to thank the doctoral committee members: Chairman of the committee, Dr G. K Dey and other members: Dr A P Tiwari, Dr J. Chattopadhyay, Dr M. K. Samal and Dr A. Chakravarty for their critical evaluation and encouragement. Their comments widened my research perspective and have encouraged me throughout these years.

I am also thankful to Shri Avinash Moharana for the technical discussions and providing the infrastructure in performing my task. I express my sincere thanks to Smt. S. Jayashree for her suggestions and guidance. I would thank the MOD Lab Chemistry division for carrying out the analysis of the samples. I am highly indebted to the workshop staff without whom the fabrication of the experimental setup was not possible. I express my sincere thanks to all the members of Thermal Hydraulic Section, RED, BARC and RDDG group for their needful help in various things.

I thank all my PhD. seniors Dr. Naveen N., Dr Archana V., Dr. Mohit Sharma, Dr. Sapna Singh, Dr. Sunil Kumar, Dr. Neelam and Dr. Manju who introduced me to HBNI. I would be particularly highly grateful to Dr. Nitendra for all the discussions on nuclear stuff and the cooking classes we had. I cannot forget to thank Dr. Nitin Minocha, Dr. Eshita Pal, Dr.

Jayaraj K., Dr. Amit Chandrakar, Dr. Parul Goel, Suresh Sahu, Amita Bedar and Satendra for being a part of this beautiful journey. In line with this is Sakshi Mukhija, Sai Rajgopal, Rakesh Kumar and Samyak Munot with whom I had fun while in office as well. Thanks for being there!

I would also like to thank all Dean, Homi Bhabha National University, Dean, Academic, administration and staff members for their constant cooperation in all administrative activities.

I would grab this opportunity to thank all my family members and my friends who have instilled in me the confidence and have always boosted me in low times. Their support has made me the person I am and I just cannot thank them enough for things they have done for me.

Thanks again for all your encouragement!

# TABLE OF CONTENTS

TABLE OF CONTENTS.....	i
Synopsis .....	i
List of figures.....	xvii
List of tables.....	xxii
List of abbreviations .....	xxiv
Nomenclature.....	xxvi
Chapter 1. Introduction .....	1
1.1. Background.....	1
1.2. Past Severe Nuclear Accidents and their Impact.....	8
1.3. Issue of radioactivity release .....	10
1.4. Filtered Containment Venting System (FCVS).....	18
1.5. Literature Review .....	22
1.6. Studies on submerged operation.....	23
1.6.1. Studies on self-priming operation .....	24
1.6.2. Non-Submerged operation or Forced Feed Operation .....	25
1.7. Major Scientific issues associated with FCVS .....	32
1.8. Outline of the thesis.....	36
1.9. Closure.....	37
Chapter 2. Concept Design of FCVS for an Advanced Indian Reactor.....	39

2.1. Introduction .....	39
2.2. Advanced Heavy Water Reactor (AHWR) description.....	39
2.3. Filtered Containment Venting System Description.....	40
2.4. Design Objectives of FCVS .....	42
2.5. Design Parameters .....	43
2.5.1. Flow profile from Containment.....	43
2.5.2. Estimation of Fission Product Release to FCVS.....	46
2.5.2.1. Mechanism of Fission Product Release in the Reactor .....	46
2.5.2.1. Estimation of inventory for the present reactor.....	47
2.6. Assumptions for the design of venturi scrubber.....	50
2.7. Design Calculations for FCVS .....	53
2.8. Arrangement of venturi scrubbers manifold in the scrubber tank.....	62
2.9. Closure.....	64
Chapter 3. Description of the Experimental Facility for FCVS.....	65
3.1. Introduction .....	65
3.2. Scaling of the experimental facility.....	65
3.2.1. Geometric Scaling .....	66
3.2.2. Flow Scaling.....	66
3.3. Details of the experimental Setup.....	67
3.3.1. Scrubber Tank and Venturi Scrubber.....	67
3.3.1.1. Scrubber Tank .....	67

3.3.1.2. Venturi Scrubber .....	69
3.3.1.3. Demister Pad .....	70
3.3.2. Iodine Dispenser.....	70
3.4. Instrumentation.....	71
3.5. Operating Procedure and Measurements .....	73
3.6. Closure.....	76
Chapter 4. Performance Evaluation of the Simulated FCVS in Experimental Facility .....	78
4.1. Introduction .....	78
4.2. Hydrodynamics of venturi scrubber .....	78
4.2.1. Results and Discussion.....	79
4.2.1.1. Effect of Upstream Pressure.....	80
4.2.1.2. High upstream pressure conditions .....	80
4.2.1.3. Low upstream pressure conditions .....	83
4.2.1.4. Effect of submergence height.....	85
4.3. Iodine vapour retention.....	86
4.3.1. Effect of gas flow rate .....	86
4.3.2. Effect of submergence height on iodine retention .....	89
4.3.3. Iodine vapour decontamination.....	90
4.4. Theoretical Evaluation of pressure drop across the venturi scrubber.....	92
4.4.1. Evaluation of liquid loading.....	94
4.4.2. Prediction of pressure drop from empirical models in the literature.....	96

4.5. Closure.....	98
Chapter 5. Development and Benchmarking of CFD Model for predicting FCVS performance.....	101
5.1. Introduction .....	101
5.1.1. Eulerian Gas Flow .....	102
5.1.2. Lagrangian Tracking of Droplets and Aerosols .....	104
5.1.2.1. Analysis of drag coefficient .....	105
5.1.3. Droplet Size Distribution .....	107
5.1.3.1. Collision of droplets .....	107
5.1.4. Capture of aerosol .....	108
5.1.5. Numerical Algorithm .....	109
5.2. Results and Discussion .....	111
5.2.1. Model Development and Validation .....	111
5.2.2. Scrubbing efficiency of aerosols .....	121
5.2.3. Effect of Operating and Geometric parameters.....	122
5.2.3.1. Effect of throat gas velocity .....	122
5.2.3.2. Effect of liquid flow rate .....	124
5.2.3.3. Effect of nozzle diameter .....	126
5.2.3.4. Effect of throat length .....	128
5.3. Application of the model to the present experiments .....	130
5.4. Absorption of iodine vapours .....	131
5.5. Results of Model Validation with the present experimental results .....	132

5.5.1.	Evaluation of liquid loading .....	132
5.5.2.	Droplets trajectory and size distribution .....	134
5.5.3.	Pressure loss in venturi scrubber .....	136
5.5.4.	Scrubbing of iodine vapour .....	138
5.6.	Design improvements for Self-priming operation .....	140
5.6.1.	Injector system with different nozzle diameters .....	142
5.6.2.	Multi-Stage Injection.....	145
5.7.	Closure.....	146
Chapter 6. Performance of FCVS for reactor prototypic conditions.....		149
6.1.	Introduction .....	149
6.2.	Case Settings.....	150
6.3.	Results and Discussion .....	152
6.3.1.	Pressure profile in the venturi scrubber.....	152
6.3.2.	Droplets Sizes.....	154
6.3.3.	Iodine absorption.....	155
6.4.	Closure.....	156
Chapter 7. Conclusions and Future Work .....		158
7.1.	Concept design of FCVS .....	158
7.2.	Understanding hydrodynamics of venturi scrubber involving multi-phase and multi-component systems.....	159
7.3.	Generation of test data and understanding the scrubbing of iodine vapour .....	160
7.4.	Development of CFD model for venturi scrubber performance.....	161

7.5. Performance of venturi scrubber for actual reactor conditions .....	162
7.6. Recommendations and Future Work .....	163
References.....	165

# List of figures

<i>Figure 1.1 Schematic of fission process</i> .....	2
<i>Figure 1.2 Greenhouse gas emissions in terms of equivalent CO<sub>2</sub> produced from various sources of energy (<a href="https://www.world-nuclear.org/nuclear-basics/nuclear-energy-and-climate-change.aspx">https://www.world-nuclear.org/nuclear-basics/nuclear-energy-and-climate-change.aspx</a> (2018))</i> .....	2
<i>Figure 1.3 Percentage of sources of energy contributing to electricity generation as per 2017 statistics <a href="http://world-nuclear-news.org/Articles/Nuclear-Innovation-Clean-Energy-Future-(NICE-Future%202018))">http://world-nuclear-news.org/Articles/Nuclear-Innovation-Clean-Energy-Future-(NICE-Future (2018))</a></i> .....	3
<i>Figure 1.4 India's three-stage nuclear power programme</i> .....	4
<i>Figure 1.5 A typical nuclear power plant</i> .....	6
<i>Figure 1.6 Overview of Filtered Containment Venting</i> .....	18
<i>Figure 1.7 Line diagram of FCVS</i> .....	21
<i>Figure 1.8 Geometry of venturi scrubber</i> .....	22
<i>Figure 1.9 Schematic of a venturi scrubber installed in a FCVS</i> .....	23
<i>Figure 1.10 Schematic of a self-priming venturi scrubber</i> .....	24
<i>Figure 1.11 Schematic of a forced feed venturi scrubber</i> .....	26
<i>Figure 2.1. Schematic of Advanced Heavy Water Reactor (AHWR)</i> .....	40
<i>Figure 2.2. Pressure transient from the containment during venting</i> .....	44
<i>Figure 2.3. Mass flow rate of gas from the containment during venting</i> .....	45
<i>Figure 2.4 Plot of (a) scrubbing efficiency and (b) cut diameter as a function of dimensionless liquid loading ratio (B)</i> .....	56
<i>Figure 2.5 Impaction parameter as a function of cut diameter</i> .....	58
<i>Figure 2.6. Pressure drop from Calvert equation for the calculated liquid loadings</i> .....	59
<i>Figure 2.7. Dimensions of venturi scrubber (m)</i> .....	62

<i>Figure 2.8 Arrangement of FCVS considered in the present study .....</i>	<i>63</i>
<i>Figure 3.1 Schematic of the experimental facility comprising of a venturi scrubber held vertically in a scrubber tank and an iodine dispenser at an elevated height to simulate the hydrodynamic behavior and scrubbing efficiency pertinent to nuclear reactor.....</i>	<i>68</i>
<i>Figure 3.2 Photograph of (a) Scrubber Tank and (b) Venturi Scrubber.....</i>	<i>69</i>
<i>Figure 3.3 Location of sampling ports in the experimental set-up for measuring the iodine retained by the alkaline pool.....</i>	<i>76</i>
<i>Figure 3.4 Cascade of bottles arrangement used for measuring bulk DF of iodine vapours .</i>	<i>76</i>
<i>Figure 4.1 Pressure drop as a function at different gas flow rates for high flow conditions for initial submergence height of 4.5 m.....</i>	<i>81</i>
<i>Figure 4.2 Radial pressure across the throat at different gas flow rates for initial submergence height of 4.5 m.....</i>	<i>82</i>
<i>Figure 4.3 Pressure drop (for low flow conditions) as a function at different gas flow rates for initial submergence height of 4.5 m.....</i>	<i>84</i>
<i>Figure 4.4 Radial pressure across the throat at different low gas flow rates for initial submergence height of 4.5 m. ....</i>	<i>84</i>
<i>Figure 4.5 Comparison of radial pressure across the throat for two submergence heights: 4 m and 4.5 m.....</i>	<i>86</i>
<i>Figure 4.6 Percentage iodine retained during experiments for flow rates varying from 0.04-0.1 kg/s at the submergence height of 4 m.....</i>	<i>88</i>
<i>Figure 4.7 Percentage iodine retained during experiments for different gas mass flow rates at two submergence heights: 3 m and 4 m.....</i>	<i>89</i>
<i>Figure 4.8 Theoretical prediction of liquid loading and corresponding pressure drop across venturi scrubber .....</i>	<i>96</i>
<i>Figure 4.9 Comparison of predicted pressure drop with measured pressure drop.....</i>	<i>98</i>

*Figure 5.1 Dimension of venturi scrubber (in mm) and the computational mesh..... 110*

*Figure 5.2 Radial penetration of droplets as a function of axial distance from injection plane for three drag models in the throat section..... 112*

*Figure 5.3 Comparison of (a) centreline velocity of continuous phase in the throat section and (b) contours of velocity of continuous phase for the venturi scrubber for three different drag models. .... 114*

*Figure 5.4 Distribution of (a) Instantaneous Weber number and (b) SMD distribution in the throat section at liquid loading  $2.75 \text{ l/m}^3$  and gas throat velocity  $70 \text{ m/s}$ . .... 116*

*Figure 5.5 Pressure drop for different liquid loadings at throat gas velocity  $70 \text{ m/s}$  compared with experimental results. .... 117*

*Figure 5.6 Pressure drop profiles for different liquid loading at throat gas velocity  $50 \text{ m/s}$  118*

*Figure 5.7 Predicted liquid flux distribution in venturi throat at six axial locations for throat gas velocity  $70 \text{ m/s}$  and liquid loading of  $2.75 \text{ l/m}^3$  compared with experimental results. ... 119*

*Figure 5.8 Predicted liquid flux distribution in venturi throat at six axial locations for throat gas velocity  $70 \text{ m/s}$  and liquid loading of  $1.1 \text{ l/m}^3$  compared with experimental results. .... 120*

*Figure 5.9 (a) Axial pressure drop variation for different gas velocities at liquid injection velocity- $5.03 \text{ m/s}$ . (b) Sauter mean diameter variation with gas velocity in the throat section. (c) Comparison of liquid flux profiles at axial distance downstream of injection with variation in gas velocity at  $x$ - $10 \text{ mm}$ ,  $20 \text{ mm}$ ,  $40 \text{ mm}$ ,  $70 \text{ mm}$  from injection..... 123*

*Figure 5.10 (a) Sauter mean diameter variation in liquid flow rates at throat gas velocity- $70 \text{ m/s}$ . (b) Comparison of liquid flux profiles at axial distance downstream of injection with variation in gas velocity at  $x$ - $10 \text{ mm}$ ,  $20 \text{ mm}$ ,  $40 \text{ mm}$ ,  $70 \text{ mm}$  from injection plane..... 126*

*Figure 5.11 a) Axial pressure drop variation with variation in number of nozzles at throat gas velocity  $70 \text{ m/s}$  and liquid loading  $1.1 \text{ l/m}^3$ . b) Comparison of liquid flux profiles at axial*

<i>distance downstream of injection with variation in nozzle diameter at x-10 mm, 20 mm, 40 mm and 70 mm from injection. ....</i>	<i>128</i>
<i>Figure 5.12 (a) Axial pressure drop variation with variation in throat length at throat gas velocity 70 m/s and liquid loading 1.1 l/m<sup>3</sup>. (b) Comparison of liquid flux profiles at axial distance downstream of injection with variation in throat length at throat end. (c) Sauter mean diameter variation with throat length in the throat section. ....</i>	<i>129</i>
<i>Figure 5.13 Dependence of K on air Reynolds number.....</i>	<i>134</i>
<i>Figure 5.14 Instantaneous distribution of droplet velocities and centreline continuous phase velocity for 0.074 kg/s gas mass flow rate and 3 m submergence height. ....</i>	<i>135</i>
<i>Figure 5.15 Instantaneous distribution of droplet diameter for 0.074 kg/s gas mass flow rate and 3 m submergence height.....</i>	<i>135</i>
<i>Figure 5.16 Instantaneous distribution of droplet diameter for 0.043 kg/s gas mass flow rate and 3 m submergence height.....</i>	<i>136</i>
<i>Figure 5.17 Pressure characteristics in the venturi scrubber for different gas mass flow rates at the submergence height of 3 m. ....</i>	<i>137</i>
<i>Figure 5.18 Pressure characteristics in the venturi scrubber for different gas mass flow rates at the submergence height of 4 m. ....</i>	<i>138</i>
<i>Figure 5.19 Percentage scrubbing of iodine vapours at submergence height of 3 m with varying gas mass flow rates.....</i>	<i>139</i>
<i>Figure 5.20 Percentage scrubbing of iodine vapours at submergence height of 4 m with varying gas mass flow rates.....</i>	<i>140</i>
<i>Figure 5.21 (a) Variation of efficiency with changing liquid injection velocity for gas velocity of 70 m/s. (b) Variation of efficiency with gas velocity for liquid injection velocity of 5.03 m/s. ....</i>	<i>141</i>
<i>Figure 5.22 Representation of nozzles considered for an x-aligned venturi scrubber. ....</i>	<i>143</i>

*Figure 5.23 (a) Axial pressure drop variation with variation in arrangement of nozzles at throat gas velocity 70 m/s and liquid loading  $\sim 1.1 \text{ l/m}^3$ . (b) Sauter mean diameter variation with different arrangement of nozzles in the throat section for throat gas velocity 70 m/s and liquid loading  $1.1 \text{ l/m}^3$  (c) Comparison of liquid flux profiles with variation in arrangement of nozzles at the throat end for gas velocity 70 m/s and liquid loading  $1.1 \text{ l/m}^3$  ..... 144*

*Figure 5.24 Multi-stage injection in a venturi scrubber..... 145*

*Figure 6.1 Pressure and mass flow rate from containment calculated from RELAP5 ..... 150*

*Figure 6.2 Dimensions of venturi scrubber (in m) along with boundary conditions ..... 151*

*Figure 6.3 Steps followed for predicting the hydrodynamics in the venturi scrubber at reactor prototypic condition..... 152*

*Figure 6.4 Liquid loading expected in the venturi scrubber. .... 153*

*Figure 6.5 Pressure characteristics in the venturi scrubber for different air flow rates at different times of venting process ..... 153*

*Figure 6.6 Droplet sizes in venturi scrubber for (a) 22 kg/s and (b) 2 kg/s containment gas mass flow..... 155*

*Figure 6.7 Percentage absorption of iodine vapours in the venturi scrubber..... 156*



# List of tables

<i>Table 1.1. Classification of fission products.....</i>	<i>13</i>
<i>Table 1.2 Release fraction to the containment.....</i>	<i>14</i>
<i>Table 1.3 Chemical Composition and forms of existence.....</i>	<i>15</i>
<i>Table 1.4 Thermal-hydraulic initial and boundary conditions at the beginning of the venting .....</i>	<i>19</i>
<i>Table 1.5 Load on the filter system by the fission product (Related to core inventory).....</i>	<i>19</i>
<i>Table 1.6 Differences between venturi scrubber for chemical, process industries and nuclear reactor application.....</i>	<i>33</i>
<i>Table 2.1 Calculated release fractions of different elements during severe accident.....</i>	<i>48</i>
<i>Table 2.2 Summary of design Parameters for FCVS for an advanced Indian reactor.....</i>	<i>50</i>
<i>Table 2.3. Values of parameter B (Equation (2.9)) with varying <math>K_p</math>.....</i>	<i>57</i>
<i>Table 2.4 Specifications of Scrubber Tank for reactor application.....</i>	<i>63</i>
<i>Table 3.1 Scaling of the experimental set-up.....</i>	<i>66</i>
<i>Table 3.2 List of instruments their range and accuracy in the experimental set-up .....</i>	<i>72</i>
<i>Table 4.1 Experimental conditions for iodine retention .....</i>	<i>87</i>
<i>Table 4.2 Summary of DF of iodine measured during experiments .....</i>	<i>91</i>
<i>Table 4.3 Summary of experimental works in forced feed venturi scrubbers.....</i>	<i>93</i>
<i>Table 4.4 Empirical relation for pressure drop in the venturi scrubber .....</i>	<i>96</i>
<i>Table 5.1 Summary of Solver Settings .....</i>	<i>110</i>
<i>Table 5.2 Results of validation studies .....</i>	<i>121</i>
<i>Table 5.3 Results of Parametric Study.....</i>	<i>130</i>
<i>Table 5.4 Summary of cases simulated.....</i>	<i>133</i>

*Table 5.5 Scrubber performance for different nozzle arrangements at different throat gas velocities for the injection velocity of 5.03 m/s..... 145*

*Table 5.6 Comparison of scrubber performance for multi-stage injection at throat gas velocity 70 m/s..... 146*

## **Chapter 1. Introduction**

### **1.1. Background**

The industrial revolution and the invention of machines marked a turning point in the growth and development of human beings. Human beings started using machines for their daily errands, which they previously used to do with hands. Before the revolution, most people lived in the country and worked on farms. During the revolution, people started moving to the cities to work in factories. Before this, people travelled by horse or walking, now new ways of travel were introduced including railroads and automobiles. This improved the standard of living and the demand of energy for functionalising these industries increased. For running these industries, fossil fuel was the primary source of energy. As a consequence of these events, energy became an essential part of everyone's daily life and became the parameter for measuring the growth and prosperity of the nations across the globe.

With time, population and machines on our planet Earth increased, which further increased the requirement of energy and this led to the depletion of their reserves. The accumulation of pollutants in the atmosphere brought in new challenges like respiratory diseases, greenhouse effect, acid rain, disturbing the eco-system, etc. The changes in ecosystem and other effects initiated the search for clean and sustainable sources of energy. Another issue that aroused the search for other sources of energy was that the fossil fuel reserves are localized to specific regions on earth, so their import by other countries caused a huge impact on their financial budget. With such concerns, the discovery of renewable sources started. But the renewable sources of energy e.g. solar energy, tidal energy, etc. couldn't be used to meet the requirement round the clock because of their seasonal dependence and scattered source.

The discovery of radioactivity by Henry Becquerel in 1896 and the fission opened new doors for a new source of energy termed as "Nuclear Energy". This was primarily based on the

fission of heavy nuclei e.g.  $^{235}\text{U}$  into lighter and stable fission products accompanied by release of neutron and energy when bombarded with a neutron (Figure 1.1). This releases a huge

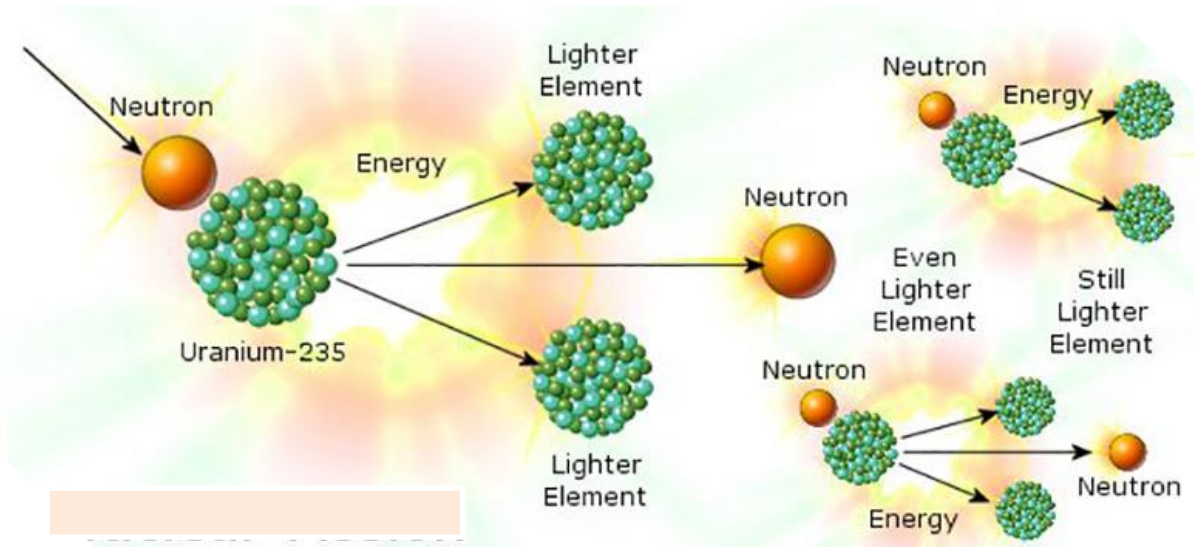


**Figure 1.1 Schematic of fission process**

amount of energy as per mass-energy equivalence. A kilogram of Uranium-235 releases almost three million times more energy than a kilogram of coal burned. In addition, the carbon footprints of nuclear energy are negligible compared to the fossil fuels (Figure 1.2).

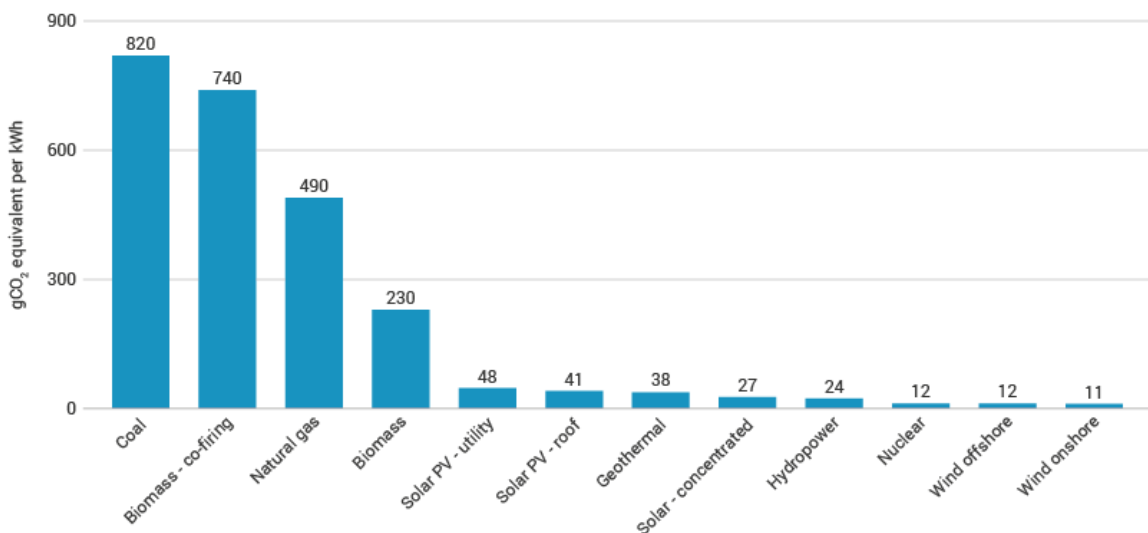


**Figure 1.2 Greenhouse gas emissions in terms of equivalent CO<sub>2</sub> produced from various sources of energy** (<https://www.world-nuclear.org/nuclear-basics/nuclear-energy-and-climate-change.aspx> (2018))

The control of this reaction to exploit the emitted energy during fission reactions was the initial challenge and the starting point of the research. The developed nations like United States started exploring this option as a part of military research programme. The first success happened when Enrico Fermi and team built the first nuclear reactor “Chicago-Pile” in 1942. In parallel to this, the ongoing political developments in the developing countries led to the fear of war amongst themselves and the idea of using nuclear fission reactions to make weapons in warfare originated. The use of nuclear bombs in Second World War created havoc and this had unanticipated and undesired effect on the inhabitants of Japan. This clearly stated to the world that the nuclear energy could be a great source of energy if properly controlled.

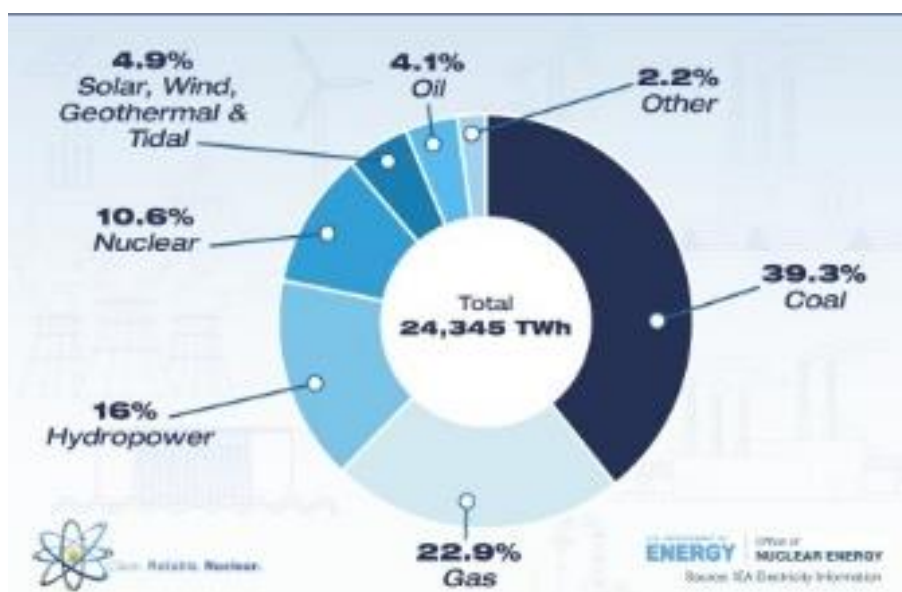


**Figure 1.3 Percentage of sources of energy contributing to electricity generation as per 2017 statistics** ([http://world-nuclear-news.org/Articles/Nuclear-Innovation-Clean-Energy-Future-\(NICE-Future \(2018\)\)](http://world-nuclear-news.org/Articles/Nuclear-Innovation-Clean-Energy-Future-(NICE-Future%20(2018))))

The research on nuclear reactors for electricity generation and as potential weapons started in other countries as well. With the depletion of carbon fuels and the increasing demand of energy, it became essential to look for sustainable and clean source of energy. This motivated the scientists to explore nuclear energy for meeting the increasing energy requirements. The

nuclear reactors currently contribute to nearly 10.6% of the electricity requirements (Figure 1.3).

In the developing countries like India, the research on nuclear energy started as more of a necessity to meet the energy requirements in the year 1956 with the establishment of Atomic Energy Commission of India. Dr. Homi Bhabha initiated this programme in collaboration with Sir Dorabji Tata. Dr. Homi Bhabha conceived a visionary three-stage nuclear power programme for India (Figure 1.4) based on closed fuel cycle concept to optimize the fuel and minimize the waste. The ultimate goal was to provide the resources for the country's growing energy requirement by using thorium reserves abundantly present in the coastal regions of South India.

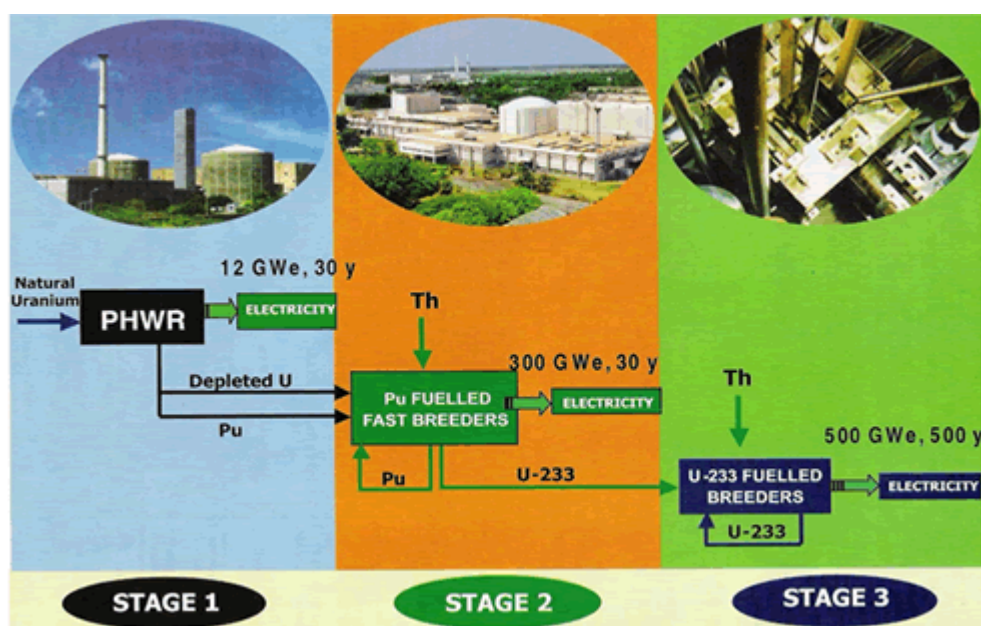


*Figure 1.4 India's three-stage nuclear power programme*

Presently, the energy requirements of our country are fulfilled with a mixed source of renewables and non-renewables with the nuclear energy contributing nearly to 1.9% as of 2019 statistics (*Government of India Ministry of Power*)

A typical nuclear reactor is shown in Figure 1.5. The key components of a typical nuclear reactor are:

- **Reactor core:** The core of the reactor contains the nuclear fuel and generates all of the heat from the fission reactions. The core comprises of fissile fuel as pellets within the fuel pins, which are then arranged in sub-assemblies in various orientations.
- **The moderator** is the material which is used to slow down the high energy neutrons emitted during fission reactions.
- **The coolant** is the material that passes through the core, transferring the heat from the fuel to a turbine. It could be water, heavy-water, liquid sodium, helium etc. depending on the type of reactor.
- **The turbine** converts the heat from the coolant to electricity, just like in a fossil-fuel plant.
- **The containment** is the structure that separates the reactor from the environment. These are usually dome-shaped, made of high-density, steel-reinforced concrete.

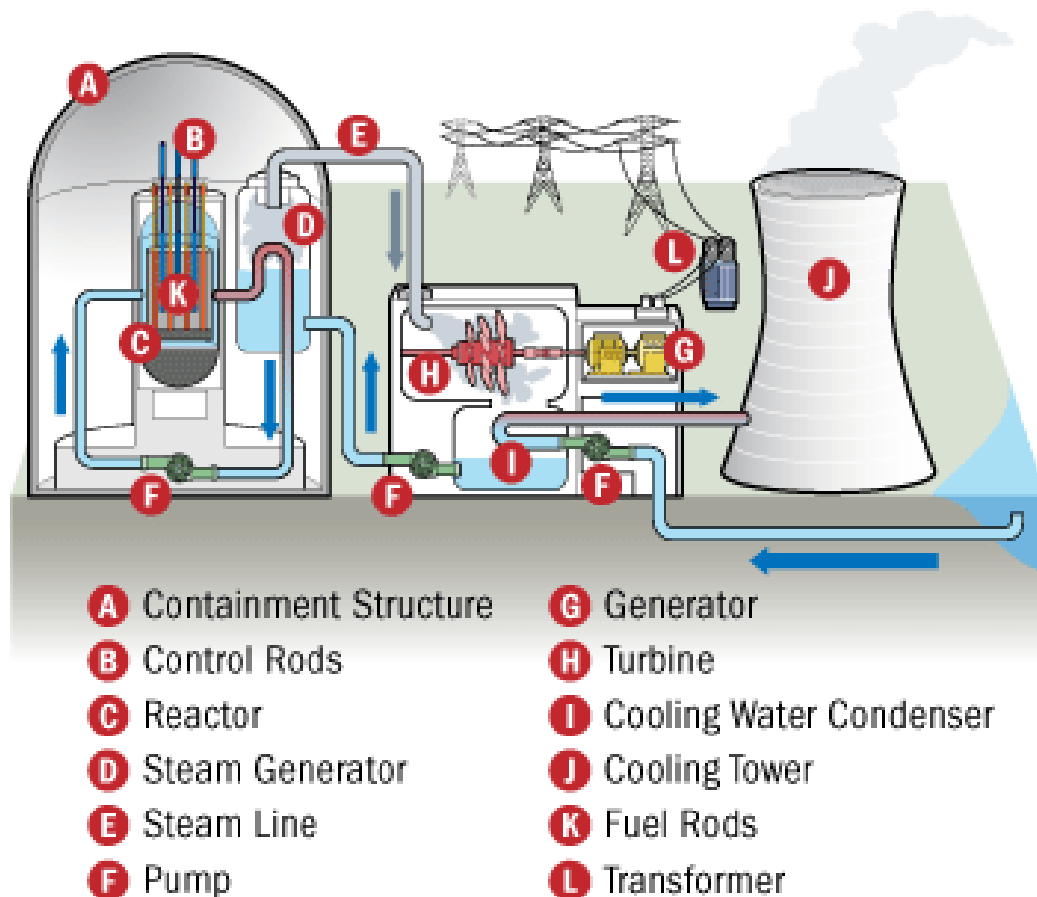


**Figure 1.5** A typical nuclear power plant

There are various types of nuclear reactors depending on the moderator, coolant and number of coolant loops in the nuclear power plant. The nuclear reactor produces energy by the fission reactions. The fission products are the by-products of these reactions and they accumulate in the reactor core during the operation in various chemical states. During normal operation, these reactions are controlled by various mechanisms like insertion of control rods etc. and the desired amount of energy is extracted. In contrast to this, in the event of sudden reactor shut down due to any natural calamity or due to any other reason, the heat production continues due to decay of fission products and this may lead to undesirable consequences as was seen in three past accidents in the history of nuclear power plants (Kessler *et al.* (2014)).

The assessment of reactor safety under such postulated scenarios is dependent on the reactor type. Under these postulated scenarios, there are various sources of energy (Knief (1981)) which are present in the reactor:

- a) The energy stored in the structural material depends on the time of operation and the fuel cycle.
- b) The decay heat of the reactor reduces to 7% of the original power just at the time of shutdown, which keeps on reducing with time. This is a huge source of energy under shutdown scenarios when there is no external source of heat removal.
- c) The inventory of the fission products is directly proportional to thermal power of reactor.
- d) The inventory of long-lived radionuclides is directly proportional to its burnup.
- e) The interactions of fuel with the structural material, moderator and the clad can produce significant heat. For example, zirconium cladding in the nuclear fuel causes production of hydrogen in the case of water-cooled reactors.
- f) Additional sources of energy and fission products can be positive feedback of reactivity.

Other uncertainties include the propagation of the accident sequence. Owing to these reasons, the analysis of each reactor is different.

If due to any unforeseen situation, safety systems are not available, then the reactor may operate in accidental conditions. This may pose threat to the safety of environment. Such scenarios need to be addressed to ensure the safety of environment and prevent any possibility of radioactivity release. Such incidents have happened in the past.

## 1.2. Past Severe Nuclear Accidents and their Impact

The three major misfortunes namely The Three Mile Island (TMI) (1979), The Chernobyl (1986) and recent Fukushima (2011) have exposed safety breaches in the installed and successful implementation in safety of future nuclear reactors (Kessler *et al.* (2014)).

In TMI accident, containment was full of fission products but only a limited amount of radioactive iodine escaped to the environment along with some noble gases. It has been estimated that about 0.9% inventory of noble gases and about 0.00003 percent of the radioiodine of the total core inventory were released to the environment at the TMI-2 site (Rogovin (1979)). The food products analysis showed negligible amount of radioiodine and other fission products.

Another major severe accident happened in Chernobyl on 26 April 1986. The reactor building got damaged and reactor core melted during the accident. The release of radioactivity continued for more than a week. The damaged core got oxidized and large release of radionuclides was observed. It was estimated that about 50% of the iodine and cesium inventory released into the atmosphere. The denser material was found closer to the reactor site while the lighter materials were carried by wind to some areas of Europe. To extinguish the blaze from the reactor building; sand, clay and dolomite was dropped from helicopters from the second day to the tenth day of the accident. This accident caused exposure of the rescue team to high radiation dosage and certain casualties were also reported. In addition, the inhabitants of the nearby cities were evacuated. The site cleaning took years and people are still afraid to move to nearby place. The exclusion zone is still contaminated and abandoned.

The recent Fukushima accident that took place on March 11, 2011 has shaken public confidence in the safety of nuclear reactors. Earthquake hitting Japanese northeast coast resulted in loss of onsite power at operating nuclear power plants. These triggered emergency

generators to function to help remove residual heat in reactors to cool the core. However, tsunami hitting the coast flooded the generator. This affected in removing the decay heat resulting in core heating, large amount of hydrogen were produced due to metal-water reaction at high temperature. Degradation of core and subsequent pressurization in the containment followed. When the concentration of hydrogen reached the threshold level, auto ignition of hydrogen occurred resulting in damage of confinement building and release of radioactive aerosols mainly iodine-131, cesium-124 and cesium-137. People living within 3, 10 and 30 km radius zone were evacuated with fear of exposure to radioactive dosage. Despite all the emergency measures taken promptly nearby environment has been contaminated by an appreciable dosage of radioactivity. Post Fukushima event analysis reported high concentrations of iodine in the soil and water samples nearly 4000 times the permissible limits (Sehgal (2012)). The associated effects of groundwater contamination and food product are relatively less as compared to Chernobyl. The nearby population did not report any health damage due to the radiation. However, it is still beyond permissible limit and work is ongoing to clean the site (Steinhauser *et al.* (2014)). Such accidents cause a huge financial burden on the economy because accidental site needs to be decontaminated for re-habitation.

Hence, to sum up the sequence of events, failure to remove the decay heat may lead to overheating of fuel enclosed in clad resulting in clad damage thus exposing the fission products to coolant. Prolongation of this scenario may build-up pressure within the containment which if ruptures exposes radioactivity to environment. Such beyond design basis events need to be assessed and new safety measures need to be implemented to manage severe accidents. Safe shut down of reactor, removal of decay heat, depressurization and confinement of radioactive materials are the important measures for managing severe accidents in nuclear reactors.

### 1.3. Issue of radioactivity release

Five major analytical programmes have been conducted since the late 1970s (Sehgal (2012)):

SASCHA in Germany

HI/VI in the United States

CRL in Canada

VEGA in Japan

HEVA/VERCORS in France

- 1) SASHA series (the first analytical experiment of its kind) provided preliminary estimates for iodine and cesium releases in irradiated fuel up to 2000 °C.
- 2) ORNL conducted the HI/VI programme between 1981 and 1993 (13 tests in total). This programme provided highly representative results on the release of fission products, especially for long-lived FPs (mainly  $^{85}\text{Kr}$ ,  $^{106}\text{Ru}$ ,  $^{125}\text{Sb}$ ,  $^{134}\text{Cs}$ ,  $^{137}\text{Cs}$ ,  $^{144}\text{Ce}$  and  $^{154}\text{Eu}$ ). These tests were qualitative as the samples were not re-irradiated prior to the tests.
- 3) AECL's CRL programme was another analytical programme conducted to study CANDU fuels. It consisted of many tests on fragments of irradiated fuel varying from 100 mg to 1 g and on short sections of clad fuel up to 2100 °C. One of its important contributions is the release of ruthenium into the air.
- 4) VEGA was performed by JAERI (Japan). A total of 10 tests were carried out: eight on  $\text{UO}_2$  fuel and two on MOX fuel. Some of the tests were carried out in a steam atmosphere up to fuel melting temperatures. The irradiation time of fuel

was shorter than the in-reactor irradiation time. This series included tests at a pressure of 10 bar which notably demonstrated a reduction in cesium releases.

- 5) HEVA/VERCORS in France aimed at quantifying releases of FPs and actinides, their kinetics and total release rates from irradiated nuclear fuel under conditions representative of a core melt accident. Twenty-five tests were carried out between 1983 and 2002 in three phases.

Another important series in this reference is the VERDON. This aimed to address very-high-burnup  $\text{UO}_2$  fuels (70 GWd/t and beyond), MOX fuels, and accidents with in-vessel ingress of air or in-vessel fuel reflooding.

In addition to several analytical experiments (listed above) integral tests were conducted for simulating behaviour in a nuclear reactor during severe accident. The notable amongst this is the Phebus FP programme. The Phebus FP programme (integral test series) aimed at simulating a large-break loss-of-coolant accident with a rupture located in the cold leg of the primary circuit. The test results clearly revealed a link between the kinetics of fission product release and the progression of fuel degradation. Other important conclusions drawn from Phebus experiments are (Lemire and Dickson (2003)):

- The iodine released from the overheated fuel is in both gaseous and particulate form. CsI is one of the particulate form. With Silver-indium-cadmium rods cadmium iodide is also a probable form. Silver rods react with iodine to form insoluble AgI and hence limit the concentration of iodine available for release. When the control rod is of boron carbide, the release of gaseous iodine is even greater.
- Cesium is released from the overheated fuel in the form of Cesium Molybdate vapour which condenses in RCS during its transport. This re-vaporizes to some extent in the presence of high temperature steam as  $\text{CsOH}$  and goes to the containment.

- The concentration of volatile iodine in the containment vessel depends mainly on physio-chemical reactions in the gaseous phase. This in turn depends on the concentration of volatile iodine coming from the primary circuit which itself depends on the affinity of the iodine for the surfaces of the vessel (paint, material, etc.).
- There was a major difference in the release behaviour of Barium (from analytical experiments) due to the possible interactions with the cladding and possibly iron, which reduced its volatility and hence release.

Hence, the release of fission products to the containment occurs in phases and is closely related to the degree of fuel melting, reactor pressure vessel integrity and interaction of melt with concrete below the reactor cavity by MCCI. The radionuclide release occurs in several phases, for example,

- a) coolant Activity Release
- b) gap Activity Release
- c) early In-Vessel Release
- d) ex-Vessel Release
- e) late In-Vessel Release, etc.

On the basis of similarity in chemical behavior, radionuclides are divided into 8 groups as reported in U.S. Nuclear Regulatory Commission (WASH-1400 (1975)), and given in Table 1.1.

**Table 1.1. Classification of fission products**

1. Noble gases:	Xe, Kr
2. Halogens:	I, Br
3. Alkali metals:	Cs, Rb
4. Tellurium group:	Te, Sb, Se
5. Barium, Strontium:	Ba, Sr
6. Noble metals :	Ru, Rh, Pd, Mo, Tc, Co
7. Lanthanides:	La, Zr, Nd, Eu, Nb, Pm, Pr, Sm, Y, Cm, Am
8. Cerium group:	Ce, Pu, Np

An earlier study reported on BWRs, relates the correspondence of these fission products with the phases of radio-nuclide release (U.S. Nuclear Regulatory Commission WASH-1400 (1975)). The summary of the same is given in Table 1.2 along with the fractional release to the containment. Further, the chemical compositions of existence in the containment atmosphere for each fission product are given in (Table 1.3).

**Table 1.2 Release fraction to the containment**

	<b>Gap Release (after 0.5 hrs)</b>	<b>Early In-Vessel (after 1.5 hrs)</b>	<b>Ex-Vessel (after 3 hrs)</b>	<b>Late In-Vessel (after 10 hrs)</b>
<b>Noble Gases</b>	0.05	0.95	0	0
<b>Halogens</b>	0.05	0.25	0.3	0.01
<b>Alkali Metals</b>	0.05	0.2	0.35	0.01
<b>Tellurium group</b>	0	0.05	0.25	0.005
<b>Barium, Strontium</b>	0	0.02	0.1	0
<b>Noble Metals</b>	0	0.0025	0.0025	0
<b>Cerium group</b>	0	0.0005	0.005	0
<b>Lanthanides</b>	0	0.0002	0.005	0

As shown in Table 1.2, noble gases (Kr, Xe), volatile fission products (Cs, I) and relatively less volatile fission products (Sr, Sb, Te, Ba, Ru, Zr) in form of aerosols, form the radioactive inventory inside the containment.

Table 1.3 Chemical Composition and forms of existence

Element	Chemical State during normal operation	Released as aerosol
Xe, Kr	No chemical reactions, gaseous form	-
I, Br	Single phase halide solution CsI, I <sub>2</sub>	>80%
Cs, Rb	Will form compounds with most other elements in the fuel. Alkali metal halides, compounds with uranates and Cs <sub>2</sub> MoO <sub>4</sub>	>80%
Te, Se	Mainly elemental form. Other possible forms are single phase chalcogenide solution (Cs <sub>2</sub> Te) and products from reactions with Zircaloy	20-90% (influenced by reactions with Zircaloy and by oxidation potential in the melt)
Ba, Sr	Oxides which can dissolve to some extent in the fuel and form separate phases BaO, Ba <sub>2</sub> (Zr-U-Pu)O <sub>3</sub>	2-40 % (influenced by reactions with Zircaloy and by oxidation potential in the melt)
Mo, Tc, Ru, Rh, Pd	Single phase metallic alloy	<5% (influenced by reactions with Zircaloy and by oxidation potential in the melt)
La, Y, Zr, Nb, Lanthanides	Oxides which dissolve in fuel	-

Iodine in reactor can be present in a number of chemical forms including the familiar iodide ion, the volatile I<sub>2</sub> form and the highly oxidized iodate ion form. The interconversion among these forms of iodine is relatively slow under normal operating conditions. A radiation field or high pH of the containment present in the containment can greatly accelerate the formation of various chemical forms of iodine in water. The observations from the various integral tests conducted in PHEBUS series showed that for a reactor equipped with silver alloy control rods, the primary circuit of the reactor is the main source of volatile iodine in the vessel. When the control rod is of boron carbide, the release of gaseous iodine increases. During its transport from the RCS, 20-30% of iodine settles due to thermophoresis. The effect of boron carbide can highly effect the iodine speciation within RCS. Apart from CsI, other probable vapour compositions present are AgI, RbI, CdI<sub>2</sub> and InI<sub>x</sub>. It was also observed that a high fraction of iodine is present at the beginning of each PHEBUS experiment that could have been released from RCS at temperature as low as 150 °C. The major takeaway from the literature is the speciation and release behaviour of iodine is highly sensitive to the conditions in the containment (Clement *et al.* (2007)).

The surfaces in the reactor containment may be painted or simple steel. Clean steel surfaces are not good iodine absorbers. However, studies have shown that zinc present in the coated surfaces of containment effectively absorbs iodine at pH ~ 9-10. This is believed to occur through formation of some metallic complexes or divalent compounds. These divalent compounds are stable in nature when pH of the solution is in the range of 9-10. However, at lower or higher pH these may further dissociate to release iodine in organic form to the containment atmosphere. Another metal which has great affinity for iodine is silver. This was shown in various experiments conducted in LOFT FPT-2, PHEBUS FPT0 and FPT1 series in which silver-indium-cadmium control rod materials were released into the containment model

of the test facility. Iodine present in the containment atmosphere precipitates in the form of insoluble silver iodide (AgI). (NEA/CSNI/R(2000)9 (2000))

These fission products can interact directly with the human beings (inhalation) or can enter the food chain through various other mechanisms. For example: The effluents from the nuclear power plants contaminate the ground water. This ground water when consumed for irrigation by human beings enters the food chain. Another possible mechanism is the direct consumption of the contaminated aquatic life by human beings. Some radionuclides are short-lived (I-131 half life is 8 days) while others have high long life (Cs-137 half life is 30 years).

Of the fission products listed in Table 1.1, volatile products are the primary concern. Iodine 131 isotope has a half-life of 8 days (other isotopes of iodine being short-lived for few hours only), poses a health hazard if present in high concentrations due to easy and almost irreversible transport to the human thyroid gland, where it can locally induce malicious cell growth leading to cancer. Iodine has been a long-standing concern in safety analysis because of its radiological hazards combined with its chemical and physical properties particularly its volatility. Iodine is mainly released in the combination of ionic, volatile and organic form (CsI (95%), HI, I<sub>2</sub>, CH<sub>3</sub>I (5%)). The release of iodine in organic and elemental form can be controlled by maintaining the pH of the containment more than 7. Apart from Iodine, Cs-137 is another fission product which needs mitigation. The main problem with cesium-137, which is present in the form of salts, is its high water solubility. Cesium-137 ions are readily distributed in the body, and especially in the muscle tissues. The biological half-life is 110 days.

Based on long-term land contamination and Thyroid dose to public, Cs-137 and I-131 are the most important radioactive fission products which needs high decontamination. Therefore, it is prudent to seek for engineered safety systems to prevent the release of these

products into the environment to mitigate further consequences. Soffer *et al.* (1995) compared the composition of fission products in PWR and BWR and it was found that the inventory of radionuclides predicted during severe accident constituted same products with variation in their composition. This variation in the composition decides their strategy of retention using Filtered Containment Venting System (FCVS).

#### 1.4. Filtered Containment Venting System (FCVS)

Filtered Containment Venting System (FCVS) is one such system aiming at controlled filtered venting of nuclear reactors hence arresting the radionuclides and helping in depressurization of the containment under extreme events.

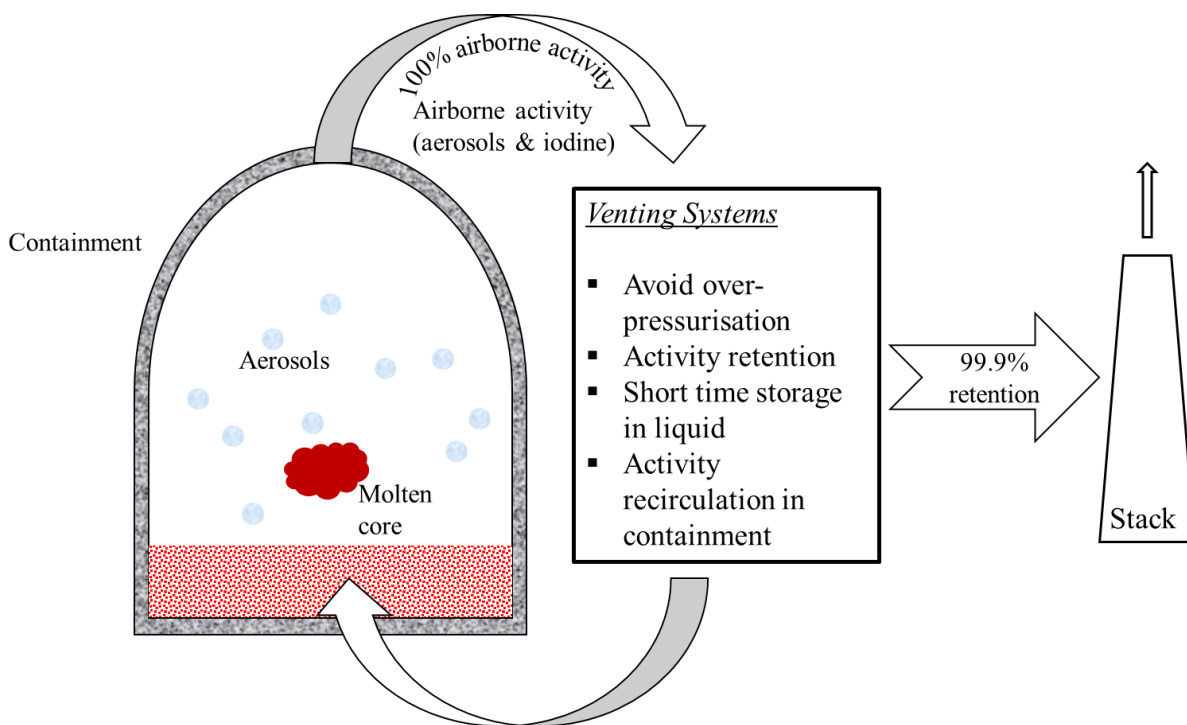


**Figure 1.6 Overview of Filtered Containment Venting**

The typical boundary conditions given by German Reactor Safety Commission (Jacquemain, D. (2014)) for BWR and PWR are summarised below:

**Table 1.4 Thermal-hydraulic initial and boundary conditions at the beginning of the venting**

	PWR	BWR
Operating pressure	< Testing pressure of containment	
Start of venting	2 to 3 days (according to the decay heat when reaching the testing pressure)	>4 hrs (according to the decay heat when reaching the testing pressure)
Mass flow rate	According to decay heat by taking into account potential heat sinks and water injection in case of venting	According to decay heat after the consumption of heat capacity of the wet well

**Table 1.5 Load on the filter system by the fission product (Related to core inventory)**

	PWR	BWR
Elementary Iodine	0.001	$4 \times 10^{-4}$
Organic Iodine	$10^{-3}$	$2 \times 10^{-4}$
CsI, CsOH	$2 \times 10^{-4}$	$3 \times 10^{-2}$
Aerosol mass	40 kg	20 kg
Decay heat		
Aerosols	2 kW	180 kW
Gaseous Iodine	5 kW	7 kW

An overview of FCVS process is shown in Figure 1.6. The airborne activity flows to the venting system in the event of pressurization of the containment. The venting system is intended to depressurize it passively and retain the airborne activity thus passing filtered gas to the stack. The existing filtration technologies currently implemented in Nuclear power plants are broadly categorized into (Jacquemain *et al.* (2014), Yang *et al.* (2018)):

[1]. **Dry Scrubbers:** This technique employs bed filters like dry filter method (German PWR) or sand bed filters (used in French PWR). The limitations and associated problems with such scrubbers are:

- Useful for Small sized Nuclear Power Plants
- Suitable for venting of smaller containment volumes and venting during normal operation
- Cannot be used to handle large steam and radioactive load during severe accident
- Filter clogging and the reduced filter efficiency in wet conditions.

[2]. **Wet Scrubbers:** Filtration in such systems is ensured by a liquid pool scrubber and is usually coupled with a droplet separator or deep-bed fine aerosols filters as second stage to improve efficiency. These type of scrubbers are capable of managing severe accidents and can be designed for any reactor type. The available commercial designs are:

- a. FILTRA-MVSS installed in Swedish Nuclear Power plants
- b. CCI-FCVS designed by Westinghouse and installed in Swiss Power plants.
- c. High speed sliding pressure venturi (HSSPV) designed by AREVA

The design of FCVS is chosen based on the inventory of fission products and the reactor type. It is also strategic and proprietary in nature. Based on the advantages offered by the wet scrubbers, it is wise to choose one of its designs for managing severe accidents.

The FCVS design considered in the present study comprises of a venturi manifold and a metallic fibre filter to ensure the removal of radioactive fission products in the form of aerosols, vapours or gases released through the containment vent line. The filtered venting line (Figure 1.7) is attached to the containment boundary via rupture disk and an isolation valve that can be activated manually at design pressure or passively. Iodine and cesium products emitted during fission are arrested in the scrubber tank by wet scrubbing of venturi manifold.

Since elemental iodine is poorly soluble in water caustic soda is added to maintain alkalinity of scrubber tank at pH~10-12 to enhance its absorption. The absorption of iodine in caustic soda is instantaneous.

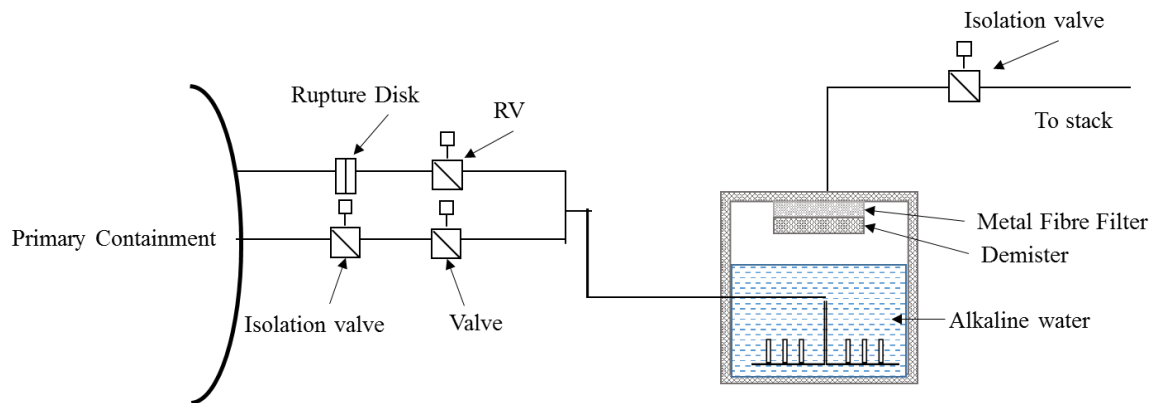


**Figure 1.7** Line diagram of FCVS

The FCVS chiefly comprises of a scrubber tank accommodating circumferentially distributed venturi manifold and a metallic fibre filter. The steam load expected from the containment decides the water inventory in the tank. The venturi scrubber (Figure 1.8) is a major component of FCVS. It mainly comprises of three segments: converging section which accelerates the gas and particulate aerosols, throat section wherein liquid droplets and aerosols drifting with gas interact and diffuser section which accounts for the pressure recovery and decrease in gas velocities. During operation in a nuclear reactor, the venturi inlet velocity may decrease with time depending on the upstream pressure. Consequently, the liquid entrainment rate from the nozzles which is governed by difference of hydrostatic head and pressure of flowing gas increases.

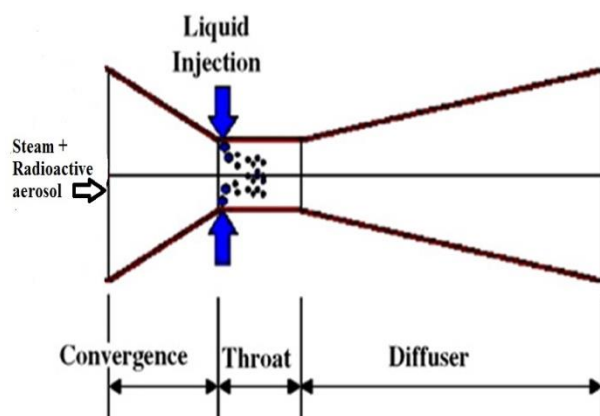


**Figure 1.8 Geometry of venturi scrubber**

The pressure difference between the nozzle inlet and the scrubber tank draws in water from the scrubber tank initiating the self-priming action. The relative velocity of the gas stream and the water causes entrainment of the liquid, the interaction of the two forms droplets thus increasing the surface area of contact between the two. The drops act as inertial collectors for particulates in the gas stream.

The working of venturi scrubber is hence highly dependent on the interaction of three phases comprising of aerosols, vapours (coming from the containment), liquid droplets (from the scrubbing liquid) and continuous gas stream. The entrainment of liquid into droplets due to the gaseous cross-flow, spatial characterization of droplets and interaction with radionuclides in the gaseous stream collectively makes it a highly complex physical process. The challenges in designing of venturi scrubber are primarily due to the complex behavior of multi-phase flow.

## 1.5. Literature Review

For the nuclear reactor application and retention of radionuclides in the postulated severe accident scenarios, the upstream conditions of flow vary during operation. In such a system for an advanced Indian reactor, FCVS comprises of a manifold of venturi scrubbers submerged in an alkaline pool. The flow from the containment will swell the pool according to the upstream pressure and flow. Hence, the liquid loading to the scrubber is controlled by the

whole dynamics happening in the system. This poses a complex scenario to decode, so we began with looking in the literature on venturi scrubber operation in such a scenario.

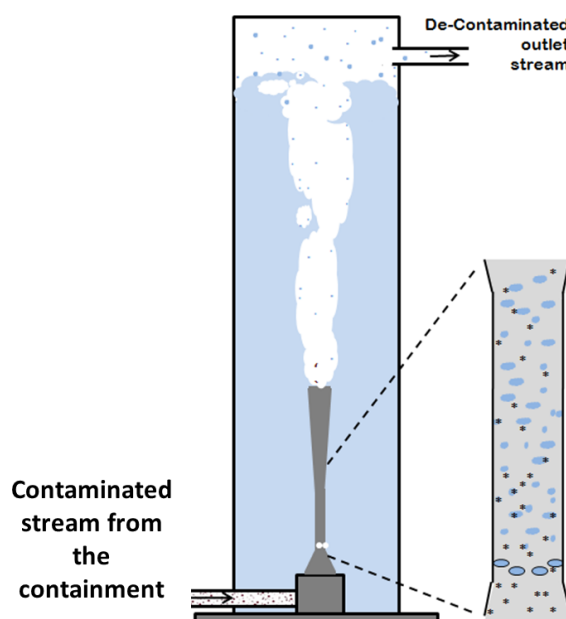


**Figure 1.9 Schematic of a venturi scrubber installed in a FCVS.**

### 1.6. Studies on submerged operation

For the first time, Lindau (1988) discussed the applicability of such a wet scrubbing unit for both PWRs and BWRs in Swedish Nuclear Power Plants. There are very limited studies on the scrubbing behavior of venturi scrubber in submerged operation.

Ali *et al.* (2013) measured the liquid flow rate entrained in the scrubber in submerged mode of operation. The operating height was 0.30 and 0.60 m with throat gas velocities ranging from 130 to 200 m/s. The experimental data showed that the increase in iodine removal efficiency was 12% for 240 m<sup>3</sup>/hr of gas flow rate as compared to marginal increase of 4% at 340 m<sup>3</sup>/hr gas flow rate. This implies that the submergence does not enhance the removal efficiency at high airflow rates (after a certain flow rate). However, they did not report the pressure drop characteristics of the venturi scrubber. Iodine removal efficiency in a submerged venturi scrubber at different gas flow rates was also measured and the efficiency was observed

to increase with high inlet concentration of iodine and liquid flow rate with negligible effect of gas flow rate.

Gulhane *et al.* (2015) studied the effect of pH on the solubility of iodine in self-priming venturi scrubber. The experimental results showed that the iodine solubility was sensitive to pH and maximum removal rate was obtained at pH=10.

### 1.6.1. Studies on self-priming operation

There are some studies on the hydrodynamic behavior and the scrubbing characteristics in the venturi scrubber in the submerged operation, which provide an overview on the working of venturi scrubber qualitatively. However, to gain a better understanding, on the flow physics in the venturi scrubber other modes of operation of venturi scrubber are reviewed. To simulate this behavior, there are some experimental studies on self-priming operation (Figure 1.10) in which liquid loading at the nozzles is governed by the hydrostatic head maintained in an overhead reservoir.

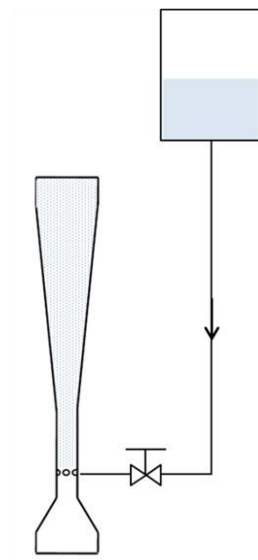


**Figure 1.10 Schematic of a self-priming venturi scrubber**

Lehner (1998) studied the venturi scrubber operating behavior with an external tank for providing the hydrostatic head. The hydrostatic head was varied from 1-2 m at the throat gas

velocity of 30-75 m/s. The disintegration of jet was observed visually at various gas flow rates. At high gas velocity, only 40% of the throat is covered with water droplets forcing more of the water to flow by side of wall. Also, the scrubbing efficiency of titanium dioxide particles was measured. The efficiency was observed to increase more with liquid flow rate, the reason being more interaction with water droplets and enhanced throat coverage.

Horiguchi *et al.* (2014) observed the entrainment behavior in such a venturi scrubber and found that at high gas velocity there is no suction of liquid in the venturi scrubber. It was also observed that with increasing gas velocity, the liquid flow suctioned through the nozzles at the throat first increases and then decreases to almost zero.

Nakao *et al.* (2016) studied the two phase flow characteristics in the venturi scrubber. The quantification of the liquid film formed in the venturi scrubber was done at varying throat gas velocities from 25-292 m/s. It was found that the amount of liquid suctioned and the liquid film present in the venturi scrubber both decreased with the increase in gas velocity.

Zhou *et al.* (2016) measured the iodide vapour absorption efficiency in a self-priming ejector type venturi scrubber under different conditions of gas and liquid flow. It was found that the absorption efficiency increased rapidly with increasing aqueous solution flow rate, while the absorption efficiency stabilises at 99% stably at excessively high flow of aqueous solution.

### 1.6.2. Non-Submerged operation or Forced Feed Operation

Venturi scrubbers are applied in various chemical and process industries to remove effluent from industries in forced feed mode (Figure 1.11). Difference between the forced feed and the submerged venturi scrubber is that the forced feed scrubbers are operated at the desired flow conditions by pumping the scrubbing liquid externally to the venturi at the throat section. So, in order to gain insight on the basic governing physics and working of venturi scrubber a literature review in this aspect is done.

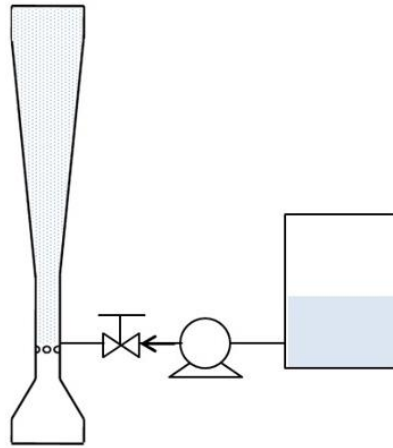


**Figure 1.11 Schematic of a forced feed venturi scrubber**

The earliest model to predict pressure drop and performance of venturi scrubber was suggested by Calvert (1970). The underlying assumptions for pressure drop modeling were one dimensional flow, uniform size and distribution of droplets; droplets attain gas velocity at the throat end and complete atomization at the entrance. The model neglected wall friction and acceleration of gas in the throat. Though simple to use the model did not account for any geometrical design. The performance was analyzed using experimental correlation of Walton and Woolcock (1960) derived for single drop target efficiency.

Boll (1973) developed a mathematical model to the predict pressure drop, particle scrubbing efficiency and Sauter mean diameter based on experimental findings. The pressure drop model included momentum exchange from gas stream to entrained droplets. The visual observations revealed liquid film flowing along the walls. The model was validated against three different geometries. The failure of accurate prediction of pressure drop can be attributed to consideration of single drop size.

Several other authors (Hesketh (1973) and Leith *et al.* (1985)) gave the pressure drop model based on their experimental findings.

A thorough theoretical and experimental analysis of pressure drop was done by Azzopardi and Govan (1984) characterizing two-phase flow in venturi, illustrating various components of pressure drop mainly quantifying entrainment of drop and their dispersion. The model accounted for existence of various sizes droplets and their deposition on the wall. The 1-D model proposed from experimental findings over-predicted pressure recovery in the diffuser section.

Annular flow model was proposed by Viswanathan *et al.* (1985). The model suggested using Lockhart Martinelli factor for two phase frictional pressure drop and incorporating droplet trajectory from the experimental observations.

Allen and Van Santen (1996) performed experimental studies in a test facility and found that single phase flow pressure drop estimation is one of the important design criteria for short throat scrubbers. The droplets were found accelerating in the diffuser section also.

Hills (1995) formulated the basic equations of mass transfer relevant to the infinitely rapid reactions encountered in the venturi scrubber. They further compared the model with the given literature data for sulphur dioxide and carbon dioxide gas in alkaline solution absorption.

Pressure drop in 0.12 m throat diameter was measured by Silva *et al.* (2009a). The gas flow rate was varied from 0.483-0.987 kg/s while liquid flow rate was varied from 0.013-0.075 kg/s. The liquid injection was carried out using both film mode and through holes in the throat. The overall pressure drop was observed to be a function of throat velocity. The pressure drop observed was more for film injection at high liquid flow rate. This is attributed to the location of injection upstream the throat where more liquid is accelerating inducing more pressure drop. They also measured drop sizes in the set-up (Silva *et al.* (2009b)) and suggested two competing mechanisms for droplet formation based on measurements: turbulent break up and coalescence, the coalescence being dominant for high gas velocity and liquid loading.

Pak and Chang (2006) numerically predicted pressure drop and scrubbing efficiency of Haller *et al.* (1989) geometry using an Eulerian frame for gas phase and Lagrangian frame for aerosol and droplets. The model assumed continuous injection of nozzle diameter droplets as water stream which is deformed under the action of high speed transverse air stream. The secondary break up is simulated by Wave break up model. The results were in agreement with experimental data for pressure drop in the converging section and throat but under-predicted pressure recovery in the diverging section.

Similar numerical studies on the same geometry were conducted by Goniva *et al.* (2009) using Open FOAM. The results for simulated pressure drop were in good agreement with experimental data but the predicted scrubbing efficiency was not satisfying for higher gas flow rates. The algorithm employed Eulerian-Lagrangian approach to solve the flow dynamics along with TAB breakup model.

Ali *et al.* (2013) simulated venturi scrubber performance using Ansys CFX and validated the methodology with their experimental results. Their simulations results concurred well with experimental values at low gas velocities but gave qualitative trend for efficiency calculation at high gas velocities. The maximum efficiency of 99.5% was achieved at 200 m/s throat velocity.

Sharifi and Mohebbi (2014) conducted numerical studies to calculate pressure drop using Eulerian-Eulerian two fluid model and MUSIG model for droplet distribution and validated the model with Vishwanathan *et al.* (1998) results. They further investigated effect of nozzle diameter and nozzle arrangement on the pressure drop. Their results revealed that the pressure drop is unaffected by variation of nozzle diameter and their arrangements within the venturi for identical operating conditions.

The drop size and their distribution is one of the key parameters in designing venturi scrubber. The reports on this front are limited and statistical. The most widely used correlations in venturi scrubber are Rossin-Rammler, Nukiyama and Tanasawa (1938) and Boll (1973). The recent studies by Alonso *et al.* (2001), Costa *et al.* (2004), Silva *et al.* (2009b) by Laser diffraction technique have concluded that atomization in venturi occurs at various points and droplet dynamics is governed by turbulent diffusion. The droplet statistics showed multiple peaks at low liquid flow rates meaning that drops are more poly disperse at low liquid flow rates. The droplet size was also observed to vary downstream the diverging section. So, a single correlation might not be adequate as design input. The drop size decreases with increasing gas flow rate.

Similar study on drop size distribution was done by Viswanathan *et al.* (2005) using PDPA for recording the droplet data. One of the important findings in this study was droplet diameter which was observed to follow mass mean diameter for throat velocity greater than 75 m/s.

Liquid flux distribution was experimentally studied by Vishwanathan *et al.* (1984) in a Pease-Anthony scrubber. The film flow rate was measured by using porous sintered metal plates located at different locations along the venturi length. The key findings were optimum distribution of liquid in venturi occurred at medieval range of liquid loading ratio of 7-9 l/m<sup>3</sup>. In the range of low liquid flow rates, the flow is more at the walls while for high flow rates the entrained liquid escaped the domain without interaction. An increase in gas velocity at a fixed volumetric liquid flow did not affect liquid flux distribution.

Modeling of droplet dispersion was simulated by Ahmadvand and Talaie (2010) in a two dimensional axisymmetric geometry using single injection nozzle. The Eulerian two-phase model uses k- $\epsilon$  model to validate experimental results in a cylindrical venturi scrubber. The

analysis focussed on importance of distribution of droplets due to turbulent flow conditions. The droplet size was found to decrease on increasing droplet eddy diffusivity.

Numerical studies by Guerra *et al.* (2012) implemented Eulerian-Eulerian technique for identifying the distribution of liquid in the throat section at varying gas velocities and liquid flow rates concluding that jet penetration is a function of number of nozzles and their arrangement at a constant liquid flow rate. They also carried out image analysis for different throat velocities and jet velocities to measure jet spreading angle. The jet spreading angle was observed to be a strong function of jet velocity and was found proportional to the ratio of Reynolds number to Weber number.

Gonçalves *et al.* (2003) proposed a one dimensional mathematical model for atomization, trajectory and dispersion of transverse jet exposed to a subsonic air stream. The model assumes disintegration of jet in venturi after a certain distance. The trajectory is calculated by force balance. The model constants are estimated using experimental results. The jet was observed to have different atomization points and the loss in mass due to formation of drops was along the trajectory. Gonçalves *et al.* (2004) proposed a mathematical model for droplet dispersion incorporating the source term due to different sized droplets in each computational volume. The injected liquid breaks into parcels following drag force.

Ananthanarayanan and Viswanathan (1999) investigated the effect of nozzle arrangement numerically demonstrating single line, symmetric, triangular and three row arrangements. The study reveals that better distribution of liquid in the throat could be attained by a wise configuration of multiple nozzles, however liquid flux remains constant. The non-uniformity in flux was observed if the nozzle to nozzle distance exceeds 10% of its width. The authors proposed a dimensionless number venturi number to predict optimal liquid flux distribution for maximum scrubbing performance.

Mayinger and Neumann (1978) studied atomization of paraffin wax particles in a rectangular venturi scrubber at superficial gas velocities of 40-115 m/s. The images show formation of parachute like sheets and then atomization into droplets.

Economopoulou and Harrison (2007a) and Economopoulou and Harrison (2007b) developed graphical tools from experimental data of Calvert and Yung to determine scrubbing efficiency and droplet dispersion. Nomographs were developed to theoretically evaluate a new venturi design. An algorithm was suggested to evaluate the parameters and create the nomographs for the desired operating conditions if they are not in the suggested range.

Goel and Hollands (1977) modified single drop target efficiency correlation derived from Walton and Woolcock (1960) experimental data to account for change in relative velocity in diffuser. The author also suggested charts to illustrate dependence of various factors on scrubbing efficiency. However, the validation showed discrepancy due to the initial drop prediction from Nukiyama and Tanasawa (1938) correlation and Schiller and Naumann (1935) spherical drag coefficient.

Rudnick *et al.* (1986) measured pressure drop and grade efficiency for 23 size intervals Wesson oil particles. The data was further compared with Calvert (1970), Yung *et al.* (1977) and Boll (1973) model. It was found that Yung *et al.* (1977)'s model predicted comparatively well. All the models were found to have less error when large diameter throat was calculated. Also the models did not take into account the type of injection of the scrubbing liquid.

The performance of venturi scrubber is, therefore, a function of various operating parameters such as drop size, volumetric liquid flow rate, throat velocity and pressure drop across the scrubber. To analyse this multidimensional problem and optimize the input parameters, various authors have performed studies using other mathematical tools.

Ravi *et al.* (2002) optimized the design of venturi scrubber using genetic algorithm. The objective function was fixed to maximize efficiency and minimise pressure drop while inputs given were throat velocity, liquid-gas loading ratio and throat width to diameter ratio. The optimum values of the above parameters were found to be 40-100 m/s, 1 l/m<sup>3</sup> and 2.5 aspect ratio respectively. The uniformity in distribution of liquid flux was found to be desired outcome in design, which was dependent on the above variables.

Nasseh *et al.* (2009) predicted pressure drop in venturi scrubber using neural network modeling. The networks were trained from five different sets of experimental values available in the literature.

### 1.7. Major Scientific issues associated with FCVS

The venturi scrubber has been traditionally implemented in chemical and process industries to remove effluent from the venting gas from these plants. The venturi scrubbers used in these industries, operate in forced feed mode and the effluent gas to be treated is having a fixed mass flow rate and a fixed concentration of pollutants. There are a few studies on the scrubbing characteristics of such forced feed scrubbers. However, for nuclear power reactors, the design of venturi scrubbers is not straight forward. This is primarily because the flow conditions in the venturi scrubber vary with time with venting of containment and the radionuclides inventory in the reactor at the time of operation is dependent on the fuel composition, burn-up, operational conditions, etc. Therefore, to design the FCVS catering to such conditions is much more complicated than what is understood for chemical and process industries. Additionally, the proprietary nature of the design leads to the scarcity of the information in literature for the particular application. The venturi scrubber designed for nuclear reactors is different from what is typically used for scrubbing gases in chemical and process industries because of the following reasons:

**Table 1.6 Differences between venturi scrubber for chemical, process industries and nuclear reactor application**

	<b>Chemical and process industries</b>	<b>Nuclear reactor application</b>
Operation	Continuous	Once in lifetime of reactor in the event of severe accident
Inlet flow	Constant	Dependent on pressure difference from the containment and ambient. Initially very high later decreases to almost constant flow (Figure 2.3)
Liquid loading	Constant, forced feed, Independent parameter	Dependent on inlet flow from the containment and the alkaline liquid level in the scrubber tank
Scrubber duty in terms of effluents/ radionuclides loading	Have known loading characteristics (typically constant or in a narrow range)	Release behaviour and amount is highly variable. Dependent on pressure difference between the ambient and containment, temperature, pH condition in the containment, its probable interaction with containment internals in its path and accident progression along with the reactor type.

The radionuclides emitted during containment venting (in either aerosol or vapour form) have residual decay heat. This decay heat increases the temperature of alkaline pool present in

FCVS tank, which in turn affect the properties of fluid mainly their density and viscosity. So, overall this complicates the process and affects the interactions between gas, aerosol, vapour, alkaline liquid in the FCVS. On the other hand, a normal waste effluent gas treated by a forced feed scrubber will not affect the flow properties in the scrubber. Also, a radionuclide isotope has health hazards, which makes its retention in FCVS highly important.

The FCVS configuration considered in the present study consists of a manifold of wet scrubbing unit, i.e. a set of venturi scrubbers submerged in a pool of scrubbing liquid along with a demister and metal fiber assembly at the top. A single venturi would not be sufficient for following reasons:

- For nuclear reactor application, the liquid loading to the scrubber is dependent on the hydrostatic head at the throat nozzles. If a single venturi is designed to handle the peak flow conditions encountered from containment it would need a very long tank to provide for that hydrostatic head.
- A single venturi scrubber would not be able to handle peak flow conditions encountered during scrubbing. For peak flow condition, the scrubber would operate in supersonic regime.
- Additionally, the total iodine inventory from the containment is very high, so the designed scrubber should provide for larger surface area for absorption or large number of droplets.
- A manifold of venturi scrubbers provides enough redundancy, which must be ensured for passive safety systems.

The venturi scrubber has three different geometrical cross-sections. The converging section accelerates the contaminated gas; then it arrives at the throat section having several nozzles and finally the diverging section which allows for recovery of pressure. The throat

section is having nozzles which allow entrainment of scrubbing liquid due to the large radial pressure difference created between the scrubber tank and the fluid at the throat. The entrained liquid encounters high speed gas in the throat section which shears it to droplets and enhances area for interaction of aerosols and vapour from the contaminated gas. Hence, the flow in a venturi scrubber comprises of gas, aerosols, scrubbing liquid, air and vapour. The interaction among these phases determines the efficiency of the venturi scrubber. Other parameters which influence the performance of venturi scrubber are its geometry, operating conditions and size and number of the nozzles. The scarcity of the test data and unavailability of required models to design such systems is a challenge and hence is the motivation of this study. The major scientific issues identified from the literature for the design of an efficient venturi scrubber are enlisted below:

- a) The hydrodynamic behavior of venturi scrubber: This is complex due to the interaction of the different phases present in the venturi scrubber and it plays an important role in deciding the scrubbing behavior and retention of radionuclides.
- b) Lack of test data: This creates major issues in understanding the fundamentals in the scrubbing behavior, especially the influence of operating parameters and geometry of the venturi scrubber on the scrubbing.
- c) Flow phenomena inside the venturi scrubber is multi-dimensional and CFD model needs to be developed to treat the complex flow physics inside the venturi scrubber.
- d) Performance of venturi scrubber for actual reactor applications is not known since it is influenced by large number of operating and geometric parameters. This primarily include the quantification of entrainment of water droplets at the throat section, its transient behavior with the change in inlet gas flow along with its distribution in the scrubber. Further the applicability of droplet size correlations developed to the submerged operation.

Therefore, the objective of the thesis are:

- To design filtered containment venting system for advanced reactors comprising of submerged venturi scrubber and metal fibre filter.
- To understand the jet entrainment behavior and flow physics inside venturi scrubber.
- To understand the scrubbing of iodine vapours as a function of operational parameters.
- To develop a CFD model which will validate the experimental findings.

## 1.8. Outline of the thesis

The above studies have been described in the following chapters of the thesis. The thesis is divided into seven chapters. Each chapter ends with a closure. The essence of each chapter is given as follows:

**Chapter 1** discusses the introduction of the thesis providing the necessity for research on retention of radionuclides during severe accident in a nuclear reactor. This chapter highlights the importance of FCVS along with the state of art in this area. The literature survey is concluded with identifying unresolved scientific and technical objectives which is addressed in the thesis.

**Chapter 2** presents a conceptual design of a venturi scrubber. Following the heuristic approach, a design of venturi scrubber is proposed for reactor prototypic conditions.

The setting up of the scaled experimental facility (encompassing a single venturi scrubber and metal fibre filter) for demonstrating the performance of the proposed design is discussed in

**Chapter 3**. Its fabrication and instrumentation details are highlighted.

**Chapter 4** focusses on the experimental results. This is divided in two different sections i.e. hydrodynamics and scrubbing of iodine vapour. The two phase axial pressure measurements across the venturi scrubber has been reported across the axial length of venturi scrubber. The

overall pressure drop incurred is compared with the empirical models available in the literature. The measurements on the bulk decontamination factor achieved by the experimental facility and the iodine retention by the alkaline pool are discussed in relation to the observed hydrodynamics.

**Chapter 5** presents the development of a CFD model and its benchmarking with results published in literature on a forced feed venturi scrubber. In addition, the effect of different operating and geometric variables on the pressure drop; liquid flux distribution and aerosol capture in the venturi scrubber is investigated. The application of CFD model to the passive venturi scrubber in experimental facility is further discussed. The injection characteristics in such conditions; resultant hydrodynamics and the interaction with iodine vapours in the venturi scrubber are presented by validation of the model with the experimental results presented in Chapter 4.

In the subsequent **chapter 6**, the developed and validated numerical model is applied to predict the performance of venturi scrubber (both hydrodynamics and percentage iodine absorption) at prototypic reactor conditions.

**Chapter 7** concludes the thesis with the key findings of the research and future recommendations of the work.

## 1.9. Closure

This chapter introduces the nuclear energy which is currently being pursued as a potential alternative energy source. Though this is a clean and sustainable energy source, it is also associated with a history of accidents like any other industry. In the background of the accidents that nuclear industry has encountered in past years, the safety measures in the design philosophy of nuclear reactors has also evolved. The integrity of the reactor containment building holds prime importance in such events. One of the suggested measures is installation

of Filtered Containment Venting System (FCVS). Various designs of FCVS have been reviewed. One such design is a manifold of venturi scrubber in a pool of scrubbing liquid along with a demister and metal fibre assembly at the top. The flow in a venturi scrubber comprises of gas, aerosols, scrubbing liquid, air and vapour. The interaction among these phases determines its overall efficiency. Further, detailed literature review on the design aspects of venturi scrubber is done which leads us to the scientific issues in designing a new venturi scrubber for reactor prototypic conditions. In the light of the scientific issues highlighted from the literature survey, the organization of thesis chapters is discussed, which laid an outline on how these grey areas have been resolved in the present thesis.

## **Chapter 2. Concept Design of FCVS for an Advanced Indian Reactor**

### **2.1. Introduction**

The proprietary nature and strategic importance of the design of Filtered Containment Venting System (FCVS) led to the scarcity of information in literature on the present topic. This creates a fundamental issue in gaining understanding, an insight of the working and the design steps to be followed for such a system for nuclear reactor application. Therefore, for addressing these issues, outlining a conceptual design of FCVS is first required. For this, the design parameters i.e. the flow conditions from the containment and the radioactive fission product inventory during accident scenarios are first determined. Based on these conditions, a FCVS design is proposed which is equipped with a manifold of venturi scrubbers submerged in an alkaline pool.

### **2.2. Advanced Heavy Water Reactor (AHWR) description**

The concept design of FCVS has been made for Indian AHWR. The AHWR is a 300 MWe pressure tube type boiling light water cooled, heavy water moderated reactor, as shown in Figure 2.1 (Sinha and Kakodkar (2006)). It is an innovative Indian reactor designed as a bridge between the second and the third stage of India's nuclear programme. It employs a significant fraction of thorium as its fuel because India has high reserves of thorium. The use of thorium as reactor fuel offers additional advantages because its neutron capture cross-section area is 2.47 times that of  $^{238}\text{U}$ . This contributes in the reduction of fuel requirement as much as 13% for producing the same amount of energy (Sinha (2011)).

AHWR design is based on natural circulation principles under normal, transient and accident conditions, which eliminate all accident scenarios resulting from pump failure

besides reducing capital and operating costs. The reactor is provided with double containment philosophy. The reactor is equipped with several safety-engineered features like Gravity Driven Water Pool (GDWP), Emergency Core Cooling System (ECCS) and Filtered Containment Venting System (FCVS).

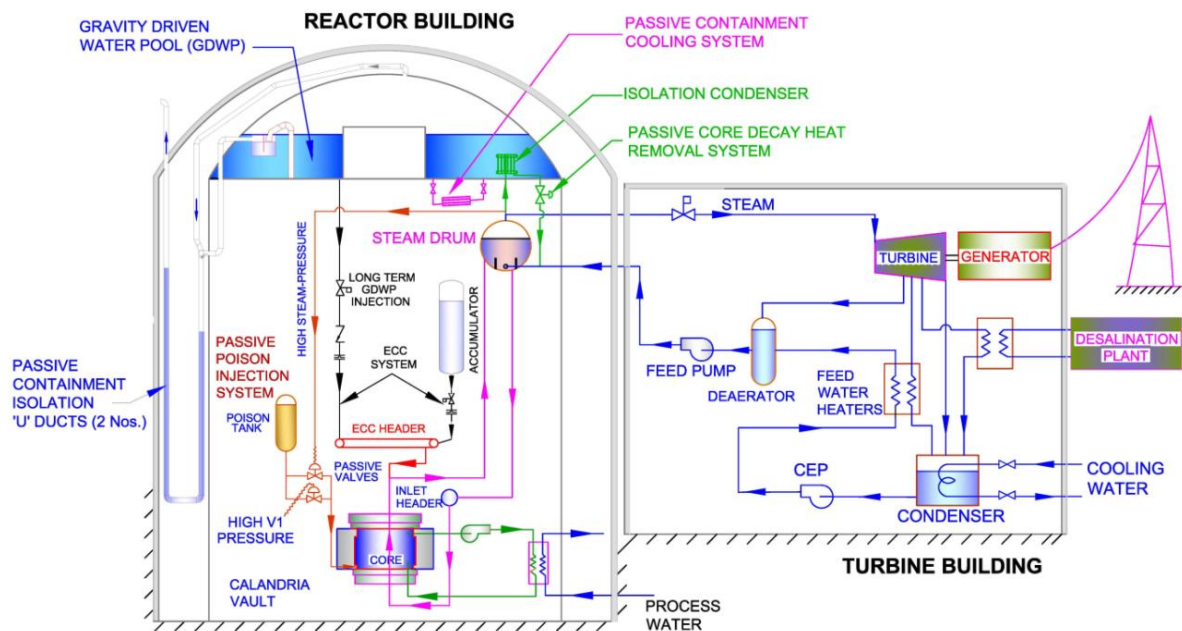


**Figure 2.1. Schematic of Advanced Heavy Water Reactor (AHWR)**

The design features of AHWR are capable of removing the core decay heat by passive means for a grace period of several days during a station blackout situation without significant rise in the clad temperature. With several passive concepts adopted in the reactor design, the probability of a Core Damage Frequency (CDF) has been estimated to be as low as  $10^{-7}$  per year in this reactor.

### 2.3. Filtered Containment Venting System Description

Under severe accident conditions involving multiple safety system failures in a reactor, the primary containment pressure may increase beyond the design pressure limit and must therefore be depressurized at high pressure to maintain the containment integrity. In addition,

the radioactivity released due to core melt down conditions, must be retained so as not to release beyond allowable limit at the public domain. These functions are carried out by a Filtered Containment Vent System (FCVS). In such postulated events, the containment pressure increases beyond the design limit and the rupture disk connected in the vent line bursts. This allows the actuation of the venting system and the flow of gases along with volatile fission products and aerosols from the containment to the scrubber tank and eventually to the venturi scrubber manifold. While passing through the venturi converging section, the gas velocity increases, resulting in a low pressure region at the throat section. The scrubber solution (supplemented by chemicals to enhance the solubility of the vapours) from the pool enters the throat through the nozzles due to radial pressure difference existing between water pool and the throat of the venturi scrubber. The vent gas, owing to their high velocities in the throat section shears the liquid entrained, producing enormous number of tiny droplets. Radioactive fission products in the form of vapour and aerosols drifting with the vent gases interact with the formed droplets. The probability that the aerosol would be retained by the droplet is primarily governed by inertial impaction wherein the aerosols separate from the gas stream line to collide with the droplets. The inertial impaction is physically the ratio of the distance to which the aerosol would travel before coming to rest for a given velocity in a medium where no force except drag is present to the radius of droplet. This depends on the velocity distribution of the flowing gas, trajectory of the aerosol and the size of the droplet. For the vapours, the retention depends on the time of interaction in addition to the drop sizes and their distribution and the mass transfer is thought to play an important role. Therefore, the scrubbing efficiency depends on the droplet sizes and their distribution in the venturi scrubber. Due to this phenomena, volatile radioactive materials such as Iodine and Cesium will get dissolved in the water droplets and hence get retained in the scrubber pool. The mixture exiting the venturi

scrubber forms large air bubbles, which passes through the bulk water in the scrubber tank, where further dissolution and scrubbing takes place.

When the gas bubbles rise from the free water surface of the scrubber tank, the bubble breaker ensures breakage of large bubbles and further downstream the demister arrests the fine entrained droplets carried along with the gas flow. In addition to the demister pad, a metal fiber filter is employed to retain very fine aerosol particulates present in the gas stream. Thus, following this two stage filtration process in the scrubber tank, the air-steam mixture is decontaminated or filtered before it is discharged through the stack into the environment.

So, the design of the FCVS needs understanding of the multi-phase interaction and its mathematical formulation. This multi-variable dependence in deciding the performance of venturi scrubber forced researchers to propose empirical correlations which have limitations on applicability. The design steps of a venturi scrubber for nuclear reactor application are adopted from chemical industry in the present work since the steps are not explicitly defined for the type of venturi scrubber discussed in this thesis. This is basically a heuristic approach involving iteratively solving empirical correlations termed as Calvert Cut diameter technique.

## 2.4. Design Objectives of FCVS

The main design objectives of FCVS are:

- Prevent over-pressurization of the containment beyond design pressure limit that may occur due to failure of multiple engineered safety systems arising from an extreme event.
- Additionally, it should also retain the radioactivity that may be released during such postulated events using venturi scrubber manifold. This would minimize release of activity beyond the containment boundary to avoid long term land contamination while

simultaneously limiting their dose to the public. The efficiency of the system is expressed in terms of decontamination factor, which is the ratio of initial activity to the final activity of the radionuclide. It is designed to achieve a minimum decontamination factor as follows:

- Elemental iodine -100
- Organic iodine -10
- Aerosols – 1000.

## 2.5. Design Parameters

### 2.5.1. Flow profile from Containment

The safety assessment of AHWR has been carried out for postulated accidental scenarios using the best estimate code RELAP5/Mod3.2. RELAP5 is a generic code which has been widely used for the prediction of thermal-hydraulic behavior in nuclear power plants. The code includes many generic component models from which general systems can be simulated. The component models include pumps, valves, pipes, heat releasing or absorbing structures, reactor kinetics, electric heaters, jet pumps, turbines, compressors, separators, annuli, pressurizers, feed-water heaters, ECC mixers, accumulators, and control system components. The flow is assumed one-dimensional and transient in nature. This two-fluid model uses constitutive relations for various interactive forces like drag etc. based on the flow regimes.

The postulated scenarios considered were Station Black Out (SBO), Loss of Coolant Accident (LOCA), Loss of GDWP water etc. (Kulkarni *et al.* (2016)). The flow from the containment was calculated in such circumstances using RELAP5 code. RELAP5 calculations were used as basis for providing input mass flow and pressure to the venturi scrubber. A severe accident code would have given more detailed and accurate result but

computationally it would have been more expensive. Severe accident codes are more preferred for reactor component analysis rather than the whole reactor analysis. Given these restrictions, the RELAP5 analysis is advantageous which allows the user to simulate a plant scale domain in one single analysis with considerable accuracy and in reasonable time.

For the present reactor, the FCVS is not designed for MCCI phase of severe accident.

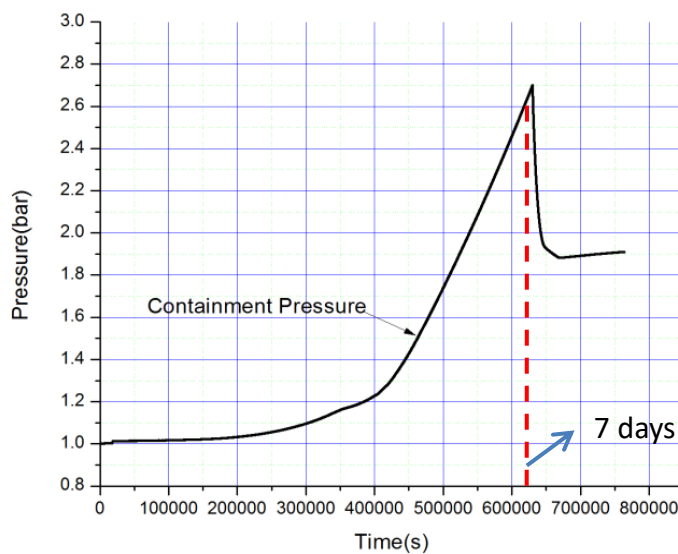


**Figure 2.2. Pressure transient from the containment during venting**

The present reactor is equipped with Core Catcher to hold the molten core. The FCVS is expected to actuate only after 7 days of an extreme event for the current reactor design. The corresponding decay heat is 0.3% and therefore, the steam load to the scrubber tank is 1.37 kg/s. The steam load is accounted while sizing the scrubber tank and its inventory. The non-condensable gas fraction considered is 70%. It was found that before venting, the containment pressure builds up initially and then at the set pressure, the rupture disk bursts thus allowing the flow to the containment as shown in Figure 2.2. This allows the flow of pressurised air-steam mixture along with radionuclides (Figure 2.3) from the containment to the manifold of venturi scrubbers. The flow and pressure transients calculated indicates that just at the start of the venting, there is a high flow rate but as venting continues both the flow and the pressure released from the containment decreases. This gives the flow

conditions for which the FCVS will operate for the considered reactor. The flow rate from the containment suddenly rises to nearly 22 kg/s and then drops very fast to about 2.5 kg/s, and then remains steady at nearly 1 kg/s. Hence, the flow remained within 2.5 to 1 kg/s at 78 kPa (g) for most part of the transient venting conditions. The pressure at the inlet of venturi scrubber system in the reactor is expected to be around 100 kPa (g) to 70 kPa (g).

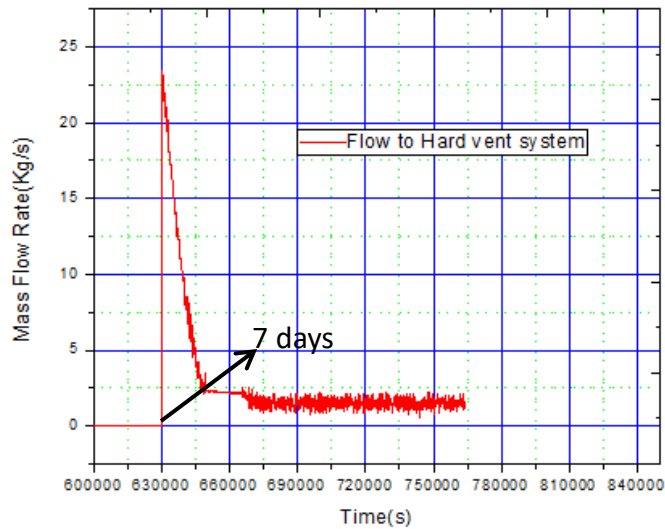


**Figure 2.3. Mass flow rate of gas from the containment during venting**

The containment venting is expected to actuate after 7 days of a severe accident (calculated from RELAP5 calculations for the present reactor) when the containment pressure builds up, exceeds the set pressure limit (2.75 bar for the present case) and ruptures the disk. As soon as the pressure limit exceeds and the flow to the containment starts after bursting of rupture disk, there is both high flow and pressure condition. However, later on as venting proceeds, there is a decrease in both flow and pressure. Therefore, if a FCVS is designed for peak flow just at the start of venting it would result in an overdesign while if only the later part of venting is targeted then it would result in underperforming scrubber. Due to this large variation in flow conditions encountered from the containment during venting, the venturi is designed for mean flow conditions.

## 2.5.2. Estimation of Fission Product Release to FCVS

### 2.5.2.1. Mechanism of Fission Product Release in the Reactor

Fission products released from the failed fuel rods are transported through the reactor coolant system and later released to the containment. (Sehgal (2012), Lemire and Dickson (2003))

#### a) Gaseous Fission Products:

During fuel irradiation, fission gases form as atoms in the grains of fuel. These atoms of gas may either diffuse toward the grain boundaries or precipitate into bubbles. These bubbles may then redissolve and reach the grain boundaries mainly by atomic diffusion. On the grain surface, the fission gases tend to coalesce and fill the boundaries. Their release from the surface usually follows two pathways depending on the temperature: burst phase and release via thermal diffusion.

The first release method usually occurs at the beginning of the temperature rise at around 1000 °C. The second phase involves the release of the intra-granular gases via a thermally activated diffusion process that begins with dissolved atoms. The gases trapped in the intra-granular bubbles are the last to be released, which generally occurs when the fuel melts.

#### b) Other FPs: Other FPs also follow a two-phase process:

(1) Fission products formed in the solution can either precipitate or diffuse to the grain boundary depending on their concentration.

(2) Once it has reached on the grain surface, vaporisation of it in either initial form or in other chemical forms (such as molybdates, zirconates, etc.) takes place.

Once out of the fuel matrix, the interaction of fission products with the cladding and components of the core structures might change their chemical form and reduce their volatility through the formation of other species. When all of the fission products have come out of the core, a significant fraction of the low volatile FPs condenses in the colder sections of the upper core structures before even reaching the hot legs of the RCS or the containment. However, in highly volatile FPs this condensation behaviour is less probable.

Fission product transport in containment:

The chemical forms of FPs reaching the containment is highly governed by their volatility, affinity towards tank internals etc. The various products are expected to be well mixed within the particles. To investigate the effect of containment thermal hydraulics on the speciation of fission products several experiments like Phebus, ThAI have been conducted in the past. The presence of steam and high humidity promotes the growth of aerosols. With the growth of aerosol in size, its probability of deposition also increases.

In conclusion, the larger particles settle while smaller ones remain air-borne. With time, there is a drastic decrease in containment source term.

#### 2.5.2.1. Estimation of inventory for the present reactor

Following degradation of core under postulated accidental scenarios, the molten core will react with concrete. This will give rise to the formation of aerosols. In the U.S. Nuclear Regulatory Commission WASH-1400 (1975) report, fission product release during this stage has been calculated and divided in the following groups:

- i) Noble gases group: Kr and Xe; released within a short interval of core damage.
- ii) Low volatile FPs: exists in either oxide/ metallic form; volatilizes at temperature ~ 2200 K hence condenses easily in the containment atmosphere to form aerosols.

iii) High volatile FPs: released shortly after core-concrete interaction.

The heat transport from the core melt into the coolant, as well as the release of fission products, will result in a pressure increase inside the closed containment. This serves as the prime basis for containment venting such that over-pressurization of the containment can be avoided. During venting, Noble gases (Kr, Xe), volatile fission products (Cs, I) and a quantity of less volatile fission products (Sr, Te) in form of aerosols will get released from the containment to the FCVS where as other less volatile fission products and activated product of fuel would remain in the core debris, primary heat transport system and on the walls of containment in condensed form. The iodine is present in the containment in both organic and elemental form. The partition coefficient of methyl iodide is 5 at 20 °C is very less as compared to that for elemental (volatile) I<sub>2</sub> (Partition coefficient of elemental I<sub>2</sub> = 90 at 20 °C). Therefore, the probability that organic iodine goes to containment is also very less and hence these are not considered in the calculations (Jacquemain *et al.* (2014)). The major elements and their release fractions are shown in the Table 2.1.

**Table 2.1 Calculated release fractions of different elements during severe accident**

Element	Release Fraction	Volatilized as
<b>Cs</b>	<b>100%</b>	CsOH
<b>I</b>	<b>100%</b>	CsI
La	<0.1%	
Mo	2%	MoO <sub>3</sub>
Nb	<0.1%	
<b>Sb</b>	<b>100%</b>	Sb <sub>2</sub>
Sn	0.2%	Sn
Sr	<0.1%	
Ag	3%	Ag
<b>Te</b>	<b>79%</b>	Te
Ru	<0.1%	

FCVS is intended to retain both aerosols and vapors present in the vent gases coming from the containment. The expected flow rate of radionuclides to the FCVS is dependent on pressure difference between the ambient and containment, temperature, pH condition in the containment, its probable interaction with containment internals in its path and accident progression along with the reactor type. In the case of AHWR, it is estimated that the core inventory can produce a maximum of 12 kg of Iodine and 99 kg of Cesium during a severe accident progression. The maximum release from the fuel bundle through the vessel is limited to 60 % of the total inventory (*Guide No. AERB/NPP-PHWR/SG/D-21 (2007)*). Further, on release to the containment, most of the fission products are plated-out on the large open surfaces present inside the containment volume. A factor of 50 % deposition (plate-out) is considered for evaluating the final inventory available for the FCVS (*Guide No. AERB/NPP-PHWR/SG/D-21 (2007)*). Following the above assumptions, the design basis load to the FCVS is approximately 3.6 kg Iodine and 30 kg Cesium.

- Cesium released during accident primarily exists in the form of CsOH and the rest combines with iodine to form CsI. CsI is highly soluble in water. It dissociates and remains as ions in water. Cesium hydroxide also being a strong base dissociates into ions when it is discharged in aqueous media during venting. The dissociation of Cesium hydroxide does not affect the solubility of elemental iodine.
- Assuming a conservative approach for evaluating the fission product, the total iodine released is considered to be of elemental form.

Therefore, the thesis is focussed on addressing the retention of iodine in volatile form in FCVS. These two parameters i.e. flow conditions and the expected inventory of radionuclides form the basis for the design of FCVS for a given nuclear reactor and are tabulated in Table 2.2.

**Table 2.2 Summary of design Parameters for FCVS for an advanced Indian reactor**

Parameters	Reactor Conditions
Input Pressure (Figure 2.2)	2.7 kg/cm <sup>2</sup> (abs)
Input Flow rate (max-min) (Figure 2.3)	2.5 kg/s - 1 kg/s
Target Decontamination Factors	Aerosols: 1000
	Molecular Iodine: 100
	Organic Iodine: 10
Iodine Inventory	3 kg

## 2.6. Assumptions for the design of venturi scrubber

Yung *et al.* (1978) performed a material balance for aerosol concentration in a differential volume of a venturi scrubber assuming a constant liquid hold-up, constant gas velocity, constant droplet diameter and its velocity. They derived the following equation:

$$-\frac{dc_s}{c_s} = \frac{1.5|u_s - u_d|}{u_d d_d} \left( \frac{Q_l}{Q_g} \right) \eta dz \quad (2.1)$$

where  $c_s$  is the instantaneous concentration of the aerosol,  $u_s$  is the velocity of aerosol,  $u_d$  is the droplet velocity,  $Q_g$  and  $Q_l$  are the volumetric flow of gas and liquid respectively,  $\eta$  is the single droplet scrubbing efficiency and  $d_d$  is the droplet diameter. To solve this equation, certain assumptions were made:

- 1) The flow is one dimensional, incompressible and isothermal.
- 2) The droplets have zero axial velocity at the throat entrance.
- 3) Liquid drop diameter ( $d_d$ ) is predicted by Nukiyama and Tanasawa correlation given by equation (2.2). The droplets are considered to have uniform diameter with uniform distribution.

$$d_d = \frac{50}{v_g} + 148.87 \left( \frac{Q_l}{Q_g} \right)^{1.5} \quad (2.2)$$

where  $v_g$  is the superficial gas velocity at the throat section.

- 4) The only force acting on the droplets is drag force and their velocity ( $u_d$ ) is calculated by the following force balance equation in the axial direction of flow ( $z$ ), i.e.

$$\frac{du_d}{dz} = \frac{3}{4} \left( \frac{\rho_g}{\rho_l} \right) \frac{(u - u_d)^2}{u_d d_d} C_d \quad (2.3)$$

where  $C_d$  is drag coefficient and is approximated by Goel and Hollands (1977) correlation,  $u$  is the velocity of the gas and  $\rho_g$  and  $\rho_l$  are the density of the gas phase and the droplets respectively.

- 5) The scrubbing phenomenon is observed only in throat section only.  
6) Scrubbing occurs primarily due to inertial impaction ( $K_p$ ). Here Calvert's single drop capture efficiency ( $\eta$ ) is used as given below:

$$K_p = \frac{\rho_s d_s^2 (u_s - u_d)^2}{9\mu d_d} \quad (2.4)$$

where  $\rho_s$  is the density of the aerosol,  $d_s$  is the diameter of aerosol and  $\mu$  is the viscosity of the gas phase.

$$\eta = \left( \frac{K_p}{K_p + 0.7} \right)^2 \quad (2.5)$$

- 7) The interaction of drops with walls is neglected.  
8) The interaction between droplets and gas is considered one way i.e. the movement of particulates is influenced by the continuous flow.

9) The aerosols are moving with the same velocity as that of gas phase i.e.  $u_s = u$ .

The flow of gas, droplets induce pressure drop in the venturi scrubber which is calculated from the Calvert's empirical model as given by (Calvert (1970))

$$\Delta P = 10^{-3} v_g^2 \left( \frac{Q_l}{Q_g} \right) \quad (2.6)$$

Equations (2.1) to (2.6) gave the governing equations for the design of venturi scrubber. This set of equations have no analytical solution therefore, they were non-dimensionalised with the help of superficial gas velocity at the throat entrance ( $v_g$ ), initial concentration of aerosols at the throat entrance ( $c_{ini}$ ) and characteristic length scale (L) as given in equation (2.7).

$$\frac{l}{L} = \frac{2}{3} \left( \frac{d_d}{C_d} \right) \frac{\rho_l}{\rho_g} \left( \frac{v_g}{v_g - u_d} \right)^{0.5} \quad (2.7)$$

This process helped in reducing the complexity of equation and generalising them. Now the aerosols to be scrubbed have a size distribution specific to application. The traditional method for calculating the efficiency has been to divide the particle sizes into bins and to sum up the efficiency for each of it to calculate the overall efficiency. However, Sundberg (1974) suggested a simplified approach and showed that the overall scrubbing efficiency of wet scrubbers can be related to distribution parameters: mass median diameter and standard deviation of the aerosol size distribution and the aerosol diameter for which the efficiency is 50% (cut diameter) only for aerosols which can be represented by a log normal size distribution. This diameter is termed as separation cut diameter and the corresponding impaction parameter is known as critical impaction parameter. This design technique relates the separation cut diameter to the overall efficiency and the size distribution parameters (equation (2.8)).

$$K_p = K_{p50} \frac{d_{sg}}{d_{pa50}} \quad (2.8)$$

where  $d_{sg}$  is aerodynamic geometric mean diameter for aerosol,  $K_{p50}$  is critical impaction parameter and  $d_{pa50}$  is performance cut diameter of aerosol or the diameter of aerosol for which efficiency of venturi scrubber is 50%.

Graphical solutions of the equation (2.1) is given in terms of inertial impaction parameter for 50% efficiency ( $K_{p50}$ ), dimensionless liquid loading ratio (B) (equation (2.9)) and aerosol diameter for which 50% efficiency is calculated ( $d_{pa50}$ ). These curves are given for capturing aerosols in the venturi scrubber up to 99% efficiency.

## 2.7. Design Calculations for FCVS

The total mass flow rate from the reactor containment as a function of time is given in Figure 2.3. The mean flow rate is considered for the design which is 4.25 kg/s (4 m<sup>3</sup>/s). The performance curves given by Calvert technique are limited to 99% efficiency. Therefore, the design objectives are:

- Minimum retention efficiency = 99 %
- The size of aerosol is having mass median diameter ( $d_{sm}$ ) of 1.5 microns and log mean size distribution of 2.5 (Jacquemain *et al.* (2014))

The flow conditions to the venturi scrubber are characterised in terms of two significant parameters, i.e. inertial impaction parameter (equation (2.4)) and dimensionless liquid loading (B) (equation (2.9)).

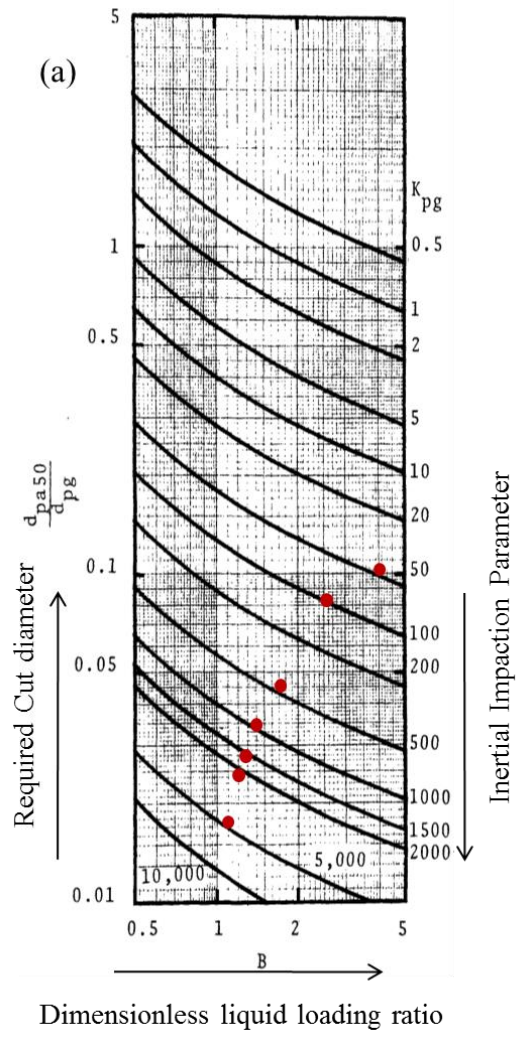
$$B = \left(\frac{1}{C_d}\right) \left(\frac{Q_l}{Q_g}\right) \left(\frac{\rho_l}{\rho_g}\right) \left(\frac{v_g}{v_g - u_d}\right)^{0.5} \quad (2.9)$$

The design steps followed for arriving at an efficient design (Yung *et al.* (1977)) for the above conditions are:

- I.) Determine required cut diameters.
- II.) Determine performance cut diameters.
- III.) Determine required pressure drop.
- IV.) Determine throat cross-sectional area.
- V.) Determine throat length.
- VI.) Determine convergence and divergence angles.

### **Step I. Determining required cut diameters**

The aerodynamic geometric mean diameter for aerosol ( $d_{sg}$ ) is defined as  $d_{sg} = d_{sm}(C \rho_s)^{0.5}$  where  $C$  is Cunningham correction factor = 1.01 and  $\rho_s$  is aerosol density = 4.933 g/cm<sup>3</sup>. This correction factor is included to account for the non-continuum effects while calculating the drag force on small particles (<15 micron). This gives the aerodynamic geometric mean diameter as 3.43 micron. Using this value, the required cut diameters for overall efficiency of 99% (penetration = 1-0.99=0.01) are calculated from the graphical solutions provided (Figure 2.4) (Yung *et al.* (1977)). The values thus obtained are tabulated in Table 2.3.



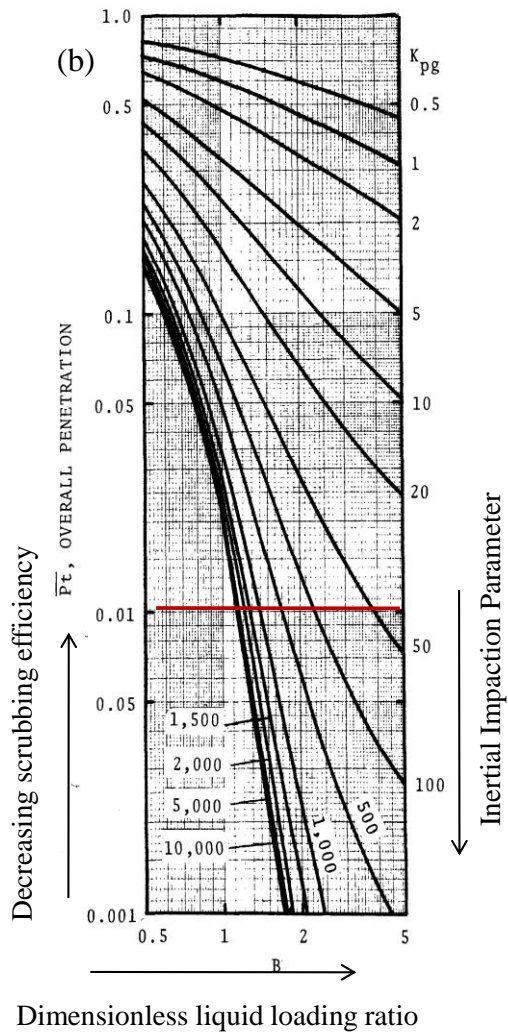


Figure 2.4 Plot of (a) scrubbing efficiency and (b) cut diameter as a function of dimensionless liquid loading ratio ( $B$ )

**Table 2.3. Values of parameter B (Equation (2.9)) with varying  $K_p$** 

<b>B</b>	$K_p$	$d_{pa50}/d_{sg}$	$d_{pg50}$ (micron)
4	50	0.1	0.15
2.3	100	0.085	0.1275
1.7	500	0.043	0.0645
1.4	1000	0.033	0.0495
1.3	1500	0.027	0.0405
1.2	2000	0.025	0.0375
1.1	5000	0.017	0.0255

**Step II. Specifying performance cut diameters**

A number of performance curves are drawn with impaction parameter as y-axis and  $d_{pa}$  on x-axis. For this, a throat gas velocity is assumed and for each throat gas velocity following parameters are calculated across a range of liquid loading.

- a) Droplet diameter is calculated using Nukiyama- Tanasawa equation for drop size.
- b) Reynolds number, drag coefficient, parameter B, critical inertial impaction parameter ( $K_{p50}$ ) (equation (2.10)) and impaction parameter ( $K_p$ ) are calculated. The other relevant equations are given in section 2.6.

$$K_{p50} = 0.2087 + \frac{0.946}{B} + \frac{0.48}{B^2} \quad (2.10)$$

for  $0.5 \leq B \leq 5$

The steps (a) and (b) are repeated for a range of operating condition (throat gas velocity and a range of liquid loading). The resultant variation in  $K_p$  with cut diameter for various liquid loading ratios is plotted in Figure 2.5.

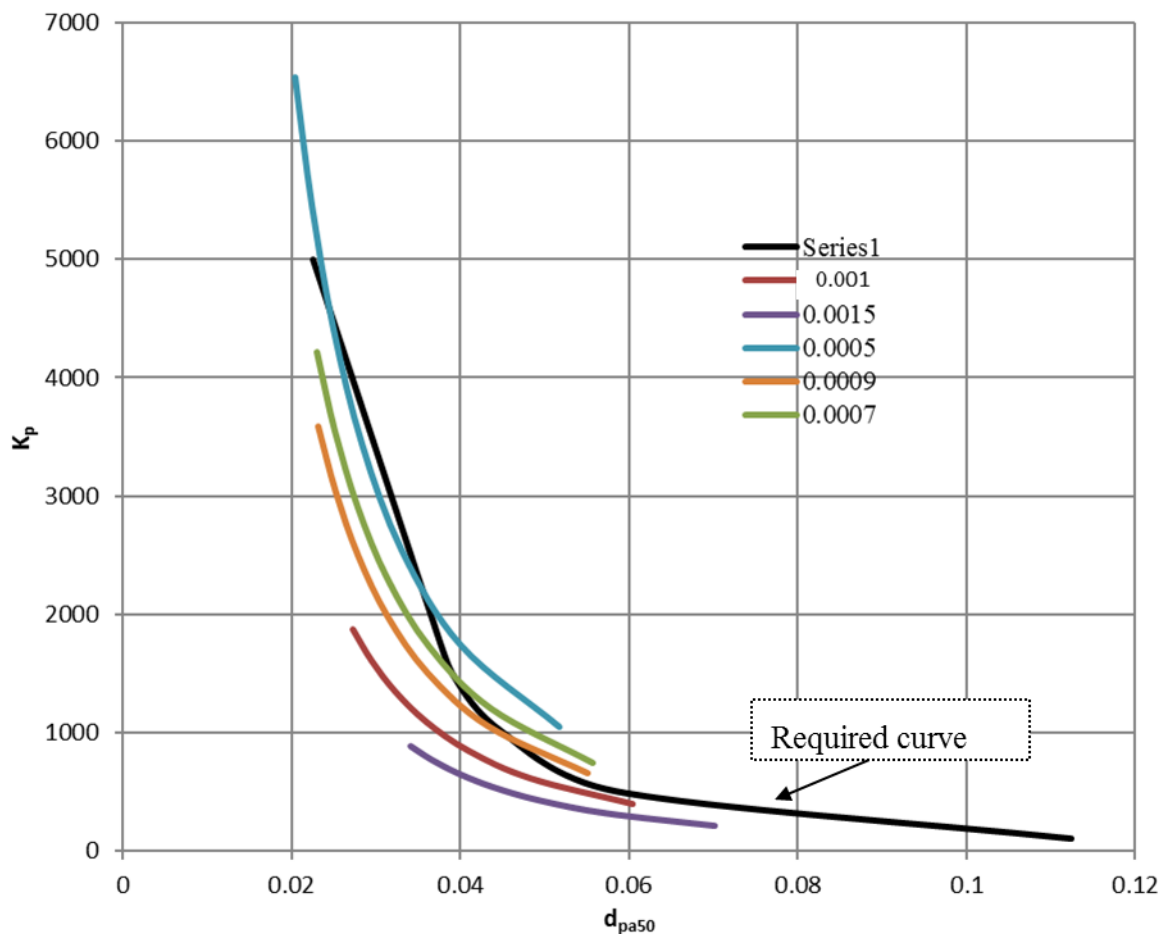


**Figure 2.5 Impaction parameter as a function of cut diameter**

The intersections of the calculated values thus plotted (as shown in Figure 2.5) with the requirement lines (shown by black line) (Table 2.3) determine the liquid loading ratios ranging from 0.0005 to 0.0009 for the present scrubber operation. The intersection points refer to the design points for the scrubber operation.

### Step III. Determine required pressure drops

The intersection of the performance curves and the required curves gives the design points i.e. liquid loadings and the corresponding operating gas velocity (Step II). Using these values, the pressure drop across the venturi scrubber is calculated using Calvert empirical relation (2.6) (Figure 2.6). Based on the allowable pressure drop across the venturi scrubber, liquid loading has been chosen and further dimensions of venturi scrubber are calculated.

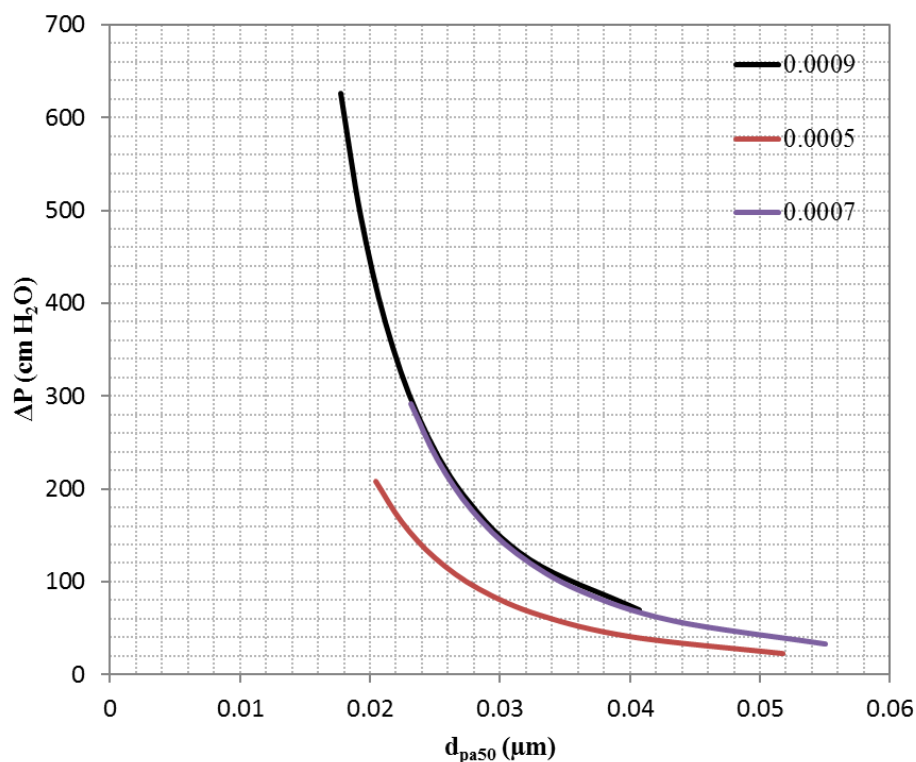


Figure 2.6. Pressure drop from Calvert equation for the calculated liquid loadings

### Step IV. Determine flow through a single venturi scrubber (both liquid and gas)

From the above steps, we get a range of operating conditions for attaining the desired efficiency. For the present case, the venturi scrubber is designed to operate at a limiting throat gas velocity of 150 m/s and operating throat gas velocity of 90 m/s across a 5 cm

throat cross-section. The above steps give the corresponding liquid loading,  $K_p$  value and  $Q_l/Q_g$  value. This gives the volumetric flow of gas as  $0.169 \text{ m}^3/\text{s}$ .

#### **Step V. Determine throat length**

The throat section plays a pivot role in the design of the venturi scrubber. A longer throat section would incur high pressure drop while a minimum length is required for allowing interaction of aerosols and scrubbing liquid. This limits the non-dimensional length ( $L$ ) of the throat section to be 2-3 (Yung *et al.* (1977)) as given in equation (2.7). It was found that increasing the non-dimensional length beyond 3 would not help in increasing efficiency of the venturi scrubber. Therefore, the non-dimensional length ( $L$ ) is fixed to 2.

$$l = \frac{2}{3} L \frac{d_d \rho_l}{C_d \rho_g} \left( \frac{v_g}{v_g - u_d} \right)^{0.5} \quad (2.11)$$

Using Step II.), the liquid loading to the venturi scrubber is fixed as 0.0008. The corresponding diameter of aerosol for 50% efficiency ( $d_{pa50}$ ) is found to be 0.0451 and  $K_p=950$  as given in Figure 2.5.

Substituting the value of  $K_p$  in equation (2.4), we get

$$v_g = 5.0206 \times 10^5 d_d \quad (2.12)$$

Using Nukiyama-Tanaswa correlation in equation (2.12), the throat gas velocity  $v_g$  is calculated to be 5926 cm/s and droplet diameter ( $d_d$ ) = 0.012 cm.

Putting these values in equation (2.11) and taking  $L=2$ , we get throat length = 52 cm.

#### **Step VI. Determine convergence and divergence angles**

For sustaining the self-priming operation, the inlet pressure expected at the inlet of venturi manifold is maximum 2 bar (abs) after subtracting frictional pressure drop in pipe from RELAP5 calculations at the minimum scrubbing pool height of 6 m. These pressure conditions govern the length of the venturi scrubber.

Maximum convergence angle to avoid flow separation =  $21^\circ$

The convergent section should provide sufficient acceleration to the gas flow. This will help in attaining the required liquid loading at the nozzles in the throat section. Therefore, maximum convergent angle is kept and this gives us the convergent section length= 10 cm and inlet diameter= 12 cm. The pressure due to the hydrostatic head at nozzles= 1.6 bar (abs) (minimum).

Therefore, divergent section length= 1.4 m with divergent angle of  $1.5^\circ$

### **Step VII. Number of nozzles in the throat section.**

The pressurised flow from the containment is maximum at about 2 bar (abs) to the venturi manifold. The hydrostatic Pressure at the throat section nozzle = 1.6 bar (abs). This is the minimum hydrostatic head maintained at the nozzles.

These two constraints gives the area of flow required at the nozzles.

For the liquid loading to the scrubber 0.0008 (Refer Step II.) and  $Q_g = 0.169 \text{ m}^3/\text{s}$  (Refer Step IV.), the pressure drop across the converging section = 0.5 bar. The pressure drop across the nozzles for entrainment is calculated from the difference of hydrostatic pressure at the nozzles and the pressure at the throat section due to the gas flow. i.e. 1.6 bar- (2-0.5) bar = 0.1 bar. Using this pressure drop across the nozzles to calculate the velocity of scrubbing liquid entrained, we get  $v_l = 3.8 \text{ m/s}$ .

Equating the maximum allowable liquid flow rate through the nozzles from the values

above to the  $\text{no. of nozzles} * \pi * \frac{\text{diameter of nozzles}^2}{4} * v_l$

And taking nozzle of diameter 2.5 mm, no. of nozzles required= 13 (approx).

The diameter of 2.5 mm is chosen because a very small nozzle diameter may choke during entrainment of scrubbing liquid from the tank while a very large diameter will not facilitate in jet breakup in small droplets.

### **Step VIII. Number of venturi scrubbers required.**

The total flow rate to the venturi manifold was calculated from RELAP5 and the mean flow rate considered for the design purpose is  $4 \text{ m}^3/\text{s}$  (Refer Section 2.7).

Flow rate per venturi scrubber is  $0.169 \text{ m}^3/\text{s}$  (Refer Step IV)

Therefore, number of venturi scrubbers required =  $4/0.169 \sim 25$ .

The final dimensions of the venturi scrubber are shown in Figure 2.7.

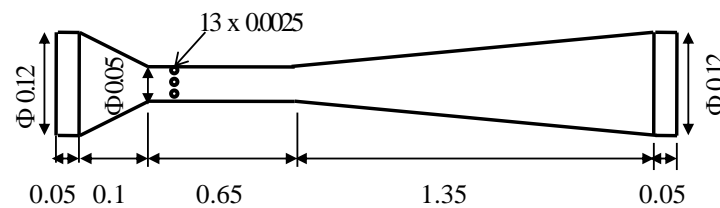


Figure 2.7. Dimensions of venturi scrubber (m)

## 2.8. Arrangement of venturi scrubbers manifold in the scrubber tank

The FCVS is conservatively designed for pressure of  $3 \text{ kg/cm}^2$  (g) and temperature of  $150^\circ\text{C}$ . A 300NB Sch 40 pipe is laid from the top of primary containment and is routed through the annular region between primary and secondary containment. At an elevation, it leaves the secondary containment and is connected to the building housing the scrubber tank (Figure 2.8). FCVS inlet line from the reactor containment enters the scrubber tank (Table 2.4) from side at around  $7 \text{ m}$  of the tank shell height.

The following points have been considered while sizing the scrubber tank:

- The venturi scrubbers should be always submerged.
- Due to the steam loading and heat of reactions, the water in the tank will evaporate. The inventory of water in the scrubber tank should be such that the venturi scrubbers should work for sufficient number of hours beyond which it will be refilled.

- There are other internals like demister in the scrubber tank. The tank height is optimised to accommodate swell following that the demister should not be submerged in any condition.
- A minimum hydrostatic head should always be maintained to ensure desired decontamination.

Following the above requirements, an optimised tank height is decided.

**Table 2.4 Specifications of Scrubber Tank for reactor application**

Sr. No.	Description	Particulars
1.	Diameter	4 m
2.	Cylindrical Height	10 m
3.	Design pressure	3 kg/cm <sup>2</sup> (g)
4.	Design temperature	150°C
5.	Material of Construction	CS (ASTM-A-516 Gr.70/ IS 2002 Grade B)
6.	Design and manufacturing code	ASME section-III-ND

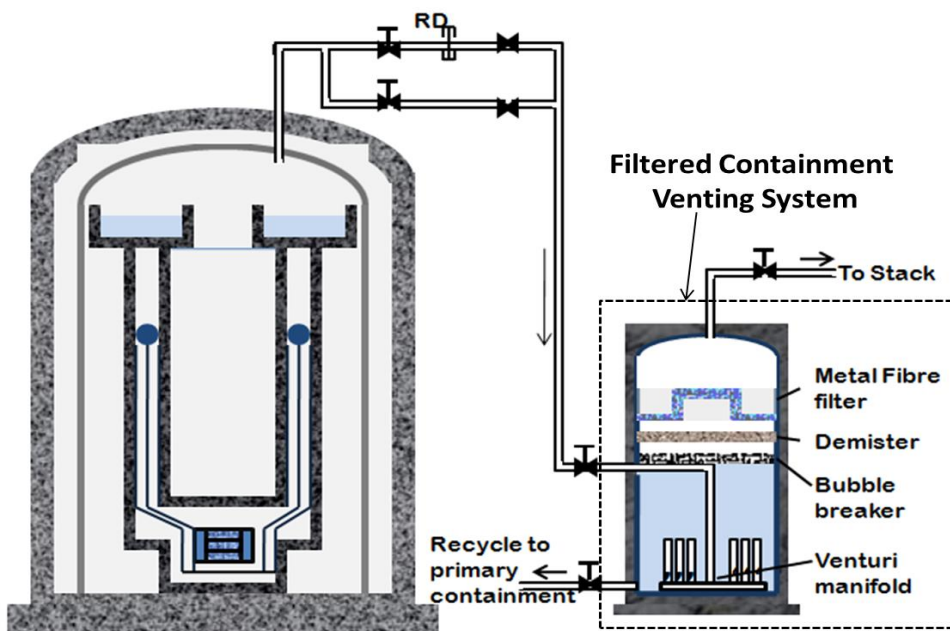


**Figure 2.8 Arrangement of FCVS considered in the present study**

It goes up to the centre of the tank and then runs vertically down up to 0.2 m from tank bottom. Here, it is branched into six cross arms, separated from each other by  $60^\circ$  to facilitate proper distribution of the exhaust gases. On each arm, five venturi scrubbers, pointing vertically upwards are installed. Thus, total number of venturi scrubbers considered in FCVS are 30.

## 2.9. Closure

The design features of an advanced Indian reactor AHWR are discussed. AHWR is a thorium fuel based reactor and is designed with several engineered safety features to mitigate the consequences of accidental scenarios. As a post Fukushima measure, installation and design of engineered safety systems including FCVS is considered. The working of FCVS in the reactor is described and its design objectives are discussed. The design parameters, i.e. flow conditions for FCVS are calculated using best estimate code RELAP5/mod3.2. The radionuclide fission inventory to be retained using this system is specified. Following this, the Calvert cut diameter technique, is used to calculate the dimensions and number of venturi scrubber in FCVS manifold. Based on this, the dimensions of the scrubber tank and the arrangement of the venturi scrubbers in the scrubber tank is laid out. The FCVS manifold is divided into 6 inclined branches. On each arm, five venturi scrubbers are installed.

## **Chapter 3. Description of the Experimental Facility for FCVS**

### **3.1. Introduction**

The literature lacked substantial studies for a venturi scrubber operated in a submerged mode due to the proprietary nature. However, a few studies which are available indicated the multidimensional nature of the flow physics inside the venturi scrubber. The performance of venturi scrubber was found to be dependent on its geometry, the operating conditions and size and number of the nozzles from which the scrubbing liquid is entrained. This created a fundamental gap in literature in gaining understanding and how to start the design process for an Indian reactor. To help resolve this issue, the design of venturi scrubber is first discussed from the pressure and flow conditions for the prototypic reactor conditions in the previous chapter. A scaled experimental facility is built such that the flow to the venturi scrubber is proportional to the number of the venturi scrubbers present in the manifold of the FCVS and dimensions are scaled at 1:1. In this chapter, the details of the experimental facility built for investigating hydrodynamics and scrubbing behavior of FCVS are discussed. The prototypic experimental facility is provided with adequate instrumentation. It is aimed to demonstrate the performance of the proposed design of venturi scrubber for an advanced Indian reactor prototypic conditions.

### **3.2. Scaling of the experimental facility**

It is difficult to perform experiments in a complete venturi manifold as designed for FCVS. Therefore, a scaled experimental facility is built which simulates the hydrodynamics and the scrubbing behavior for iodine vapour retention in a single venturi scrubber. A series of experiments have been performed in this facility by varying the parameters namely gas flow

rate, amount of iodine, submergence height and pressure conditions to understand their implications on the performance of designed venturi scrubber.

### 3.2.1. Geometric Scaling

A single venturi scrubber is fabricated having the dimensions similar to that designed for reactor conditions. The nozzles at the throat section are actual holes drilled in the metallic venturi during fabrication.

### 3.2.2. Flow Scaling

For most duration of the venting the mass flow from the containment remained within 2.5 to 1 kg/s at 78 kPa (g). The experiments are conducted to simulate the flow behaviour in this range in the scaled facility. The flow rate to the facility is scaled in proportion to the total number of venturi scrubbers.

**Table 3.1 Scaling of the experimental set-up**

	Reactor (30 venturi	Experimental Facility	Ratio
<b>Geometric Scaling</b>			
No. Of Venturi	30	1	1:30
Converging length	0.10	0.10	1:1
Throat length (m)	0.65	0.65	1:1
No. of nozzles	13 no. (2.5 mm)	13 no. (2.5 mm)	1:1
Diverging length	1.35	1.35	1:1
<b>Flow Scaling</b>			
Flow to the venturi	2.5-1	0.10-0.02	1:30
Hydrostatic head	6	3-4.5	
Iodine load (g)	3000	35-200	

It is submerged in an alkaline pool and the height of this pool is varied in the experiments. The amount of iodine is also varied to understand the scrubbing behavior of FCVS under various loading instances pertinent to the prototypic nuclear reactor.

### 3.3. Details of the experimental Setup

The schematic diagram of the experimental facility built to study the hydrodynamic characteristics and the scrubbing behavior of iodine vapours in a submerged venturi scrubber is shown in Figure 3.1 and Figure 3.2. There are three major components of the experimental set-up: Scrubber Tank, Venturi Scrubber and Iodine Dispenser.

#### 3.3.1. Scrubber Tank and Venturi Scrubber

##### 3.3.1.1. Scrubber Tank

The scrubber tank is 7 m in height and 1 m in diameter. The material of construction is CS with epoxy paint on the inside. To build the tank, two sheets are rolled and flanged with a 5 mm rubber gasket in between to erect the scrubber tank. The tank is provided with a drain line at the bottom for cleaning and the filling line at the top which is connected to the DM water supply tank at the top.

The venturi scrubber stands vertically inside the scrubber tank at its bottom. The venturi scrubber is made of SS316. It is bolted on a support made of CS at the bottom of scrubber tank. The support is connected to the gas flow supply line (0.12 m) from the compressor. The compressed air is supplied through a reservoir of 7 kg/cm<sup>2</sup> pressure. The air is supplied to the experimental facility at the venturi inlet. The supply line is of the same diameter as that of the venturi inlet i.e. 0.12 m. At the top of the scrubber tank, an exhaust line of 0.05 m diameter and length 10 m is provided to vent the gases from the facility to the atmosphere.

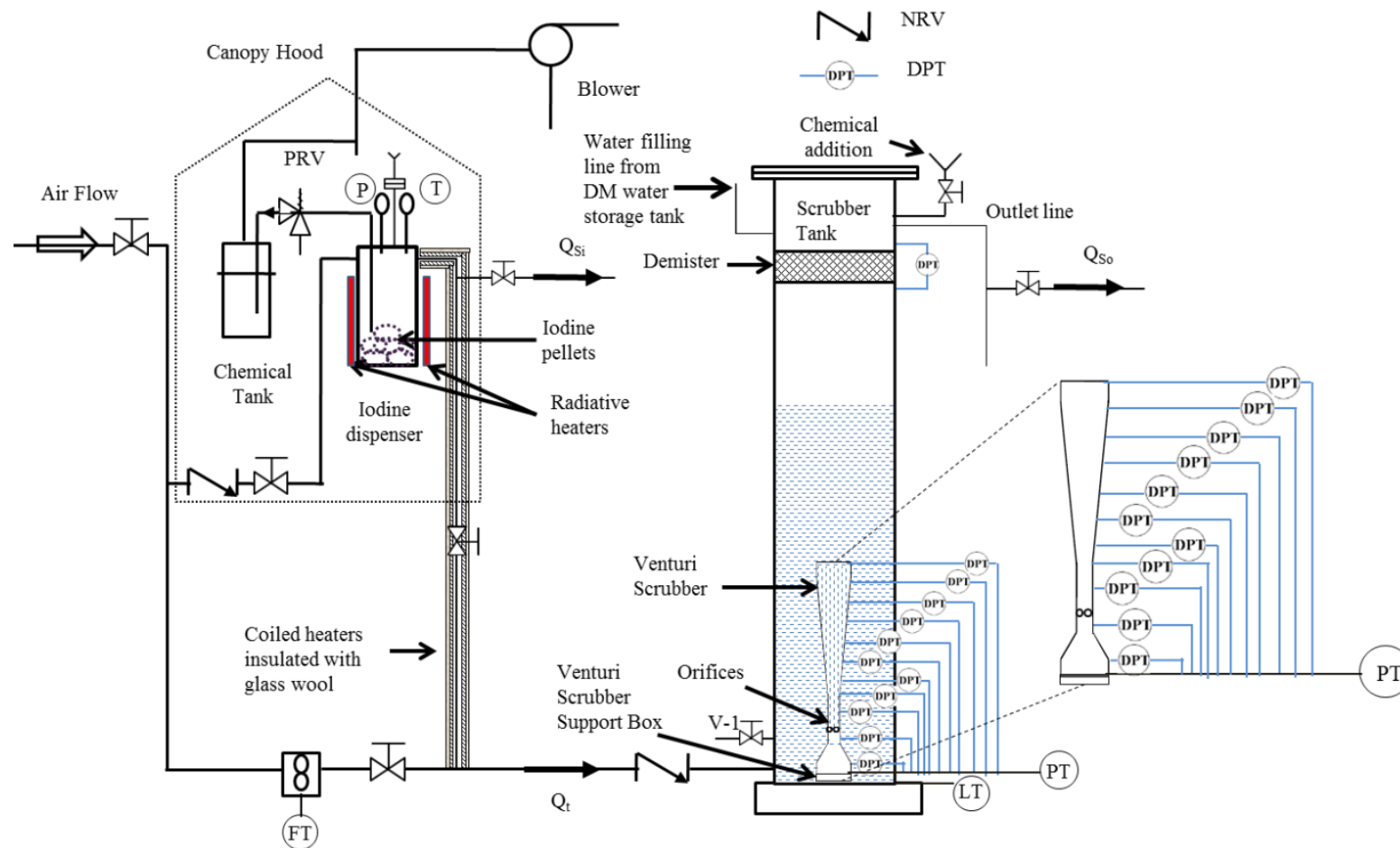


**Figure 3.1** Schematic of the experimental facility comprising of a venturi scrubber held vertically in a scrubber tank and an iodine dispenser at an elevated height to simulate the hydrodynamic behavior and scrubbing efficiency pertinent to nuclear reactor

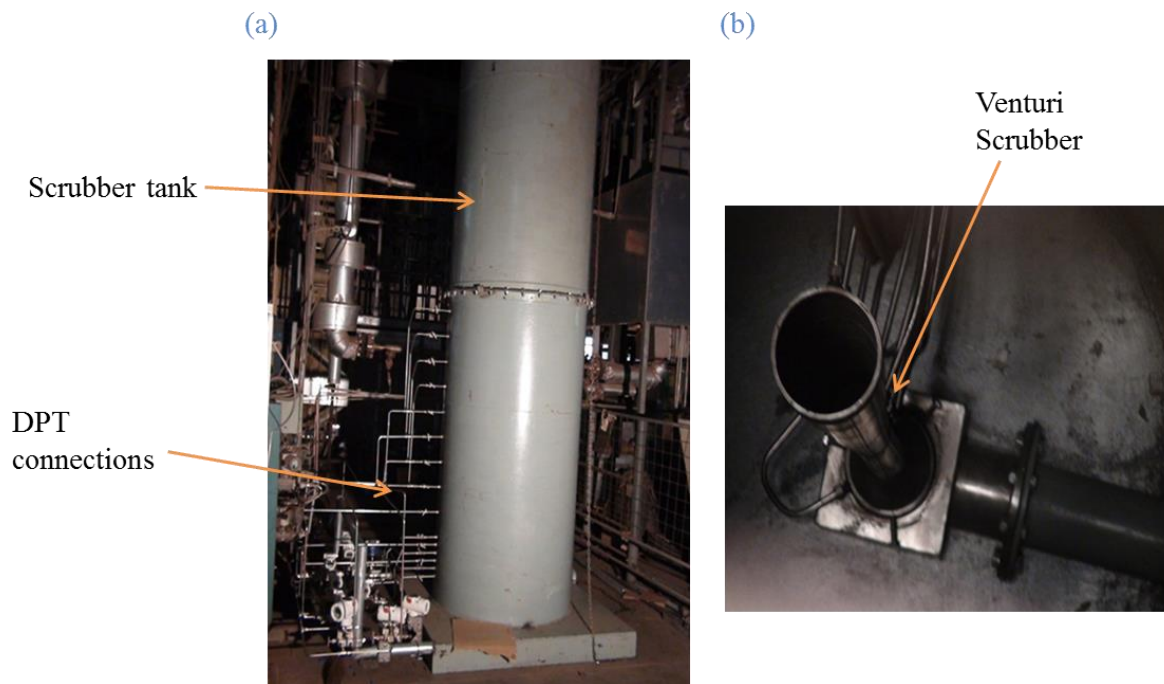


**Figure 3.2 Photograph of (a) Scrubber Tank and (b) Venturi Scrubber**

### 3.3.1.2. Venturi Scrubber

Owing to the health hazards associated with the release of iodine in the environment it is extremely important to contain the vapours inside the containment. Keeping these aspects in consideration and the high reactor volume of reactor under consideration, venturi scrubber sizing was done. The design inputs are therefore the upstream pressure and volumetric flow rate of contaminated gases in the containment. This further gives the liquid loading required for attaining desired decontamination. Consequently, for achieving the liquid loading to the venturi scrubber passively by creating the radial pressure difference across the nozzles located at the throat section; operating height, number of nozzles and dimensions of nozzle for venturi scrubber operation was fixed. The final dimensions of venturi scrubber are shown in the Figure 2.7. A flow developing length of 0.05 m is provided in the throat section before having thirteen nozzles radially in the venturi scrubber.

### 3.3.1.3. Demister Pad

A demister pad is installed at the top of the scrubber tank to remove the droplets from the outgoing air. The demister has a voidage of 97.98%, bulk density of  $160 \text{ kg/m}^3$  and surface area of  $530.96 \text{ m}^2/\text{m}^3$ . The demister pad size is 1 m in diameter and 0.1 m thick. The Demister Pad is made of steel wire mesh duly knitted and crimped. The pad is in mattress form (in segments) and each of its segments is supported by the top and bottom support grids. The demister pad is fixed at 0.5 m below the top of the tank.

### 3.3.2. Iodine Dispenser

The Iodine dispenser is a cylindrical SS316 vessel of diameter 0.15 m, height 0.4 m and thickness 0.007 m and is supported on a bench (bottom insulated by a Bakelite sheet). A SS pipe of 0.02 m diameter with flange connection is bolted at the top of the vessel for filling iodine pellets in the dispenser prior to the experiment. To ensure no leakage of iodine vapours during experiment, a gasket is placed between the flanges during bolting. The vessel is provided with an inlet air purge line which carries the iodine vapour generated by heating the iodine pellets to the air inlet line of the scrubber tank. A valve is provided at the outlet of the iodine dispenser to manually adjust the iodine concentration to the air inlet line. The outlet line of iodine dispenser is insulated by glass wool to avoid condensation of vapours before it mixes with the air.

In an extreme condition of pressure rise in the dispenser unit, a pressure relief valve is provided to vent the dispenser into a chemical tank. The tank is filled with sodium thiosulphate solution and sodium hydroxide solution to maintain pH~11 because it reacts instantaneously with the iodine vapours. To ensure safety during experiments, a canopy hood having an air blower is designed to forcefully dispense adjoining air or any leakage of iodine vapour at a high altitude.

### 3.4. Instrumentation

The details of the instruments in the experimental set-up are given in (Table 3.2). There are 14 DPTs which are connected along with one PT (at venturi inlet) to measure the pressure drop characteristics in the venturi scrubber. The location of DPTs is given in Table 3.2. Total 15 DPTs are installed in the set up out of which two are in converging section of venturi scrubber, seven are in throat section and five are in diverging section of the venturi scrubber. One DPT is located across demister pad. One level transmitter (LT) is provided at the bottom of the scrubber tank to measure the pool swelling during the experiment.

The experimental facility has been provided with Differential Pressure Transmitters (DPTs) which are attached to the Pressure Transmitter (PT) at the entrance of the venturi scrubber for measuring the pressure drop across the venturi scrubber (at different axial locations) as shown in Table 3.2. It gives the local pressure drop. The submergence depth is measured with the Level Transmitter (LT) located at the entrance of the venturi scrubber.

One pressure transmitter is provided at the iodine dispenser to monitor the pressure during experiments. Four thermocouples are connected to the radiative heaters provided at the circumference of the iodine dispenser and two thermocouples record the temperature of the bulk gas inside the iodine dispenser. The pipe connecting to the outlet of the scrubber tank to the inlet of the venturi scrubber is heated by coil heaters to ensure that iodine vapours are not condensed and insulated by glass wool. There are four thermocouples arranged in the outlet pipe of the iodine dispenser. Pressurised gas from the compressor is supplied to the venturi scrubber to simulate non-condensable gases coming from containment. The gas flow rate is adjusted by a valve present at the inlet of the venturi scrubber. The flow rate of gas is measured by a turbine flow meter. Just before the inlet to the venturi scrubber, a check valve is provided to prevent the backflow of water in the flow line.

**Table 3.2 List of instruments their range and accuracy in the experimental set-up**

Instrument	Location from bottom of scrubber tank	Range			Accuracy
		Min	Max	unit	
PT-1	0.025 m	0	1	kg/cm <sup>2</sup>	± 1%
DPT_2	0.1m	-300	300	mmWC	± 1%
DPT_3	0.15 m	-300	300	mmWC	± 1%
DPT_4	0.18 m	-300	300	mmWC	± 1%
DPT_5	0.21 m	-300	300	mmWC	± 1%
DPT_6	0.25 m	-300	300	mmWC	± 1%
DPT_7	0.4 m	-400	400	mmWC	± 1%
DPT_8	0.55 m	-550	550	mmWC	± 1%
DPT_9	0.7 m	-700	700	mmWC	± 1%
DPT_10	0.8 m	-800	800	mmWC	± 1%
DPT_11	1.05 m	-1050	1050	mmWC	± 1%
DPT_12	1.35 m	-1350	1350	mmWC	± 1%
DPT_13	1.65 m	-1650	1650	mmWC	± 1%
DPT_14	1.95 m	-1950	1950	mmWC	± 1%
DPT_15	2.2 m	-2200	2200	mmWC	± 1%
DPT_16	Across demister pad	-2200	2200	mmWC	± 1%
FT	Pressurised air flow measurement	0	12000	lpm	± 1%
LT	Level Transmitter	0	7000	mmWC	± 1%
TE	Thermocouples	0	400	°C	± 0.75%
ICP-MS	Iodine concentration measurement in the exiting air	1.1		ppb	± 5%
ICP-OES	Iodine concentration measurement in the scrubber tank	0.5		ppm	± 10%

The amount of iodine retained in the scrubber tank and the decontamination factor of the experimental set-up is measured by ICP-MS and ICP-OES techniques. These techniques

are basically spectroscopic methods to measure the amount of the iodine present in the sample collected after each experiment.

### 3.5. Operating Procedure and Measurements

Before the start of each experiment, the scrubber tank is filled up to a height greater than 3 m (such that all of the DPTs are submerged in water) with demineralized water by opening the filling line at the top of the scrubber tank. Then venting of all DPTs is done. This is essential for ensuring that there is no air entrapped in the DPT which may cause error in measurement during experiment. During the venting procedure, it is maintained that all the pressure transmitters are submerged in water. After this, the scrubber tank is filled to the desired height with DM water.

The working fluid is added to the scrubber tank prior to each experiment through a funnel arrangement provided in the scrubber tank (Figure 3.1). For the present experiments, the working fluid is an alkaline solution comprising of sodium hydroxide and sodium thiosulphate in the weight ratio of 5:2 following the chemical reaction (3.1).



The pH of the tank is checked before the start of the experiment and is maintained at 10-11 owing to the higher solubility of iodine in alkaline environment. After putting a known weight of iodine pellets and closing the flange at the top of the iodine dispenser, air blower and the radiative heaters arranged at the circumference of the iodine dispenser are switched on and their temperature is monitored in the recorder. Once the temperature of the iodine dispenser reaches 200<sup>0</sup> C, the pipe heaters connecting the outlet of the dispenser to the inlet of the venturi are switched on. In the meanwhile, inlet valve of compressed air is opened and the flow of air through the scrubber tank is fixed at the desired flow rate. The water and compressed air used

in the experiment are at room temperature. The air flow from the compressor is allowed to stabilise, the air supply to the iodine dispenser is started and outlet valve of iodine dispenser is opened sequentially to allow iodine vapour mixed with air to enter at the bottom of the scrubber tank. The measurements namely air flow rate by turbine flow meter, pressure readings by PT and DPTs are recorded at every second in the data logger during the experiment. The results report averaged values of the measurements.

The analysis of iodine vapour removal in the scrubber tank is performed by ICP-OES analysis of scrubber tank solution taken before and after each experiment is finished. The samples are collected after each experiment in different sampling bottles and they are sealed to avoid any losses. There are two sampling ports provided in the experimental set up for measuring iodine concentration as shown in Figure 3.3. The required number of bottles in the cascade (Figure 3.4) is identified through an iterative process in initial few experiments and optimized number of bottles was found to be three at every sampling location. Figure 3.3 shows the locations at which sampling are done to quantify the iodine concentration retained in the scrubber tank (location 1) and the iodine concentration escaping the facility (location 2).

At the end of each experiment, the samples for analysis of iodine absorbed were collected (approximately 50 ml in volume in each sampling bottle). The different samples taken were:

- a) The iodine retained in the scrubber tank is calculated from the scrubber tank solution after the experiment has ended (Location 1, Figure 3.3).
- b) Three separately tagged samples from each of the sampling bottles in the vent outlet line (Location 2, Figure 3.3).

After the samples were collected from the experiment in the sampling bottles, the calibration of the instrument is done which included sample with varying known concentrations

of iodine. The blanks containing the same amount of sodium thiosulphate and sodium hydroxide as the scrubber tank were prepared and then analysed. This removed any possible effect of sodium thiosulphate and sodium hydroxide in the analysis. Now the sample collected from the experiment typically 3-5 ml in volume is loaded in the instrument. The sample passes through the nebuliser and then reaches the plasma (Approximately 5% of the sample loaded in the instrument reaches the plasma.) (in case of ICP-OES) and we get the spectra. From this spectra, we calculate the concentration from the calibration graph previously plotted.

The analysis procedure followed above is making matrix matched standards to eliminate matrix interference. The method was validated by a spike recovery experiment. This method removes the possible disturbance caused by the sodium ions present in the samples of experiments analysed. The samples were diluted to bring the matrix concentration within the allowed limit of the instrument. There is a very less probability of losses on the analyser walls as the calibration process is repeated before each analysis and the instrument is cleaned after each analysis.

The retention of iodine in the scrubber tank is measured by collecting the scrubber tank solution after the experiment is finished. Figure 3.4 shows a schematic of the sampling technique adopted for measuring iodine vapour decontamination factor. To measure the decontamination factor, iodine vapour concentration is measured by connecting cascade of bottles containing 2% by weight sodium carbonate solution to the sampling port at location 2 through silicone tubing during the whole experiment. The air is bubbled throughout the experiment through these bottles. The flow rate is adjusted by the needle valve and measured by rotameter manually. The samples from these bottles are analyzed for the amount of iodine (by ICP-MS) in the air escaping from the facility.

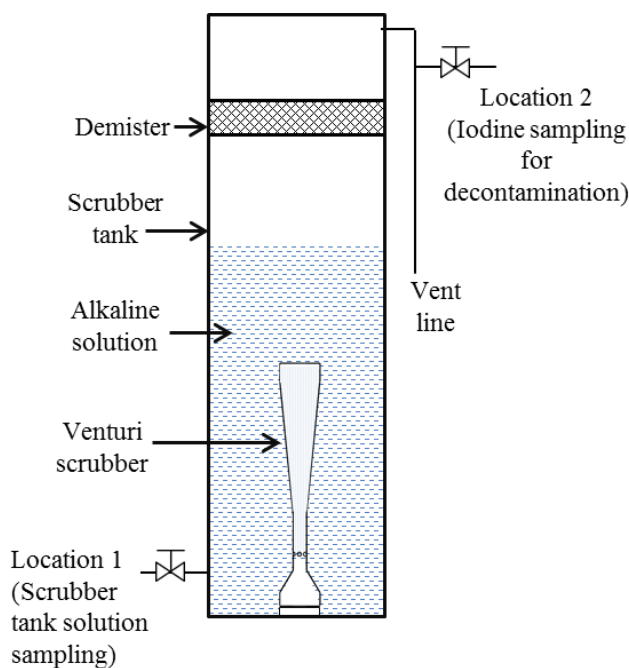


**Figure 3.3** Location of sampling ports in the experimental set-up for measuring the iodine retained by the alkaline pool

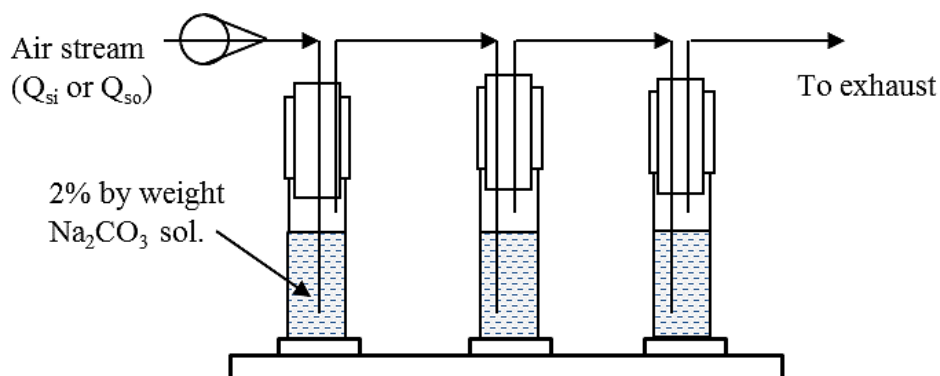


**Figure 3.4** Cascade of bottles arrangement used for measuring bulk DF of iodine vapours

### 3.6. Closure

The FVCS is having a manifold of venturi scrubbers arranged in six branches. To simulate the performance of FCVS for an advanced Indian reactor, a scaled experimental facility is built. The scaling is done keeping the flow to the single venturi scrubber similar as expected in the reactor conditions. The dimensions of the venturi scrubber and the hydrostatic head are maintained as 1:1. This will essentially give us the behavior of a single venturi

scrubber amongst the manifold arrangement. The experimental facility fabrication details and instrumentation are further discussed.

- The experimental facility comprises of a single venturi scrubber of the dimensions calculated in previous chapter and is enclosed in a tank containing alkaline solution.
- To understand the hydrodynamic behavior in the venturi scrubber differential pressure transmitters (DPTs) are provided along the length of the scrubber.
- For measuring the vapour scrubbing in this set-up iodine dispenser is built where in the vapours of iodine will be generated and it is made to flow through the scrubber arrangement to measure its retention during the experiments.

## **Chapter 4. Performance Evaluation of the Simulated FCVS in Experimental Facility**

### **4.1. Introduction**

In spite of the various studies on the forced venturi scrubbers as mentioned in first chapter, the literature lacks the fundamental understanding of the performance of submerged venturi scrubber installed in FCVS. This led us to design the FCVS for prototype conditions and fabricate a scaled experimental facility to gain an understanding of the same. This chapter presents experimental study on the hydrodynamic behavior and iodine vapour scrubbing in it. The experiments were conducted for different gas flow rates and submergence heights of the scrubber tank to investigate the hydrodynamics as identified for the present nuclear reactor. Additionally, the retention of radioactive iodine in this safety system (which has been a concern during severe accident scenarios) has been simulated using laboratory grade iodine of similar chemical behavior.

The presented experimental analysis is important not only for creating database for future model development but also for understanding the submerged operation of venturi scrubber and gas-water interaction within the scrubber. The results have been divided in two headings:

- 1) Hydrodynamics of venturi scrubber
- 2) Iodine retention and bulk Decontamination Factor of the experimental set up for iodine vapour

### **4.2. Hydrodynamics of venturi scrubber**

There is almost no data on pressure drop occurring in the venturi scrubber for submerged conditions as relevant to nuclear reactors in the open literature. In the nuclear reactors, performance of venturi scrubber needs to be understood not only at high pressure

condition of containment when venting starts (Figure 2.3) but also under low pressure conditions when venting continues for prolonged period.

From the RELAP analysis (Figure 2.3), it was found that the containment pressure builds up initially to 2.75 bar and then decreases to 1.9 bar. The flow rate from the containment suddenly rises to nearly 22 kg/s and then drops very fast to about 2.5 kg/s, and then remains steady at nearly 1 kg/s. The transition time for the decrease in pressure is very small. Hence, the flow remained within 2.5 to 1 kg/s at 78 kPa (g) for most part of the transient venting conditions (i.e. 0.10-0.02 kg/s per venturi scrubber). This was therefore marked as area of interest for the experiments conducted in the prototypic set-up designed in the present study.

Hence, to understand the venting characteristics of submerged venturi scrubber in such scenarios, a venturi scrubber was designed (shown in Figure 3.1) and investigated for measuring the effect of relevant parameters (i.e. upstream pressure, gas flow rate and submergence heights) for nuclear applications. The two phase axial pressure drop across the venturi scrubber has been measured and the radial pressure difference across the nozzles at the throat section has been studied. The pressure drop profiles have been used for predicting the flow distribution in the venturi scrubber. The decrease in submergence height of scrubber tank is done to understand its implications on liquid loading in venturi scrubber. The theoretical models discussed in literature have been employed for predicting the overall pressure drop in the venturi scrubber and is compared with the experimental results.

#### 4.2.1. Results and Discussion

The venturi scrubber operates because of the radial pressure difference across the nozzles at the throat section which draws liquid from the scrubber tank. Hence, this radial pressure difference causes liquid entrainment in the venturi scrubber. The radial pressure ( $P_{\text{tank}} - P_{\text{th}}$ ) is measured as the difference of the pressure in the scrubber tank and inside of venturi

scrubber at the nozzles in the throat section. Therefore, the two phase pressure drop characteristics measured in the venturi scrubber are related to the measured radial pressure difference across the nozzles in the throat section. Each experiment was repeated 4-5 times.

#### 4.2.1.1. Effect of Upstream Pressure

During venting in accidental scenarios, the upstream pressure from the nuclear reactor is marked by an initially high value at the start, and as time proceeds for prolonged scenarios, it sees a decreased value. So, there is clearly a requirement to understand the effect of upstream pressure on the pressure drop characteristics in the venturi scrubber.

#### 4.2.1.2. High upstream pressure conditions

Figure 4.1 shows the variation in axial pressure drop in the scrubber with gas flow rate ranging from 0.07-0.25 kg/s at high pressure conditions (gas pressure at the inlet of the venturi scrubber is varying from 47 to 54 kPa (g)) at the submergence height of 4.5 m. The pressure drop is found to increase with flow rate in converging section as shown in Figure 4.1. The flow in converging section is only single phase flow and hence the pressure increases with the flow rate as expected. Following Bernoulli's principle, in the converging section, with the decrease in cross-sectional area, the flow velocity will increase resulting in loss in pressure. In the present system, the reference point is taken at the inlet of the venturi scrubber and the pressure drop is measured with respect to that. Consequently, absolute pressure drop measured at different axial locations in the converging section of the venturi scrubber keeping reference as inlet will increase for the converging section. The venturi scrubber throat section starts from 0.15 m, while the nozzles are created 0.05 m after the start of the throat section. The pressure drop stays nearly constant in the throat section ( $0.15 \text{ m} < \text{axial position} < 0.2 \text{ m}$ ) before the nozzles in the throat section indicating that the friction losses are negligible. After the injection of liquid through the nozzles, the pressure further decreases due to the momentum exchange between the entrained liquid and the gas. Hence, the pressure drop is observed to increase in the throat

section after the injection of water at the nozzles in the throat section. In addition to this, the entrained liquid at the throat section of the venturi scrubber also experiences shear because of the difference in velocities and this follows the break-up and the formation of droplets. This occurs at the expense of momentum transferred (interaction) by the gas phase to the entrained liquid. Higher is the interaction, higher will be the decrease in pressure, consequently smaller droplets will be formed. In the diverging section of the venturi scrubber, pressure recovery is seen. The pressure drop is recovering up to axial position of 1.6 m for all the flow rates after that it is constant.

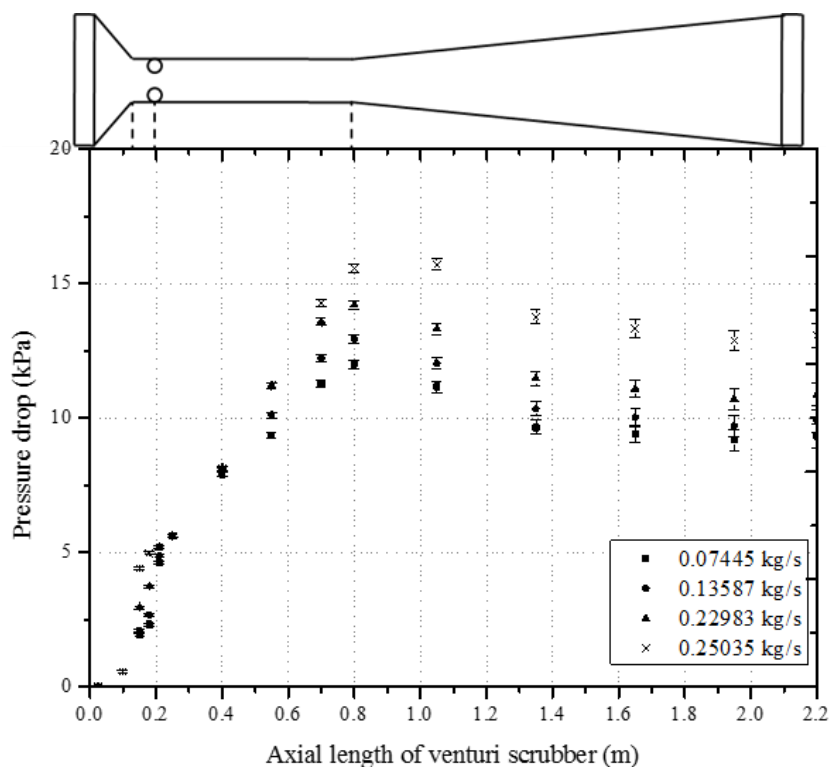


**Figure 4.1** Pressure drop as a function at different gas flow rates for high flow conditions for initial submergence height of 4.5 m.

Figure 4.2 shows the radial pressure difference at the throat section for the gas flow rates ranging from 0.07-0.25 kg/s. At high gas flow of 0.25 kg/s, a sudden decrease in radial pressure difference across the throat is observed, which indicates that the liquid suction decreases at high gas flow rates.

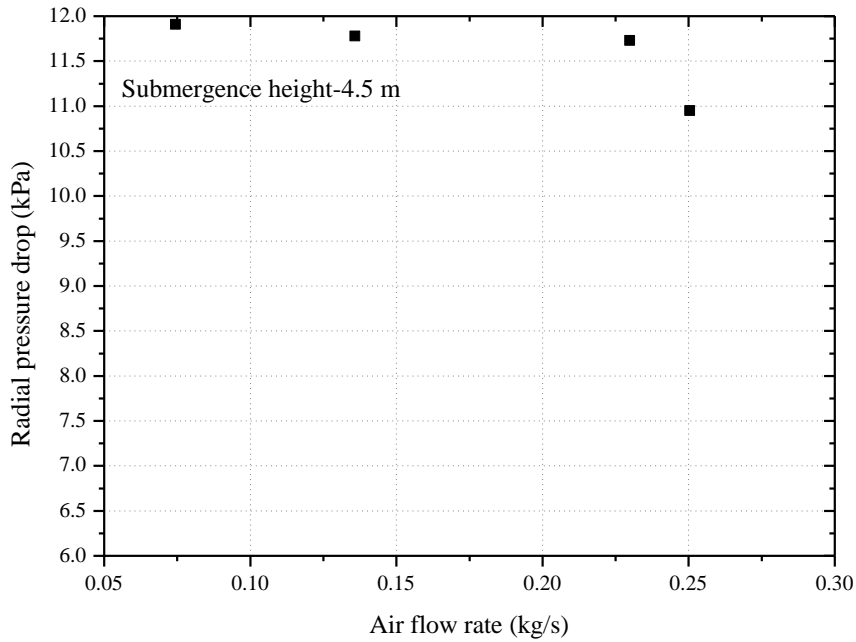


**Figure 4.2 Radial pressure across the throat at different gas flow rates for initial submergence height of 4.5 m.**

The trend of pressure drop observed in the experimental measurements is similar for all the flow rates though the magnitude differs in all the cases (Figure 4.1). The increase in pressure drop in the throat section is the highest for the flow rate of 0.25 kg/s indicating that the momentum exchange between the entrained fluid and the continuous phase is the highest. The sudden decrease in radial pressure in Figure 4.2 is supported by the pressure drop variation in venturi scrubber shown in Figure 4.1. The sudden decrease in radial pressure indicates a sharp increase in liquid loading which should result in higher pressure drop across the venturi scrubber. The data shown in Figure 4.1 connects with this logic.

The pressure does not start recovery just at the start of the diverging section at the axial location of 0.8 m for this flow rate unlike that for other flow rates. This implies that the inertia of the gas phase is high enough to accelerate the liquid entrained in the diverging section which also compensates its recovery in the axial location in the venturi scrubber for this gas flow rate. The magnitude of pressure drop observed in the venturi scrubber throat section indicates the

extent to which entrained liquid has disintegrated into droplets and accelerated in the domain. Therefore, with the increase in gas flow rate, it can be said that the fraction of droplets i.e. dispersed phase existing in the throat section is increasing.

#### 4.2.1.3. Low upstream pressure conditions

Figure 4.3 shows the variation in axial pressure drop in the scrubber with gas flow rate ranging from 0.04-0.10 kg/s at low pressure conditions (gas pressure at the inlet of the venturi scrubber is varying from 37 to 42 kPa) at the submergence depth of 4.5 m. In the converging section of the venturi scrubber, the pressure drop is found to increase with gas flow rate in the similar way as observed in high pressure conditions in Figure 4.3. In the throat section, after entrainment at the throat nozzles, there is an increase in the pressure drop similar to that seen in Figure 4.1. The increase in pressure drop is however lesser as compared to Figure 4.3. For low pressure and flow conditions, there is a slight increase in the pressure drop in the diverging section unlike that observed at high pressure condition. For all the flow rates, the overall pressure drop is found to increase with the gas flow rate.

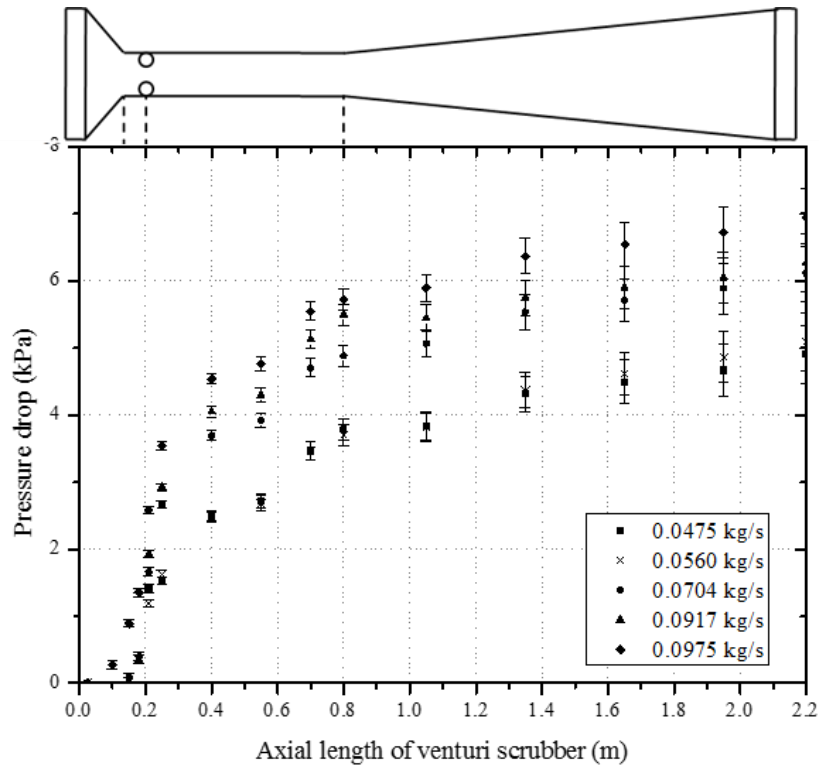


*Figure 4.3 Pressure drop (for low flow conditions) as a function at different gas flow rates for initial submergence height of 4.5 m.*

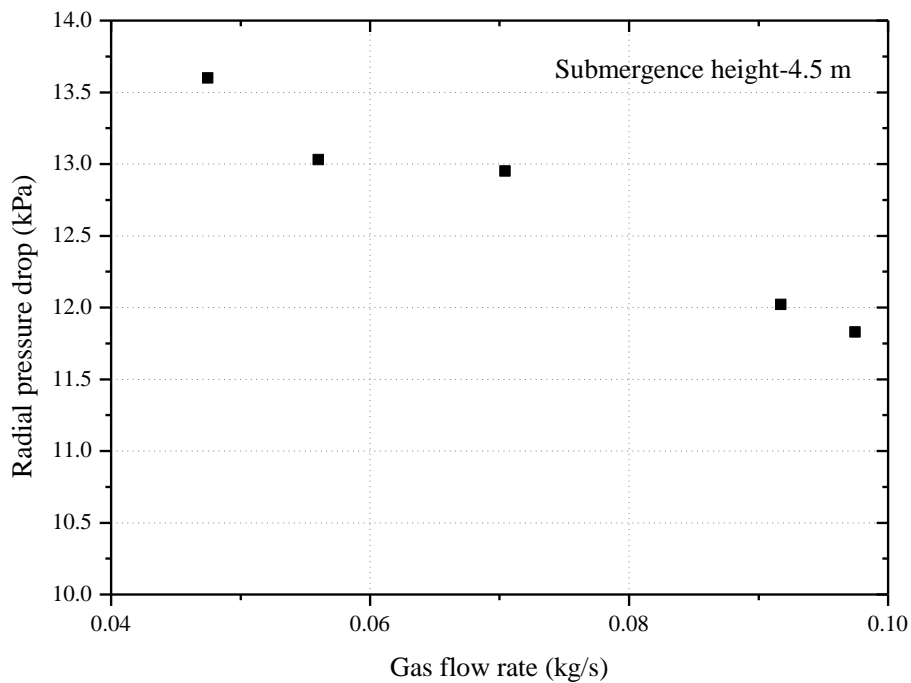


*Figure 4.4 Radial pressure across the throat at different low gas flow rates for initial submergence height of 4.5 m.*

The reason of this pressure drop profile is closely related to the two-phase flow distribution expected in the venturi scrubber in the condition of low inertial gas phase. The momentum exchange between the two phases is lesser in the cases shown in Figure 4.3 due to which the deformation, acceleration and disintegration of entrained liquid is lesser and hence the fraction of liquid film is higher. This is indicated by the radial pressure difference across the throat which is in the range of 11 kPa and above for the high upstream pressure (Figure 4.2) which allows lesser inflow of liquid compared to Figure 4.4. In the diverging section, the interfacial friction is more than the momentum gain by the gas flow and entrained liquid which prevents pressure recovery.

On comparing the radial pressure difference across the nozzles for the case  $\sim 0.07$  kg/s in Figure 4.2 and Figure 4.4, it can be seen that the values are 11.91 and 12.95 kPa respectively. These two experiments were conducted for the same gas flow rate at different operating pressure (measured by the Pressure Transmitter located at the bottom of the venturi scrubber). In the condition of high pressure, the Pressure transmitter reading was 47 kPa(g), while in low pressure conditions the recorded gauge pressure at the inlet of venturi scrubber was 37 kPa(g). This clearly implies that at low pressure conditions, the driving force for the suction of entrained liquid is higher and hence the expected inflow of liquid is higher.

#### 4.2.1.4. Effect of submergence height

To investigate the effect of submergence height on the suction pressure at the throat section, experiments were conducted for two submergence heights of liquid, i.e. 4.5 m and 4 m as shown at low pressure conditions for different gas mass flow rates as shown in Figure 4.5. The gas mass flow rates are varied in the range of 0.04-0.10 kg/s for both the submergence depths. Figure 4.5 shows that for lower submergence depth of water column (4 m), the radial pressure difference across nozzles is lower for all the flow rates as compared to that for 4.5 m.

This indicates higher suction of liquid is occurring at 4.5 m depth of water column as compared to 4 m submergence depth especially for low gas flow rates.

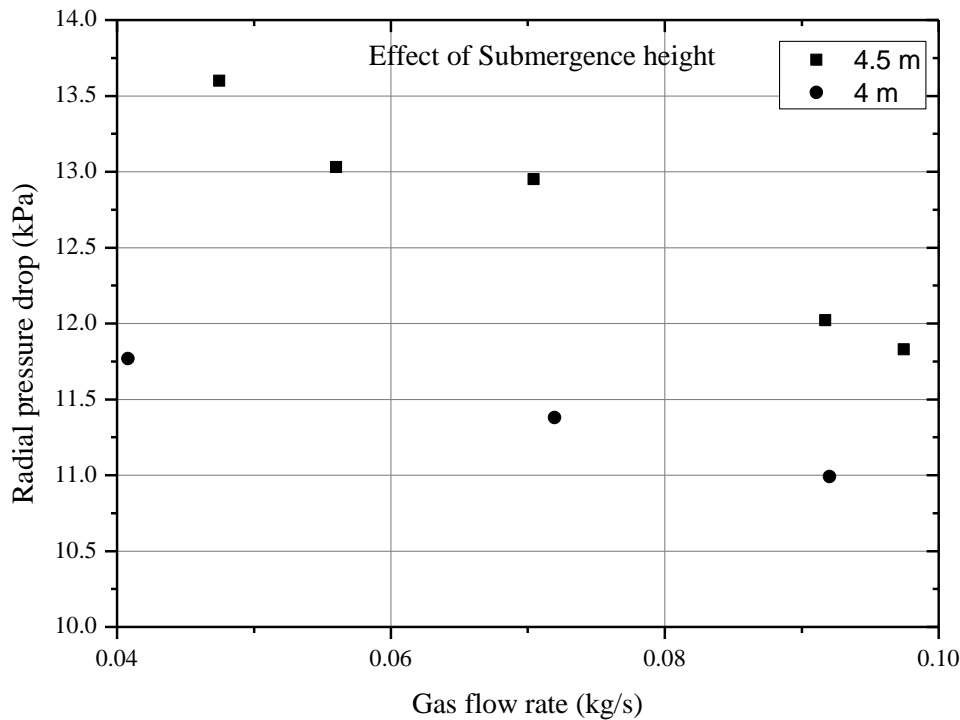


**Figure 4.5 Comparison of radial pressure across the throat for two submergence heights: 4 m and 4.5 m.**

### 4.3. Iodine vapour retention

The two important parameters affecting the system hydrodynamics as seen in the previous section are the gas flow rate and the submergence height. Since the hydrodynamics is closely linked with the vapour retention in the experimental facility, these two parameters are investigated and the measurements on the retention are discussed.

#### 4.3.1. Effect of gas flow rate

The iodine retained in the scrubber tank is shown in Figure 4.6 for submergence height of 4 m and the gas mass flow rates varying in the range of 0.04-0.10 kg/s. In all these experiments (Table 4.1), a known weight of iodine was charged in the iodine dispenser. The

quantity of the residual iodine left after the experiment in the scrubber tank (sample collected from location 1 (Figure 3.3)) was analyzed by ICP-OES technique.

**Table 4.1 Experimental conditions for iodine retention**

Expt No.	Gas mass flow rate (kg/s)	Iodine charged in the iodine dispenser (g)
Submergence height:3 m		
Expt No. 1	0.044	100
Expt No. 2	0.055	100
Expt No. 3	0.074	100
Expt No. 4	0.086	100
Submergence height:4 m		
Expt No. 5	0.045	100
Expt No. 6	0.060	100
Expt No. 7	0.082	100
Expt No. 8	0.090	100
Expt No. 9	0.094	100
Submergence height:4.5 m		
Expt No. 10	0.121	35
Expt No. 11	0.055	140
Expt No. 12	0.097	200

The iodine retention in the scrubber tank is found to increase steeply at flow rates upto 0.06 kg/s after that the increase is smaller. Overall, there is a monotonic increase in iodine removal efficiency with the gas flow rate as shown in Figure 4.6. An efficiency of more than 95% is recorded for the mass flow rate of 0.1 kg/s.

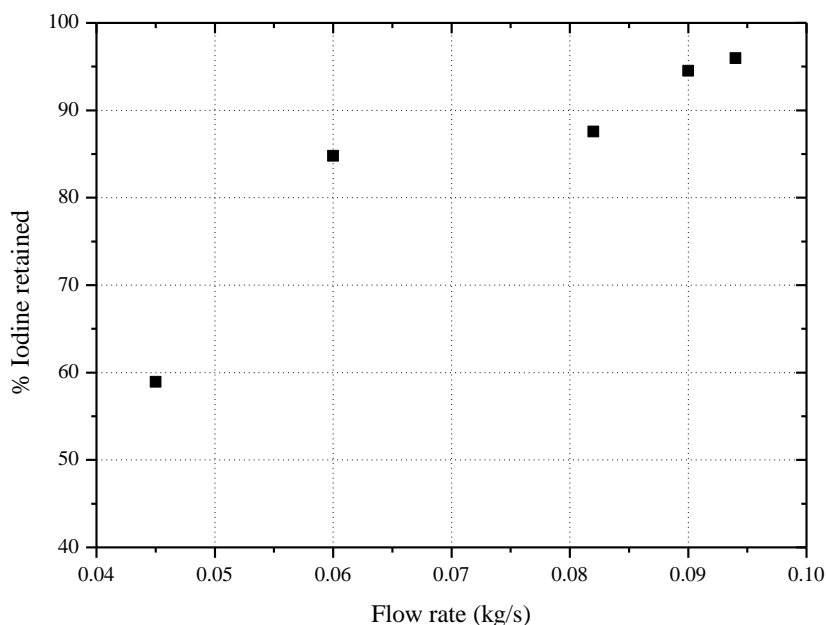


**Figure 4.6 Percentage iodine retained during experiments for flow rates varying from 0.04-0.1 kg/s at the submergence height of 4 m.**

As discussed in the previous section, an increase in gas flow rate increases the number of droplets in the venturi scrubbers. These droplets act as collector surface for absorbing the incoming iodine vapours. So, a higher efficiency is expected when the aqueous solution is highly dispersed in the venturi scrubber. According to the correlations suggested in the literature (Nukiyama and Tanasawa (1938); Boll (1973)) the diameter of the droplets is inversely proportional to the gas flow rate. So, higher is the number of droplets, higher will be interfacial area available for vapour absorption. Therefore, increase the number of droplets increases the mass transfer of iodine in it.

### 4.3.2. Effect of submergence height on iodine retention

Under identical mass flow conditions (ranging from 0.04-0.1 kg/s), the measurements of iodine retention in the scrubber tank were compared for two submergence heights of 3 m and 4 m is shown in Figure 4.7. The sample is collected from location 1 after the experiment is done. The scrubbing performance of the system increases with increasing flow rate. On comparing the two submergence depths, it is observed that at mass flow rate of  $\sim 0.045$  kg/s the effect of submergence height on the overall removal efficiency is appreciable but as the flow rate increases the experimental values for both of the submergence heights converge to similar values.

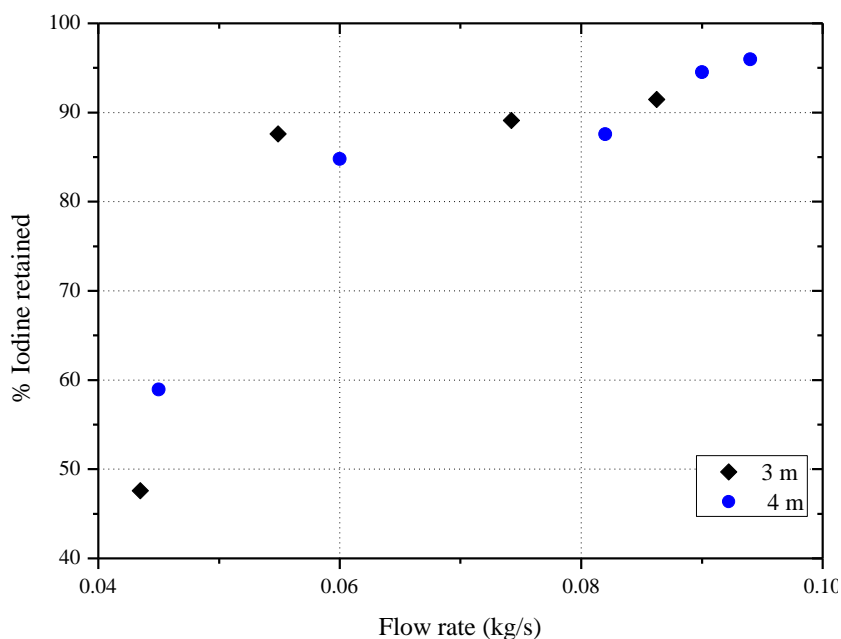


**Figure 4.7 Percentage iodine retained during experiments for different gas mass flow rates at two submergence heights: 3 m and 4 m.**

After escaping from the venturi scrubber, the gas plume passes through the submerged bed in the form of bubbles and interacts with the alkaline solution in it. In case of higher submergence, the probability of interaction or in other words retention time of iodine vapours in the scrubber tank increases, hence higher efficiency is expected in the case of 4 m height.

Another important conclusion that can be drawn from Figure 4.7 is that at high gas flow rates the water column above the venturi scrubber does not contribute to the retention of iodine vapour scrubbing because the interaction time is reduced by high flow rate.

Hence, it is seen that the major contribution to the scrubbing or retention of iodine vapours is coming from venturi scrubber and alkaline pool. This study is further extended to study the overall decontamination for few cases considering the scrubber tank; tank internals; demister pad and vent line to be the participating components of the test facility in the measurement.

### 4.3.3. Iodine vapour decontamination

Although the iodine retained in the scrubber tank solution gives an absolute idea of the minimum decontamination achieved by the system, there is a further need to quantify the amount of iodine escaping the facility untreated. This essentially differentiates the performance of the submerged venturi scrubber from the tank internals and other components of the facility.

For this purpose, sampling of iodine vapours concentration is done at the outlet of scrubber tank at location 2 by purging compressed air from the experimental facility in three flasks containing 2% by weight of sodium carbonate solution. The samples are further analyzed by ICP-MS technique to quantify the amount of dissolved iodine in the bottles and hence the outlet concentrations of iodine vapours are calculated. After 30 min of experimentation, the dissolved iodine in each flask is measured. This gives an estimate of the total amount of iodine leaving untreated through the facility. Table 4.2 presents the decontamination of the experimental facility; the amount of iodine vapours escaping from the facility along with the retention of iodine vapours by the submerged venturi scrubber for submergence height of 4.5 m. The concentration of iodine dissolved in the sampling bottles containing sodium carbonate solution is measured to calculate the decontamination by the facility.

**Table 4.2 Summary of DF of iodine measured during experiments**

Gas mass flow rate (kg/s)	Amount of iodine charged (g)	Concentration of dissolved iodine at the outlet of venturi scrubber (ppb)			Total amount of dissolved iodine at the outlet of venturi scrubber ( $\mu\text{g}$ )	Calculated amount of Iodine leaving untreated (g)	DF	Iodine removed by the venturi scrubber and alkaline pool(%)
		F-1	F-2	F-3				
0.12	35	BDL *	BDL *	BDL *	-	-	Very high	70.63
0.056	140	1971	967	932	1935	0.6148	228	84.32
0.097	200	165	92	87	172	0.0811	2466	82.15
* BDL-Below Detection Limit -1.1 ppb								

F-1, F-2 and F-3 represent the concentration of the dissolved iodine (in ppb) in the samples of ICP-MS collected from the outlet of the venturi scrubber sampling bottles (shown in the Figure 3.4) for each experiment. The values given in each column are cumulative values calculated from the samples collected at the end of each test.

Sample Calculation for Table 4.2 :

$$\text{Total amount of dissolved iodine } (\mu\text{g}) = \sum_{i=1}^3 (\text{Conc in each bottle (ppb)})$$

$$* \text{ Volume of alkaline solution in sampling bottle } (= 0.5 \text{ l})$$

$$=(0.5 \times 165)+(0.5 \times 92)+(0.5 \times 87)$$

$$=172 \mu\text{g}$$

The sampling line at Location 2 (shown in Figure 3.3) is a 3/16 inch pipe with a valve in it. This outlet line is connected to three sampling bottles containing 2% by weight sodium carbonate solution through silicone tubing during the whole experiment. The concentration of

iodine collected from the vent line exiting the venturi scrubber at the inlet flow rate of the gas =  $172 \times 7 \text{ lpm} / 3300 \text{ lpm} (=0.097 \text{ kg/s: gas mass flow rate at venturi scrubber inlet}) = 0.0811 \text{ g}$

The ratio of inlet iodine to the outlet iodine weight calculate from above procedure gives the Decontamination Factor (DF).

$$DF = \frac{\text{Inlet concentration of iodine}}{\text{Outlet concentration of iodine}} = \frac{200}{0.0811} = 2466.5$$

From the above values, it is observed that, the amount of iodine escaping the facility is found to be insignificant irrespective of the amount of iodine charged into the system. This is because of the substantial affinity of iodine vapour to deposit on internal surfaces existing prior to the sampling port present in the facility. Just upon escape from the pool of alkaline solution, the demister pad and tank wall serves as potential surfaces for iodine deposition. From the experiments conducted, it is found that the contribution of tank internals towards overall decontamination is appreciable. The decontamination observed at the outlet is a trade-off between the retention in the scrubber pool and the deposition on the tank internals, which includes the demister pad, un-wetted tank walls and outlet pipeline to the sampling point. Nonetheless, the performance of the facility is largely governed by the venturi scrubber design where significant amount of the bulk decontamination takes place although the presence of tank internals further improves the DF of the total facility.

#### 4.4. Theoretical Evaluation of pressure drop across the venturi scrubber

Mathematical modeling of pressure variation in the venturi scrubber is complicated because of the multiphase flow behavior and the complex interaction of the multiple phases. In the present case, the superficial throat gas velocity varies from 14-70 m/s. Therefore, experiments have been done in the past to model for forced feed venturi scrubbers (Table 4.3).

**Table 4.3 Summary of experimental works in forced feed venturi scrubbers**

	Throat velocity (m/s)	Liquid loading (l/m <sup>3</sup> )
Allen and Van Santen (1996)	45-115	0.2-1.2
Boll (1973)	45-92	0.6-2.4
Gamisans <i>et al.</i> (2002)	8-27	2.9-23.5
Guerra <i>et al.</i> (2012)	59-74	0.1-0.25
Haller <i>et al.</i> (1989)	50-100	0.55-2.75
Silva <i>et al.</i> (2009)a	34-70	0.015-0.19
Viswanathan <i>et al.</i> (1985)	46-76	0.4-1.2

It was concluded in our studies that the pressure drop across the venturi scrubber increased with increase in gas velocity, which is similar to the observation in all the studies conducted on forced feed venturi scrubbers (referred in Table 4.3). Pressure drop models have been proposed for such systems in which the liquid entrainment is an input to the scrubbing system unlike that in submerged venturi scrubber system. In this context, first simplified theoretical model was suggested by Calvert (1970) where the sole reason of pressure drop was stated to be the acceleration of the entrained phase. Boll (1973) discussed differential equations accounting for wall friction and momentum exchange between the two phases in the pressure drop calculation. The model assumed complete atomization of the liquid and their size was estimated from Nukiyama and Tanasawa (1938) equation similar to Calvert's model. Hesketh (1973) proposed an experimental correlation by fitting the data from many experiments. He

incorporated throat area ( $A_t$ ) in his correlation. Goel and Hollands (1977) presented the solution of Boll's differential equation in dimensionless number and charts which were simple to use. Till now, the complete atomization of entrained liquid and mono disperse droplets were considered. This shortcoming was identified by Azzopardi and Govan (1984) and Viswanathan *et al.* (1985) and they proposed annular film model for pressure drop estimation. Azzopardi and Govan (1984) discussed that the roughness of the wall film also contributes to pressure drop in the venturi scrubber. Viswanathan *et al.* (1985) experimentally measured the liquid film fraction for the venturi scrubber and proposed to evaluate it empirically for finding the pressure drop in a new scrubber. An annular two-phase flow model was hence developed for the accurate prediction of the pressure drop using film-flow correlation.

From the literature, it is clear that there are a few models reported as above for forced feed venturi scrubber systems in which the liquid entrainment is an input to the scrubbing system unlike that in submerged venturi scrubber system. In absence of any models for submerged venturi scrubber system, it is prudent to apply these models to submerged systems and check their applicability and limitations.

#### 4.4.1. Evaluation of liquid loading

The pressure drop across the scrubber has been estimated from the theoretical models available in the literature and compared with the experimental values. These models require the liquid loading as an input. The liquid loading across all the cases for submergence height of 4 m and 4.5 m has been estimated from the measured radial pressure difference across the nozzles in the throat section as given in equation (4.1).

$$P_{th} - P_{tank} = \frac{K}{2} \rho_l v_l^2 \quad (4.1)$$

where  $v_1$  is the velocity of entrained droplets into the throat section,  $P_{th}$  indicates the pressure at the inside of venturi scrubber due to gas flow and  $P_{tank}$  indicates the hydrostatic pressure in the scrubber tank just outside of the nozzles in the throat section. The measured pressure drop ( $P_{th} - P_{tank}$ ) has been equated with the pressure loss due to flow of droplets through the small sized nozzles located in the throat section. The  $P_{th} - P_{tank}$  is given by the difference of pressure reading given by the value of DPT at  $x=0.18$  m and Level Transmitter (Table 3.2). Their accuracies are  $\pm 0.686$  kPa and  $\pm 0.0588$  kPa respectively. The uncertainty in analysis in pressure difference is therefore  $\pm 0.75$  kPa.

The loss coefficient (K) is considered to be 0.4 at the nozzle entrance (McCabe *et al.* (1957)). The liquid loading ( $q_l$ ) is defined as the ratio of total volume of liquid entrained in the venturi scrubber to the volumetric gas flow in the venturi scrubber (in  $l/m^3$ ). The liquid loading has been estimated from the velocity of liquid ( $v_L$ ) (equation (4.2)).

$$q_l = \frac{\text{no. of nozzles} * (\rho_l * \text{Area of nozzle} * v_L)}{\rho_g * \text{Inlet Area of venturi} * \text{velocity at inlet of venturi}} * 1000 \quad (4.2)$$

The calculated values of liquid loading to the scrubber are found to decrease with the increase in flow rate of gas as seen in Figure 4.8. This is consistent with the self-priming behavior of the Venturi scrubber (Lehner (1998); Ali *et al.* (2013)). It is also seen in Figure 4.8 that the liquid loading to the scrubber in low pressure conditions is 3-4 times higher than the values calculated for high pressure conditions.

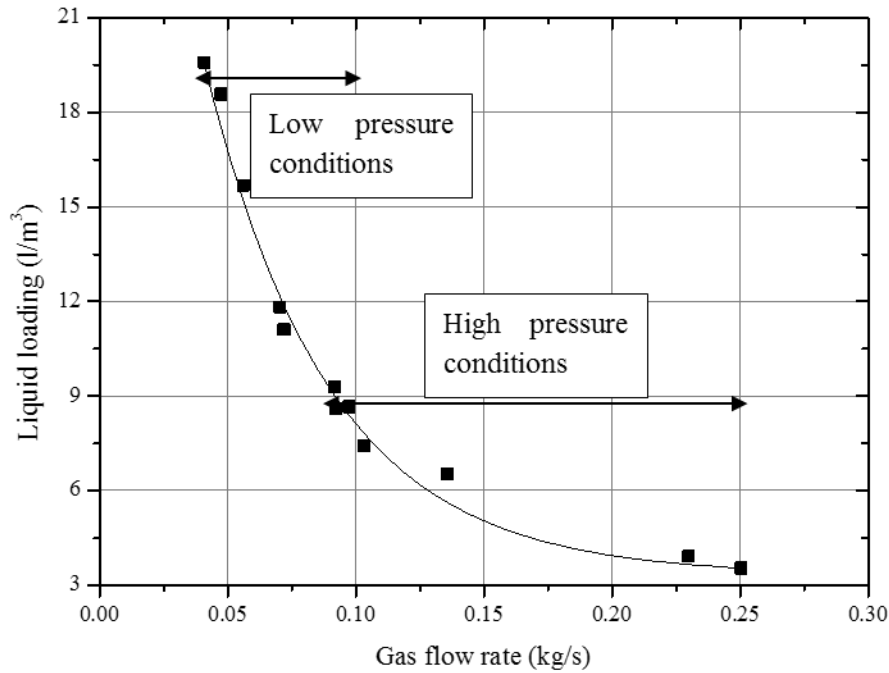


**Figure 4.8** Theoretical prediction of liquid loading and corresponding pressure drop across venturi scrubber

#### 4.4.2. Prediction of pressure drop from empirical models in the literature

Thus, knowing liquid loading to the scrubber, the pressure drop across the scrubber is estimated from the theoretical models available in the literature and compared with the experimental values as shown in Figure 4.9. The equations of pressure drop are summarised in Table 4.4.

**Table 4.4** Empirical relation for pressure drop in the venturi scrubber

Hesketh model for pressure drop given in equation (4.3) as

$$\Delta P = 1.36 * 10^{-4} * v_g^2 * \rho * \left( \frac{Q_l}{Q_g} \right) * A_t^{1.33} [0.56 + 935 (q_l) + 1.29 * 10^{-5} (q_l)^2] \quad (4.3)$$

Calvert model for pressure drop given in equation

(4.4) as

$$\Delta P = 10^{-3} v_g^2 \left( \frac{Q_l}{Q_g} \right) \quad (4.4)$$

The terms appearing in equation (4.3) and (4.4) are  $Q$  (volumetric flow rate ( $\text{m}^3/\text{s}$ )),  $A_t$  (throat cross-sectional area ( $\text{m}^2$ )),  $\rho$  (density of gas ( $\text{kg}/\text{m}^3$ )),  $v_g$  (Superficial gas velocity in the throat section ( $\text{m}/\text{s}$ )) and  $q_l$  (Liquid to volumetric gas flow rate ratio ( $1/\text{m}^3$ )).

It is seen that Calvert's model prediction is close to measured values for all the cases as compared to other two models. A closer look to the experimental profile of pressure drop in Figure 4.3 suggests that the pressure recovery is not seen which is attributed to either wall film formation or high mass liquid loading. The Calvert's model assumes that the sole reason of pressure drop is liquid acceleration and the liquid is disintegrated into monodispersed droplets having the velocity of continuous phase. Either of the two reasons is not accounted in the empirical correlation and therefore, it can be claimed that the Calvert's model over predicts the pressure drop due to its simplified basis. Hesketh correlation failed for all the cases for the present case. Though Hesketh considers throat area but the model has been derived for short throat lengths and here the venturi scrubber has a relatively larger throat length. Such empirical correlations fail to predict reasonably when applied to conditions far from where they were obtained.

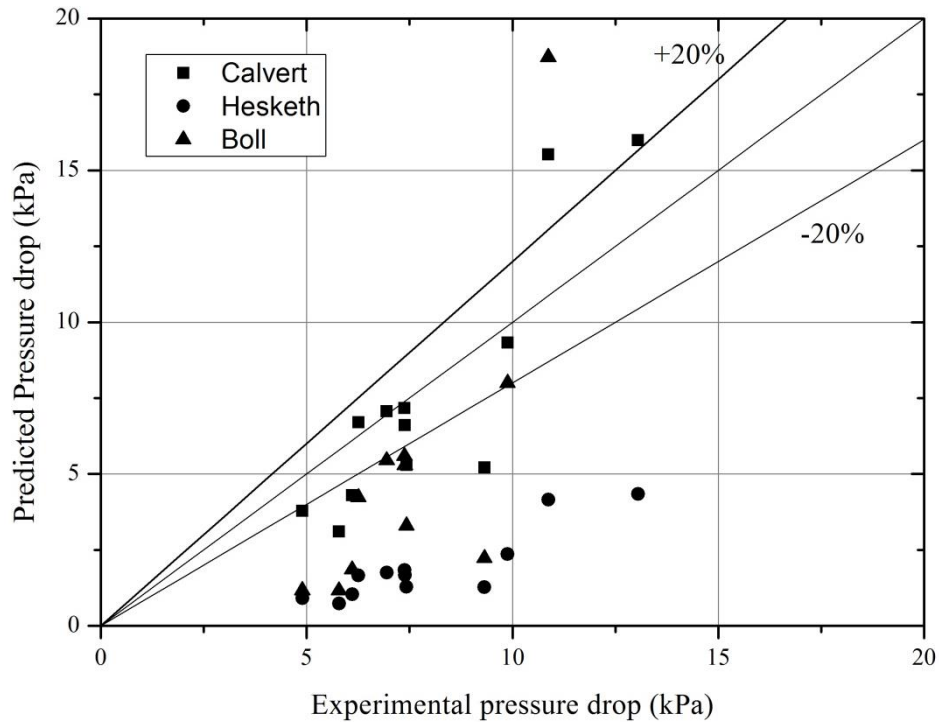


**Figure 4.9 Comparison of predicted pressure drop with measured pressure drop**

The Boll's model accounts for gas wall friction, gas acceleration and the liquid acceleration in the differential equations of pressure drop and assumes 100% atomization. It is also assumed that the coefficient of friction is constant which gives a good prediction for the cases verified in the derivation. Another probable reason for difference in pressure drop prediction can be the incorrect estimation of liquid loading to the scrubber. The liquid entrainment in the venturi scrubber is opposed by the co-flowing compressed air in the venturi scrubber. So, the interfacial friction may vary from a constant value of 0.4 as considered here. The open literature available for self-priming venturi scrubbers have no model for liquid loading. Therefore, this simplistic model for liquid loading cannot be validated.

#### 4.5. Closure

The FCVS design is important for protecting the integrity of the containment under beyond design basis scenarios. It helps in depressurization and retention of radionuclides, which could spread in the environment. Amongst all the radionuclides generated by the fission

reactions, iodine in vapour form is one of the most detrimental radionuclide to human health, hence its retention is a stringent requirement. The scrubbing behavior of FCVS to retain radionuclides when operated in submerged mode depends on the hydrodynamics occurring inside the venturi scrubber for which limited studies are available. Therefore, full scale experimental facility is built with the objective to simulate iodine vapour retention as a function of gas mass flow rate using alkaline solution of sodium thiosulphate and sodium hydroxide solution in the scrubber tank. The characterization of hydrodynamics in the venturi scrubber is done by measuring the axial pressure drop at various axial locations and the radial pressure drop at the nozzles of the scrubber which allows passive injection of aqueous solution from the scrubber tank. The experiments for investigating scrubbing efficiency were also carried out under various submergence height of the venturi scrubber (3 m and 4 m). The major observations are:

Hydrodynamics of submerged venturi scrubber:

- a) In general, it is found that the pressure drop increases with gas flow rate for both low and high pressure conditions.
- b) For high pressure conditions, the radial pressure at the nozzles in the throat is almost invariant for the flow rates 0.07-0.25 kg/s but at very high gas mass flow rate of 0.25 kg/s, a sudden decrease in pressure is observed. The pressure drop values in the venturi scrubber reveal an increase in the converging section, a sharp increase in the throat section after the entrainment and gradual recovery in the diverging section.
- c) In low pressure conditions, there is no pressure recovery in the diverging section of the venturi scrubber unlike that at higher gas pressure cases.
- d) The radial pressure difference across the nozzles in the throat increases with the decrease in gas flow rate, which is an important aspect for scrubbing liquid loading into the venturi scrubber.

- e) At low inlet pressure, submergence height of venturi scrubber is decreased to 4 m. This decreased the radial pressure across the throat. This measured radial pressure difference is employed to predict liquid loading to the scrubber. The estimated liquid loading at the nozzles in the throat section is found to decrease with increase gas flow rate both at high and low pressure conditions.
- f) The overall pressure drop incurred in the submerged venturi scrubber is estimated from correlations of forced feed venturi scrubbers of Boll, Calvert and Hesketh. It was found that none of the correlation gave results within  $\pm 20\%$  range for all the cases studied.

Results on iodine scrubbing measurements in the experimental facility showed that

- a) The total amount of iodine exiting through the vent line is insignificant.
- b) The scrubbing behavior of submerged scrubber was measured as a function of gas mass flow rate (from 0.04-0.1 kg/s). It was found that an increase in gas flow rate from 0.045 kg/s to 0.06 kg/s, increased the percentage retention of iodine in the scrubber tank increased from 60% to 85%. However, a further increase in gas flow rate showed a lesser effect on the scrubbing performance of the submerged venturi scrubber with the efficiency rising to 95% for 0.1 kg/s.
- c) Effect of submergence depth of venturi scrubber on the retention of iodine vapours in the scrubber tank was investigated for submergence height of 3 m and 4 m. The scrubbing performance appreciably improved with the submergence depth for the gas flow rate of  $\sim 0.045$  kg/s, but for high gas flow rates, the experimental values for both the submergence heights converge to similar values.

## **Chapter 5. Development and Benchmarking of CFD Model for predicting FCVS performance**

### **5.1. Introduction**

The complex three-phase flow occurring in the venturi scrubber represents an intricate case of interacting phases resulting in deformation, breakup and coalescence of the droplet phase. These droplets interact with aerosols and vapours to retain them. The hydrodynamics of the venturi scrubber depends on the jet penetration, droplet distribution and the extent to which these droplets intercept the incident aerosol particulates. For passive operation, as in the case of nuclear industry, the venturi scrubber is required to achieve high capture efficiency for a wide range of aerosol size at varying operational transients without any external intervention. Though there are studies in the literature on droplet break-up mechanisms, none demonstrates the spray characteristics of the multi-jet injection with respect to the application of the venturi scrubber to such imposing conditions. Hence, in order to arrive at an efficient scrubber design for submerged operation, there is a need to develop an analytical tool, which can predict the scrubber performance based on the multi-jet characteristics prevailing in the throat section of the scrubber. There has been no attempt to model self-priming venturi scrubber in literature. Another additional issue is that the liquid loading in self-priming venturi scrubber is not an independent parameter (as in forced feed venturi scrubber) rather it is a function of flow parameters. Therefore, first attempt was made for forced feed venturi scrubbers due to the availability of inputs i.e. gas velocity and liquid loading at the nozzles in the throat section. It was found that the empirical models could not predict the measured values and were off by more than  $\pm 20\%$ . Then the same model was applied for self-priming venturi scrubbers.

Since, the spray characteristics inside the scrubber do not depend on the mode of operation, a computational model based on Euler-Lagrangian framework was employed to simulate the flow characteristics in the scrubber operating in forced-feed mode while subjecting it to various operating conditions. The first step taken here to achieve this is to validate this model against published results on forced feed venturi scrubbers (Haller *et al.* (1989)). The present model differs from earlier proposed models of Pak and Chang (2006), Goniva *et al.* (2009) and Ali *et al.* (2013) by incorporating the inertial effects assisting droplet breakup, the increased momentum source and droplet coalescence for regions of high liquid concentration.

The particle laden gas flow interacts with the multi-jet liquid injection occurring at the throat section of the scrubber. The shear force acting on the jet surface results in the entrainment of smaller droplets into the gas domain. Depending on the flow conditions prevailing in the throat section of the venturi scrubber, the extent of droplet deformation, breakup and coalescence is realized. The gas phase flow is modeled through an Eulerian framework while the dispersed droplets and the particulates are tracked in a Lagrangian framework. To reduce the computational complexity, particles having identical diameter, velocity and spatial position are clubbed and referred as parcels (O'Rourke (1981)).

### 5.1.1. Eulerian Gas Flow

The gas flow is assumed to be incompressible, turbulent and isothermal. The Reynolds-averaged Navier–Stokes equation along with the RNG  $k$ – $\epsilon$  turbulence model (Orszag *et al.* (1993)) is employed to simulate the continuous air flow. The generalised momentum equation, accounting the volume occupied by the dispersed phase, is given by equation (5.1). Since the volume fraction of the droplets is less than 10%, equation (5.2) represents a simplified form of the carrier phase momentum equation. The details of each term in the equation can be found elsewhere (Anderson and Jackson (1967)).

$$\begin{aligned} \frac{\partial}{\partial t} ((1 - \alpha_d)\rho\mathbf{u}) + \nabla \cdot ((1 - \alpha_d)\rho\mathbf{u}\mathbf{u}) & \quad (5.1) \\ & = -(1 - \alpha_d)\nabla P + \nabla \cdot [(1 - \alpha_d)\boldsymbol{\tau}] + (1 - \alpha_d)\rho\mathbf{g} + S \end{aligned}$$

where  $\alpha_d$  is the volume fraction of the droplets in the computational cell,  $\rho$  is the density of the gas phase,  $\mathbf{u}$  is the gas velocity,  $P$  is the pressure,  $\boldsymbol{\tau}$  is the stress tensor and  $S$  is the source term due to the interaction with droplets

$$\frac{\partial}{\partial t} (\rho\mathbf{u}) + \nabla \cdot (\rho\mathbf{u}\mathbf{u}) = -\nabla P + \nabla \cdot \boldsymbol{\tau} + \rho\mathbf{g} + \frac{S}{(1 - \alpha_d)} \quad (5.2)$$

$$\text{where } \boldsymbol{\tau} = \mu \left[ (\nabla\mathbf{u} + \nabla\mathbf{u}^T) - \frac{2}{3}\nabla \cdot \mathbf{u} \mathbf{I} \right]$$

where  $\mu$  is viscosity,  $\mathbf{u}$  is velocity and  $\mathbf{I}$  is unit tensor.

The volume fraction (equation (5.3)) is evaluated as the ratio of summation of the volume occupied by each parcel to the volume of the computational cell. In conditions of high liquid loadings, the volume fraction may locally exceed the limiting value. For such conditions, equation (5.4) corrects the momentum source by accounting the volume fraction of the droplets occupied in the computational cell. The momentum source to the gas phase is due to the drag forces acting on the dispersed phase and is proportional to the number of parcels present in the respective computational cell.

$$\alpha_d = \frac{1}{dV} \sum N_d V_d \quad (5.3)$$

$$S = -\frac{1}{dV} \sum N_d \left[ C_D \left( \frac{\rho(\mathbf{u} - \mathbf{u}_d)^2}{2} \right) (A_p) \right] \quad (5.4)$$

where  $dV$  is the volume of the computational cell,  $\mathbf{u}_d$  is the droplet velocity,  $A_p$  is the droplet surface area,  $C_D$  is the drag coefficient and  $N_d$  is the number of particles in a droplet parcel.

### 5.1.2. Lagrangian Tracking of Droplets and Aerosols

The aerodynamic drag force is assumed to dominate the flow of the droplets and the aerosol particles in the scrubber and therefore, is considered as the only force governing the dispersed phase trajectory, given by equation (5.5). As the density of continuous phase (i.e. air) is much smaller than the dispersed phase density, the effect of added mass and Basset history force can be neglected.

$$m_p \frac{d\mathbf{u}_p}{dt} = C_D \left( \frac{\rho(\mathbf{u} - \mathbf{u}_p)^2}{2} \right) (A_p) \quad (5.5)$$

where  $m_p$  is the mass of the particulate phase.

Depending on the turbulent intensity of the gas flow field, the turbulent eddies also affect the trajectory of the dispersed phase (Gosman and Loannides (1983)). This is incorporated by accounting the fluctuating gas velocity through the eddy lifetime model. The extent of turbulent dispersion affecting the dispersed phase trajectory depends on the size of the particulates interacting with the turbulent eddies. The micron sized aerosol particles, as compared to the droplet phase, get largely influenced by the fluctuating gas velocity.

The presence of high aerodynamic forces in the near injection region results in the deformation of the droplet. The extent of deformation is characterised by the droplet's instantaneous Weber number (equation (5.6)). The magnitude of deformation was incorporated to predict the deformed diameter of the droplets by the model of Hsiang and Faeth (1992) as given below.

$$\frac{d_{ef}}{d_d} = \begin{cases} 1 + 0.19 We^{0.5} & We \leq 100 \\ 2.9 & We > 100 \end{cases} \quad (5.6)$$

$$We = \frac{\rho(\mathbf{u} - \mathbf{u}_d)d_d^2}{\sigma_d} \quad Re = \frac{\rho(\mathbf{u} - \mathbf{u}_d)d_d}{\mu} \quad A_p = \frac{\pi d_{ef}^2}{4} \quad (5.7)$$

where  $d_{ef}$  is deformed droplet diameter,  $d_d$  is droplet diameter,  $We$  is Weber number,  $\sigma_d$  is the surface tension of drop,  $\mu$  is the viscosity of the gas and  $Re$  is Reynolds number of droplet.

The aerosol particles are considered to follow the spherical drag coefficient proposed by Schiller and Naumann (1935). The deformed droplets experience higher drag forces (equation (5.10)) due to change in projected area and shape. The shape correction is accounted by incorporating the time-resolved drag correction suggested by Schmehl *et al.* (2000) as given by equation (5.8) to the spherical drag model proposed by Clift *et al.* (1978), as shown in equation (5.9).

$$\text{correction} = We(0.2319 - 0.1579 \log Re + 0.047 (\log Re)^2 - 0.0042 (\log Re)^3) \quad (5.8)$$

$$C_{D,sph} = \frac{24}{Re} (1 + 0.16 Re^{.687}) + \frac{0.42}{4.25^{10^4}(Re^{-1.16})} \quad (5.9)$$

where,

$$C_D = C_{D,sph} + \text{correction} \quad (5.10)$$

where  $C_{D,sph}$  is the spherical drag coefficient.

The near-injection region of the venturi scrubber comprise of multiple column like structures which undergo shape distortion and breakup due to interaction with the high cross flow velocity. Since the above models are developed for isolated droplets, the drag coefficient used in the present analysis is corrected to account for this effect. The presence of the liquid column offers greater resistance to the inertial forces causing the deformation. Hence, a factor of 0.6 was introduced in the deformation equation to limit the peak diameter of the droplets associated with the column structure.

#### 5.1.2.1. Analysis of drag coefficient

The atomization process is caused by the disruption of liquid jet due to the momentum transfer between the entrained jet and air injected. The area of interest in this regard, is therefore, the rate of momentum transfer against their inertial properties. The process of

transferring momentum to the liquid phase is usually promoted by the onset of a relative motion between phases, inducing the inception and propagation of wavy disturbances. Wave crests can eventually evolve in elongated ligaments and undergo detachment from the liquid.

If the liquid phase is highly energetic as in pressure atomizer or on the contrary, the air phase has a significantly high fraction of energy as in air-blast atomizers, the modeling or understanding of disintegration is easier because in such processes the inertia of the liquid can be neglected. However, for the present case of the venturi scrubber, the liquid jet entrained at the nozzles has a radial velocity initially and air injected have kinetic energies, due to which the near injection phenomenon is complex to model. The effect of aerodynamic pressure on the injected jet causes it to deform, which increases its interfacial area and it starts thinning in the direction of flow by forming child droplets at the interface.

The physics of particle laden jets has been reviewed by Faeth and Dahm (2006) and Chen *et al.* (1993). The study focussed on existence of two regions in particle-laden flows: dense region observed near the nozzle and dilute region subsequent to complete breakup. Due to the presence of a column like structure in the near injection region, the resistance to inertial forces resulting in distortion and oscillation is higher as compared to spherical droplets. In view of this, the drag coefficient suggested for isolated droplet cannot be used in the near injection region and therefore, the spherical drag coefficient is corrected to account for the presence of the cylindrical column. As the relative velocity between the drop and continuous phase increases, the inertial forces start to dominate over surface tension forces. Experimentally it is observed that the droplets starts to deform when  $We > 1$ . The droplet break up progresses by the initiation of oscillations at  $We = 1$ . These oscillations continue to grow till the drop surface energy is exceeded by inertial energy which is reported at  $We = 12$ .

### 5.1.3. Droplet Size Distribution

The presence of high interfacial shear on the multi-jet injection results in the growing surface oscillation and subsequent breakup. The sizes of the droplets are governed by the amplitude of the fastest growing wave on the droplet surface. In the near injection region, the droplets get accelerated upon interaction with the carrier phase. The inertial effects of the droplets are therefore accounted by the use of the Kelvin-Helmholtz and Rayleigh-Taylor (KH and RT) breakup model proposed by Beale and Reitz (1999). The model assumes the presence of a liquid column through the injection, given by the Levich core length, where the droplet sizes are evaluated from the wavelength and growth rate of the K-H instability, while for droplets outside the liquid core, both K-H and R-T effects are considered for breakup. The diameter of the child droplet is set proportional to the wavelength of the fastest growing unstable surface wave on the parent droplet. Furthermore, the rate of change of droplet diameter depends on the breakup time, which is inversely proportional to the growth rate of the fastest surface wave. Depending on the nozzle dimensions and relative velocities between the phases (i.e. shearing), the size of the child droplet and the breakup time is evaluated for the parent droplet of diameter based on the fastest growing wave following the K-H or R-T instability. The breakup is allowed only when the mass accumulated from the parent droplet at a rate evaluated from the breakup time which is equal to 5% of the initial mass. Subsequent to breakup, the droplet takes the dimension of the child droplet and the velocity is adjusted so that the momentum is conserved. The detailed model description can be found in Beale and Reitz (1999).

#### 5.1.3.1. Collision of droplets

Conversely, in the region of high droplet concentration, the collision of droplets may result in coalescence and the exchange of momentum between the droplets. The collision model of O'Rourke (1981) is implemented in the present analysis to predict the droplet size and the

velocity distribution of the colliding droplets. For conditions of high liquid loading, the coalescence of the droplets is found to be prominent in the throat section of the venturi scrubber.

#### 5.1.4. Capture of aerosol

Inertial impaction is the dominating mechanism for capture of micron size aerosol in the throat section of venturi scrubber. The single droplet capture efficiency due to inertial impaction depends on the size of the target particles and the relative velocity between them. The efficiency is modeled as a function of the ratio of aerosol stopping distance to the radius of the collector droplet, referred to as the inertial impaction parameter, given in equation (5.11) and (5.12) and evaluated using the model of Calvert (1970).

$$K_p = \frac{\rho_s(u - u_d)d_s^2}{9\mu d_d} \quad (5.11)$$

$$\eta = \left(\frac{K_p}{K_p + 0.7}\right)^2 \quad (5.12)$$

where  $K_p$  is inertial impaction parameter,  $\rho_s$  is the density of aerosol,  $\eta$  is target efficiency and  $d_s$  is aerosol diameter.

The capture of aerosols in the venturi scrubber is modeled with the prime assumption that capture occurs only when the aerosols and droplets occupy the same computational cell. For a parcel containing  $N_s$  number of aerosol particles interacting with a single droplet parcel with  $N_d$  number of droplets, the number of aerosols captured due to inertial impaction is evaluated by equation (5.13) as

$$N_{cap} = \eta \frac{\pi}{4} d_d^2 |\mathbf{u}_s - \mathbf{u}_d| \frac{N_d N_s}{dV} \Delta t, \quad (5.13)$$

where  $N_{cap}$  is number of aerosol particles captured by one droplet in a computational cell,  $u_s$  is aerosol velocity,  $N_s$  is number of particles in an aerosol parcel and  $\Delta t$  is particle time step. The cell velocities of gas phase, droplet and aerosol velocities were used in the calculation.

The total number of aerosols captured is the summation of all the aerosols captured by the total number of droplet parcels present in the cell. The overall scrubbing efficiency of aerosols is evaluated by averaging the cell-based efficiency over the number of participating computational cells.

### 5.1.5. Numerical Algorithm

The finite volume method was employed to obtain the numerical simulation of the dispersed three-phase flow through the venturi scrubber. Using a coupled algorithm, the RANS and  $k-\varepsilon$  equations were set to a simulation framework to obtain the converged gas flow field. The droplets and aerosol particles were then introduced as surface injections at the throat nozzle and the venturi inlet respectively. The mass flow rate is area weighted and the velocity of injection is perpendicular to the flow direction. The dispersed particles were tracked based on the particle time step of the injection. The particle time step is defined as the time difference between two successive injections. At each particle time step, particles in domain are tracked and their position, velocities, diameter and injection of new particles is monitored.

Since the aerodynamic forces experienced by the particles are much higher than the gravitational force, the source term (coupling terms) only include the particle-induced drag terms. The entrainment of the liquid jet is computed through the breakup model as discussed earlier. Collision with the wall surface is assumed to be perfectly elastic for both the dispersed phases. The solution to the above numerical setup provides a distribution map of the dispersed phases throughout the domain of the venturi scrubber. This information, namely the particle position, velocity, number of particles per parcel, is further extracted to compute the scrubbing efficiency of aerosols in the venturi scrubber. The computed efficiency corresponds to a steady configuration of the dispersed phase. Therefore, a number of configurations are analyzed to arrive at an averaged capture efficiency of the scrubber. The model was developed based on

the experimental results reported by Haller *et al.* (1989). The geometry of the venturi scrubber along with the computational mesh is shown in Figure 5.1. The summary of solver settings is given in Table 5.1.

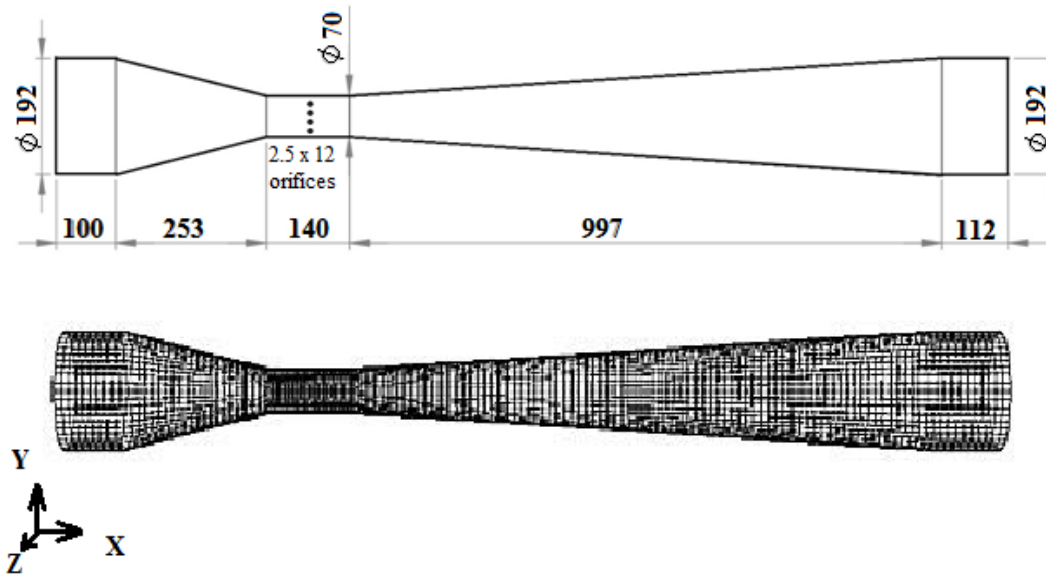


Figure 5.1 Dimension of venturi scrubber (in mm) and the computational mesh

Table 5.1 Summary of Solver Settings

<b>Viscous model</b>	Turbulent k- $\epsilon$ RNG model with standard wall function	
<b>Particle time step</b>	5e-04 s	
<b>Breakup model</b>	KHRT (Break up parameters: ( $B_0$ -0.61, $B_1$ -17, $C_{rt}$ -0.3, $C_{\tau}$ -0.2, $C_L$ -5))	
<b>Boundary Conditions:</b>		
<b>Region</b>	Type	Specification
<b>Venturi Inlet (air)</b>	Velocity Inlet	2.5-12.57 m/s
<b>Venturi Inlet (particulates)</b>	Silica particles	Median diameter (1 micron) (Pak and Chang (2006))
<b>Outlet</b>	Pressure Outlet	Atmospheric
<b>Nozzles</b>	Droplet Injection	Liquid velocity ; Droplet diameter:2-3.5 mm

The scrubber was operated in forced-feed condition for varying gas and liquid flow rates. The results are the measured local liquid to gas mass flow ratios normalized with the overall liquid loading ratio to represent the liquid flux distribution in the throat section of the scrubber. The study also calculates the pressure drop across the scrubber and the scrubbing efficiency of aerosols for particulates (silica particles) of 1-micron median diameter.

## 5.2. Results and Discussion

### 5.2.1. Model Development and Validation

The model for venturi scrubber is validated with Haller *et al.* (1989) results. The initial drop diameter is equal to the diameter of nozzle for all simulations (Wu *et al.* (1997)). The case of 70 m/s throat gas velocity and liquid loading of  $2.75 \text{ l/m}^3$ , defined as the volume of liquid injected into the scrubber per unit volume of air flow, is first discussed cited in Haller *et al.* (1989). The two most important aspects governing the flow through the venturi scrubber is the shear-induced breakup of the multi-jet injection occurring in the throat section and the extent to which these entrained droplets intercept the incident aerosol particles. From modeling point of view, the hydrodynamics of the multi-jet atomization in cross flows significantly depends on the drag and breakup models chosen for the simulation framework. Following the various stages of jet break-up, a single droplet based drag model proves inadequate to capture the spray trajectory (Mashayek *et al.* (2011)), particularly in the near injection region where the jet behaves as a continuous column like structure. Thus in the present study, the drag model is corrected to account for the change in the drag force experienced by the spray injection. In addition to the drag model, the breakup model also plays an important role in shaping the jet trajectory. Unlike cases of Jet-In-Cross-Flows (JICF) (Wu *et al.* (1997); Inamura and Nagai (1997)) here the bulk air flow field gets affected by the presence of multiple injections at the throat section. The change in the inertial frame of reference justifies the use of KHRT breakup

model to simulate the shear-induced atomization of the jet injection. As a modeling parameter, the time constants of the respective instabilities resulting in breakup, govern the mass shedding rate of the multi-jet injection which in-turn affects the trajectory of the droplets.

The effect of different drag models in predicting the multi-jet trajectory of the spray injection for the above operating condition is shown in Figure 5.2. The plot represents the instantaneous droplet position, scaled to its diameter in the venturi throat section (droplet diameter at injection=2.5 mm). Figure 5.2 shows the droplet size evolution with a) spherical drag coefficient (Clift *et al.* (1978)), b) Schmehl *et al.* (2000) model and c) Corrected drag model.

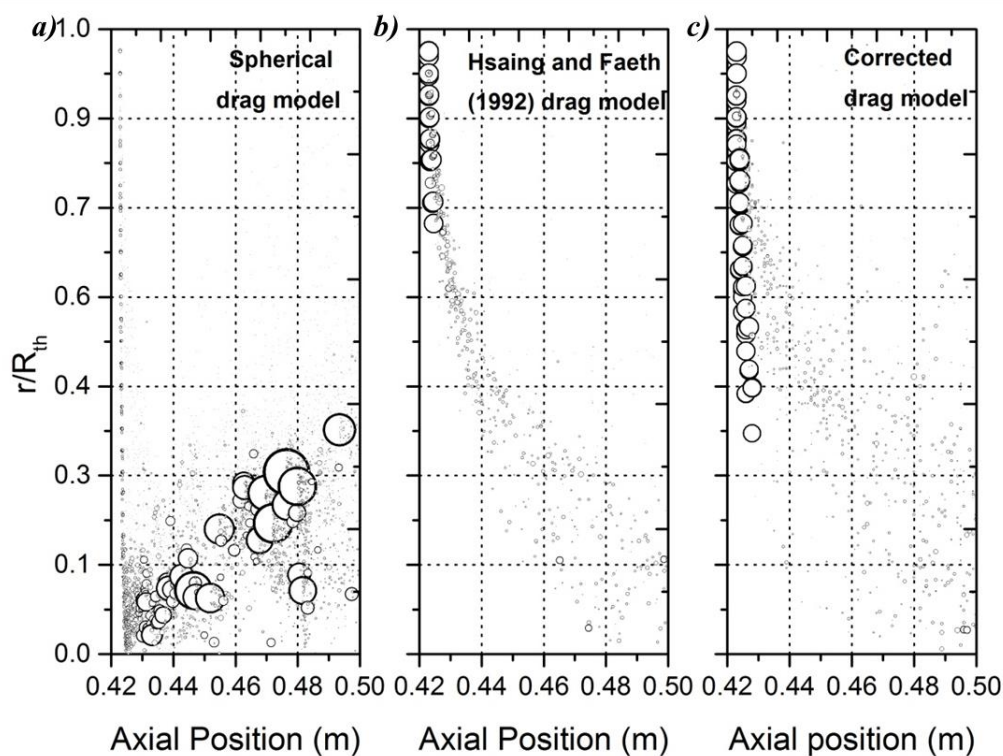


**Figure 5.2 Radial penetration of droplets as a function of axial distance from injection plane for three drag models in the throat section.**

The drag model quantifies the extent of momentum transfer taking place between the phases. With spherical drag coefficient (Figure 5.2 (a)), the momentum exchange is lower,

hence the droplets retain their velocities, size and transverse to the centre of the throat section where they interact with droplets of other streams to form bigger droplets. However, when the modified droplet drag coefficient given by Schmehl *et al.* (2000) (Figure 5.2 (b)) is applied, the droplet drag is more, droplets lose their initial inertia in the radial direction and are deflected in axial direction. The higher resistive (drag) forces make them unstable and shed smaller droplets. The near-injection region of the venturi scrubber comprise of multiple column like structures which undergo shape distortion and breakup due to interaction with the high cross flow velocity. Since the above models are developed for isolated droplets, the drag coefficient used in the present analysis is corrected to account for this effect. A factor of 0.6 was introduced in the deformation equation associated with the column structure. The resultant droplet sizes are shown in Figure 5.2 (c). The correction in the drag model corresponding to the high Weber number region helped in achieving the required dispersion of the droplets as cited by Haller *et al.* (1989).

The retention of inertia results in the occurrence of delayed droplet breakup as observed in the trajectory plots shown in Figure 5.3. The centerline velocity and the contours of velocity of the carrier phase for each drag model are shown in Figure 5.3. The gradual acceleration of the gas velocity is marked by the presence of the multi-jet column in the near injection region (Figure 5.3a). Further downstream, the momentum exchange between the dispersed droplets and the continuous phase results in the deceleration of the gas flow. The substantial change in the carrier phase velocity justifies the use of KH-RT type breakup model (Figure 5.3b).

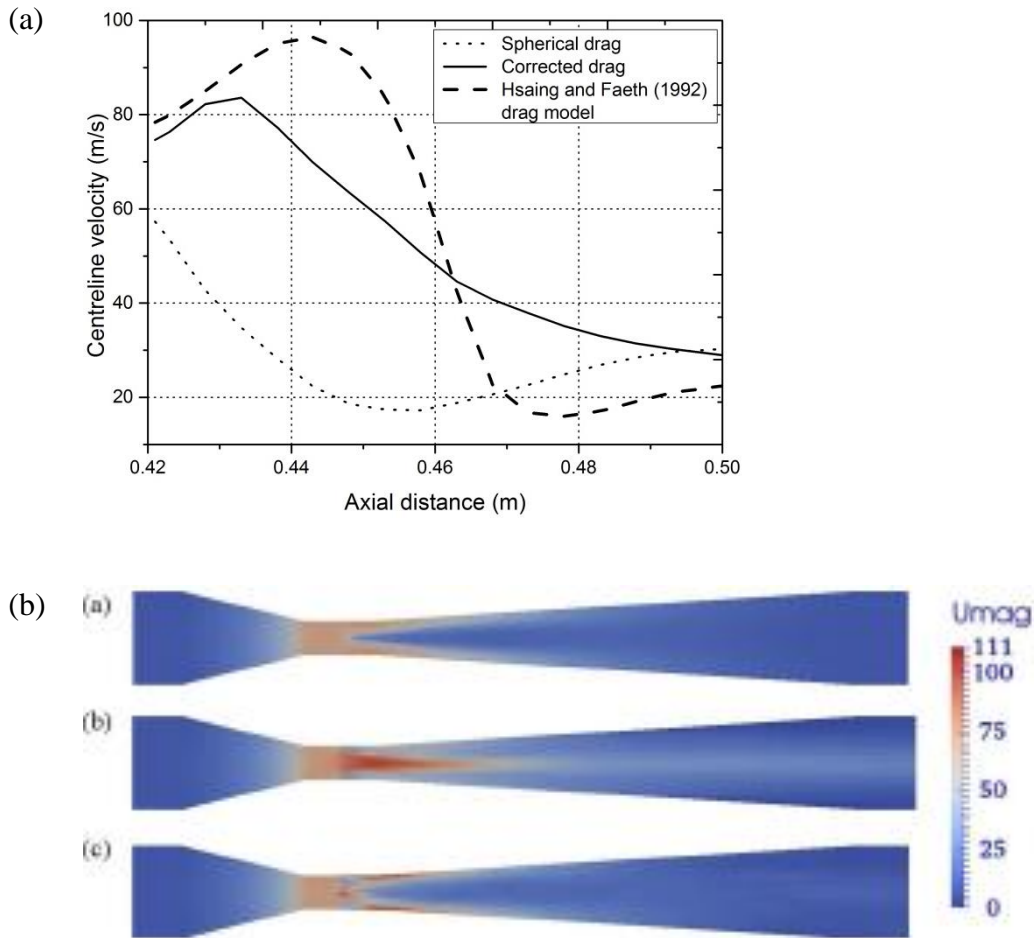
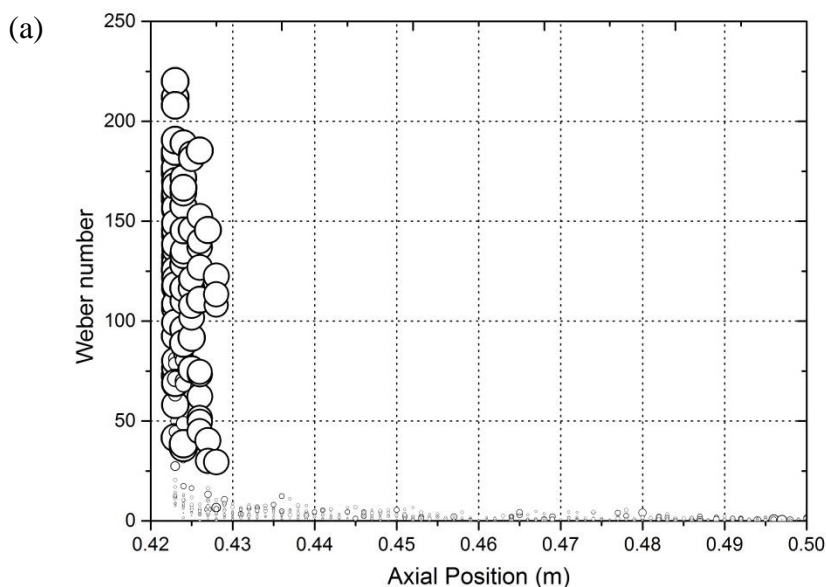


**Figure 5.3 Comparison of (a) centreline velocity of continuous phase in the throat section and (b) contours of velocity of continuous phase for the venturi scrubber for three different drag models.**

With the increase in the drag coefficient from spherical drag to the full deformation model, the rate at which the gas phase is decelerating is increasing. Consequently, the velocity of the gas phase is decreasing at a faster rate on increasing the drag coefficient (Figure 5.3a Figure 5.3b). In other words, the inertia of the jet injection is long retained for spherical drag model as compared to the full deformation model proposed by Schmehl *et al.* (2000). The consequence of this is seen in Figure 5.2 where it can be seen that the droplets are coming to the center of the throat section and coalescing to form bigger droplets when the drag coefficient is spherical. When the drag is increased to full deformation model, the individual jet is deflected

at the near injection regime resulting in its break-up and it is not able to interact with other streams injected at the nozzle. With the modified drag model, the near injection deflection is controlled such that its initial trajectory is captured and the required dispersion is seen.

Figure 5.4a shows the distribution of Weber number droplets formed in the throat section as a result of the shear between the two phases. It basically reflects the change in the relative velocities of the droplets and the continuous phase. The distribution suggests that this difference is significant in the near injection plane. Additionally, it shows that the child droplets do not undergo further breakup, but at the same time re-distributes itself upon interaction with the turbulent gas phase flow. This is also indicated by the area averaged SMD plot shown in Figure 5.4b. The extent of the droplet dispersion achieved in the throat section governs the capture efficiency of the scrubber which is quantified by the liquid distribution plots explained in the subsequent sections.



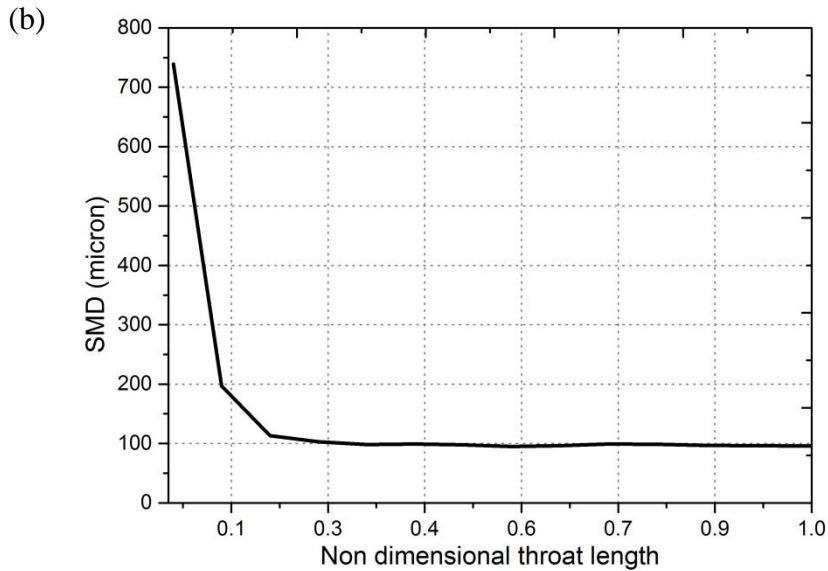


**Figure 5.4 Distribution of (a) Instantaneous Weber number and (b) SMD distribution in the throat section at liquid loading  $2.75 \text{ l/m}^3$  and gas throat velocity  $70 \text{ m/s}$ .**

In the limit of high volume fraction occupied by the droplet phase (i.e. locally exceeding 10% the cell volume), the momentum exchange term to the continuous phase flow equation is corrected by incorporating the effect of volume fraction in that particular computational cell. The computational model hence developed successfully captures the hydrodynamic behavior occurring in the venturi scrubber and can be depicted from the validation plots of axial pressure drop profiles shown in Figure 5.5 and Figure 5.6. The predicted pressure drop values are compared with experimental data. The pressure drop increases in the converging section following Bernoulli's principle. With the introduction of liquid in the throat section, the momentum transfer from the gas phase to the liquid results in sharp increase in the pressure drop. The pressure drop continues to increase till the end of the throat section. In the diverging section, the continuous phase and dispersed phase decelerates resulting in pressure recovery. The predicted values show a good match with the experimental values. The results of validation of pressure drop across the scrubber for different liquid loadings at gas throat velocity of  $70 \text{ m/s}$  and  $50 \text{ m/s}$  are shown in Figure 5.5 and Figure 5.6 respectively. With the increase in liquid

loading, the pressure drop was found to increase for both the throat gas velocities of 50 m/s and 70 m/s.

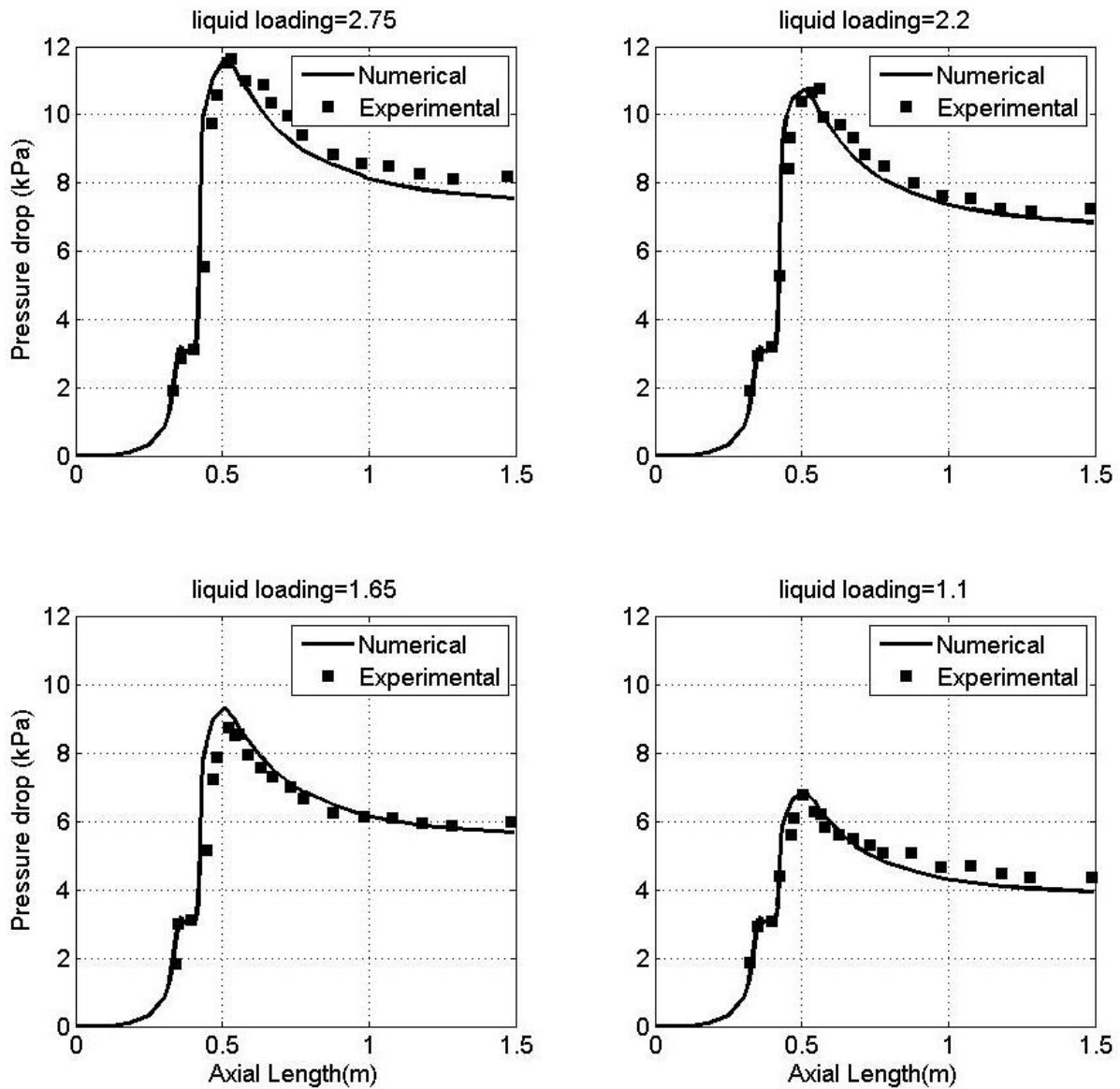


**Figure 5.5** Pressure drop for different liquid loadings at throat gas velocity 70 m/s compared with experimental results.

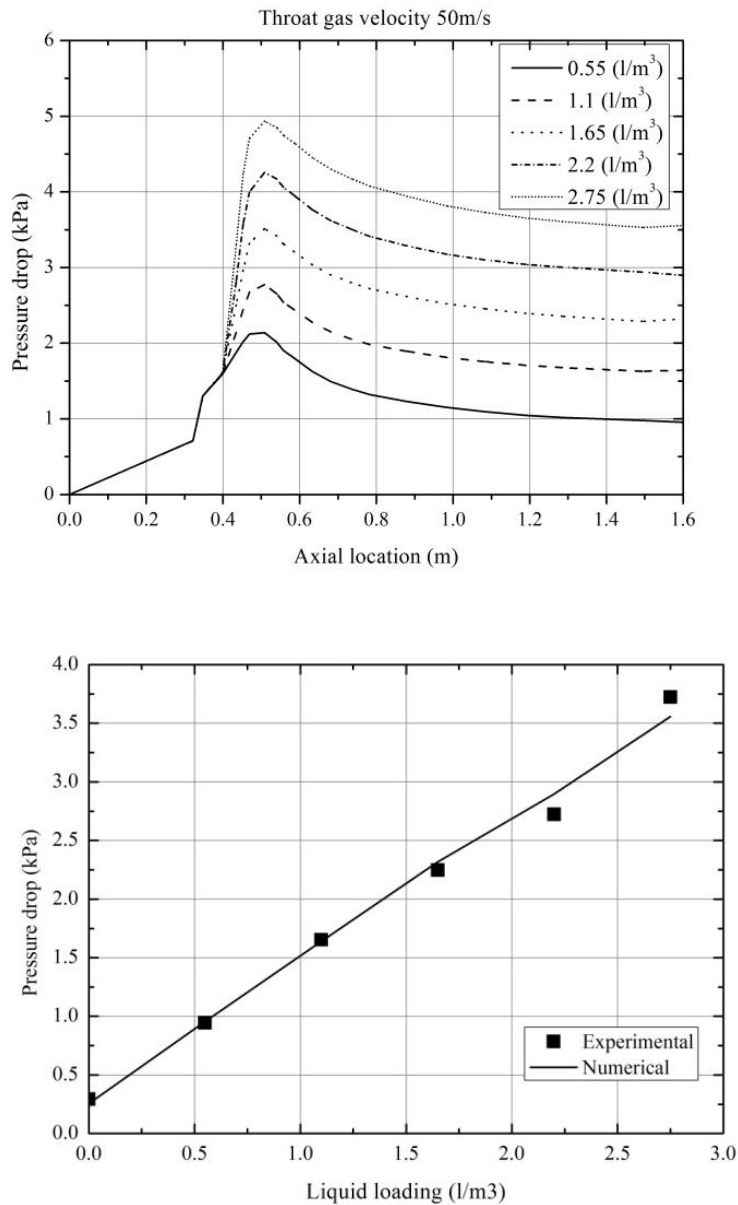


**Figure 5.6** Pressure drop profiles for different liquid loading at throat gas velocity 50 m/s

Secondly, the extent of the entrained droplets intercepting the particulates is evaluated by the overall average of the capture efficiency obtained for each computational cell. The scrubbing efficiency of the venturi scrubber largely depends on the hydrodynamic behavior of the flow condition. For the present case of validation (for liquid loading 2.75 l/m<sup>3</sup>), the liquid flux profile is shown in Figure 5.7. The data shown in Figure 5.7 is the comparison of numerical prediction of liquid loading against the experimental data given by Haller *et al.* (1989). Haller *et al.* (1989) measured the axial liquid loading in the experiments. For this, the liquid was

siphoned at six different axial locations after the injection at the throat section with a U-shaped probe.

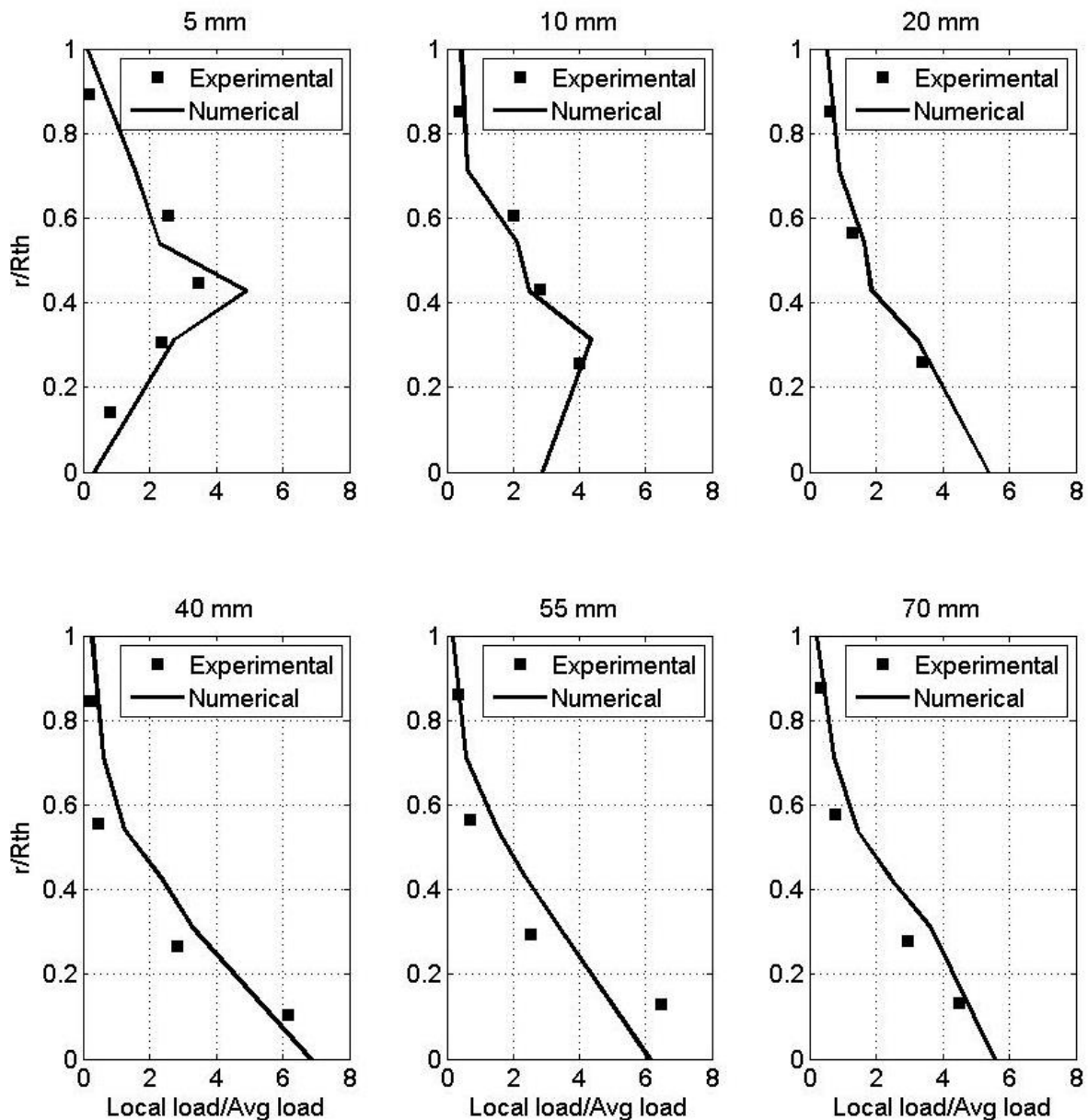


**Figure 5.7 Predicted liquid flux distribution in venturi throat at six axial locations for throat gas velocity 70 m/s and liquid loading of  $2.75 \text{ l/m}^3$  compared with experimental results.**

The liquid flux profiles are analyzed by the radial penetration of the multi-jet injection and the throat coverage. The jet penetration is calculated by locating the radial position of the peak value of the local loading ratio at the throat outlet. The liquid flux distribution is plotted

against its radial location ( $r$ ) scaled to the radius of the throat section ( $R_{th}$ ). The prediction of liquid flux in the throat is compared with the experimental values at 5 mm, 10 mm, 20 mm, 40 mm, 55 mm and 70 mm from injection plane (Figure 5.7). For calculating the liquid flux distribution in the throat section, the throat section is divided into radial clips of 4 mm.

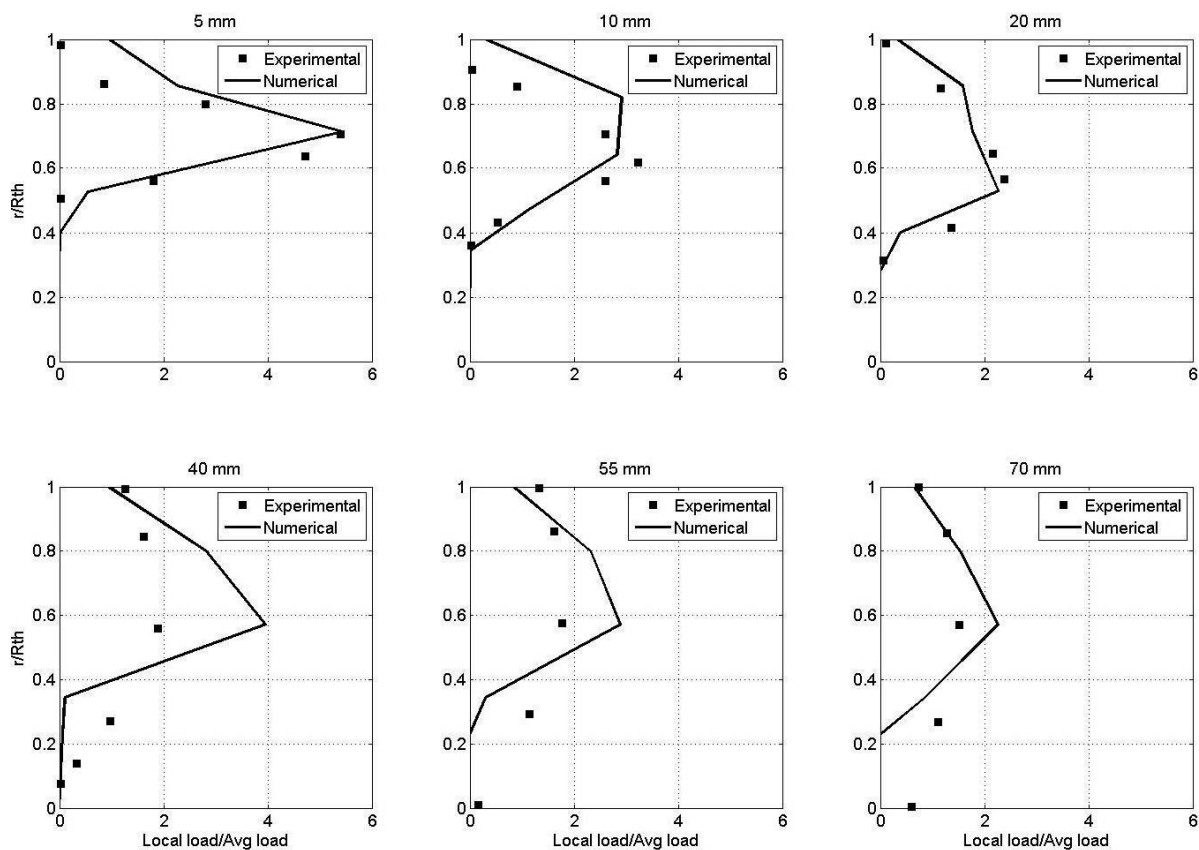


**Figure 5.8 Predicted liquid flux distribution in venturi throat at six axial locations for throat gas velocity 70 m/s and liquid loading of  $1.1 \text{ l/m}^3$  compared with experimental results.**

The values reported in Figure 5.7 are time averaged and area averaged. In the present case, 100 % radial penetration is observed at a distance of 20 mm from injection plane. The liquid flux profiles for the case of  $2.75 \text{ l/m}^3$  liquid loading shows a good match with the cited values. The droplet coalescence effects and the volume occupied by the droplets become dominant for the cases of high liquid loading (2.75 and 2.2). The inclusion of these effects in the numerical model helped achieving a close match with the measured pressure drop values. The droplet

dispersion effects are more appreciable for the cases of lower liquid loading, as seen in the validation plots for  $1.1 \text{ l/m}^3$  liquid loading (Figure 5.8).

### 5.2.2. Scrubbing efficiency of aerosols

The scrubbing efficiency is calculated using equation (5.13) while for calculating target efficiency ( $\eta$ ), equations (5.11) and (5.12) are used. The high relative velocity at the throat injection and subsequent distribution of child droplets results in shaping the trajectory of the injected jet in the throat section. Following the liquid flux profiles for the cases of validation, the scrubbing efficiency of aerosols is found to increase with the high jet penetration and high throat coverage by the dispersed child droplets. From validation point of view, the predicted results correlate well with the experimental values (Haller *et al.* (1989)) and are within 7% as listed in Table 5.2. The corresponding radial jet penetration and the SMD obtained at the throat outlet of the scrubber are also calculated. The efficiency of the scrubber is found to increase with increase in radial penetration and decrease in the SMD of the droplets.

**Table 5.2 Results of validation studies**

Throat gas velocity (m/s)	Liquid loading ( $\text{l/m}^3$ )	SMD ( $\mu\text{m}$ )	Jet Penetration	Efficiency (%)		
				Expt	Numerical	Error(%)
50	0.55	229	throat wall	86.67	83.40	3.27
50	1.10	236	0.40	88.91	95.00	6.09
50	1.65	193	0.50	91.48	97.20	5.72
50	2.20	190	0.50	92.65	97.50	4.85
50	2.75	189	0.50	93.28	97.60	4.32
70	0.55	84	0.20	94.00	91.30	2.90
70	1.10	90	0.35	98.00	91.60	6.50
70	1.65	84	0.35	98.90	93.90	5.10
70	2.20	100	0.60	99.40	96.00	3.40
70	2.75	98	1.00	99.70	97.60	2.10
100	0.55	68	throat wall	93.70	97.30	3.60
100	1.10	57	throat wall	96.70	99.10	2.40

### 5.2.3. Effect of Operating and Geometric parameters

With relevance to self-priming operation, the change in upstream pressure or the change in operating height changes the throat gas velocity and the liquid injection velocity to the scrubber. In view of this, in the following sections, the effect of change in gas velocity, liquid velocity along with variation in throat lengths and nozzle diameter on the performance of the scrubber is discussed. These effects are analyzed by comparing the axial pressure drop, the droplet SMD, liquid flux distribution at different axial location in the throat section and the scrubbing efficiency of aerosols obtained for each case.

#### 5.2.3.1. Effect of throat gas velocity

The effect of changing throat velocity is demonstrated at constant liquid injection velocity of 5.03 m/s. With the increase in gas velocity, the extent of momentum transfer to the spray injection increases and hence the pressure drop increases, which is evident from the pressure drop plots shown in Figure 5.9a. The enhanced momentum transfer also results in the formation of smaller liquid droplets (Figure 5.9b) hence, increasing the number of collector surfaces. The plot for SMD, shown in Figure 5.9b, shows the relative effect of the changing gas velocity as a function of the scrubber throat length. The SMD is found to decrease from 130 micron to 40 microns for 50 m/s to 100 m/s change in gas velocity at the throat outlet. This explains the increase in scrubbing efficiency of aerosols attained for high gas velocities, (Table 5.2). For the same volume of liquid injection, Figure 5.9c shows the relative difference in the liquid flux distribution at different axial planes from the injection location. The increase in gas velocity restricts the jet radial penetration into the throat section. This increases the peak liquid flux value at the throat wall.

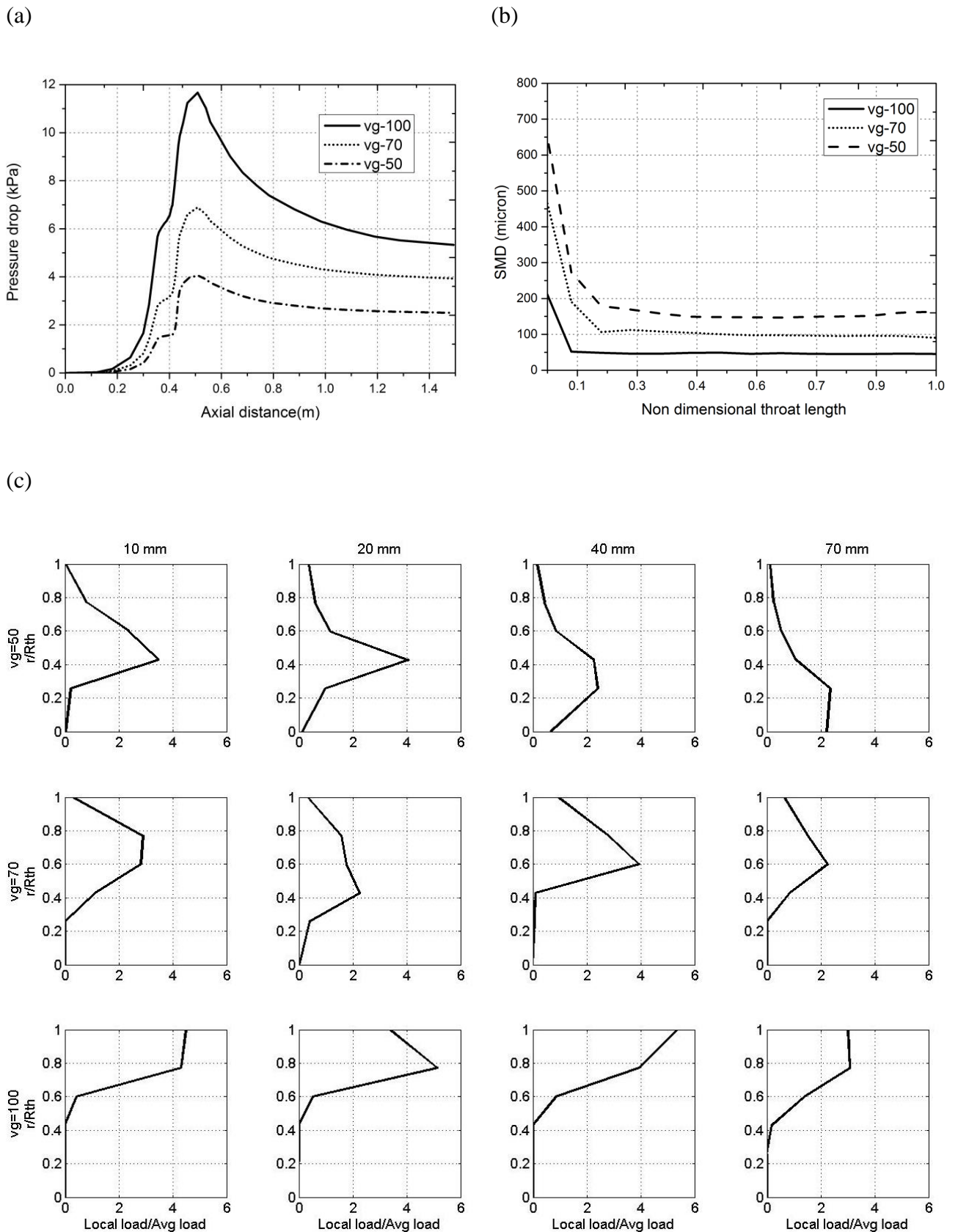


**Figure 5.9 (a) Axial pressure drop variation for different gas velocities at liquid injection velocity-5.03 m/s. (b) Sauter mean diameter variation with gas velocity in the throat section.**

***(c) Comparison of liquid flux profiles at axial distance downstream of injection with variation in gas velocity at x-10 mm, 20 mm, 40 mm, 70 mm from injection.***

#### 5.2.3.2. Effect of liquid flow rate

This case is similar to that cited by Haller *et al.* (1989) where the liquid loading ratio is varied for a constant throat gas velocity of 70 m/s. We have discussed (in section 5.2) the effect of increasing liquid loading on pressure drop (Figure 5.5) in the venturi scrubber. As expected, the increased liquid volume adds to the resistance offered to the gas flow, hence increasing the pressure drop incurred in the throat section and the overall pressure drop also. On the other hand, the SMD plots, (Figure 5.10a), show negligible change in the predicted droplet diameters. This implies that the SMD is significantly governed by the gas velocity and is a weak function of liquid injection velocity for the present case of variations i.e. from 2.5 m/s to 12.5 m/s. Similar observations were reported by Alonso *et al.* (2001) who performed experiments at throat gas velocities of 50-90 m/s and liquid loading ratios of 0.5-2 l/m<sup>3</sup>. Therefore, the increased liquid volume results in generating more number of entrained droplets in the scrubber. This also explains the change in the recovery pressure drop across the diverging section of the scrubber considering the fact that the droplets reach their terminal velocity by the end of the throat section. The liquid flux profiles for all the cases (at different axial locations in the throat section) are shown in Figure 5.10b. The increase in jet inertia with the increase in liquid loading resulted in high radial penetration as evident from the liquid flux profiles (Figure 5.10b). The increase in penetration as well as the number of child droplets helps in improving the scrubbing efficiency of aerosols of the scrubber, as depicted in Table 5.2. The trend in variation of the scrubber performance shows that, with the realisation of complete throat coverage, the efficiency only increase by a marginal amount with further increase in liquid loading while contributing largely to the rise in pressure drop values.

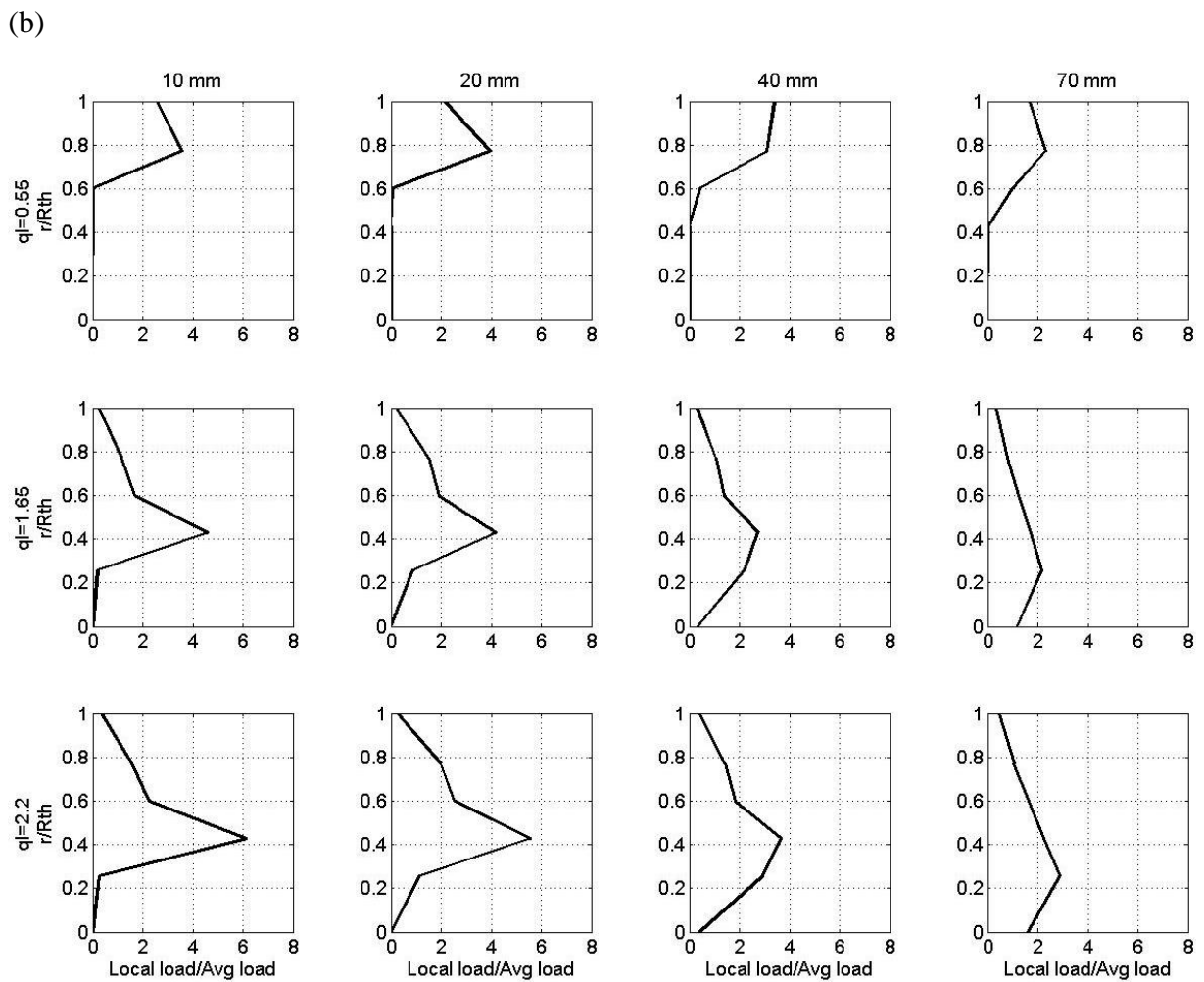
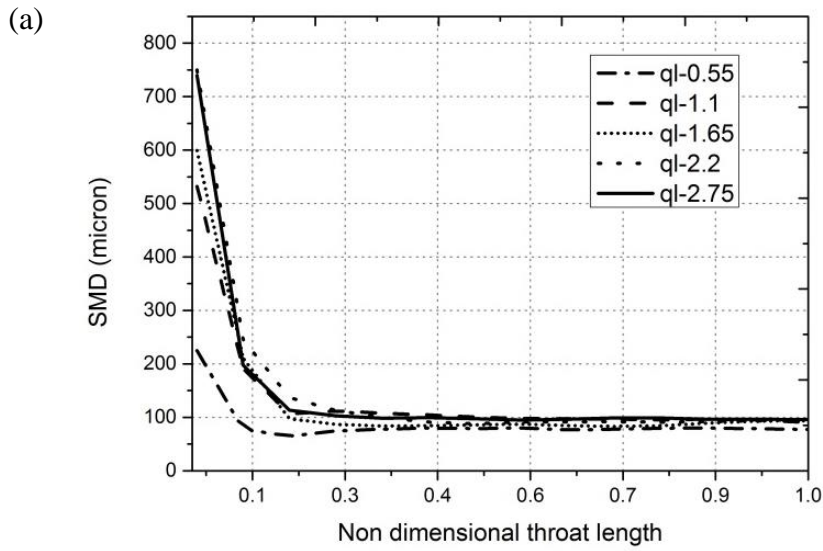


**Figure 5.10 (a) Sauter mean diameter variation in liquid flow rates at throat gas velocity-70 m/s. (b) Comparison of liquid flux profiles at axial distance downstream of injection with variation in gas velocity at x-10 mm, 20 mm, 40 mm, 70 mm from injection plane**

#### 5.2.3.3. Effect of nozzle diameter

In this section, the effect of nozzle diameter on scrubbing efficiency and pressure drop is investigated. The scrubber was operated at a constant gas velocity of 70 m/s with a liquid loading of  $1.1 \text{ l/m}^3$ . Different nozzles of diameter 2 mm, 2.5 mm, 3 mm and 3.5 mm, placed concentrically, were considered to study the effect on the performance of the scrubber. Figure 5.11a shows pressure drop values for the change in the nozzle diameter. The highest pressure drop was recorded for 16 number of nozzles of 2 mm each. The increased number of nozzles provide more surface area for stripping to occur while, offering higher blockage to the gas phase flow area at the near injection region. This, though, had negligible effect on the predicted droplet size distribution (Table 5.3) which implied that the droplet size is weakly affected by the initial diameter of the droplet. The jet penetration at different axial locations is shown in Figure 5.11b. It is seen in the plots that a larger diameter of nozzle (3.5 mm, 6 no.) would allow the jet to penetrate to the centre of the throat (Jet penetration=0.6). However, for the smaller nozzle diameters, the liquid flux at the centre of the throat is decreased (Diameter of nozzle=2 mm, 16 no. of nozzles, Jet penetration=0.35). This is because a larger initial drop diameter would resist the continuous phase more strongly compared to a shorter initial drop diameter. The improved penetration obtained for high nozzle diameters helped in achieving better scrubbing efficiencies (Table 5.3). The scrubbing efficiency of 93% is achieved for 3.5 mm nozzle diameter. Therefore, with the same volume of liquid injection, the efficiency can be improved by increasing the nozzle diameter, without incurring additional pressure drop in the system.

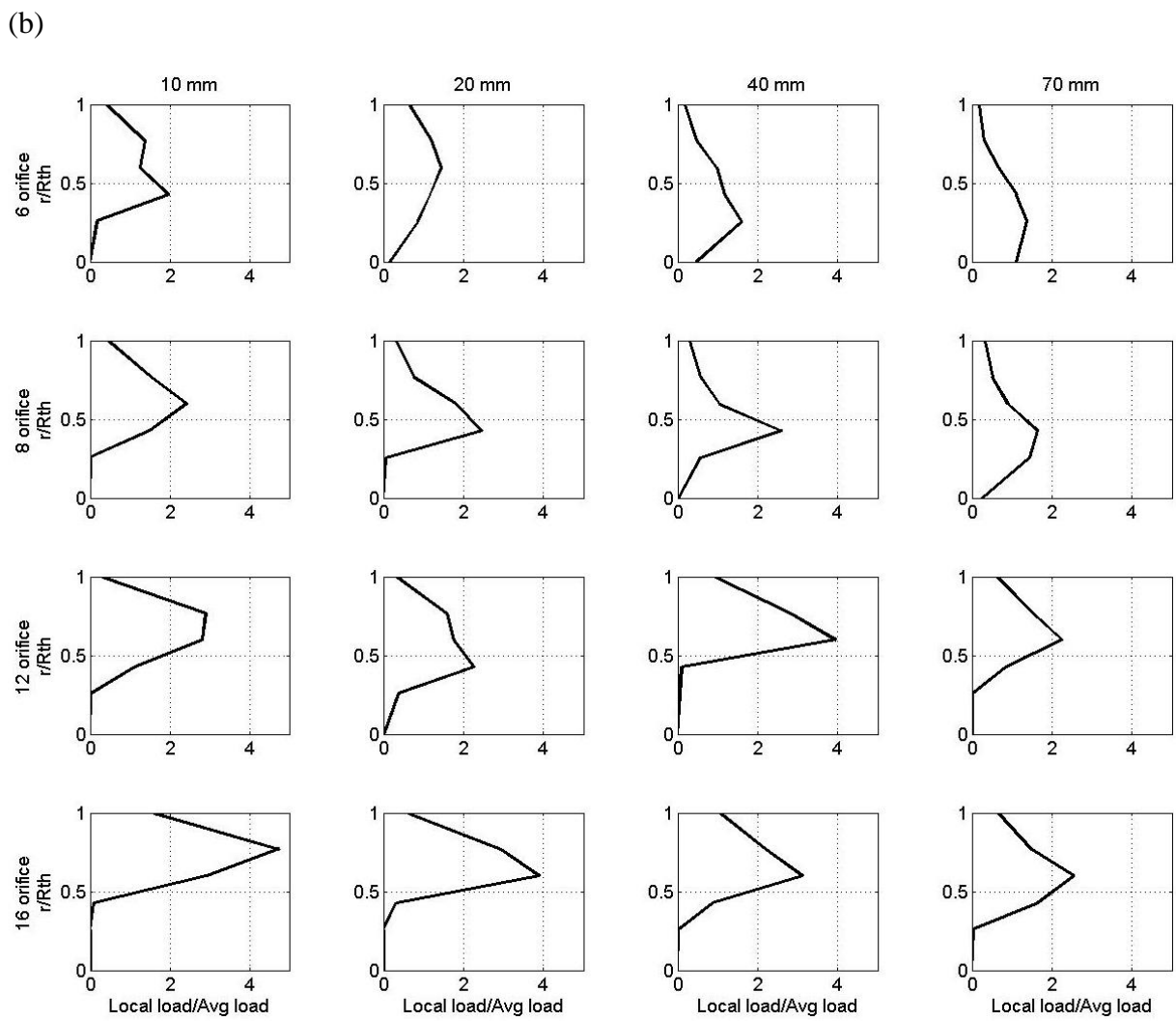
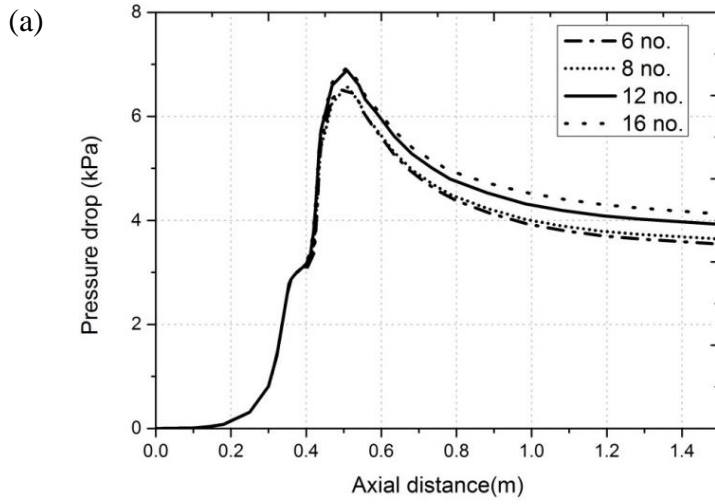


*Figure 5.11 a) Axial pressure drop variation with variation in number of nozzles at throat gas velocity 70 m/s and liquid loading 1.1 l/m<sup>3</sup>. b) Comparison of liquid flux profiles at axial distance downstream of injection with variation in nozzle diameter at x-10 mm, 20 mm, 40 mm and 70 mm from injection.*

#### 5.2.3.4. Effect of throat length

The throat length was varied from 50 mm to 80 mm for 70 m/s gas velocity and 1.1 l/m<sup>3</sup> liquid loading. The pressure drop profiles, shown in Figure 5.12a, shows that below 70 mm throat length the peak pressure drop decreases with decrease in throat length. This implies, for the present operating condition, 70 mm downstream throat length is sufficient for the droplets to attain their terminal velocities. Figure 5.12b shows the effect of throat length on liquid flux profiles at the throat end for each case. It can be seen that a longer throat would allow re-distribution of liquid flux marked by a decrease in peak liquid flux value. Figure 5.12c shows no change in the SMD of the droplets as the droplet break-up gets saturated by 20 mm of the available throat length. Hence, with the increase in throat length the child droplets get more dispersed by the end of the throat length. This is also evident in the liquid flux profiles obtained at the throat outlet, as shown in Figure 5.12b. Nevertheless, these marginal variations in the liquid flux profile did not contribute much to affect the scrubbing efficiency of the scrubber (Table 5.3).

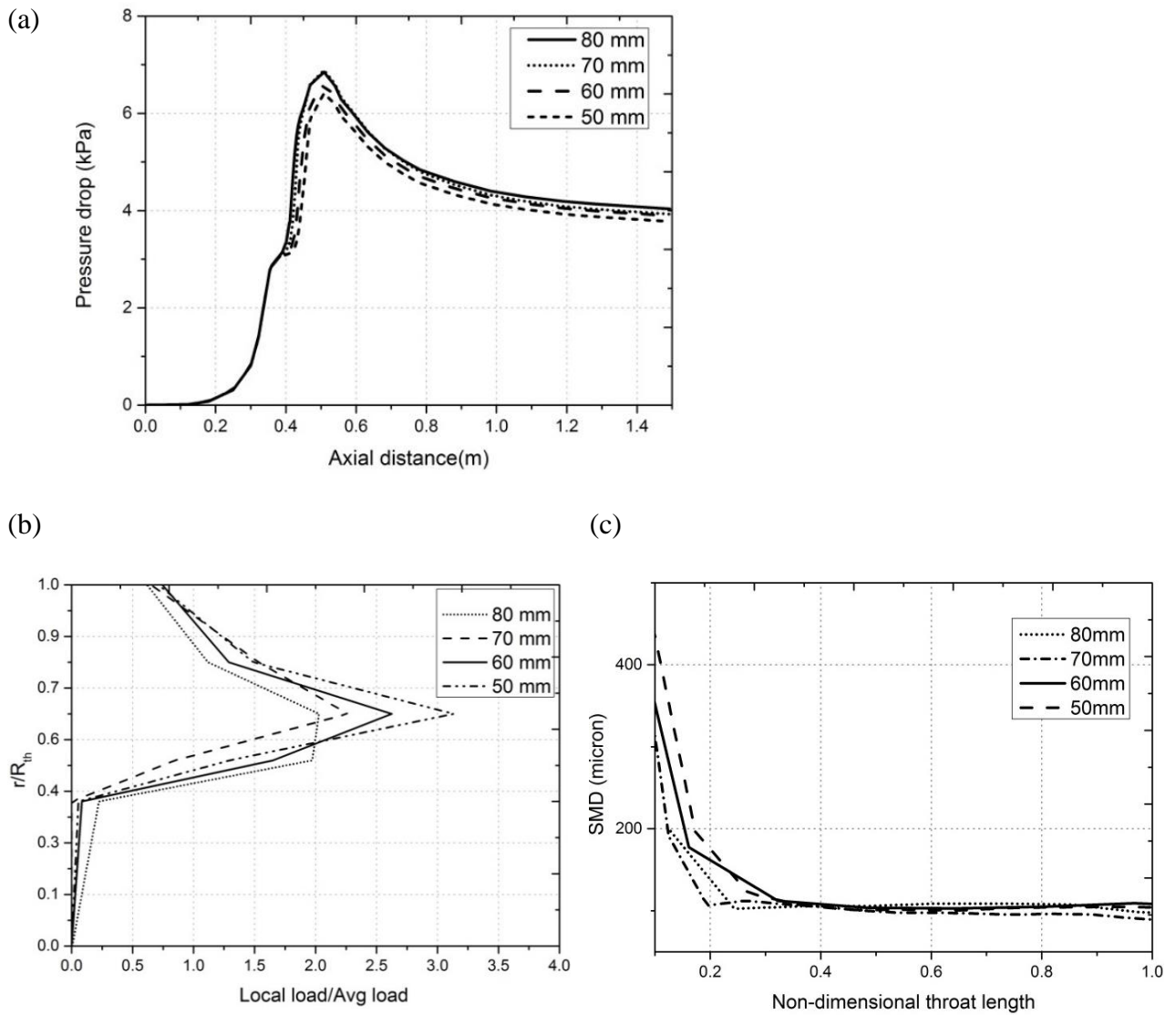


**Figure 5.12** (a) Axial pressure drop variation with variation in throat length at throat gas velocity 70 m/s and liquid loading 1.1 l/m<sup>3</sup>. (b) Comparison of liquid flux profiles at axial distance downstream of injection with variation in throat length at throat end. (c) Sauter mean diameter variation with throat length in the throat section.

**Table 5.3 Results of Parametric Study**

	Throat gas velocity (m/s)			Throat length (mm)				Nozzle Diameter (mm)			
	50	70	100	50	60	70	80	2	2.5	3	3.5
Jet penetration	0.6	0.4	0.22	0.4	0.4	0.4	0.4	0.35	0.4	0.5	0.6
SMD(micron)	147	90	44	105	100	90	95	91	90	104	92
Efficiency	92.1	91.6	97.5	91.8	91.8	91.6	91.7	92.3	91.6	91	93

### 5.3. Application of the model to the present experiments

The benchmarking of the CFD model with the forced feed venturi scrubber showed its adequacy in modeling the flow physics inside the venturi scrubber. The inputs to the CFD model are the velocity of the continuous phase at the inlet of the venturi scrubber, the initial diameter, the velocity of the dispersed phase and the pressure at the outlet of the venturi scrubber. The model validation with the experiments conducted in the present work is detailed in the following segment. When the venturi scrubber is operated in a submerged mode, its entrainment characteristics are not known a priori unlike forced feed venturi scrubber, but the radial pressure difference driving this entrainment is known. So, the present section deals with calculating the entrainment characteristics from the radial pressure difference across the nozzles. The CFD model is developed assuming that the volumetric loading of the droplets to the scrubber is less than 10% of the computational volume such that the droplets can be treated in Lagrangian framework. The governing equations, the source terms for interaction of the two phases and the solver algorithm are discussed in sections 5.1.1-5.1.5. For the absorption of iodine vapours, the model description is given here.

#### 5.4. Absorption of iodine vapours

The removal of iodine from the venturi scrubber is modeled assuming that the reaction rate is kinetically fast and mass transfer of iodine from gas in the droplet is gas film controlled (Hills (1995), Eguchi *et al.* (1975)). The reaction will take place at the interface between gas and droplet. It is also assumed that the iodine is uniformly distributed radially and is moving with gas in the domain of the venturi scrubber. Since the reaction rate is high and the venturi scrubbers are operated in excess of reactant, concentration of iodine in the droplet is zero. The concentration of iodine at the outlet is calculated from the following equation (5.14).

$$\frac{c_{cout}}{c_{in}} = \exp\left(-\frac{4 * 3.14 * r_d^2 * k_g * t_{res}}{V}\right) \quad (5.14)$$

where  $k_g$  is mass transfer coefficient,  $r_d$  is the radius of droplet,  $V$  is the volume of gas surrounding the droplet and  $t_{res}$  is the contact time between the droplet and iodine vapour. The Sherwood number, which characterises the ratio of convection mass transfer rate to diffusive mass transfer rate, is calculated by the equation (5.15).

$$Sh = 2 + 0.347(Re * Sc^{.5})^{0.62} \quad (5.15)$$

where  $Sc$  is Schimdt number and  $Sh$  is Sherwood number.

Steinberger and Treybal (1960) correlation of Sherwood number (equation (5.15)) is used for gas-phase mass transfer coefficient for a single droplet and is valid within the ranges of  $1 < Re < 30,000$  and  $0.6 < Sc < 30,000$  (Mariana *et al.* (2004)). Another mathematical formulation of Sherwood number is given by equation (5.16). This equation is equated to equation (5.15) to obtain gas phase mass transfer coefficient and is substituted in equation (5.14) to evaluate  $c_{out}$ .

$$Sh = \frac{k_g * d_d}{D_g} \quad (5.16)$$

where  $d_d$  is the diameter of droplet and  $D_g$  is gas diffusivity.

The single droplet absorption correlation is extrapolated to the whole domain by dividing the venturi scrubber into sections of 0.05 m axial length. The input of iodine concentration to each section is equated to  $c_{out}$  from the previous section.

## 5.5. Results of Model Validation with the present experimental results

### 5.5.1. Evaluation of liquid loading

The liquid is entrained in the venturi scrubber nozzles due to the difference in radial pressure and is opposed by the air flowing inside the venturi scrubber. Therefore, the liquid loading to the scrubber is determined by the interplay of these two forces as given in equation (5.17).

$$P_{th} - P_{tank} = \frac{1}{2} K \rho_l v_l^2 ; K = f(Re_g); Re_g = \frac{\rho_g u_{gin} D_{in}}{\mu} \quad (5.17)$$

where  $P_{th}$  is the pressure in the throat section of venturi scrubber just inside the nozzles,  $P_{tank}$  is the hydrostatic pressure in the tank just outside the nozzles,  $K$  is loss coefficient,  $u_{gin}$  is the velocity of the gas phase at the inlet of the venturi scrubber,  $D_{in}$  is the diameter at the inlet of the venturi scrubber,  $\rho_l$  is density of entrained liquid,  $\rho_g$  is density of gas phase,  $v_l$  is velocity of entrained liquid and  $Re_g$  is the gas phase Reynolds number.

This is different from normally encountered flow through nozzles where the two fluids are same. In addition, the entraining liquid has to overcome the resistance of the flowing gas inside the venturi scrubber. Consequently, the loss coefficient at the nozzles of the venturi scrubber cannot be considered constant. This physical understanding led to the conclusion that the loss coefficient is a function of continuous gas flow and is proportional to the pressure difference across the nozzles.

The value of K is then assumed to find the respective value of liquid loading to the scrubber. After this, the CFD model is solved to obtain the pressure profile in the venturi scrubber. This process is repeated for all the cases listed in Table 5.4. The values of K, which finally yield the pressure profiles across the venturi scrubber, are considered to be final. The final values of K are plotted against the Reynolds number of gas flow at the inlet of the venturi scrubber in Figure 5.13.

**Table 5.4 Summary of cases simulated**

Gas mass flow rate (kg/s)	Radial pressure difference (kPa)	Gauge Pressure at the venturi outlet (kPa)	Estimated liquid velocity (m/s)	Estimated Liquid loading ( $l/m^3$ )
Submergence height : 3 m				
0.043	10.46	18.89	26.43	61.41
0.055	13.23	18.33	16.28	31.78
0.074	10.91	19.90	8.54	10.77
0.086	12.84	20.32	7.56	8.50
Submergence height : 4 m				
0.045	14.72	24.74	31.36	69.45
0.060	9.03	33.09	10.98	21.06
0.082	12.75	27.19	9.23	11.89
0.094	11.01	30.26	7.00	7.87

Table 5.4 summarises the input to the CFD code. It can be seen from the Table 5.4 that the liquid entrainment increases exponentially when the air inlet velocity is low. Physically,

this implies that when the air inlet velocity is low, the air flowing in the venturi scrubber offers lower interfacial resistance causing large volume of water to entrain. This suggests the key feature of submerged operation of venturi scrubber wherein it adjusts the liquid loading in accordance with the radial pressure and gas flow rate, unlike that in forced feed scrubbers.

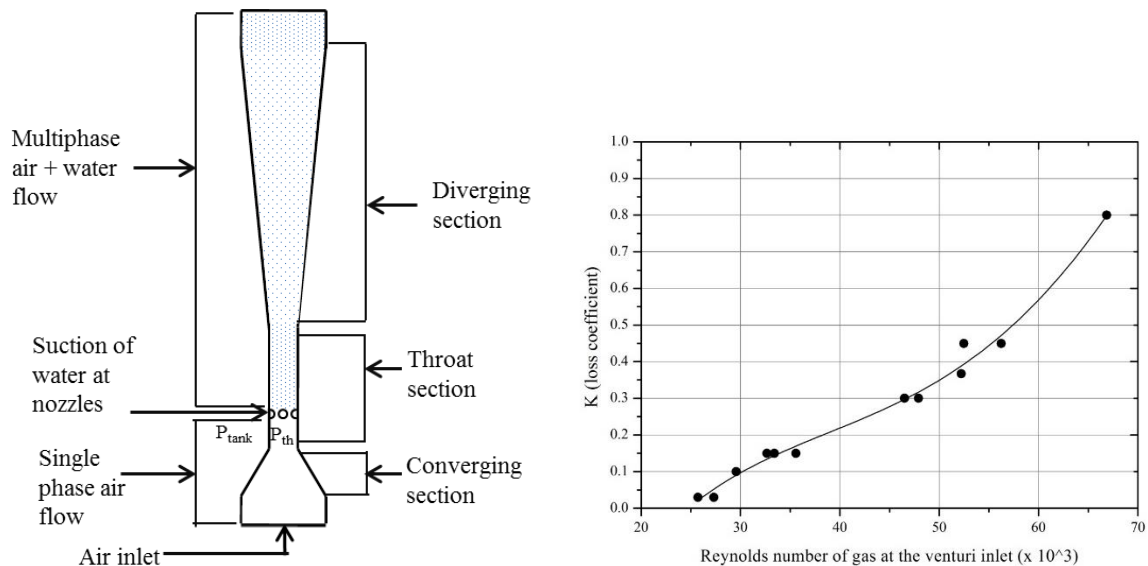


**Figure 5.13** Dependence of  $K$  on air Reynolds number

### 5.5.2. Droplets trajectory and size distribution

Detailed analysis of continuous phase flow profile and trajectory is done for the case of 0.074 kg/s gas mass flow rate where the liquid loading to the scrubber is 10.76 l/m<sup>3</sup>. The droplet trajectories and its size evolution as shown in Figure 5.14 and Figure 5.15 suggests that the droplets undergo sudden break-up upon its entrance but further downstream some droplets coalesce to form bigger droplets. It is also seen in the plot that the droplets leaving the venturi scrubber throat section have higher momentum in comparison to the gas velocity. This suggests that momentum exchange with the droplets reduces the pressure drop recovery in the diverging section of the venturi scrubber.

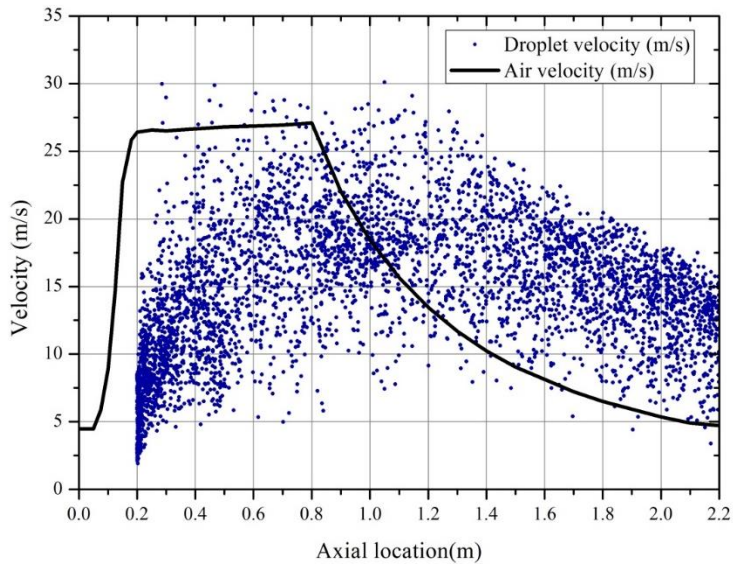


**Figure 5.14** Instantaneous distribution of droplet velocities and centreline continuous phase velocity for 0.074 kg/s gas mass flow rate and 3 m submergence height.

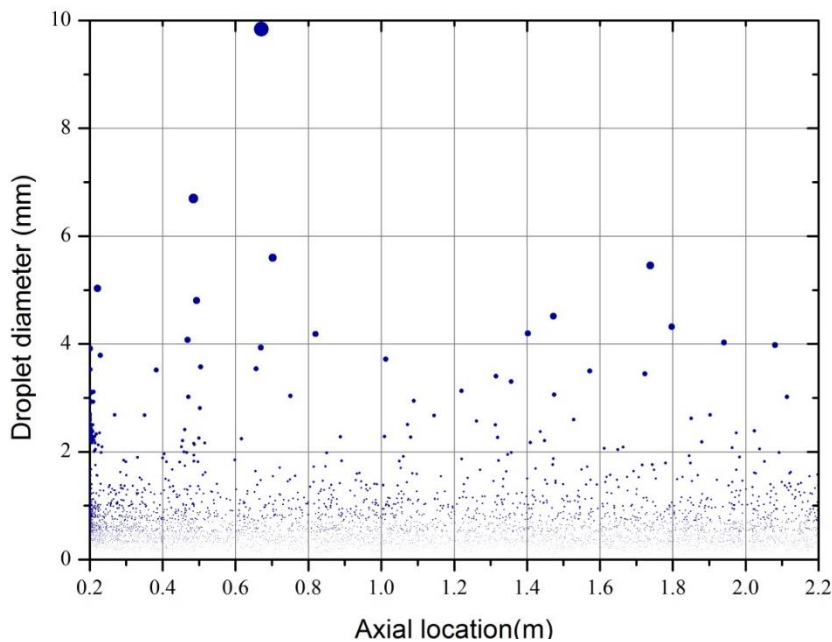


**Figure 5.15** Instantaneous distribution of droplet diameter for 0.074 kg/s gas mass flow rate and 3 m submergence height.

The instantaneous distribution of droplet diameter for the 0.043 kg/s flow rate has been shown in Figure 5.16. Comparison of this with Figure 5.15 suggest that the droplets formed are more in number and the extent to which the droplets are accelerated in the domain is more for

0.074 kg/s. The analysis showed that the venturi scrubber in the operating conditions has suctioned a large volume of water from the pool for lower air flow rate. Also the droplet coalescence is more prominent in 0.043 kg/s case. The high liquid loading to the scrubber at lower air inertia allows more droplets to interact just at the nozzle entrance thus causing it to coalesce and form bigger droplets as seen in Figure 5.16.

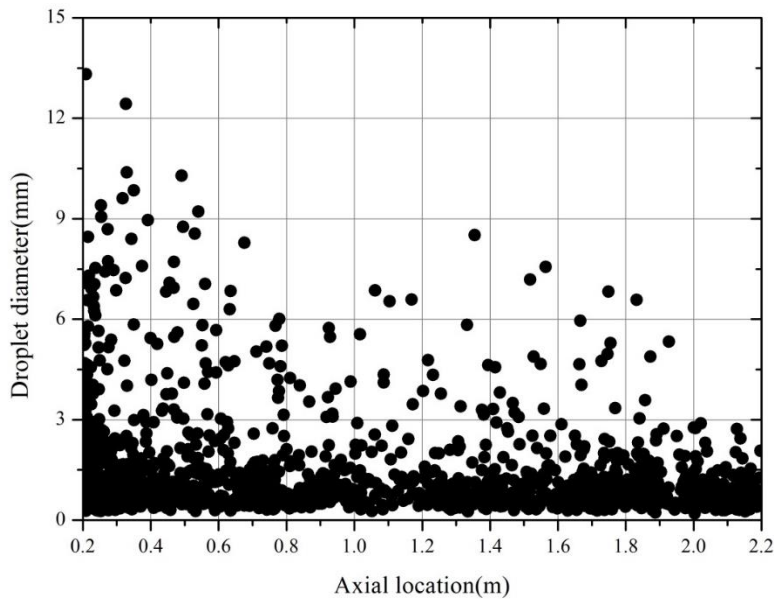


**Figure 5.16** Instantaneous distribution of droplet diameter for 0.043 kg/s gas mass flow rate and 3 m submergence height.

### 5.5.3. Pressure loss in venturi scrubber

The two phase pressure characteristics in the venturi scrubber is consequence of the flow of droplets and of air (Figure 5.17 and Figure 5.18). In the converging section of the venturi scrubber, there is single phase air which accelerates due to decrease in cross-sectional area for flow. After that it enters the throat section where there is slight decrease in pressure due to the friction. At the nozzles in the throat (at axial location of 0.2 m), there is liquid entrainment which decreases the effective area for air flow and is also gaining momentum due to the relative motion between the two phases. The high shear encountered by the entrained

droplets deflect it axially and deforms it in shape as well. This results in pressure loss. On entering the diverging

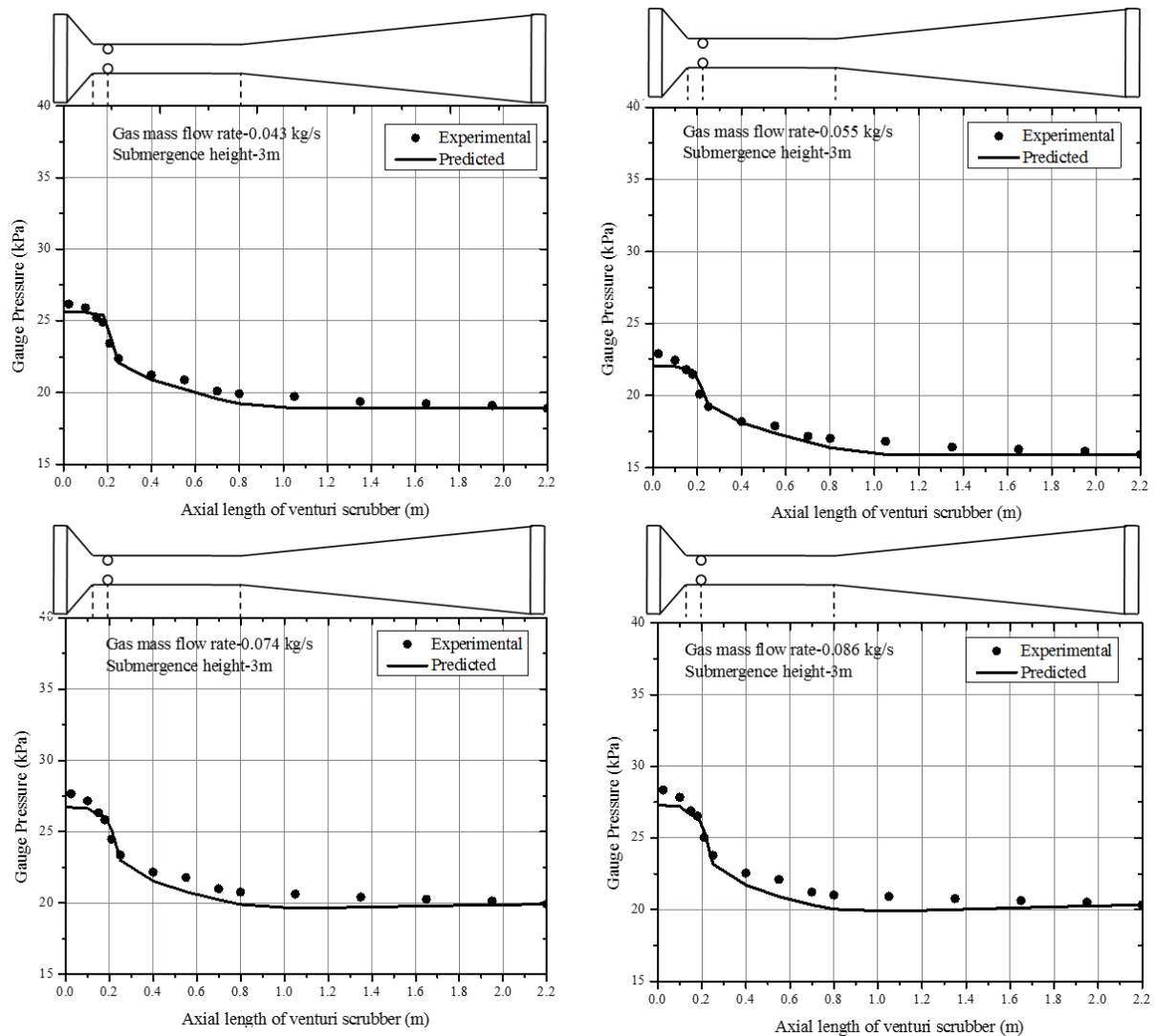


**Figure 5.17** Pressure characteristics in the venturi scrubber for different gas mass flow rates at the submergence height of 3 m.

section, the air and the droplets both decelerate but the high liquid loading in the present cases restricts the recovery of pressure. This is in close agreement with the experimental values.

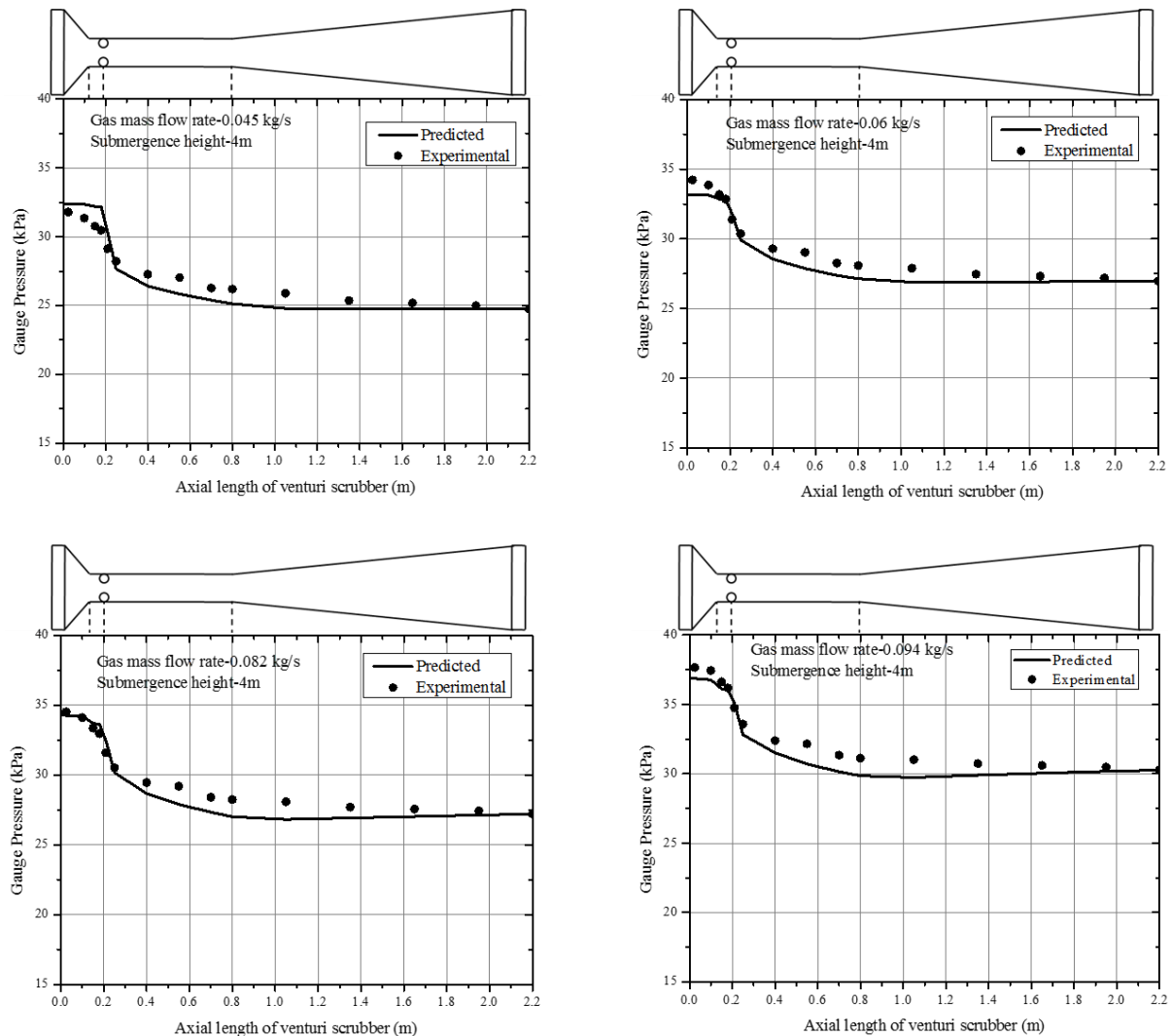


**Figure 5.18** Pressure characteristics in the venturi scrubber for different gas mass flow rates at the submergence height of 4 m.

#### 5.5.4. Scrubbing of iodine vapour

The scrubbing efficiency of the venturi scrubber was computed assuming that the reaction is instantaneous at the interface of the droplet and iodine vapour (Figure 5.19 and Figure 5.20). The scrubbing efficiency was evaluated at flow rates varying from 0.04-0.1 kg/s at the submergence height of 3m (Figure 5.19). It is found in the predicted results that the contribution of venturi scrubber to the scrubbing of iodine vapours increases with the increase in the air velocity. This is probably due to the increased number of droplets at high air velocity. This observation is similar to that measured in the experiments. The scrubbing achieved is a

combined effect of both the total surface area available and the retention time. A higher throat length allows for redistribution of droplets and hence interaction time is provided which in turn helps in increasing the iodine scrubbing.

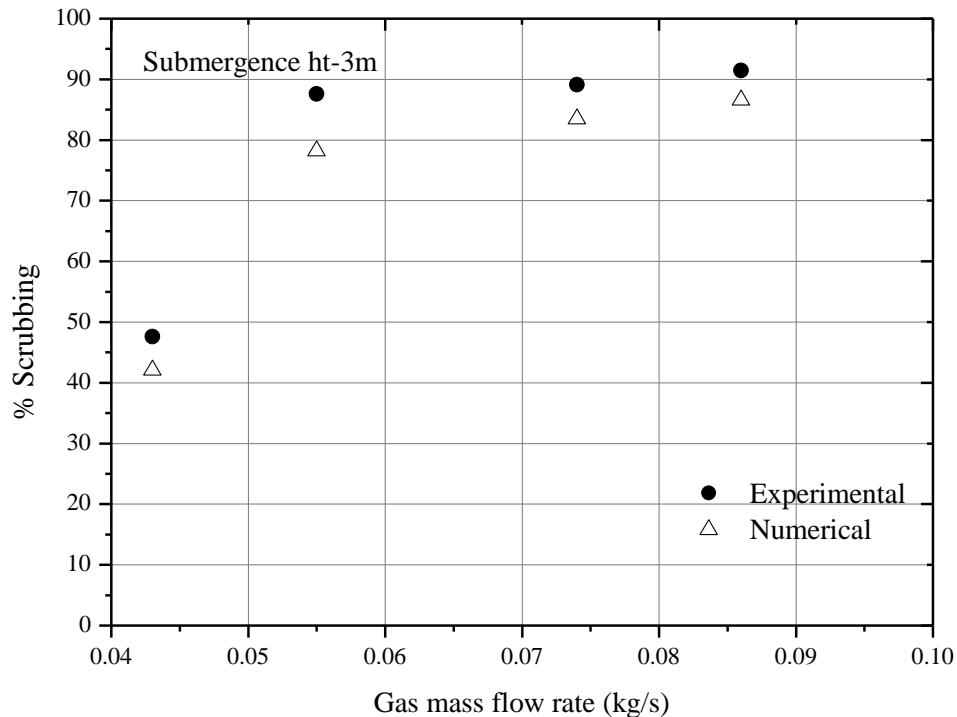


**Figure 5.19 Percentage scrubbing of iodine vapours at submergence height of 3 m with varying gas mass flow rates**

Figure 5.20 shows similar analysis for air flow rates of 0.04-0.1 kg/s for 4 m submergence height. The experimental and predicted efficiency both increases with increase in air flow rate for 4m submergence height also. Thus, at higher flow rates the increased number of droplets allow maximum retention of iodine despite the decrease in contact time.

The retention of iodine is governed by mass transfer characteristics of gaseous iodine present at the surface of entrained liquid through nozzles. This phenomenon is affected largely by two parameters: residence time of gas and interfacial area. The residence time of gas is high for low gas flow rates. In such scenarios, the entrained liquid is high but the entrained droplet sizes are also high such that the interfacial area of absorption is less and hence the resultant

absorption. While an increase in gas velocity, decreases the liquid loading, increases the number of collection surfaces or droplets, the residence time is decreased. So, the overall efficiency is a trade-off between these two factors for the present case.

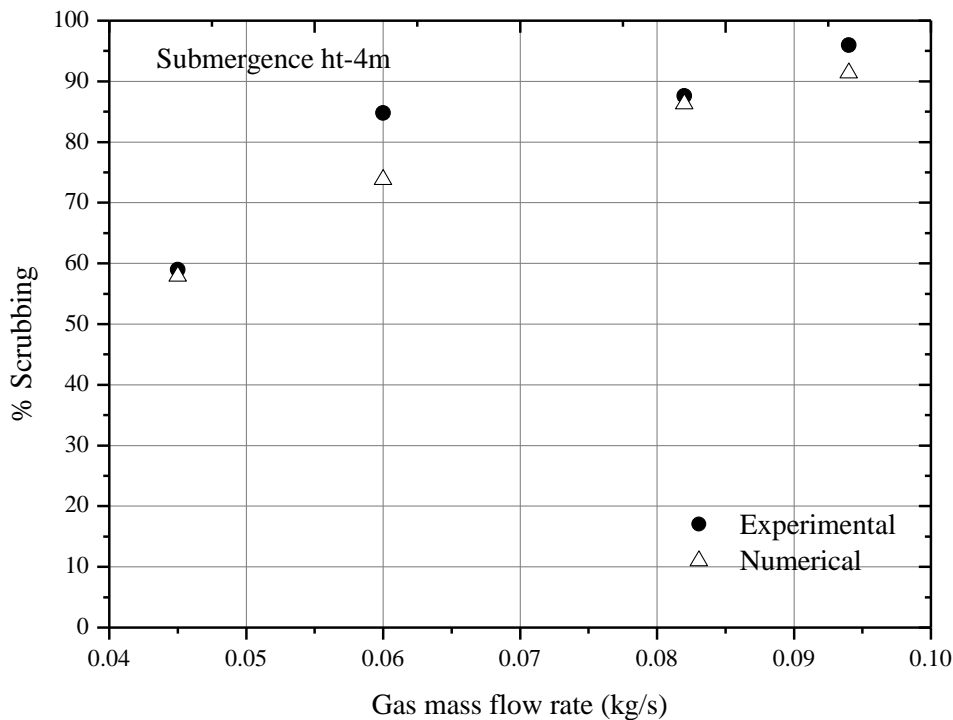
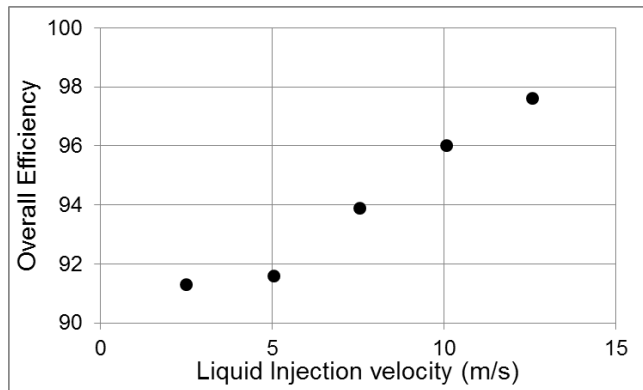


**Figure 5.20** Percentage scrubbing of iodine vapours at submergence height of 4 m with varying gas mass flow rates

## 5.6. Design improvements for Self-priming operation

Subjecting the venturi scrubber to self-priming operation, the transients often include decrease in the throat gas velocity with corresponding increase in the amount of liquid entrained into the scrubber. Under conditions of absence of wall liquid film in the throat section, the above parametric study can be used to explain the working of such a scrubber operating in self-priming mode. Figure 5.21a shows the effect of increasing liquid flow rate with the same gas velocity and Figure 5.21b shows the effect of decreasing throat gas velocities at constant liquid injection velocity.

(a)



(b)

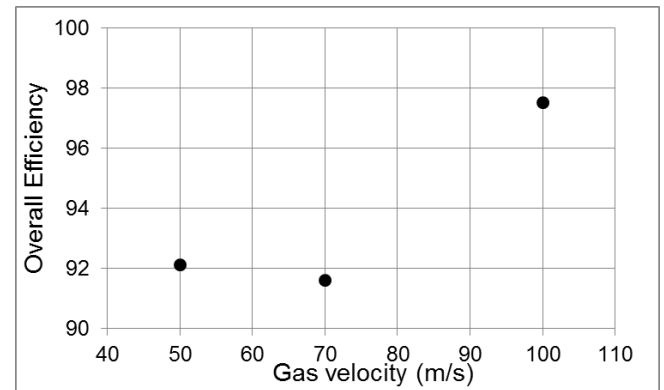


**Figure 5.21 (a) Variation of efficiency with changing liquid injection velocity for gas velocity of 70 m/s. (b) Variation of efficiency with gas velocity for liquid injection velocity of 5.03 m/s.**

Therefore, at fixed gas flow rate and increasing operating height for a self-priming scrubber, the scrubbing efficiency increases because of the increased throat coverage along with the increased number of collector surfaces. On the other hand, for cases incurring low gas velocity, the overall scrubbing efficiency is a balance between the increased jet penetration and the decreased number of collector surfaces. Therefore, in such conditions, by ensuring uniform throat coverage, a better scrubbing efficiency can be obtained (also discussed by Haller *et al.* (1989)). In other words, the scrubber should necessarily be designed for efficient utilization of the scrubber liquid for transients associated with lower gas velocities. This would eventually ensure an increase in the overall capture efficiency across all operating conditions. In addition to this, during passive operation, it is also desired to minimize the scrubber operating height so as to facilitate the upstream pressure to reach a lower limiting value. In this regard, the geometric parameters play a crucial role in achieving the above functionalities. Based on the simulation results obtained for different geometric parameters, two configurations are discussed in the following sections.

### 5.6.1. Injector system with different nozzle diameters

Based on the liquid flux profiles obtained for changing nozzle diameters, a single stage injection consisting of different nozzle sizes can be incorporated to extract the advantage of the difference in throat penetration achieved for each injection diameter. In this regard, two arrangements are considered for analysis: (a) 12 nozzles (4x 2 mm+ 4x 2.5 mm +4x 3 mm) (b) 16 nozzles (10x 1.5 mm + 4x 2.5 mm + 2x 3.5 mm), as shown in Figure 5.22. The scrubber was operated at 70 m/s gas throat velocity and 5.03 m/s liquid injection velocity, amounting to an overall liquid loading of  $\sim 1.1 \text{ l/m}^3$ . The two arrangements (A-2 and A-3) grossly differ by the volumetric contribution of each diameter to the total liquid load into the scrubber. A-3 represents an arrangement where near equal injection flow rate is allowed through each diameter set.

The relative difference in the liquid flux profiles obtained for these arrangements as compared to the single nozzle set is shown in Figure 5.23c. The liquid flux profiles showed that for a higher nozzle diameter the tendency of the entrained jet to go the centre of the throat section increases. The variation in the nozzle arrangement also influenced the droplet mean diameter and was found to have decreased with increasing number of smaller nozzles, as shown in Figure 5.23b, while having no effect on the saturation length of droplet breakup ( $\sim 30\%$  of the throat length). The decrease in peak liquid flux values recorded for each axial plane suggests the increase in droplet dispersion which helped in achieving a near uniform liquid flux profile at the throat outlet. Therefore, with the increase in droplet distribution coupled to the increase in the number of droplets, the overall scrubbing efficiency increased by an appreciable amount. The decrease in droplet diameter resulted in a marginal increase in the peak pressure drop, as shown in Figure 5.23a. The results of analysis for different gas flow rates are tabulated in Table 5.5. The results show a significant decrease in the SMD values for changing nozzle arrangement for lower throat gas velocities. Additionally, with the presence of high jet

penetration, the aerosol particulates get larger surface area for deposition and hence resulting in higher efficiency.

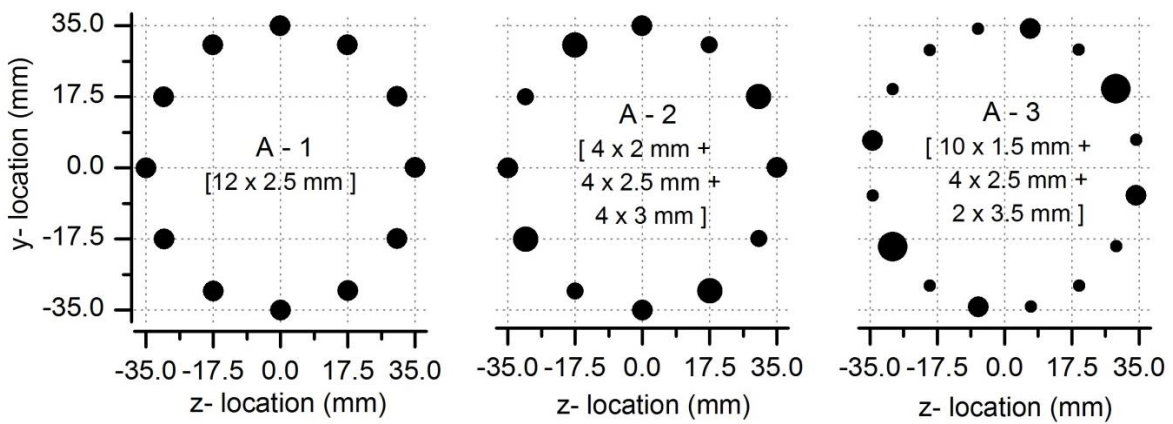
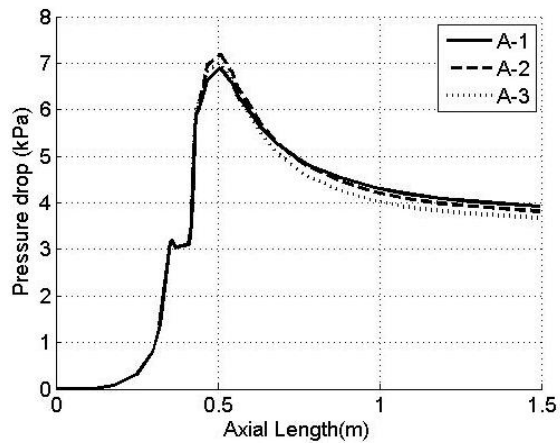
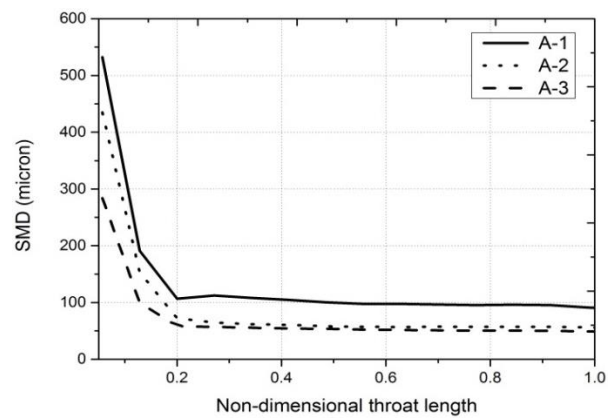


Figure 5.22 Representation of nozzles considered for an x-aligned venturi scrubber.

(a)



(b)



(c)

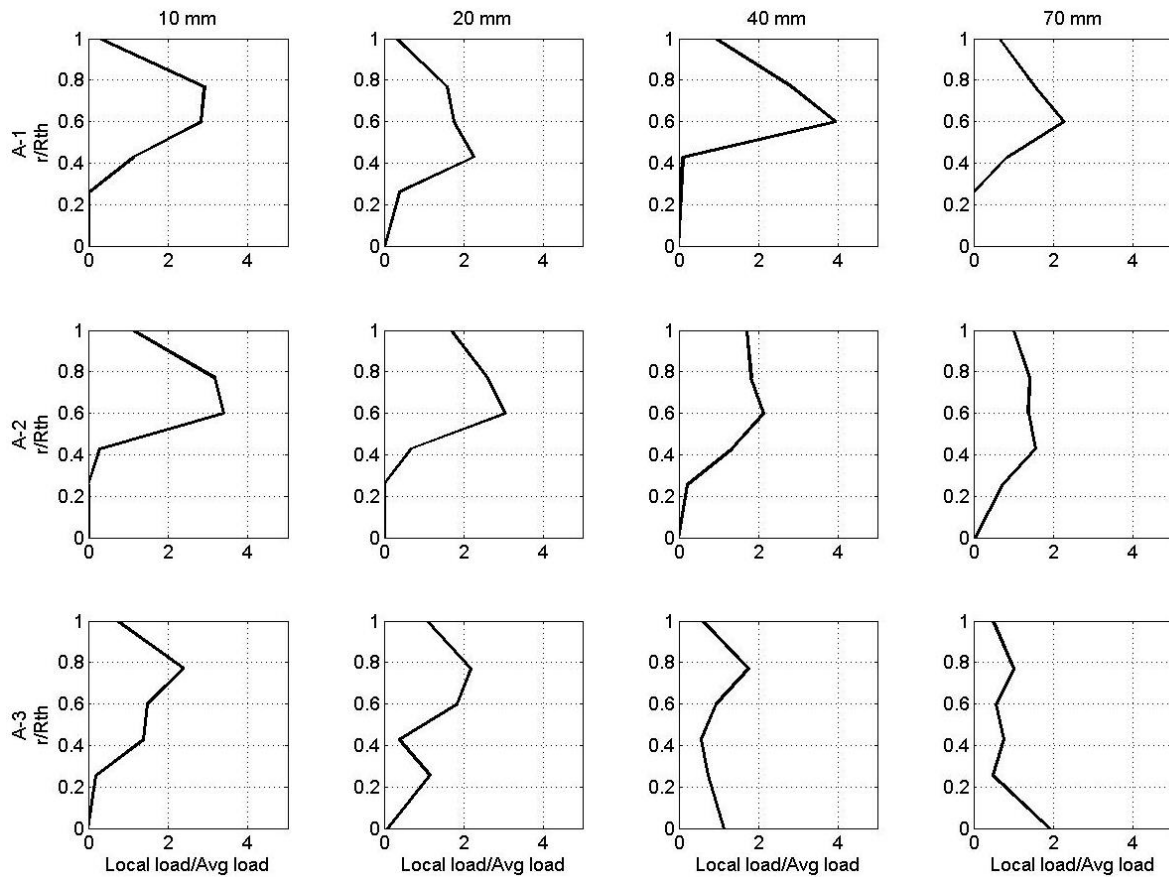


**Figure 5.23 (a) Axial pressure drop variation with variation in arrangement of nozzles at throat gas velocity 70 m/s and liquid loading  $\sim 1.1 \text{ l/m}^3$ . (b) Sauter mean diameter variation with different arrangement of nozzles in the throat section for throat gas velocity 70 m/s and liquid loading  $1.1 \text{ l/m}^3$  (c) Comparison of liquid flux profiles with variation in arrangement of nozzles at the throat end for gas velocity 70 m/s and liquid loading  $1.1 \text{ l/m}^3$**

**Table 5.5 Scrubber performance for different nozzle arrangements at different throat gas velocities for the injection velocity of 5.03 m/s**

Throat gas velocity (m/s)	50			70			100		
Arrangement	A-1	A-2	A-3	A-1	A-2	A-3	A-1	A-2	A-3
SMD (micron)	147	92	75	90	56	49	44	30	30
Jet penetration	0.6	1	1	0.4	0.6	1	0.2	0.2	0.2
Efficiency of venturi scrubber	92.1	92.7	92.8	91.6	94.3	93.7	97.5	99.99	99.98

### 5.6.2. Multi-Stage Injection

The spray characteristics for a multistage injection system are investigated by introducing two stages of injection with identical number of nozzles (12x2.5mm) separated by 20 mm axial length (Figure 5.24). Further, the liquid injection velocity is kept constant at 6.28 m/s per nozzle at 70 m/s throat gas velocity in both the cases. The calculated scrubbing efficiency is found to increase in comparison to single-stage injector (Table 5.6). The jet penetration and the SMD value has also increased because of the increase in overall liquid loading to the venturi scrubber.

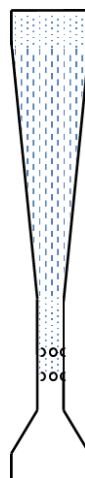


**Figure 5.24 Multi-stage injection in a venturi scrubber**

**Table 5.6 Comparison of scrubber performance for multi-stage injection at throat gas velocity 70 m/s**

Nozzle arrangement	Single stage injection ( $v_I = 6.28$ m/s) (12 x 2.5 mm)	Two stage injection ( $v_I = 6.28$ m/s) (12 x 2.5 mm separated by 20 mm)
SMD (micron)	84	120
Jet penetration	0.35	0.6
Efficiency	93.9	94.7

Therefore, multistage injectors are helpful in enhancing the efficiency of the scrubber, but the positioning of the stages plays an important role in governing the droplet size and hence the jet penetration obtained in the throat section of the scrubber. From the design point of view, the multiple stages of injection in the venturi scrubber should be separated by at least the atomization length of the prior injection. The flow through the subsequent stages of injection would attain different penetration lengths in the throat section due to gradual deceleration of the continuous gas phase.

## 5.7. Closure

The development of a CFD model is presented in detail highlighting the governing equation for both gas phase and droplets. The effect of interaction term i.e. drag term is focussed in depth. The developed computational model is shown to match well with the pressure drop, liquid flux distribution and the scrubbing efficiency of aerosols of Haller et al. data (1989) within  $\pm 10\%$ .

The developed model was implemented for predicting the effect of different parametric conditions, namely gas velocity, liquid flow rates, nozzle diameter and throat length on the performance of venturi scrubber. From the parametric study, it was found that higher jet penetration obtained for high liquid loading ratios help in increasing the scrubbing efficiency. The droplet size is strongly dependent on the continuous velocity. The axial pressure drop

profiles followed a monotonic trend of increased pressure drop with the increase in the liquid loading to the scrubber.

Further the model was applied to the experiments conducted in the submerged venturi scrubber. The retention of iodine is calculated from the gas droplet mass transfer coefficient given by Steinberg and Treybal correlation. The model is validated with the experiments conducted on a submerged venturi scrubber operation and can be employed to assess the performance of venturi scrubber under flow conditions expected in FCVS during accidental situations. The key findings from the application of the model to the present experiments are:

- The liquid loading to the scrubber is evaluated from the radial pressure drop at the nozzles in the throat section. The interfacial loss coefficient is found to follow power law correlation with Reynolds number of air at the inlet.
- The interfacial loss increases with increase in air flow rate. The liquid loading hence decreases with increase in air flow rate.
- The model was found to successfully predict the two phase pressure characteristics in the venturi scrubber. The air phase accelerates in the converging section due to which the pressure decreases. At the nozzles location (0.2 m), there is a sharp pressure drop due to the entrainment of liquid. The two phase pressure plot in the venturi scrubber showed no recovery in the diverging section.
- The iodine retention efficiency in the venturi scrubber was found to increase with increase in air flow rate despite the decrease in liquid loading to the scrubber. This is due to the enhanced number of droplets which increases the interfacial area for mass transfer of iodine vapours to droplets.

Based on the simulation results of the parametric study, the applicability of such a scrubber to self-priming mode is discussed in the context of efficient utilization of the entrained

liquid to the scrubber. It was shown that incorporating multiple diameter nozzles in the throat section improves liquid flux distribution and hence performance of venturi scrubber when it is operated in self-priming mode. Similar effect was seen by having multiple injection stages in the throat section.

## **Chapter 6. Performance of FCVS for reactor prototypic conditions**

### **6.1. Introduction**

During venting under postulated accidental scenarios, the flow and pressure from the AHWR containment was predicted by RELAP5 (Figure 6.1). The containment pressure builds up initially and then at the set pressure, the rupture disk bursts and allows the flow to the scrubber as shown in Figure 6.1. This allows the flow of gas from containment to the manifold of venturi scrubbers. This flow then experiences the friction pressure losses in the pipes and fittings and then enters the venturi manifold in the scrubber tank.

The flow and pressure transients observed indicated that there is a high flow rate initially but as venting continues, both the flow and the pressure released from the containment decreased. The flow rate from the containment suddenly rises to nearly 22 kg/s and then drops very fast to about 2.5 kg/s, and then remains steady at nearly 1 kg/s. Hence, the flow remained within 2.5 to 1 kg/s at 78 kPa (g) for most part of the transient venting conditions (0.10-0.02 kg/s per venturi scrubber). The pressure at the inlet of venturi scrubber system in the reactor is expected to be around 100 kPa (g) to 70 kPa (g).

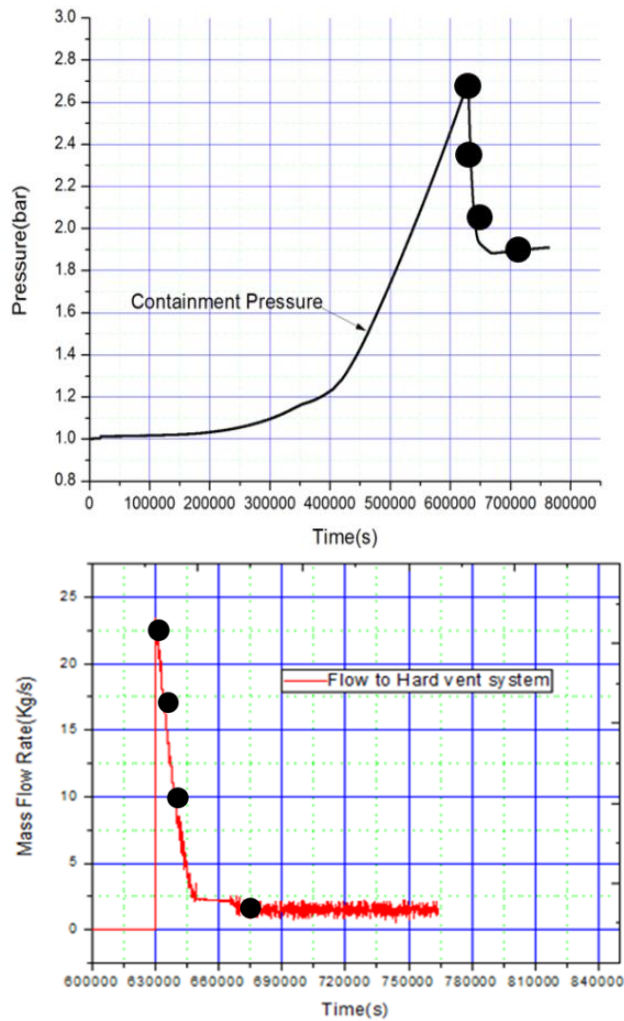


**Figure 6.1** Pressure and mass flow rate from containment calculated from RELAP5

## 6.2. Case Settings

The initial conditions of inlet pressure and flow (velocity) from the containment are calculated from the RELAP5. The friction losses in the connecting pipe to the scrubber tank are calculated. The pressure conditions and gas flow rate are hence obtained at the entrance of venturi manifold. The four different mass flow rates (Figure 6.1) (shown by black circles and mentioned by the mass flow rates value in the next sections) are chosen at different times from the containment for the performance evaluation of venturi scrubber. The total flow from Figure 6.1 is divided equally in all venturi scrubbers (total 30 numbers). The geometry of a single

venturi scrubber is shown in Figure 6.2 along with the boundary specifications taken in the computational analysis.

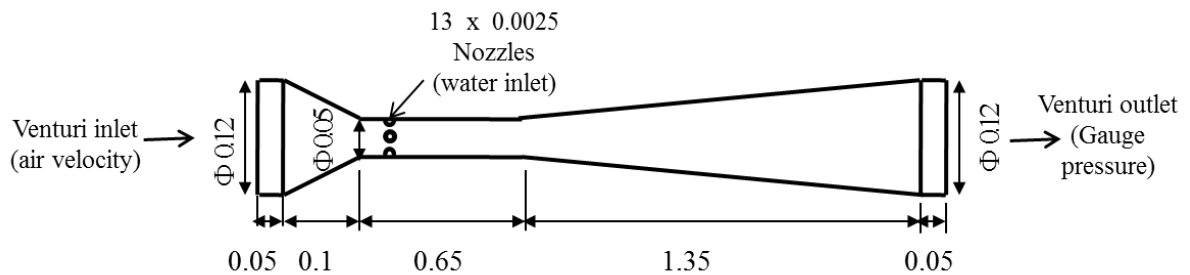


**Figure 6.2 Dimensions of venturi scrubber (in m) along with boundary conditions**

The velocity of droplets and outlet pressure are not known for CFD simulation. So, an iterative approach is adopted in which the outlet pressure and the liquid loading to the venturi scrubber is varied to match the inlet pressure (Figure 6.3). The values of liquid loading and the outlet pressure which match the known flow and pressure at the inlet of the venturi scrubber are assumed to be prevalent under reactor prototypic conditions. The same process is repeated for all cases. The details of the governing equations and the models implemented are discussed and benchmarked in the Chapter 5.

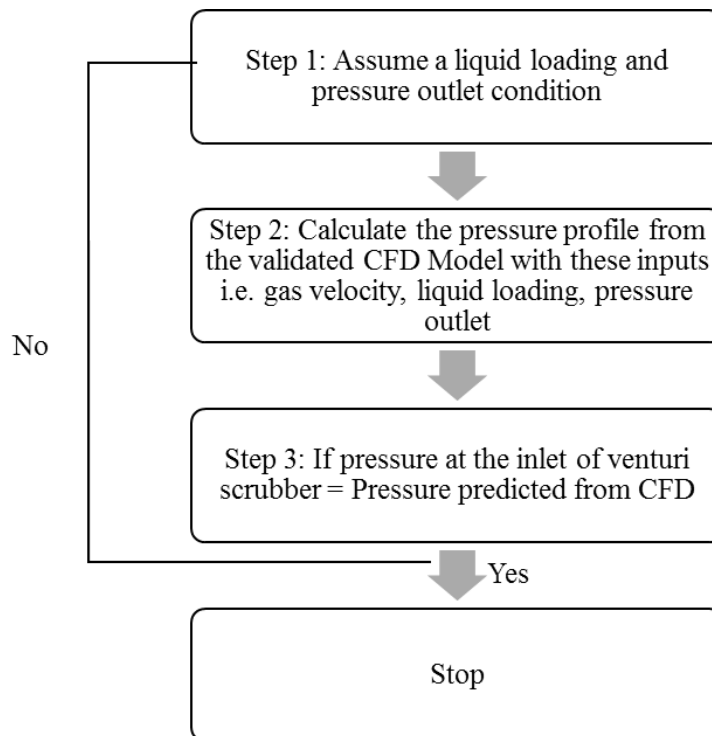


**Figure 6.3 Steps followed for predicting the hydrodynamics in the venturi scrubber at reactor prototypic condition**

## 6.3. Results and Discussion

### 6.3.1. Pressure profile in the venturi scrubber

The pressure profile is predicted in the venturi scrubber to evaluate the depressurization ability of the venturi scrubber. The values of liquid loading in a single venturi scrubber as a function of mass flow rate from containment have been calculated and are shown in Figure 6.4. The x-axis in Figure 6.4 indicate the mass flow rate from the containment to relate the instances of analysis from Figure 6.1 (though the analysis is conducted for a single venturi scrubber corresponding to which the liquid loading is represented in y-axis).

The pressure profiles are obtained for corresponding liquid loadings and gas flow rates as shown in Figure 6.5. It is seen that as the containment pressure decreases, the pressure profiles in the venturi scrubber showed different behavior in the diverging section. With the increase in

liquid loading at low gas velocities, the recovery of pressure in the diverging section decreases.

This was also observed in the experiments conducted in the submerged facility.

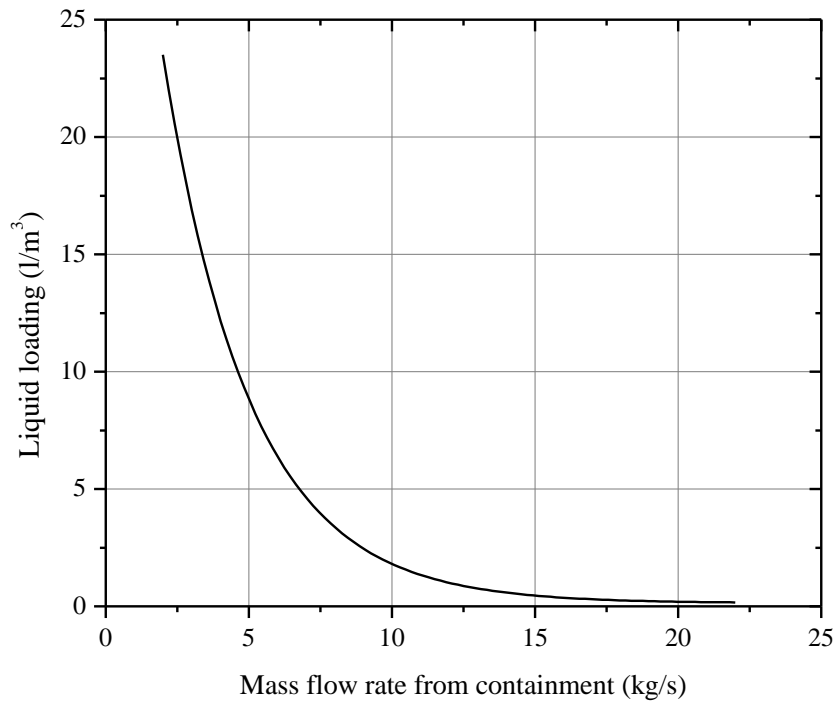


**Figure 6.4** *Liquid loading expected in the venturi scrubber.*

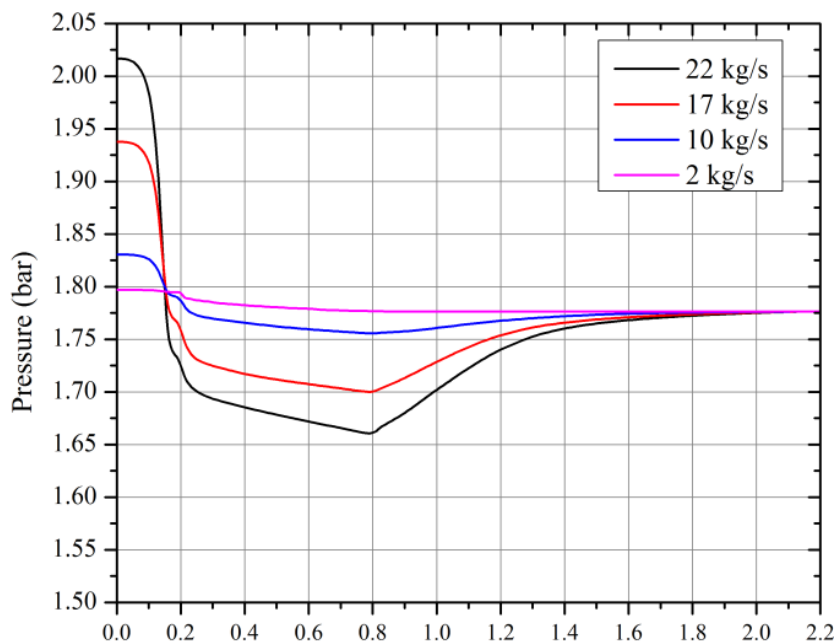
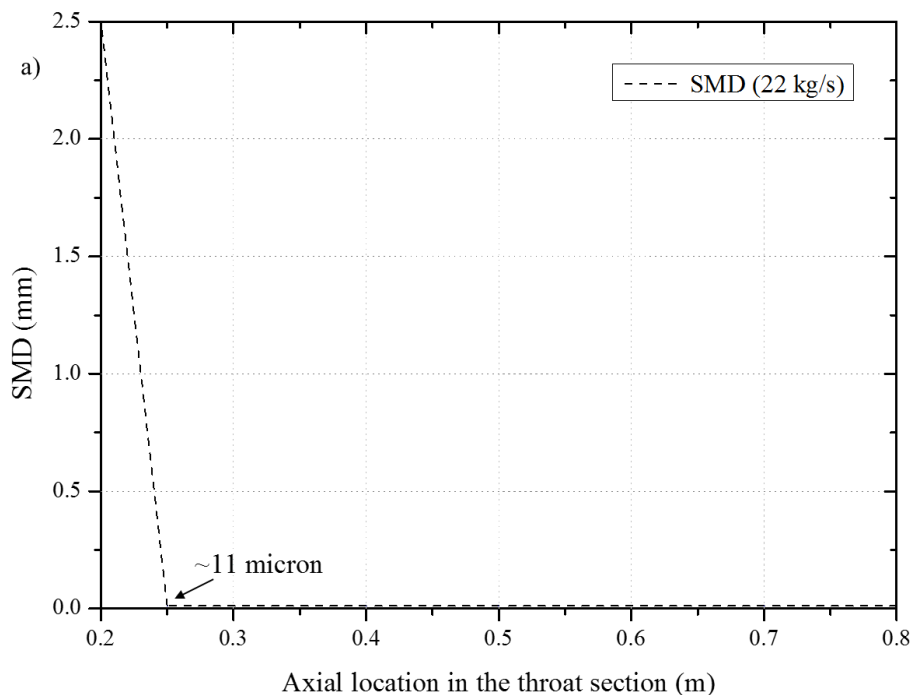


**Figure 6.5** *Pressure characteristics in the venturi scrubber for different air flow rates at different times of venting process*

It was also seen that the decrease in pressure in the throat section is also decreasing with the decrease in gas flow rate (Figure 6.5). With the decrease in gas flow rate, the amount of entraining liquid is increasing. Simultaneously, the energy of gas phase is decreasing while the inertia of entrained liquid is increasing. So, there is a decrease in momentum exchange and consequently pressure drop. The outlet pressure for all the cases is same but the pressure drop across the cases is different. This is because of different entrainment of scrubbing liquid across the nozzles in the throat section.

### 6.3.2. Droplets Sizes

This is probably due to lesser interaction of the gas phase and the droplets. This also indicates that at high gas velocities the sizes of the droplets formed is smaller. The droplet sizes predominantly decide the absorption efficiency of venturi scrubber. It was seen that for 22 kg/s gas mass flow rate from the containment, the droplets shed to micron size ( $\sim 11$  micron) at the start of injection and remain in that range throughout the downstream flow.



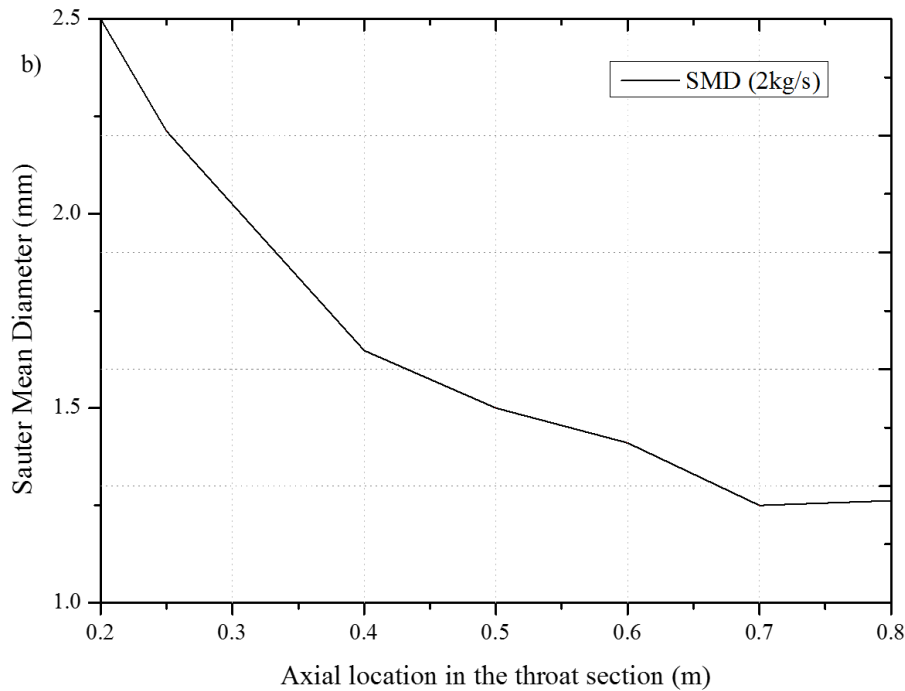


**Figure 6.6 Droplet sizes in venturi scrubber for (a) 22 kg/s and (b) 2 kg/s containment gas mass flow.**

While for 2 kg/s gas mass flow rate, the droplet sizes shown in Figure 6.6 show that the droplets didn't decrease to micron size droplets suddenly upon injection and some droplets coalesce to form bigger droplets downstream.

The governing force in the droplet size distribution is the shear. This shear experienced by the entrained phase is resisted by the inertia of the entrained liquid at the nozzles. So, after a certain distance which is approximately 0.3 m axial location in the present case the drag forces overcome the trajectory of the droplets.

### 6.3.3. Iodine absorption

The radioactive iodine vapours enter the venturi scrubber along with the gas flow. The absorption of iodine in the scrubber is attained by the addition of chemicals in the scrubber tank. The estimated inventory of iodine from the reactor fuel gave us the amount of chemicals catering to the total iodine that can be released under an extreme event involving severe core

damage. This calculated iodine is expected in gaseous form and its absorption through numerical calculation is calculated and shown in Figure 6.7.

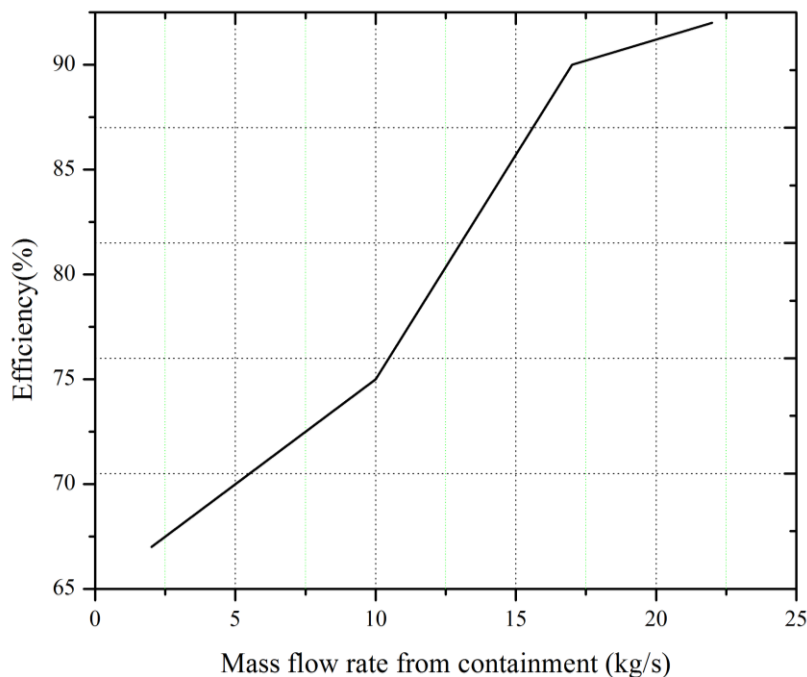


**Figure 6.7 Percentage absorption of iodine vapours in the venturi scrubber**

#### 6.4. Closure

The effectiveness of FCVS consisting of venturi scrubber in a submerged alkaline solution for depressurization and iodine absorption is investigated for an Indian advanced reactor conditions. The venturi scrubber plays an important role in depressurising the containment and filtering the contaminated gas. Therefore, its performance both pressure characteristics and iodine absorption are analyzed through a CFD framework.

- During the operation transients, the pressure and mass flow rate from the containment are expected to vary and they are predicted for prototypic reactor by RELAP5.
- The liquid loading to the venturi scrubber increases at low gas flow rates. However, the drop sizes formed are larger for low gas flow rates.

- The pressure profile predicted in the venturi scrubber numerically showed a decrease in the converging section and throat section. But for diverging section, the recovery in the diverging section decreases with the decrease in gas flow rate.
- The predicted iodine absorption efficiency is initially very high (~95%) but later it was decreasing and for prolonged period of venting it was found to be 68% due to decrease in gas flow rate.

## Chapter 7. Conclusions and Future Work

This chapter concludes the thesis highlighting the key findings and the recommendation for future work. The present study is focused to resolve several scientific aspects in the design of FCVS which is an important safety aspect installed in advanced nuclear reactors. The physics behind the working and the governing parameters of FCVS in the light of severe accidents has been brought out. Detailed study of the hydrodynamics and scrubbing behaviour of FCVS is demonstrated for an advanced Indian nuclear reactor through experiments in a scaled facility. The multi-phase interaction in the venturi scrubber is modeled through a CFD model benchmarked against the results in literature. The model is subsequently applied to predict the hydrodynamics and scrubbing behavior observed for the experiments conducted in the present study. The performance of the FCVS is predicted under reactor prototypic conditions. These flow transients during venting are calculated from thermal hydraulic code RELAP/mod 3.2. The main conclusions drawn out from the study are as follows:

### 7.1. Concept design of FCVS

- The radionuclide fission inventory to be retained using this system and the mean flow expected from the containment formed the design basis of FCVS for reactor conditions.
- Following this, the Calvert cut diameter technique, is used to calculate the dimensions and number of venturi scrubber in the FCVS manifold.
- The dimensions of the scrubber tank, the number of venturi scrubbers and the arrangement of the venturi scrubbers in the scrubber tank are finalized.

## 7.2. Understanding hydrodynamics of venturi scrubber involving multi-phase and multi-component systems

- For understanding the hydrodynamics and the interaction of the multiple phases present in the system, a scaled experimental set-up is built having a single venturi scrubber and a demister pad at the upstream enclosed in a tank. The dimension of venturi scrubber is same as that to be used in actual case.
- The set-up is provided with adequate DPTs and the sampling lines to measure the pressure drop and the scrubbing of radionuclide simulant iodine vapour.
- During venting from the containment, the flow transients indicated that for majority of duration the flow lies in the range of 2.5-1 kg/s (0.10-0.02 kg/s per venturi scrubber). The experiments were conducted in the scaled facility in this range of flow.
- In general, it is found that the pressure drop increases with gas flow rate for both low and high pressure conditions.
- The radial pressure at the throat nozzles is measured during the experiments and it was found to decrease with the increase in gas flow indicating the decrease in liquid loading to the venturi scrubber.
- With the decrease in flow pressure at 0.07 kg/s, it was found that the pressure recovery in the diverging section is not happening. This is attributed to the increased entrainment of scrubbing liquid at the nozzles indicated by the increased radial pressure at the nozzles. The radial pressure difference at the nozzles increased by 1 kPa with the decrease in flow pressure.
- Thus, a novel finding of no recovery of pressure in the diverging section of venturi scrubber was observed when multiphase flow passes with strong entrainment of large number of small sized droplets in the throat section unlike that observed in forced feed conditions for the venturi scrubbers used in chemical and process industries. This is

primarily due to the high amount of liquid entrained at the nozzles of the venturi scrubber which helps in scrubbing of radionuclides especially at low gas flow rates and flow pressure conditions.

- The measured pressure drop values were compared with the values predicted from the empirical models given in the literature and it was found that they were off by more than  $\pm 20\%$ .

### 7.3. Generation of test data and understanding the scrubbing of iodine vapour

- For the first time, the influence of gas flow rates, height of scrubbing liquid and concentration of iodine on scrubbing behaviour in submerged venturi scrubber operating in passive mode has been found out.
- It is reflected that the dependence of these factors is prominent at low gas flow rates.
- The amount of iodine scrubbed is well within the target requirements of the venturi scrubber even at high flow rates.
- The scrubbing behavior of submerged scrubber was measured as a function of gas mass flow rate (from 0.04-0.1 kg/s) at 4 m submergence depth. It was found that an increase in gas flow rate from 0.045 kg/s to 0.06 kg/s, increased the percentage retention of iodine in the scrubber tank from 60% to 85%. However, a further increase in gas flow rate to 0.1 kg/s increased the scrubbing performance to 95%.
- The effect of submergence depth on the scrubbing was investigated by decreasing the submergence depth to 3 m. It was observed that the scrubbing performance appreciably decreased by 10% with the submergence depth for the gas flow rate of  $\sim 0.045$  kg/s, but for high gas flow rates, the iodine retention converge to similar values.
- It was also observed that the iodine vapors had substantial affinity to deposit on internal surfaces of the scrubber tank existing prior to the sampling port present in the experimental facility, which enhances their retention.

#### 7.4. Development of CFD model for venturi scrubber performance

- It is found that the current empirical models available in literature fail to simulate the flow physics inside the venturi scrubber.
- A CFD model has been developed which simulates the inertial effect of entrained jet, the drag forces which determines the trajectory of the droplets, the interaction of aerosols and droplets for hydrodynamics and scrubbing of iodine inside the venturi scrubber.
- The model is found to accurately validate the hydrodynamics, liquid flux distribution at the axial locations in the throat section and retention of aerosols in forced feed mode published in the literature.
- The influence of geometric (i.e. nozzle diameter and throat length) and operating parameters (i.e. liquid loading and throat gas velocity) on the performance of venturi scrubber were investigated.
  - The droplet size is strongly dependent on the continuous phase velocity. With the increase in gas velocity, the sizes of droplets is decreased. This increase the performance of the venturi scrubber to 97.5% for throat gas velocity of 100 m/s as compared to an efficiency of 92% for 50 m/s of throat gas velocity.
  - From the parametric study, it was found that higher jet penetration obtained for high liquid loading ratios help in increasing the scrubbing efficiency.
  - The increase in throat length helps in a better dispersion of liquid flux with a marginal improvement in efficiency.
  - A higher nozzle diameter of 3.5 mm helped in achieving a better jet penetration without incurring additional pressure drop with 1.5% increase in efficiency as compared to the base case.

- The model is applied to the experiments conducted in submerged mode applicable to nuclear application. The retention of iodine vapour and the hydrodynamics including the pressure drop characteristics and the liquid injection at the throat nozzles are investigated.
  - The model successfully captured the hydrodynamic behaviour and quantified the iodine retention in the venturi scrubber.
  - The interfacial loss at the nozzles increases with increase in air flow rate and is a function of Reynolds number of gas phase at the venturi inlet. The liquid loading to the venturi scrubber, thus decreases with increase in air flow rate.
  - The iodine retention efficiency in the venturi scrubber was found to increase with increase in air flow rate due to the enhanced number of droplets despite the decrease in liquid loading to the scrubber.
- Based on the numerical model, two design modifications namely, multi-stage injection and variable throat nozzle diameter arrangement are suggested which will help in achieving a better liquid flux distribution and improving the performance of venturi scrubber.
  - Both these arrangements helped in achieving a percentage increase of 1-2% in efficiency for the cases investigated in the present study.

### 7.5. Performance of venturi scrubber for actual reactor conditions

- The CFD model was implemented for calculating the performance of a single venturi scrubber for reactor prototypic conditions to predict the iodine retention in the venturi scrubber.
  - The numerical simulations predicted that just at the start of the venting process the designed venturi scrubber would retain 95% of the incoming iodine vapor. This percentage will decrease with the decrease in gas flow rate to 68% for prolonged durations of containment venting.

- It was observed in the experiments that the iodine retention in the tank internals and the demister pad also enhances the scrubbing. Collectively, the efficiency of the venturi scrubber and the tank internals and other structures present will help in attaining the desired target of 99.9% retention.

## 7.6. Recommendations and Future Work

The installation of FCVS is mandatory for the retention of radionuclides which may be aerosol or vapour form. The design of FCVS investigated in the present study consisted of a manifold of venturi scrubbers and a demister pad upstream thus providing two stages of filtration for the retention of fission products, which can either be in aerosol or vapour form. The present experimental study investigated the efficiency of FCVS for vapour retention and development of the CFD model for the same. However, there are certain aspects, which need further investigation:

- Conducting experiments for aerosol retention with a wide range of size distribution.
  - This will involve building an aerosol generation chamber and measuring the aerosol capture efficiency.
- Conducting experiments with varying fractions of steam along with air as carrier gas.
  - It is stated in the literature that with steam the solubility of fission products increase and hence the efficiency of FCVS. This needs quantification.
- Conducting experiments with a manifold of venturi scrubbers for the same flow conditions to verify the scaling philosophy
  - This will essentially help in identifying that whether the venturi scrubber performance is affected by the presence of other scrubbers in the manifold or is independent.

- Improving the CFD model based on the above findings
  - The above experimental studies will help in understanding the loss coefficient (K) across the nozzles in the throat section of the venturi scrubber. These studies can be further utilized to develop a model on K.
  - All of the above studies will generate data, which can be further plugged in the CFD model to make more reliable and comprehensive.

# Synopsis

The three major accidents in the nuclear power plants in the past namely, Three Mile Island, Chernobyl and the much recent Fukushima have time and again emphasised that the safety of the nuclear reactors needs reassessment and better understanding, and adopt mitigatory systems so that the risk to public is almost eliminated. The nuclear community also learned that in the absence of Containment Venting systems, the containment pressure may rise and it may threaten the structural integrity of the containment and may ultimately lead to release of hazardous radionuclides to the environment. Therefore, in such instances of severe accident, many utilities have proposed and are in the process of deploying the Filtered Containment Venting System (FCVS) which would help in reducing containment pressure build-up and retain the radionuclides without releasing to the environment. The venturi scrubber has been traditionally implemented in chemical and process industries to remove effluent from the venting gas from these plants. The venturi scrubbers used in these industries, operate in forced feed mode and the effluent gas to be treated is having a fixed mass flow rate and a fixed concentration of pollutants. There are a few studies on the scrubbing characteristics of such forced feed scrubbers. However, for nuclear power reactors, the design of venturi scrubbers is not straight forward. This is primarily because the flow conditions in the venturi scrubber vary with time with venting of containment and the radionuclides inventory in the reactor at the time of operation is dependent on the fuel composition, burn-up, operational conditions, etc. Therefore, to design the FCVS catering to such conditions is much more complicated than what is understood for chemical and process industries. Additionally, the proprietary nature of the design leads to the scarcity of the information in literature for the particular application.

For the Indian advanced reactor application, as considered in the present design, the FCVS is designed to operate in a passive mode unlike the traditional scrubbers used in chemical

and process industries. The FCVS configuration considered in the present study consists of a manifold of wet scrubbing unit, i.e. a set of venturi scrubbers submerged in a pool of scrubbing liquid along with a demister and metal fiber assembly at the top. The venturi scrubber has three different geometrical cross-sections. The converging section accelerates the contaminated gas; then it arrives at the throat section having several nozzles and finally the diverging section which allows for recovery of pressure. The throat section is having nozzles which allow entrainment of scrubbing liquid due to the large radial pressure difference created between the scrubber tank and the fluid at the throat. The entrained liquid encounters high speed gas in the throat section which shears it to droplets and enhances area for interaction of aerosols and vapour from the contaminated gas. Hence, the flow in a venturi scrubber comprises of gas, aerosols, scrubbing liquid, air and vapour. The interaction among these phases determines the efficiency of the venturi scrubber. Other parameters which influence the performance of venturi scrubber are its geometry, operating conditions and size and number of the nozzles. The scarcity of the test data and unavailability of required models to design such systems is a challenge and hence is the motivation of this study. The major scientific issues identified from the literature for the design of an efficient venturi scrubber are enlisted below:

- a) The hydrodynamic behavior of venturi scrubber: This is complex due to the interaction of the different phases present in the venturi scrubber and it plays an important role in deciding the scrubbing behavior and retention of radionuclides.
- b) Lack of test data: This creates major issues in understanding the fundamentals in the scrubbing behavior, especially the influence of operating parameters and geometry of the venturi scrubber on the scrubbing.
- c) Flow phenomena inside the venturi scrubber is multi-dimensional and CFD model needs to be developed to treat the complex flow physics inside the venturi scrubber.

d) Performance of venturi scrubber for actual reactor applications is not known since it is influenced by large number of operating and geometric parameters.

The above issues are resolved in the present study. A conceptual design of venturi scrubber for an Indian advanced nuclear reactor has been made based on empirical models available in literature (Yung et al. (1978)). The inputs to the design, i.e. contaminated gas flow characteristics from the containment are calculated from RELAP5 during postulated severe accident scenario for the reactor. Thus, knowing these input conditions and the desired goal for retention of radionuclides in the scrubber, a heuristic approach has been adopted to obtain the liquid loading to the scrubber. Since the desired liquid loading to the scrubber can be achieved only passively by radial pressure difference across the nozzles, the submergence height of the scrubbing liquid and the number of nozzles have been calculated. Figure 1 shows the arrangement of Filtered Containment Venting System for the reactor considered in the present study.

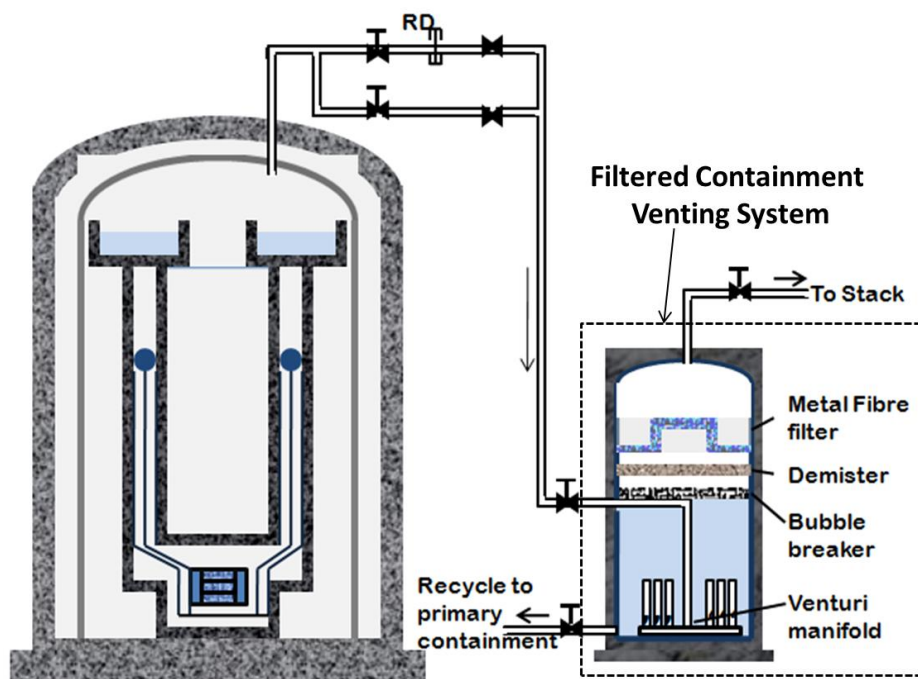


**Figure 1. Arrangement of Filtered Containment Venting System considered in the present study**

To demonstrate the performance and understand the scrubbing behavior of this venturi scrubber, an experimental set-up has been built. The setup (Figure 2) consists of a single venturi scrubber of dimensions one-to-one same as that for reactor design conditions. The inlet flow rate is scaled to that of one venturi scrubber of the prototype case, with air as the working fluid and iodine as radionuclide simulant. The inlet pressure, gas flow rate, height of scrubbing liquid and iodine concentrations were varied similar to that of the prototypic conditions to understand the hydrodynamics and scrubbing behavior. The accuracy of measurements is given in Table 1.

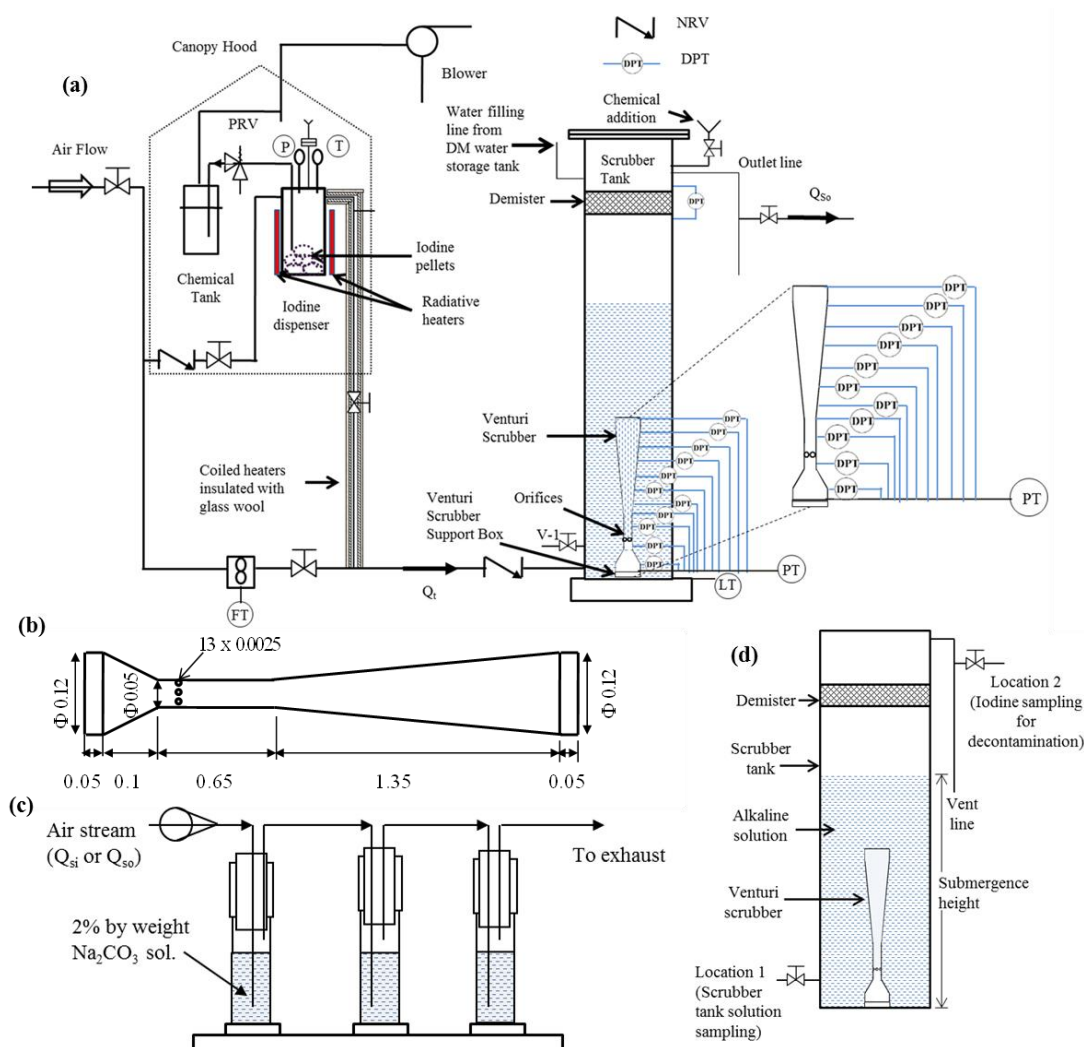


**Figure 2 (a) Schematic of the experimental setup. V-1 (Location-1): Scrubber tank sampling;  $Q_{So}$  (Location 2): Flow rate for Measuring Iodine Concentration at the outlet of the venturi scrubber;  $Q_i$ : Inlet Flow of air to the venturi scrubber (b) Venturi scrubber**

*dimensions (in m) (c) Sampling arrangement for measuring bulk iodine vapour decontamination factor (d) Location of sampling ports in the experimental set up*

**Table 1. Accuracy of the measurements**

Parameter	Instrument	Accuracy
Pressure	Differential Pressure Transmitter	$\pm 1\%$ of the measured values
	Pressure Transmitter	$\pm 1\%$ of the measured values
Flow	Turbine Flow Meter	$\pm 1\%$ of the measured values
Level	Level Transmitter	$\pm 1\%$ of the measured values
Temperature	Thermocouples	$\pm 0.75\%$ of the measured values
Iodine concentration	ICP-MS (Least measurement 1.1 ppb)	within 5%
	ICP-OES (Least measurement 0.5 ppm)	within 10%

The axial pressure drop across the venturi scrubber and the radial pressure difference across the nozzles at the throat section have been measured and shown in Figure 3. The pressure drop profiles have been used for predicting the flow distribution in the venturi scrubber. It is important to understand the adequacy of the models available in literature for predicting the pressure drop in the venturi scrubber; hence they have been used in the present study and have been compared with the experimental results (Figure 3).

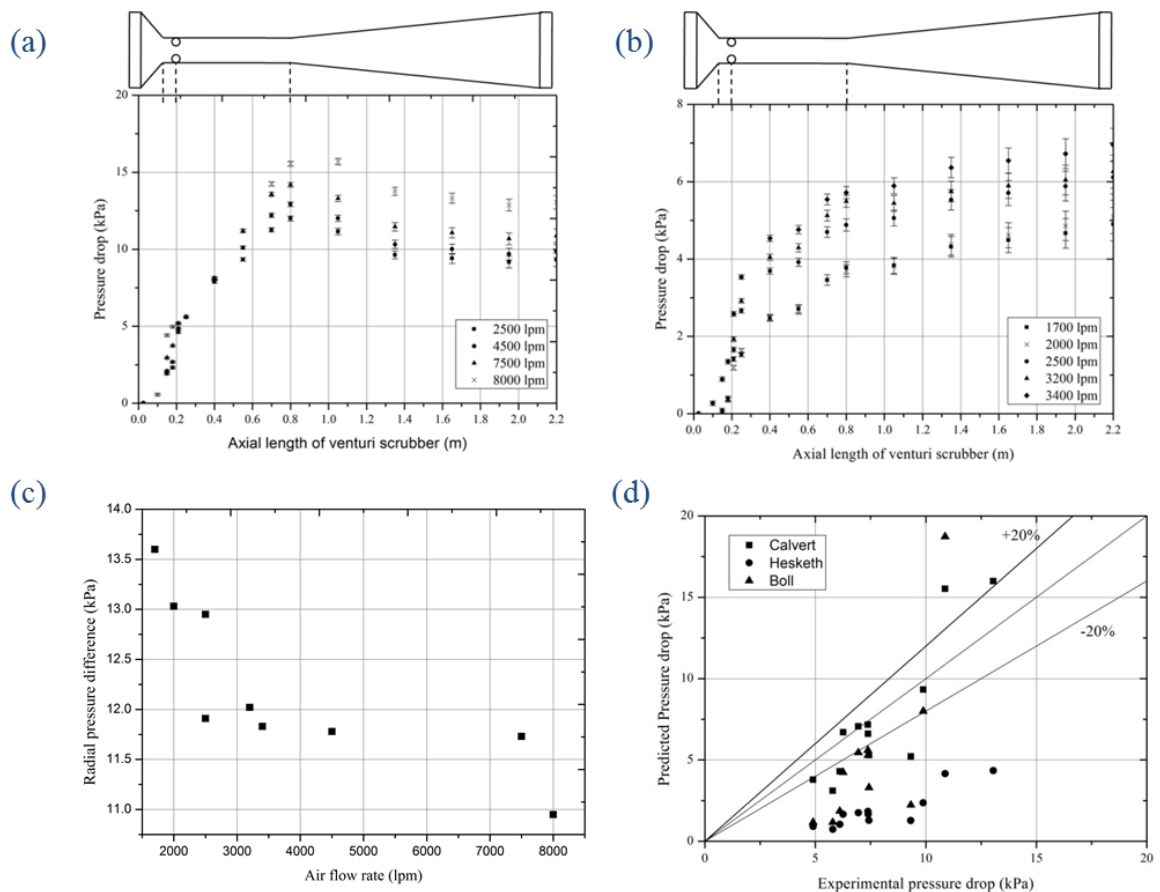


**Figure 3. Pressure drop in venturi scrubber for (a) high gas flow rates and (b) low gas flow rates at 4.5 m submergence height. (c) Radial pressure difference across the nozzles in the throat at low gas flow rates for initial submergence height of 4.5 m. (d) Comparison of predicted pressure drop with measured pressure drop**

The following conclusions were drawn:

- In general, it is found that the overall pressure drop in the venturi scrubber increases along the length of the scrubber with air flow rate for both low and high flow conditions.
- The pressure drop in the venturi scrubber reveals an increase in the converging section, a sharp increase in the throat section after the entrainment of liquid droplets from the scrubber tank and gradual recovery in the diverging section. But in low flow conditions, there is no pressure recovery in the diverging section of the venturi scrubber unlike that at higher flow rates (Figure 3(a) and Figure 3(b)). Thus, the hydrodynamic behavior of this

type of venturi scrubber operating in passive mode is completely different from that observed for forced feed ones where pressure recovery is seen in the diverging section of the venturi scrubber.

c) The radial pressure difference across the nozzles in the throat increases with the decrease in air flow rate (Figure 3(c)). This causes large scrubbing liquid influx into the venturi scrubber even at low gas flow rates to facilitate significant scrubbing, which is very important.

d) From the liquid loadings and the measured gas flow rate, the overall pressure drop incurred in the submerged venturi scrubber is calculated from the correlations of forced feed venturi scrubbers of Boll (1973), Calvert (1970) and Hesketh (1973) which are the models available in literature. It was found that large errors exist between the predictions and the measurements (Figure 3(d)).

After the hydrodynamics, the scrubbing of radionuclides especially iodine which is the most crucial aspect, has been investigated in the present experiments. This is done by heating known weight of laboratory grade iodine pellets and generating its vapour. The vapour is fed to the compressed air inlet line from where the mixture of the two enters the venturi scrubber. The tank is filled with sodium thiosulphate solution and sodium hydroxide solution (pH~11) because it reacts instantaneously with the iodine vapours. The iodine concentration retained in the scrubber tank and the bulk decontamination of iodine vapours is measured by ICP-MS analysis of the samples. The bulk decontamination (DF) is measured by passing compressed gas in three flasks arranged in series containing 2% by weight of sodium carbonate at the outlet of scrubber tank. It was found that the total amount of iodine exiting through the vent line is insignificant. The results obtained are summarised in Table 2.

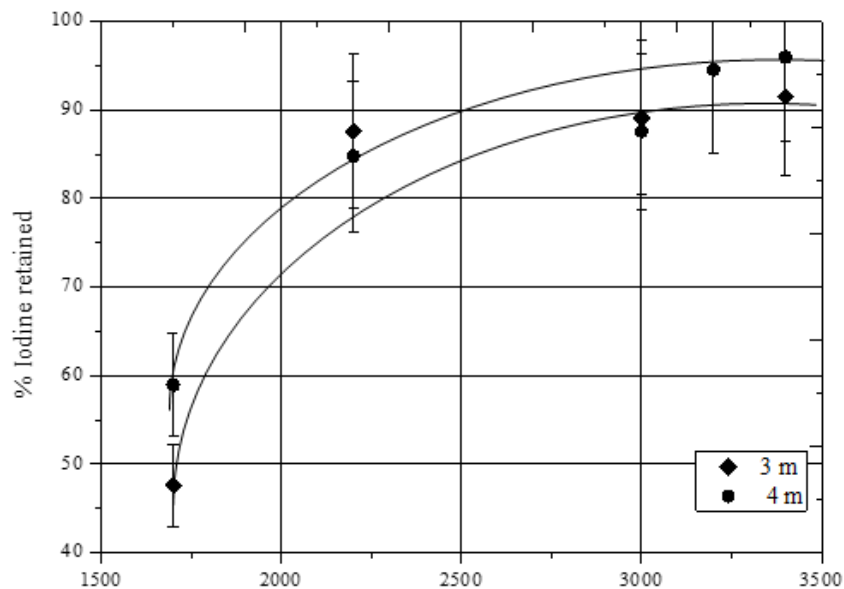
**Table 2. Summary of DF of iodine measured during experiments**

Q <sub>t</sub> (lpm)	Amount of iodine charged (one-time charge)(g) (W <sub>c</sub> )	Q <sub>so</sub> (lpm)	Concentration of dissolved iodine (ppb)			Total amount of dissolved iodine (μg) (W <sub>d</sub> )	Iodine removed by the venturi scrubber and alkaline pool(%)	Measured amount of Iodine leaving unscrubbed (g)	DF
			F-1	F-2	F-3				
2000	140	1.1	1971	967	932	1935	84.32	0.6148	228
3400	200	7	165	92	87	172	82.15	0.0811	2466
4200	35	4.5	BDL*	BDL*	BDL*	-	70.63	-	Very high

\*BDL-Below Detection Limit -1.1 ppb

The retention of iodine concentration in the scrubber tank shows the percentage of scrubbing contributed by the alkaline pool and venturi scrubber (Figure 4).

- a) At 4 m submergence depth, it was found that an increase in air flow rate from 1700 lpm to 2200 lpm, the percentage retention of iodine in the scrubber tank increased

**Figure 4. Iodine retention by the submerged facility**

from 60% to 85%. However, a further increase in air flow rate showed a lesser effect on the scrubbing performance of the submerged venturi scrubber.

- b) Effect of submergence depth on iodine retention was investigated by decreasing submergence height to 3 m. The results showed that the scrubbing performance appreciably improved (by ~10%) with the submergence depth for the air flow rate of 1700 lpm but for high air flow rates, the experimental values for both the submergence heights converge to similar values.

The experiments concluded that the FCVS configuration studied is adequate for retention of radionuclides during severe accident. After performing the experiments, CFD model was developed to simulate this multiphase flow in venturi scrubber. While developing the numerical model, several issues from literature were identified. Firstly, the formation of droplets doesn't occur instantaneously upon entrainment of liquid in the venturi scrubber and the forces governing the trajectory of entrained jet and stripping of droplets from the entrained jet needs to be explicitly studied. It was reported in the literature that the inertia of the entrained jet also governs the distribution of droplets formed in the venturi scrubber. Additionally, a mean diameter cannot account for the poly-disperse range of droplets that form in the venturi scrubber as pointed out in the literature. Therefore, a CFD model which simulates the inertial effect of entrained jet (by relaxation of drag coefficient (Schmehl et al. (2000)) near the injection) and its further break up (Beale and Reitz (1999)) because of the interfacial shear is developed. The drag forces are considered to play a pivot role in shaping the trajectory of the droplets. The interaction of aerosols and droplets is assumed to occur only through inertial impaction (Boll (1973)). The model has been benchmarked first with the experimental findings of Haller et al. (1989) for liquid flux distribution (Figure 5(b)), pressure drop (Figure 5(d)) and scrubbing efficiency (Table 3) of silica particles (aerosols) for a forced feed venturi scrubber. It was found that the CFD model is able to predict the experimental results within  $\pm 10\%$  accuracy.

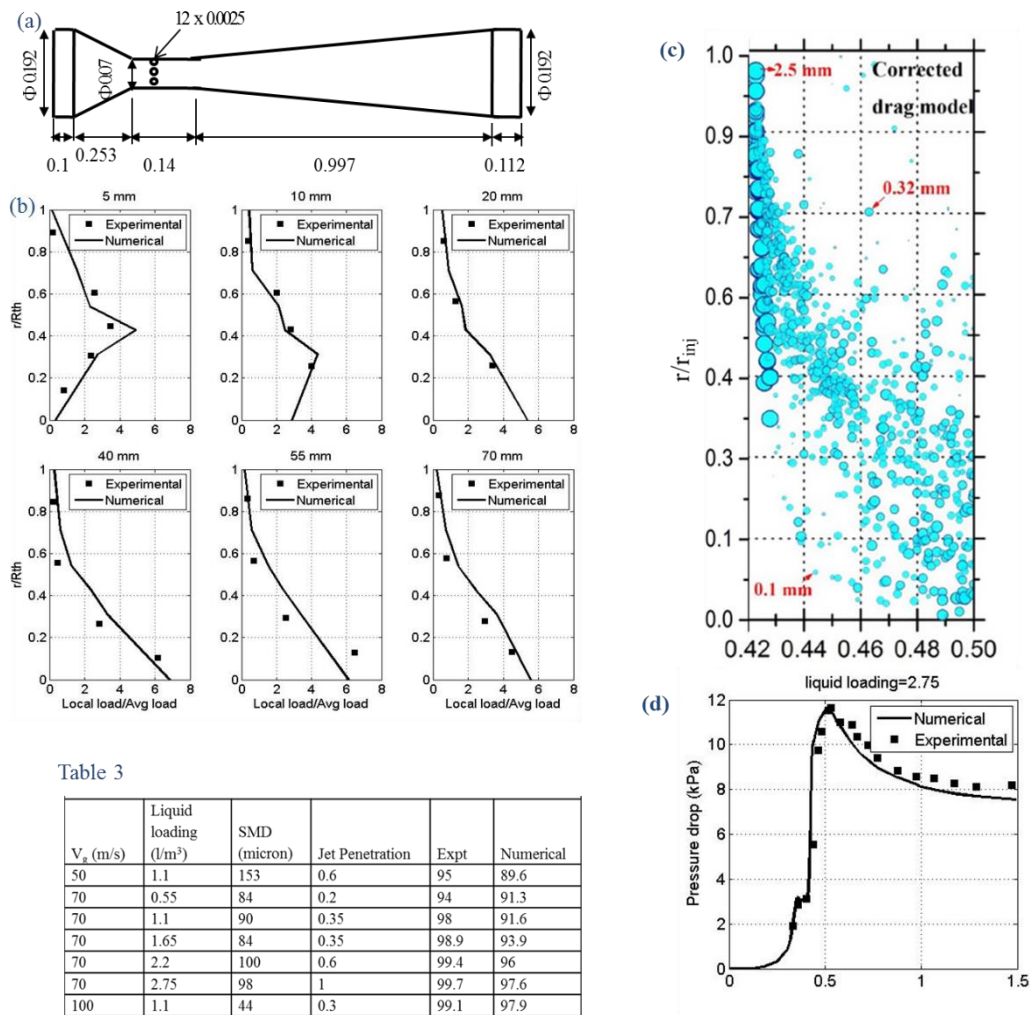


**Table 3. Results of validation studies.**

**Figure 5 (a) Geometry of venturi scrubber (b) Liquid flux distribution at different axial locations in venturi scrubber after liquid injection for 70 m/s throat gas velocity and 2.75  $l/m^3$  compared with experimental results (c) Droplet size distribution for 70 m/s throat gas velocity and 2.75  $l/m^3$  (d) Pressure drop for 70 m/s throat gas velocity and 2.75  $l/m^3$  compared with experimental results**

To understand the influence of operating and geometric parameters on the performance of venturi scrubber, parametric study for different throat gas velocities, liquid injection velocities, changing throat length and changing nozzle diameter has been done. It was concluded that a uniform distribution of liquid flux is desirable for better performance of venturi scrubber in self-priming mode. In this regard, two design modifications were proposed, i.e. variable diameter nozzle and multi stage injection which if implemented will

help in increasing scrubbing efficiency of aerosols. The CFD model thus developed has been further validated with the present experimental results obtained in the submerged experimental facility. The domain of analysis was restricted to venturi scrubber only. The pressure distribution, droplet characteristics and the percentage iodine absorption were calculated. The model accounted for the relative motion of the droplet and air phase. The following results were obtained:

- The pressure variation across the venturi scrubber observed in the experiment were predicted well with experimental values. The air phase accelerates in the converging section due to which the pressure increases. At the nozzles location (0.2 m) there is a sharp pressure drop due to the injection of droplets. The two phase pressure in the venturi scrubber showed no recovery in the diverging section (Figure 6(a)).

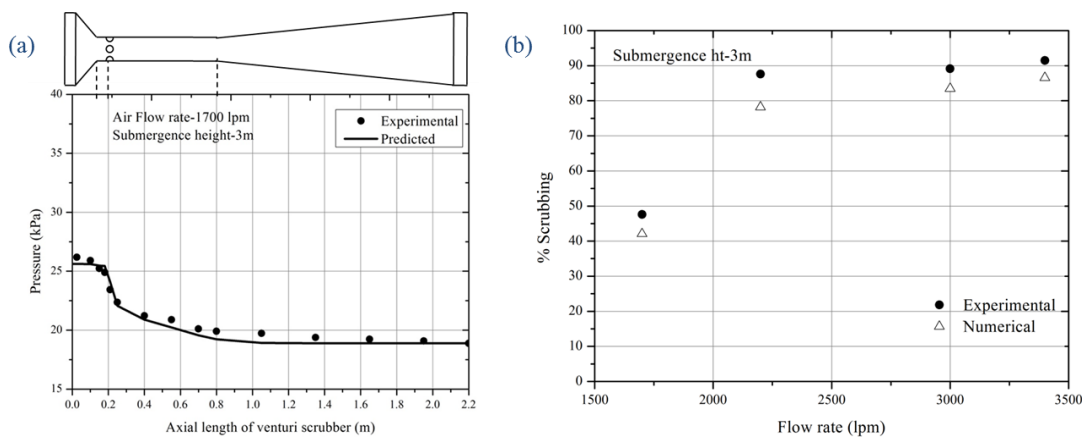


**Figure 6 (a) Pressure characteristics for 1700 lpm air flow rate at submergence height of 3m (b) and percentage scrubbing of iodine vapours at submergence height of 3m.**

- The iodine retention efficiency in the venturi scrubber was found to increase with increase in air flow rate despite the decrease in liquid loading to the scrubber. This is due to the enhanced number of droplets which increase interfacial area for mass transfer of iodine vapours to droplets (Figure 6(b)).

Next the validated CFD model has been applied to predict the performance of venturi scrubber of the actual reactor. Before venting, the containment pressure builds up initially and then at the set pressure the flow through the rupture disk starts when it bursts. This allows the flow of compressed gas from containment to the manifold of venturi scrubbers. This flow and inlet pressure to the scrubber from the containment was calculated using RELAP5. The flow and pressure transients observed indicated that there is a high flow rate initially but as venting continues, both the flow and the pressure from the containment decreased.

The pressure profile expected in the venturi scrubber at different times of venting and corresponding iodine absorption efficiency achieved in a single venturi scrubber of the manifold of FCVS was calculated. It was found that the pressure profiles (Figure 7(a)) exhibited two different behaviors in diverging section of venturi scrubber as was seen in experiments.

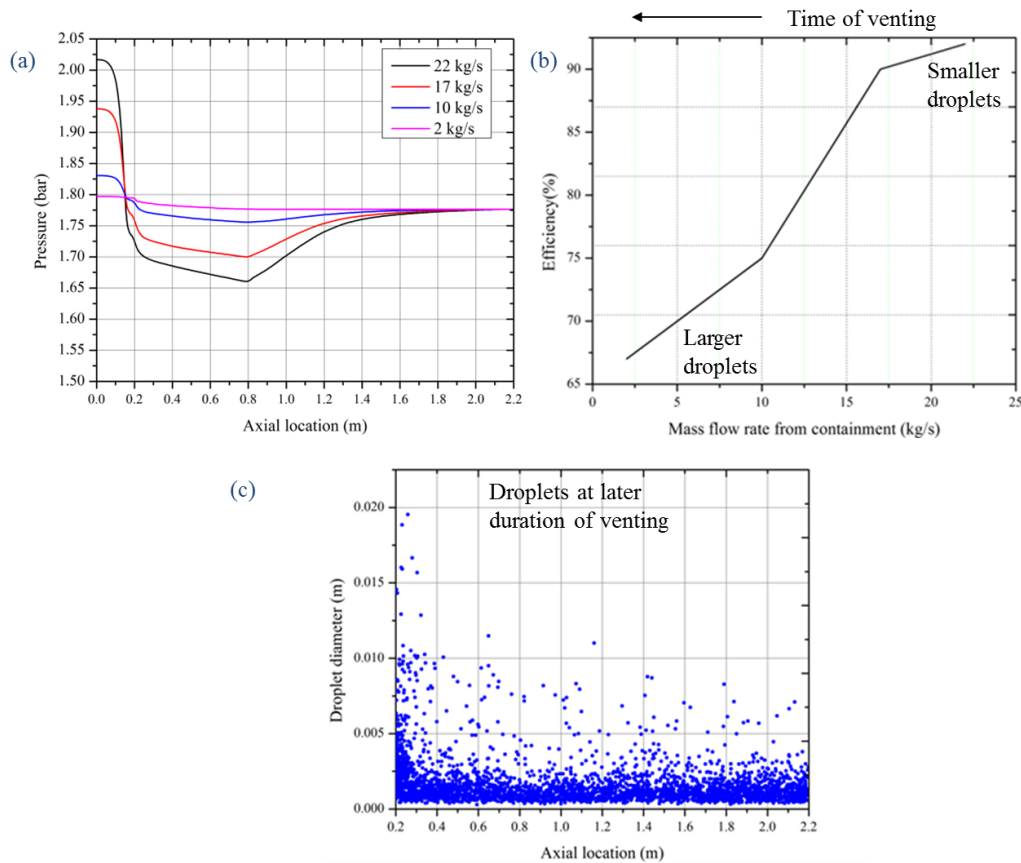


**Figure 7 (a) Pressure characteristics and (b) iodine absorption efficiency in a venturi scrubber for different mass flow rates from the containment at different times of venting process (c) Droplet sizes formed in the venturi scrubber at later duration of venting**

Initially at high pressure and mass flow from the containment, the liquid loading to the scrubber is found to be lesser as compared to prolonged durations of venting. At this situation, the interfacial drag is high due to the large difference in the velocities. This promotes the formation of small micron sized droplets as observed in the simulation. Later when the mass flow from the containment decreases, the liquid loading to the scrubber increases owing to the self-priming operation. This results in decrease of interfacial resistance (or drag) because of the increased liquid inertia and the decreased gas velocity and increase in droplet size (Figure 7(c)).

The combined effect of gas velocity and liquid loading result in the pressure profiles shown in Figure 7(a). These droplets so formed in the venturi scrubber result in significant absorption of radionuclides as shown in Figure 7(b). The formation of smaller droplets at high mass flow rates promoted higher surface area for gas absorption and hence the predicted efficiency was more (Figure 7(b)).

In summary, the following insights are obtained from this study:

- The complex flow behavior inside the venturi scrubber operated in passive mode is simulated in the experimental set-up. A novel finding of no recovery of pressure in the diverging section of venturi scrubber was observed when multiphase flow passes with strong entrainment of large number of small sized droplets in the throat section unlike that observed in forced feed conditions for the venturi scrubbers used in chemical and process industries. This is primarily due to the high amount of liquid entrained at the nozzles of the venturi scrubber which helps in scrubbing of radionuclides especially at low gas flow rates.
- For the first time, the influence of gas flow rates, height of scrubbing liquid and concentration of iodine on scrubbing behavior in submerged venturi scrubber operating in passive mode has been found out. It is reflected that the dependence of these factors is prominent at low gas flow rates. However, the amount of iodine scrubbed is well within the target requirements of the venturi scrubber even at high flow rates.
- It is found that the current empirical models available in literature fail to simulate the flow physics inside the venturi scrubber. Therefore, a CFD model has been developed which simulates the inertial effect of entrained jet, the drag forces which determines the trajectory of the droplets, the interaction of aerosols and droplets for hydrodynamics and scrubbing of iodine inside the venturi scrubber. The model is found to accurately simulate the hydrodynamics and scrubbing of radionuclide simulants in forced feed and passive

mode of operation accurately. The influence of geometric and operating parameters on the performance of venturi scrubber was investigated.

- The CFD model was implemented for the prototype reactor condition to predict the iodine retention in the venturi scrubber and it was found that design is adequate.

### **Organization of the thesis**

The above studies have been described in the following chapters of the thesis. The thesis is divided into seven chapters. Each chapter ends with a closure. Chapter 1 discusses the introduction of the thesis providing the necessity for research on retention of radionuclides during severe accident in a nuclear reactor. This chapter highlights the importance of FCVS along with the state of art in this area. The literature survey is concluded with identifying unresolved scientific and technical objectives which is addressed in the thesis. Chapter 2 presents a conceptual design of a venturi scrubber. Following the heuristic approach, a design of venturi scrubber is proposed for reactor prototypic conditions. For the validation of the proposed design, an experimental facility is built which encompasses a single venturi scrubber and metal fibre filter. The setting up of the scaled experimental facility is discussed in Chapter 3. Chapter 4 focusses on the experimental results. This is divided in two different sections i.e. hydrodynamics and scrubbing of iodine vapour. The two phase axial pressure measurements across the venturi scrubber has been reported across the axial length of venturi scrubber. The overall pressure drop incurred is compared with the empirical models available in the literature. The measurements on the bulk decontamination factor achieved by the experimental facility and the iodine retention by the alkaline pool are discussed in relation to the observed hydrodynamics. Chapter 5 presents the development of a CFD model and its benchmarking with results published in literature on a forced feed venturi scrubber. In addition, the effect of different operating and geometric variables on the pressure drop; liquid flux distribution and aerosol capture in the venturi scrubber is investigated. The application of CFD model to the

passive venturi scrubber in experimental facility is further discussed. The injection characteristics in such conditions; resultant hydrodynamics and the interaction with iodine vapours in the venturi scrubber are presented by validation of the model with the experimental results presented in Chapter 4. In the subsequent chapter 6, the developed and validated numerical model is applied to predict the performance of venturi scrubber (both hydrodynamics and percentage iodine absorption) at prototypic reactor conditions. Chapter 7 concludes the thesis with the key findings of the research and future recommendations.

## **REFERENCES**

Beale, J.C. and Reitz, R.D., (1999). Modeling spray atomization with the Kelvin-Helmholtz/Rayleigh-Taylor hybrid model. *Atomization and Sprays*. Volume 9 (6), Pages: 623–650. doi:10.1615/AtomizSpr.v9.i6.40.

Boll, R.H., (1973). Particle collection and pressure drop in venturi scrubbers. *Industrial Engineering Chemistry Fundamentals*. Volume 12, Pages: 40-50. doi: 10.1021/i160045a008.

Calvert, S., (1970). Venturi and other atomizing scrubbers. *AIChE Journal*. Volume 16, Pages: 392-396.

Haller, H., Muschelknautz, E. and Schultz, T., (1989). Venturi Scrubber Calculation and Optimization. *Chemical Engineering and Technology*. Volume 12, Pages: 188-195. doi:10.1002/ceat.270120125.

Hesketh, H.E., (1973). Atomization and Cloud Behavior in Venturi Scrubbing. *Journal of the Air Pollution Control Association*. Volume 23(7), Pages: 600-604. doi: 10.1080/00022470.1973.10469814.

Schmehl, R., Maier, G. and Wittig, S. (July 2000). CFD analysis of fuel atomization, secondary droplet breakup and spray dispersion in the premix duct of a LPP combustor. In: *Proceedings of 8th International Conference on Liquid Atomization and Spray Systems*, Pasadena, CA, USA.

Yung, S.C., Calvert, S. and Barbarika, H.F. (1978). Venturi Scrubber Performance Model. *Environmental Science & Technology*. Volume 12(4), Pages: 456-459.

## Thesis Highlight

Name of the Student: Paridhi Goel

Name of the CI: Bhabha Atomic Research Centre, Mumbai      Enrolment No.: ENGG0201304009

Thesis Title: Design of an efficient venturi-scrubber for retention of radionuclides during severe accident of a nuclear reactor.

Discipline: Engineering Sciences

Sub-Area of Discipline: Chemical Engineering

Date of viva voce: 04-01-2020

Under extreme conditions in a nuclear reactor, primary containment pressure may rise beyond design pressure and therefore, it must be depressurized to maintain containment integrity. In addition, the radioactive materials released during accident progression in the containment atmosphere must be retained to have negligible impact beyond the boundary. Filtered Containment Venting System (FCVS) is installed to carry out these functions. The design of FCVS employs a manifold of venturi scrubbers and a demister pad upstream thus providing two stages of filtration. There are several scientific issues associated with the design of the venturi scrubber such as (a) The hydrodynamic behaviour of venturi scrubber: This is complex due to the interaction of the different phases present and it plays an important role in deciding the scrubbing behaviour and retention of radionuclides. (b) Lack of test data: This creates major issues in understanding the fundamentals in the scrubbing behavior especially the influence of operating parameters and geometry (c) Flow phenomena inside the venturi scrubber is multi-dimensional and CFD model needs to be developed to treat the complex flow physics inside the venturi scrubber and (d) Performance of venturi scrubber for actual reactor application is not known since it is influenced by large number of operating and geometric parameters.

The above issues have been addressed in the present work through experiments and CFD simulations. A concept design of FCVS has been made using empirical models available in literature. The flow transients during venting are calculated from thermal hydraulic code RELAP/mod 3.2 and are used as inputs for calculating the dimension of venturi scrubber, number of venturi scrubbers and the dimensions of the scrubber tank. Detailed study of the hydrodynamics and scrubbing behaviour of FCVS is demonstrated for an advanced Indian nuclear reactor through experiments in a scaled facility (having a single venturi scrubber of 1:1 geometry) (shown in Figure 1). For relatively high pressure conditions, pressure drop reveals an increase with the gas flow rate similar to single phase flow and forced feed scrubbers. But in low pressure conditions, there is no pressure recovery in the diverging section of the venturi scrubber. The scrubbing efficiency increased with gas flow rate. The effect of submergence depth on iodine retention is prominent at low gas flow rates while at high gas flow rates the values of iodine retention converge to similar values. The overall decontamination factor of iodine vapors indicate that the target scrubbing efficiency is achieved. None of the earlier models on pressure drop could predict the measured pressure drop values. Therefore, the multi-phase interaction in the venturi scrubber is modeled through a CFD model benchmarked against the results in literature. The model is subsequently applied to predict the hydrodynamics and scrubbing behavior observed for the experiments conducted in the present study. The performance of the FCVS is predicted under reactor prototypic conditions.

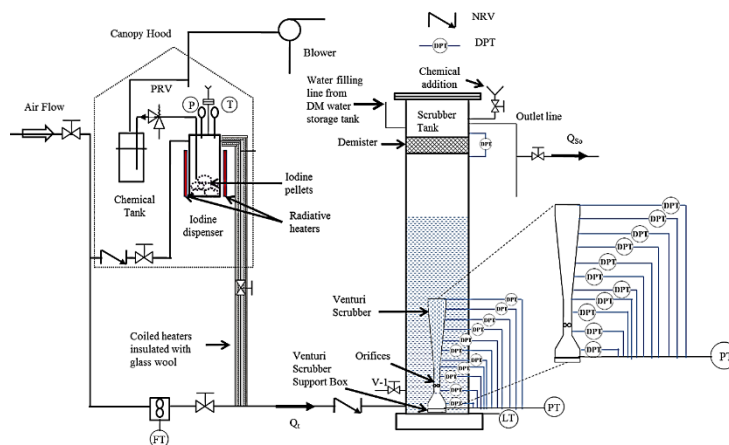


Figure 1 Schematic of experimental facility for FCVS

# List of abbreviations

AHWR	Advanced Heavy Water Reactor
BWR	Boiling Water Reactor
CDF	Core Damage Frequency
CFD	Computational Fluid Dynamics
CS	Carbon Steel
DF	Decontamination Factor
DM	Demineralized Water
DPT	Differential Pressure Transmitter
ECCS	Emergency Core Cooling System
FCVS	Filtered Containment Venting System
FP	Fission Products
FT	Turbine Flow meter for measuring flow of pressurised gas
GDWP	Gravity Driven Water Pool
HSSPV	High speed sliding pressure venturi
ICP-MS	Inductively Coupled Phase-Mass Spectrometry
ICP-OES	Inductively Coupled Phase-Optical Emission Spectrometry
KHRT	Kelvin Helmholtz Rayleigh Taylor Instability
LOCA	Loss of Coolant Accident
LT	Level Transmitter
MCCI	Molten Core Concrete Interaction
MW	Mega Watt
NRV	Non Return Valve

PDPA	Phase Doppler Particle Analyzer
PRV	Pressure Relief Valve
PT	Pressure Transmitter
PWR	Pressurised Water Reactor
RCS	Reactor Coolant System
RELAP	Reactor Excursion and Leak Analysis Program
RNG	Renormalization Group
SBO	Station Black Out
SMD	Sauter Mean Diameter
SS	Stainless Steel
TE	Thermocouples
TMI	Three-Mile Island

# Nomenclature

$A_p$	Droplet surface area ( $m^2$ )
$A_t$	Throat cross-sectional area ( $m^2$ )
$B$	Volumetric ratio of liquid to gas flow rates (dimensionless)
$B_0$	Kelvin-Helmholtz model drop size constant
$B_1$	Kelvin-Helmholtz model break up time constant
$c$	Concentration of iodine
$c_s$	Concentration of aerosol
$C_D$	Drag coefficient (dimensionless)
$C_L$	Core break up length constant
$C_{rt}$	Rayleigh-Taylor model drop size constant
$C_{\tau}$	Rayleigh-Taylor model break up time constant
$d$	diameter (m)
$d_{pa50}$	Performance cut diameter of aerosol (micron)
$dV$	Volume of computational cell ( $m^3$ )
$D_{in}$	Venturi inlet diameter (m)
$D_g$	Diffusivity of gas ( $m^2/s$ )
$g$	Acceleration due to gravity ( $9.8 m/s^2$ )
$k_g$	Mass transfer coefficient (m/s)
$K$	Loss coefficient
$K_p$	Inertial impaction parameter (dimensionless)
$K_{p50}$	Critical impaction parameter (dimensionless)
$l$	Throat length (cm)

L	Non-dimensional length
m	Mass (kg)
N	Number of particles in one parcel
$N_{\text{cap}}$	Number of aerosol particles captured by one droplet in a computational cell
$P_{\text{tank}}$	Hydrostatic pressure in the scrubber tank just outside the nozzles in the throat section (kPa)
$P_{\text{th}}$	Pressure in the venturi scrubber just inside the nozzles in the throat section (kPa)
$q_l$	Liquid to gas volumetric flow rate ratio ( $l/m^3$ )
$Q_g$	Volumetric flow of gas phase ( $m^3/s$ )
$Q_s$	Flow rate for Measuring Iodine Concentration at the outlet of the venturi scrubber (lpm)
r	Radial position in the throat section (m)
$r_d$	Radius of droplet (m)
$R_{\text{th}}$	Throat radius (m)
Re	Reynolds number for particle (dimensionless)
$Re_g$	Reynolds number of the gas at the venturi inlet (dimensionless)
S	Source term due to interaction with droplets ( $N\ m^2/m^3$ )
Sc	Schimdt number (dimensionless)
Sh	Sherwood number (dimensionless)
$t_{\text{res}}$	Contact time between droplet and iodine vapour (s)
$\Delta t$	particle time step (s)
u	Velocity vector (m/s)
$u_{\text{gin}}$	Velocity of air at the venturi inlet (m/s)
$v_g$	Superficial continuous (gas) phase velocity at the throat section (m/s)
$v_l$	Initial Velocity of entrained scrubbing liquid from the scrubber tank (m/s)
V	Volume of gas surrounding the droplet ( $m^3$ )

$V_d$	Volume of droplets ( $m^3$ )
$We$	Weber number (dimensionless)

### Sub-script

d	Droplet
ef	Deformed
g	Gas phase
in	inlet
ini	Initial concentration
l	Scrubbing liquid
out	out
s	Aerosol
sg	Aerodynamic mass median
sph	Spherical

### Greek letters

$\rho$	Density ( $kg/m^3$ )
$\tau$	Stress tensor (Pa)
$\sigma$	Surface tension ( N/m)
$\eta$	Target efficiency (dimensionless)
$\mu$	Viscosity of gas (Pa s)
$\alpha$	Volume fraction of dispersed phase (dimensionless)

## References

Ahmadvand, F. and Talaie, M. R. ((2010)) ‘CFD modeling of droplet dispersion in a Venturi scrubber’, *Chemical Engineering Journal*, 160(2), pp. 423–431. doi: 10.1016/j.cej.2010.03.030.

Ali, M., Yan, C., Sun, Z., Gu, H. and Wang, J. ((2013)) ‘Study of iodine removal efficiency in self-priming venturi scrubber’, *Annals of Nuclear Energy*, 57, pp. 263–268. doi: 10.1016/j.anucene.2013.02.014.

Ali, M., Yan, C., Sun, Z., Gu, H., Wang, J. and Mehboob, K. ((2013)) ‘Iodine removal efficiency in non-submerged and submerged self-priming venturi scrubber’, *Nuclear Engineering and Technology*, 45(2), pp. 203–210. doi: 10.5516/NET.03.2012.047.

Ali, M., Yan, C., Sun, Z., Wang, J. and Gu, H. ((2013)) ‘CFD simulation of dust particle removal efficiency of a venturi scrubber in CFX’, *Nuclear Engineering and Design*, 256, pp. 169–177. doi: 10.1016/j.nucengdes.2012.12.013.

Allen, R. W. K. and Van Santen, A. ((1996)) ‘Designing for pressure drop in Venturi scrubbers: The importance of dry pressure drop’, *The Chemical Engineering Journal and the Biochemical Engineering Journal*, 61(3), pp. 203–211. doi: 10.1016/0923-0467(95)03044-1.

Alonso, D. F., Gonçalves, J. A. S., Azzopardi, B. J. and Coury, J. R. ((2001)) ‘Drop size measurements in Venturi scrubbers’, *Chemical Engineering Science*, 56(16), pp. 4901–4911. doi: 10.1016/S0009-2509(01)00140-3.

Ananthanarayanan, N. V. and Viswanathan, S. ((1999)) ‘Effect of nozzle arrangement on Venturi scrubber performance’, *Industrial and Engineering Chemistry Research*, 38(12), pp. 4889–4900. doi: 10.1021/ie9902131.

Anderson, T. B. and Jackson, R. ((1967)) 'Fluid mechanical description of fluidized beds: Equations of Motion', *Industrial and Engineering Chemistry Fundamentals*, 6(4), pp. 527–539. doi: 10.1021/i160024a007.

Azzopardi, B. J. and Govan, A. . ((1984)) 'The Modeling of Venturi Scrubbers', *Filtration & Separation*, 21(3), pp. 196–200.

Beale, J. C. and Reitz, R. D. ((1999)) 'Modeling Spray Atomization With the Kelvin-Helmholtz/Rayleigh-Taylor Hybrid Model', *Atomization and Sprays*, 9(6), pp. 623–650. doi: 10.1615/atomizspr.v9.i6.40.

Boll, R. H. ((1973)) 'Particle Collection and Pressure Drop in Venturi Scrubbers', *Industrial and Engineering Chemistry Fundamentals*, 12(1), pp. 40–50. doi: 10.1021/i160045a008.

Calvert, S. ((1970)) 'Venturi and other atomizing scrubbers Efficiency and Pressure Drop', *AIChE Journal*, 16(3), pp. 392–396.

Chen, T., Smith, C., Schommer, D. and Nejad, A. ((1993)) *Multi-zone behavior of transverse liquid jet in high-speed flow, 31st Aerospace Sciences Meeting, Reno, NV, U.S.A.* doi: 10.2514/6.1993-453.

Clement, B., Cantrel, L., Ducros, G., Funke, F., Herranz, L., Weber, G. and Wren, C. ((2007)) *State of the Art Report on Iodine Chemistry (NEA / CSNI / R (2007)1)*.

Clift, R., Grace, J. . and Weber, M. E. ((1978)) *Bubbles, Drops and Particles*. Academic Press.  
*Containment system design for Pressurised Heavy Water Reactors Guide No. AERB/NPP-PHWR/SG/D-21 ((2007)) AERB SAFETY GUIDE.* doi: 10.1002/prs.10149.

Costa, M. A. M., Henrique, P. R., Gonçalves, J. A. S. and Coury, J. R. ((2004)) 'Droplet size in a rectangular Venturi scrubber', *Brazilian Journal of Chemical Engineering*, 21(2), pp. 335–

343. doi: 10.1590/S0104-66322004000200024.

Economopoulou, A. A. and Harrison, R. M. ((2007)a) ‘Graphical Analysis of the Performance of Venturi Scrubbers for Particle Abatement. Part I: Rapid Collection Efficiency Evaluation’, *Aerosol Science and Technology*, 41(1), pp. 51–62. doi: 10.1080/02786820601112839.

Economopoulou, A. A. and Harrison, R. M. ((2007)b) ‘Graphical Analysis of the Performance of Venturi Scrubbers for Particle Abatement. Part II: Size Distribution of Penetrating Particles’, *Aerosol Science and Technology*, 41(1), pp. 63–74. doi: 10.1080/02786820601112847.

Eguchi, W., Adachi, M., Miyake, Y. and Sakamoto, T. ((1975)) ‘Mechanism and rate of dilute iodine vapor absorption by aqueous sodium hydroxide solution’, *Journal of Nuclear Science and Technology*, 12(9), pp. 567–580. doi: 10.1080/18811248.1975.9733154.

Faeth, G. and Dahm, W. J. A. ((2006)) *Liquid Breakup in Dense Sprays*.

Gamisans, X., Sarrà, M., Lafuente, F. J. and Azzopardi, B. J. ((2002)) ‘The hydrodynamics of ejector-Venturi scrubbers and their modelling by an annular flow/boundary layer model’, *Chemical Engineering Science*, 57(14), pp. 2707–2718. doi: 10.1016/S0009-2509(02)00171-9.

Goel, K. C. and Hollands, K. G. T. ((1977)) ‘A General Method for Predicting Particulate Collection Efficiency of Venturi Scrubbers’, *Industrial and Engineering Chemistry Fundamentals*, 16(2), pp. 186–193. doi: 10.1021/i160062a003.

Gonçalves, J. A. S., Costa, M. A. M., Aguiar, M. . and Coury, J. R. ((2004)) ‘Atomization of liquids in a Pease Anthony Venturi scrubber Part II. Droplet Dispersion’, *Journal of Hazardous Materials B*, 116, pp. 147–157.

Gonçalves, J. A. S., Costa, M. A. M., Henrique, P. R. and Coury, J. R. ((2003)) ‘Atomization

of liquids in a Pease-Anthony Venturi scrubber: Part I. Jet dynamics', *Journal of Hazardous Materials*, 97(1–3), pp. 267–279. doi: [http://dx.doi.org/10.1016/S0304-3894\(02\)00266-2](http://dx.doi.org/10.1016/S0304-3894(02)00266-2).

Goniva, C., Tukovic, Z., Feilmayr, C., Bürgler, T. and Pirker, S. ((2009)) 'Simulation of offgas scrubbing by a combined Eulerian-Lagrangian Model', in *Seventh International Conference on CFD in the Minerals and Process Industries CSIRO, Melbourne, Australia*, pp. 1–7.

Gosman, A. D. and Loannides, E. ((1983)) 'Aspects of Computer Simulation of Liquid-Fueled Combustors', *Journal of Energy*, 7(6), pp. 482–490. doi: 10.2514/3.62687.

*Government of India Ministry of Power* (no date). Available at: <https://powermin.nic.in/en/content/power-sector-glance-all-india> (Accessed: 28 February 2019).

Guerra, V. G., Béttega, R., Gonçalves, J. A. S. and Coury, J. R. ((2012)) 'Pressure drop and liquid distribution in a venturi scrubber: Experimental data and CFD simulation', *Industrial and Engineering Chemistry Research*, 51(23), pp. 8049–8060. doi: 10.1021/ie202871q.

Gulhane, N. P., Landge, A. D., Shukla, D. S. and Kale, S. S. ((2015)) 'Experimental study of iodine removal efficiency in self-priming venturi scrubber', *Annals of Nuclear Energy*. Elsevier Ltd, 78, pp. 152–159. doi: 10.1016/j.anucene.2014.12.008.

Haller, H., Muschelknautz, E. and Schultz, T. ((1989)) 'Venturi scrubber calculation and optimization', *Chemical Engineering & Technology*, 12(1), pp. 188–195. doi: 10.1002/ceat.270120125.

Hesketh, H. E. ((1973)) 'Atomization and Cloud Behavior In Venturi Scrubbing', *Journal of the Air Pollution Control Association*, 23(7), pp. 600–604. doi: 10.1080/00022470.1973.10469814.

Hills, J. H. ((1995)) 'Behavior of Venturi Scrubbers as Chemical Reactors', *Industrial & Engineering Chemistry Research*. American Chemical Society, 34(12), pp. 4254–4259. doi: 10.1021/ie00039a015.

Horiguchi, N., Yoshida, H., Kaneko, A. and Abe, Y. ((2014)) 'Relationship between Flow Pattern and Pressure Distribution in Venturi Scrubber', in *22nd International Conference on Nuclear Engineering*. Prague, Czech Republic, pp. 1–6.

Hsiang, L. P. and Faeth, G. M. ((1992)) 'Near-limit drop deformation and secondary breakup', *International Journal of Multiphase Flow*, 18(5), pp. 635–652. doi: 10.1016/0301-9322(92)90036-G.

[http://world-nuclear-news.org/Articles/Nuclear-Innovation-Clean-Energy-Future-\(NICE-Future](http://world-nuclear-news.org/Articles/Nuclear-Innovation-Clean-Energy-Future-(NICE-Future) ((2018)).

<https://www.world-nuclear.org/nuclear-basics/nuclear-energy-and-climate-change.aspx> ((2018)).

Inamura, T. and Nagai, N. ((1997)) 'Spray Characteristics of Liquid Jet Traversing Subsonic Airstreams', *Journal of Propulsion and Power*, 13(2), pp. 250–256. doi: 10.2514/2.5156.

Jacquemain, D., et al. ((2014)) *NEA/CSNI/R(2014)7. OECD/NEA/CSNI Status Report on Filtered Containment Venting*.

Jacquemain, D., Guentay, S., Basu, S., et al. ((2014)) *OECD/NEA/CSNI Status Report on Filtered Containment Venting*.

Kessler, G., Vesper, A., Schlüter, F.-H., Raskob, W., Landman, C. and Päsler-Sauer, J. ((2014)) *The Risks of Nuclear Energy Technology*. doi: 10.1007/978-3-642-55116-1.

Knief, R. A. ((1981)) *Nuclear Energy Technology*. Hemisphere Publishing Corporation;

Washington, DC.

Kulkarni, P. P., Kumar, M., Kumar, N., Jayashree, S., Nayak, A. K., Prasad, T. V. S. M. H., Samal, M. K., Gopika, V., Agrawal, M. K., Mukhopadhyay, D. and Ganju, S. ((2016)) *Post Fukushima Design Modifications of AHWR*.

Lehner, M. ((1998)) ‘Aerosol Separation Efficiency of a Venturi Scrubber Working in Self-Priming Mode’, *Aerosol Science and Technology*, 28(5), pp. 389–402. doi: 10.1080/02786829808965533.

Leith, D., Cooper, D. W. and Rudnick, S. N. ((1985)) ‘Venturi scrubbers: Pressure loss and regain’, *Aerosol Science and Technology*, 4(2), pp. 239–243. doi: 10.1080/02786828508959052.

Lemire, R. J. and Dickson, L. W. ((2003)) ‘Overview of Release Phenomenology in Phebus FP and Comparison with Out-of-Pile Experiments’, in *Fifth Phebus FP Seminar*. France.

Lindau, L. ((1988)) ‘FILTRA-MVSS, A system for reactor accidents mitigation’, *Journal of Aerosol Science*, 19(7), pp. 1389–1392.

Mariana, K. I. S., Satake, T., Maezawa, A., Takeshita, T. and Uchida, S. ((2004)) ‘Experimental and modeling study on carbon dioxide absorption in a cyclone scrubber by phenomenological model and neural networks’, *Korean Journal of Chemical Engineering*, 21(3), pp. 589–594. doi: 10.1007/BF02705492.

Mashayek, A., Behzad, M. and Ashgriz, N. ((2011)) ‘Multiple Injector Model for Primary Breakup of a Liquid Jet in Crossflow’, *AIAA Journal*, 49(11), pp. 2407–2420. doi: 10.2514/1.j050623.

Mayinger, F. and Neumann, M. ((1978)) ‘Dust Collection in Venturi Scrubbers’, *German*

*Chemical Engineering*, 1, pp. 289–293.

McCabe, W., Smith, J. and Harriott, P. ((1957)) *Unit operations of chemical engineering*. Seventh Ed, *Chemical Engineering Science*. Seventh Ed. McGraw-Hill Education. doi: 10.1016/0009-2509(57)85034-9.

Nakao, Y., Horiguchi, N., Yoshida, H., Kanagawa, T., Kaneko, A. and Abe, Y. ((2016)) ‘Measurement of flow rate of droplets and liquid film in venturi scrubber’, in *International Conference on Nuclear Engineering, Proceedings, ICONE*, pp. 1–4. doi: 10.1115/ICONE24-60641.

Nasseh, S., Mohebbi, A., Sarrafi, A. and Taheri, M. ((2009)) ‘Estimation of pressure drop in venturi scrubbers based on annular two-phase flow model, artificial neural networks and genetic algorithm’, *Chemical Engineering Journal*, 150(1), pp. 131–138. doi: 10.1016/j.cej.2008.12.011.

NEA/CSNI/R(2000)9 ((2000)) *Insights into the control of the release of iodine, cesium, strontium and other fission products in the containment by severe accident management, Report NEA/CSNI/R(2000)9*. doi: NEA/CSNI/R(2000)9.

Nukiyama, S. and Tanasawa, Y. ((1938)) ‘An Experiment on the Atomization of Liquid by means of an Air Stream’, *Transactions of the Japan Society of Mechanical Engineers*, 4(15), pp. 128–135.

O’Rourke, P. J. ((1981)) *Collective Drop Effects on Vaporizing Liquid Sprays*. Princeton University, New Jersey.

Orszag, S. A., Yakhot, V., Flannery, W. S. and Boysan, F. ((1993)) ‘Renormalization group modeling and turbulence simulations’, in *International conference, Near-wall turbulent flows, Tempe, Arizona*, p. 1031.

Pak, S. I. and Chang, K. S. ((2006)) 'Performance estimation of a Venturi scrubber using a computational model for capturing dust particles with liquid spray', *Journal of Hazardous Materials*, 138(3), pp. 560–573. doi: 10.1016/j.jhazmat.2006.05.105.

Ravi, G., Gupta, S. K., Viswanathan, S. and Ray, M. B. ((2002)) 'Optimization of venturi scrubbers using genetic algorithm', *Industrial and Engineering Chemistry Research*, 41(12), pp. 2988–3002. doi: 10.1021/ie010531b.

Rogovin, M. ((1979)) *Three Mile Island: A report to the Commissioners and to the Public (NUREG/CR-1250)*, Nuclear Regulatory Commission, special inquiry group. doi: 10.1093/rpd/nch445.

Rudnick, S. N., Koehler, J. L. M., Martin, K. P., Leith, D. and Cooper, D. W. ((1986)) 'Particle Collection Efficiency in a Venturi Scrubber: Comparison of Experiments with Theory', *Environmental Science and Technology*, 20(3), pp. 237–242. doi: 10.1021/es00145a002.

Schiller, L. and Naumann, A. Z. ((1935)) 'A drag coefficient correlation', *Vereines Deutscher Ingenieure*, 77, pp. 318–320.

Schmehl, R., Maier, G. and Wittig, S. ((2000)) 'CFD Analysis of Fuel Atomization, Secondary Droplet Breakup and Spray Dispersion in the Premix Duct of a LPP Combustor', in *Eighth ILASS - Europe 2000*, pp. 1–8.

Sehgal, B. R. ((2012)) *Nuclear Safety in Light Water Reactors: Severe Accident Phenomenology*. Academic Press.

Sharifi, A. and Mohebbi, A. ((2014)) 'A combined CFD modeling with population balance equation to predict pressure drop in venturi scrubbers', *Research on Chemical Intermediates*, 40(3), pp. 1021–1042. doi: 10.1007/s11164-013-1018-2.

Silva, A. M., Teixeira, J. C. F. and Teixeira, S. F. C. F. ((2009)a) ‘Experiments in a large-scale venturi scrubber. Part I: Pressure drop’, *Chemical Engineering and Processing: Process Intensification*, 48(1), pp. 59–67. doi: 10.1016/j.cep.2008.02.001.

Silva, A. M., Teixeira, J. C. F. and Teixeira, S. F. C. F. ((2009)b) ‘Experiments in large scale venturi scrubber. Part II. Droplet size’, *Chemical Engineering and Processing: Process Intensification*, 48(1), pp. 424–431. doi: 10.1016/j.cep.2008.05.007.

Sinha, R. K. ((2011)) ‘Advanced nuclear reactor systems - An Indian perspective’, *Energy Procedia*, 7, pp. 34–50. doi: 10.1016/j.egypro.2011.06.005.

Sinha, R. K. and Kakodkar, A. ((2006)) ‘Design and development of the AHWR-the Indian thorium fuelled innovative nuclear reactor’, *Nuclear Engineering and Design*, 236(7–8), pp. 683–700. doi: 10.1016/j.nucengdes.2005.09.026.

Soffer, L., Burson, S. B., Ferrell, C. M., Lee, R. Y. and Ridgely, J. N. ((1995)) *Accident Source Terms for Light-Water Nuclear Power Plants (NUREG-1465)*.

Steinberger, R. L. and Treybal, R. E. ((1960)) ‘Mass transfer from a solid soluble sphere to a flowing liquid stream’, *AIChE Journal*, 6(2), pp. 227–232. doi: 10.1002/aic.690060213.

Steinhauser, G., Brandl, A. and Johnson, T. E. ((2014)) ‘Comparison of the Chernobyl and Fukushima nuclear accidents: A review of the environmental impacts’, *Science of the Total Environment*. Elsevier B.V., 470–471, pp. 800–817. doi: 10.1016/j.scitotenv.2013.10.029.

Sundberg, R. E. ((1974)) ‘The Prediction of Overall Collection Efficiency of Air Pollution Control Devices from Fractional Efficiency Curves’, *Journal of the Air Pollution Control Association*, 24(8), pp. 758–764. doi: 10.1080/00022470.1974.10469966.

U.S. Nuclear Regulatory Commission WASH-1400 ((1975)) ‘Reactor safety study. An

- assessment of accident risks in U. S. commercial nuclear power plants. Executive Summary. WASH-1400 (NUREG-75/014)', *Nureg 75/014*, 1400(October), p. 10. doi: 10.2172/7134131.
- Vishwanathan, S., Gnyp, A. W. and Pierre, C. C. St. ((1984)) 'Examination of Gas-Liquid Flow in a Venturi Scrubber', *Industrial and Engineering Chemistry Fundamentals*, 23(3), pp. 303–308. doi: 10.1021/i100015a007.
- Viswanathan, S., Gnyp, A. W. and St. Pierre, C. C. ((1985)) 'Annular flow pressure drop model for Pease–anthony-type venturi scrubbers', *AIChE Journal*, 31(12), pp. 1947–1958. doi: 10.1002/aic.690311204.
- Viswanathan, S., Lim, D. S. and Ray, M. B. ((2005)) 'Measurement of drop size and distribution in an annular two-phase, two-component flow occurring in a venturi scrubber', *Industrial and Engineering Chemistry Research*, 44(19), pp. 7458–7468. doi: 10.1021/ie0489195.
- Walton, W. H. and Woolcock, A. ((1960)) 'Aerodynamic Capture of Particles', *Pergamon Press, New York.*, pp. 129–153.
- Wu, P.-K., Kirkendall, K. A., Fuller, R. P. and Nejad, A. S. ((1997)) 'Breakup Processes of Liquid Jets in Subsonic Crossflows', *Journal of Propulsion and Power*, 13(1), pp. 64–73. doi: 10.2514/2.5151.
- Yang, J., Lee, D. Y., Miwa, S. and Chen, S. wen ((2018)) 'Overview of filtered containment venting system in Nuclear Power Plants in Asia', *Annals of Nuclear Energy*, 119, pp. 87–97. doi: 10.1016/j.anucene.2018.03.047.
- Yung, S.-C., Calvert, S. and Barbarika, H. F. ((1977)) *Venturi Scrubber Performance Model*. Washington, D.C.

Yung, S., Calvert, S., Barbarlka, H. F. and Leslie, E. ((1978)) ‘Venturi Scrubber Performance Model’, *Environmental Science & Technology*, 12(4), pp. 456–459. doi: 10.1021/es60140a009.

Zhou, Y., Sun, Z., Gu, H. and Miao, Z. ((2016)) ‘Performance of iodide vapour absorption in the venturi scrubber working in self-priming mode’, *Annals of Nuclear Energy*. Elsevier Ltd, 87, pp. 426–434. doi: 10.1016/j.anucene.2015.09.026.